

Copyright
by
Thomas Wade Stakesby Lewis
2013

The Dissertation Committee for Thomas Wade Stakesby Lewis
certifies that this is the approved version of the following dissertation:

**Dendrimers as Drug and Gene Delivery Vectors: A Self
Consistent Field Theory Study**

Committee:

Venkat Ganesan, Supervisor

Christopher Ellison

Vernita Gordon

Isaac Sanchez

Thomas Truskett

**Dendrimers as Drug and Gene Delivery Vectors: A Self
Consistent Field Theory Study**

by

Thomas Wade Stakesby Lewis, B.S.Ch.E.

DISSERTATION

Presented to the Faculty of the Graduate School of
The University of Texas at Austin
in Partial Fulfillment
of the Requirements
for the Degree of

DOCTOR OF PHILOSOPHY

THE UNIVERSITY OF TEXAS AT AUSTIN

August 2013

Dedicated to my parents, Jane Bell and Greg Lewis, and step-parents, Kim Lewis and Rex Bell. Their constant sacrifice, love, and support throughout my life have both provided the opportunity and inspired me to pursue my interests to my greatest potential.

Acknowledgments

I am deeply appreciative of the intellectual and emotional support I have received along my academic journey. Many people have supported me during my time at the University of Texas at Austin, all of whom I would like to thank.

First, I would like to express my deep appreciation to my advisor, Professor Venkat Ganesan. His scientific vision and expertise provided the foundation for my thesis, and his patience, feedback, and encouragement were crucial to my development as a researcher. He was always able to recognize the best of my work when I was discouraged, and helped me see the forest for the trees when I was lost. Lastly, I would like to thank him for securing funding and computational resources through the Texas Advanced Computing Center to support my work throughout the entirety of my graduate career.

Additionally, I am very appreciative of the insight and support that has been provided to me by my thesis committee members; Dr. Christopher Ellison, Dr. Vernita Gordon, Dr. Isaac Sanchez, and Dr. Thomas Truskett. They have always made themselves available to help me with my coursework and thesis projects. They have also been very helpful in providing guidance for my career after graduate school. I would like to especially thank Drs. Tom and Van Truskett for their very helpful discussions and advice on this matter.

I have been extremely fortunate to share an office with Dr. Victor Pryamitsyn for the past four years. I cannot thank him enough for all the technical questions he patiently fielded from me over the years. Along with sharing his vast knowledge of polymer physics, I also very much enjoyed our discussions on life, religion, and politics. I would also like to thank Dr. Manas Shah, Dr. Landry Khounlavong, Dr. Ben Hanson, Dr. Paresh Chokshi, Dr. David Trombly, Dr. Arun Kumar, Chetan Mahajan, Gunja Pandav, Dylan Kipp, Vaidya Sethuraman, Ahmad Omar, and Do Yong Lee for all of their help and feedback along the way.

I have also received assistance from many of the staff within the ChE Department. Jim Smitherman and Butch Cunningham were always very helpful in addressing my maintenance concerns and offered me plenty of advice for my own personal pursuits. I would like to thank Randy Rife and especially Patrick Danielewski for all of their help in sorting out my IT issues. On many occasions, Patrick went beyond the duties of his job to help me in this regard. Finally I would like to thank Eddie Ibarra, Tammy McDade, Teri Sahba, T Stockman, Kay Costales-Swift, Carrie Brown, and Jessica Kramm for all of their support in a variety of capacities.

My academic drive has been largely inspired by a multitude of great teachers including Thomas Handloser, Mike Moran, Paul Spencer, Don Curdie, Dave Rogers, Dr. Jim Turpin, Dr. Richard Ulrich, and Dr. Christa Hestekin. Their support, guidance, and in many cases, recommendations are directly tied to my academic accomplishments. In particular, Professor Hestekin provided

me with the opportunity to perform undergraduate research, an experience which helped me prepare a solid foundation for my work in graduate school.

Many friendships, both in and out of Austin, have helped to make my time at the University of Texas some of the best years of my life. I would particularly like to acknowledge my life-long friend, Reed Barrett, and his parents, Gary and Sheilah. Reed, thank you for the years of shenanigans and for always believing in me. I have been extremely fortunate to have had the opportunity to play music and cultivate friendships with Kendall Hong, Ernie Surell, Jason Bean, and Dave de Alejandro over the past four years. Making music with them will be what I miss most about Austin. I would also like to thank my close friends outside of the Ganesan Lab (in no particular order): Dr. Colin Smith, Douglas French, Peter Frailie, Zachary Smith, William Kelton, Sean Burgland, Dr. William, Emily, and Jackson Liechty, Eric, Danielle, and Fletcher Young, Joseph Cheng, Joyce Ho, Dr. David Van Wagener, Dr. Alexander Voice, Ramiro Palma, Dr. Stephanie Freeman, and James Carmer.

Most importantly, I would like to thank my family for their unconditional support and love. Most people would consider themselves lucky to have two loving parents. I have had the great fortune of being reared by four amazing parents: Jane and Rex Bell, and Greg and Kimberly Lewis. Knowing that you were always there for me, no matter what was going on in your own lives, has helped me through obstacles small and large. Your years of hard work and sacrifice have provided me with everything I could have ever needed to have a bright and successful future. Thank you. I know I can only pay

this debt forward. I would also like to thank my grandparents, James and Pearl Van Arsdale, James and Margaret Lewis, Paul and Dorothy McGuire, and Flora and Roy Cline for always believing in me. To William, Carolyn, and Rev. Jeremy Bell: thank you for years of support and laughter. I especially would like to thank Jeremy for being both a good friend and devoting countless hours to helping me to develop into a better writer. To my siblings Kristan, Kelli, James, William, and Paul: your intelligence, creativity, hilarity, and perseverance have constantly inspired me to be a better person throughout my life. Additionally, I would like to acknowledge the very helpful technical conversations that William provided regarding my thesis work. Lastly, I would like to thank my loving fiancé, Dr. Amanda Lanza, and her family Susan, Robert, and Jennifer. Amanda, you are not only my best friend and anchor, but a role model in all aspects of my life. Your love and friendship has carried me through all the challenges and frustrations of graduate school, and I look forward to spending the rest of my life with you.

Dendrimers as Drug and Gene Delivery Vectors: A Self Consistent Field Theory Study

Publication No. _____

Thomas Wade Stakesby Lewis, Ph.D.
The University of Texas at Austin, 2013

Supervisor: Venkat Ganesan

This research focuses on the modeling of dendrimer molecules for their application as delivery vectors within drug and gene therapy systems. We examine how the architecture and composition of dendrimers affect their drug and gene binding efficacies along with their interactions with anionic bilayers. We specifically focus on how the weakly basic nature of dendrimer monomers and the addition of neutral grafts to dendrimer surface groups affect their interactions with drugs, linear polyelectrolytes, and bilayers. By using polymer self-consistent field theory (SCFT) to model such systems, we develop a computationally efficient means to provide physical insights into these systems, which are intended to guide dendrimer design for delivery applications.

We study the conformational properties of weakly basic (annealed) polyelectrolyte dendrimers by developing a SCFT model that explicitly accounts for the acid-base equilibrium reaction of the weakly basic monomers.

We specifically focus on the role of local counterion concentration upon the charge and conformations of the annealed polyelectrolyte dendrimers. We compare our results to existing polymer scaling theories and develop a strong stretching theory for the dendrimer molecules.

We extend the previous study to model the interactions between weakly basic dendrimers and weakly acidic, hydrophobic drug molecules. We specifically examine the effects of excluded volume, electrostatic, and enthalpic interactions on the binding efficacies between dendrimers and drugs under a variety of dendrimer generations, solution pOH conditions, drug sizes, and Bjerrum length values.

We study the role of neutral dendrimer grafts on the conformations and drug binding efficacies of dendrimers. We then elucidate how the observed conformational changes affect the charge of the dendrimers. Furthermore, we examine how the presence of grafts affects the steric, electrostatic, and hydrophobic interactions between the drugs and dendrimers under a variety of solution conditions. We compare our results with the binding efficacies observed for non-grafted dendrimers to delineate the conditions under which the grafted dendrimers are better suited as drug hosts.

We include semi-flexible, anionic linear polyelectrolyte (LPE) molecules in our grafted dendrimer SCFT framework to model the interactions between dendrimers and negatively charged genetic materials. Specifically, we examine how neutral dendrimer grafts, LPE stiffness, and solution pOH affect the interactions between dendrimers and LPEs. We then use our SCFT potential fields

as input into Monte Carlo simulations in order to determine the dendrimer-LPE potentials of mean force and the resulting loop and tail statistics of the dendrimer-adsorbed LPE chains.

We incorporate a negatively charged bilayer into our grafted dendrimer SCFT framework to model dendrimer interactions with a cellular membrane. We specifically examine the role of dendrimer grafting length, solution pH , and membrane tension on such interactions. By comparing our results with SCFT calculations of fixed dendrimer conformations and hard sphere nanoparticles in the presence of membranes, we delineate the role of dendrimer flexibility and porosity on the interactions between dendrimers and anionic bilayers.

Table of Contents

Acknowledgments	v
Abstract	ix
List of Figures	xvi
Chapter 1. Introduction	1
1.1 Background and Motivation	2
1.2 Outline of Dissertation	11
1.2.1 Conformations of Charged Dendrimer Molecules	11
1.2.2 Encapsulation of Weakly Acidic Molecules by Polyelectrolyte Dendrimers	12
1.2.3 Effects of Neutral Grafted Chains on the Conformations and Drug Encapsulation Efficacies of Polyelectrolyte Dendrimers	13
1.2.4 Role of Neutral Grafts and Chain Stiffness on the Binding Between Weakly Basic Dendrimers and Linear Polyelectrolytes	13
1.2.5 Effects of Neutral Grafted Chains and Solution pH on Dendrimer-Membrane Interactions	14
Chapter 2. Conformations of Charged Dendrimer Molecules	16
2.1 Introduction	16
2.2 Nomenclature and Terminology	20
2.3 Scaling regimes for polyelectrolyte dendrimers	23
2.4 Self-Consistent Field Theory Method	28
2.4.1 Annealed Charge Model (Explicit Ions)	29
2.4.2 Quenched Charge Model (Explicit Ions)	34
2.4.3 Implicit ion model with Debye-Huckel interactions	35
2.4.4 Numerical Scheme	35

2.4.5	Parameters	36
2.5	Results	37
2.5.1	Effects of pOH and the fraction of dissociatable groups α_P on the conformations of AE dendrimers	38
2.5.2	Comparing the charge fraction effects of AE, QE and QI Models	44
2.5.3	Effect of salt concentration on the conformation and sizes of dendrimers	50
2.5.4	Scaling Behavior of AE, QE and QI Models	52
2.6	Strong Stretching Theory for Weak Polyelectrolyte Dendrimers	61
2.7	Summary	67
Chapter 3. Encapsulation of Weakly Acidic Molecules by Polyelectrolyte Dendrimers		69
3.1	Introduction	69
3.2	Self-Consistent Field Theory Method	74
3.2.1	Potential of Mean Force for Drug Insertion	81
3.2.2	Justification of the Model of a “Point-Like” Drug Molecule	82
3.2.3	Numerical Scheme	83
3.2.4	Parameters	84
3.3	Results	86
3.3.1	Non-Interacting Drug Molecules	87
3.3.2	Electrostatic Interaction Effects	90
3.3.3	Enthalpic Interaction Effects	98
3.3.4	Electrostatic Interaction and Enthalpic Effects	102
3.4	Summary	106
Chapter 4. Effects of Neutral Grafted Chains on the Conformations and Drug Encapsulation Efficacies of Polyelectrolyte Dendrimers		108
4.1	Introduction	108
4.2	Model and Self-Consistent Field Theory	113
4.2.1	Parameters	121
4.3	Results and Discussion	124

4.3.1	Conformations of Grafted Polyelectrolyte Dendrimers	124
4.3.2	Encapsulation of Drugs in Dendrimers: Quantities of Interest	134
4.3.3	Influence of Excluded Volume Interactions	136
4.3.4	Influence of Electrostatic Interactions	137
4.3.5	Effects of Enthalpic Interactions on Drug Encapsulation	140
4.3.6	Combined Influence of Electrostatic and Enthalpic Interactions	144
4.4	Summary	146
Chapter 5.	Role of Neutral Grafts and Chain Stiffness on the Binding Between Weakly Basic Dendrimers and Linear Polyelectrolytes	148
5.1	Introduction	148
5.2	Hybrid Self-Consistent Field Theory and Monte Carlo Approach	153
5.2.1	Self-Consistent Field Theory Model	154
5.2.2	Monte Carlo Simulation of the LPE Chains	164
5.2.3	Parameters	166
5.3	Results	168
5.3.1	Effect of Persistence Length on LPE Complexation	170
5.3.2	Effect of Grafting Length on LPE Complexation	179
5.3.3	Effect of pOH on Complexation	186
5.4	Summary	190
Chapter 6.	Effects of Neutral Grafted Chains and Solution pH on Dendrimer-Membrane Interactions	193
6.1	Introduction	193
6.2	Model	198
6.2.1	Self-Consistent Field Theory Model	198
6.2.2	Parameters	212
6.3	Results	215
6.3.1	Dendrimer-Membrane Interaction	216
6.3.2	Influence of Dendrimer Flexibility and Porosity	225
6.3.3	Effect of Neutral Grafts	230
6.3.4	Effect of pH and Membrane Tension	238
6.4	Summary	242

Chapter 7. Summary and Future Work	245
7.1 Summary of Research	245
7.2 Recommendations for Future Work	246
7.2.1 Dendrimer Flexibility	247
7.2.2 Incorporating Explicit Hydrogen Bonding	248
7.2.3 Multibody Dendrimer-Linear Polyelectrolyte Interactions	249
7.2.4 Dendriplex Interactions with a Membrane	250
Bibliography	251

List of Figures

1.1	A schematic displaying a generation 2 polyamido amine dendrimer having a triethanolamine core. Each of the corresponding generations of the dendrimer are marked by the concentric circles. Reprinted (adapted) with permission from Ref. [56]. Copyright 2012 Wiley.	3
1.2	A schematic displaying the addition of graft chains to the periphery of a generation 3 dendrimer. Reprinted (adapted) with permission from Ref. [65]. Copyright 2000 American Chemical Society.)	8
1.3	A schematic which represents the conformation of polyelectrolyte dendrimer (a), the binding between a dendrimer and model drug molecules (b), the binding between a dendrimer and a linear polyelectrolyte (c), and the interaction of a dendrimer with a bilayer membrane (d).	9
2.1	Schematic of a 2^{nd} generation dendrimer having a functionality of 3.	21
2.2	Monomer density (a) and charge dissociation $\alpha_P\alpha(r)$ (b) profiles for the $g = 3$, $n = 5$ AE dendrimers with the average dissociated charges indicated in the legend. The solution conditions correspond to a Debye screening length of $3a$. The solid lines represent the case where the bulk $pOH = 6.185$ and α_P is allowed to vary. The dotted lines represent AE dendrimers having $\alpha_P = 0.70$ where the pOH is allowed to vary. The inset in (a) displays the log-log perspective of the $\bar{\alpha} = 0.68$ density plot.	39
2.3	Density profiles for the branch points of the $g = 3$, $n = 5$, $\kappa^{-1} = 3a$ AE dendrimer with $pOH = 4.235$ (a) and $pOH = 7.635$ (b). Increasing the charge fraction results in a higher electrostatic force acting on the dendrimer monomers, forcing the shell density maxima to reside at further radial values.	42
2.4	Monomer density (a) and $\alpha_P\alpha(r)$ dissociation (b) profiles for $g = 3$, $n = 5$, $\kappa^{-1} = 3a$ AE (solid lines) and QE (dashed lines) dendrimers with $\alpha_P\alpha(r)$ values of 0.25 (black) and 0.50 (red).	46
2.5	Monomer density (a) and charge dissociation (b) profiles for $g = 3$, $n = 5$, $\kappa^{-1} = 3a$ AE, QI, and QE dendrimers with charge fraction values of $\bar{\alpha} = 0.02$ (black) and 0.58 (green). The inset in (a) displays a logarithmic plot of the density profiles for the $\bar{\alpha} = 0.58$ dendrimers.	48

2.6	The effect of salt concentration on the size of $g = 3, n = 5$ AE ($\alpha_P \alpha_b = 0.53$) and QE ($\alpha_P = 0.53$) dendrimers.	51
2.7	(a) The effect of salt concentration on the Cl^- (solid) and OH^- (dotted) density profiles inside AE dendrimers; (b) Charge dissociation profiles in the AE dendrimers as a function of salt concentrations.	53
2.8	(a) Scaling of dendrimer size of the $g = 3, n = 5, \kappa^{-1} = 3a$ AE, QI, and QE dendrimers with respect to charge fraction. (b) Scaling of dendrimer size of the $\bar{\alpha} = 0.45, n = 5, \kappa^{-1} = 3a$ AE, QI, and QE dendrimers with respect to the number of monomers.	55
2.9	(a) Effective charge in the dendrimer Q ; and (b) The fraction of uncompensated charge (ϕ_{resid}) for the $g = 3, n = 5, \kappa^{-1} = 3a$ AE, QI, and QE dendrimers as a function of $\bar{\alpha}$	57
2.10	(a) Dendrimer size scaling of the $g = 3, n = 5$ QI and QE dendrimers with respect to charge fraction for $\kappa^{-1} = 3a, 25a, 50a$. (b) Dendrimer size scaling of the $\bar{\alpha} = 0.20, n = 5, \kappa^{-1} = 50a$ QI and QE dendrimers with respect to monomer number.	59
2.11	The fraction of uncompensated charge (ϕ_{resid}) for the $g = 3, n = 5$ QI and QE dendrimers as a function of $\bar{\alpha}$ for $\kappa^{-1} = 3a, 25a, 50a$. We see that increasing κ^{-1} results in higher values of ϕ_{resid} , with ϕ_{resid} decreasing with increasing $\bar{\alpha}$ for a fixed value of κ^{-1}	60
2.12	(a) Comparison of the AE dendrimer monomer density profiles from SST and the SCFT simulations. (b) Comparison of the SST parabolic potential profiles with the results of the SCFT simulations for $g = 3, n = 5, \kappa^{-1} = 3a$ AE dendrimers.	65
3.1	Comparison of the density profiles for the point-like and sphere-like drug models. The inset displays a comparison of the $\varphi_D(r)$ for the region $r \geq R_D$	84
3.2	(a) The effect of generation number on the volume fraction profiles of drug molecules, $\varphi_D(r)$ (the size of the drug molecule $R_D = 3a$). The inset displays the dendrimer volume fraction profile, $\varphi_P(r)$. (b) The effect of generation number and R_D on drug molecule encapsulation, $\varphi_{D,excess}$, which is seen to have negative values for all cases. The inset displays the number of drug molecules encapsulated.	89

3.3	(a) The PMFs, $w_D(r)$, experienced by the drug $R_D = 0.5a$ (green and black lines) and $R_D = 2.0a$ (blue lines) in the presence of $G3$ (solid lines) and $G6$ (dashed lines) dendrimers for differing values of l_B . Note that the left hand axis corresponds to the cases where $R_D = 0.5a$, while the right hand axis corresponds to the cases where $R_D = 2.0a$. (b) The effect of l_B on the encapsulation ability of a $G3$ dendrimer in a solution of $pOH = 5.621$. (c) Effect of dendrimer generation on encapsulation ability for small ($R_D = 0.5a$) and large ($R_D = 2.0a$) drug molecules in solution with short ($l_B = 0.5a$) and long ($l_B = 5.0a$) Bjerrum lengths.	92
3.4	(a) The effect of pOH , $pK_{a,D}$, and $pK_{b,P}$ on the encapsulation ability of a $G3$ dendrimers, where $l_B = 1.0a$ and $R_D = 1.0a$. Encapsulation is seen to non-monotonic with respect to pOH . (b) Effect of pOH on the charge fraction ($\bar{\alpha}_P$), bulk polymer probability of dissociation ($\bar{\alpha}_{P,b}$), and bulk drug dissociation ($\bar{\alpha}_{D,b}$) for the cases where $pK_{a,D} = pK_{b,P} = 5.0$ (black), $pK_{a,D} = pK_{b,P} = 6.0$ (red), and $pK_{a,D} = pK_{b,P} = 7.0$ (green).	96
3.5	(a) The drug PMFs for $R_D = 0.5a$ (black and red lines) and $R_D = 2.0a$ (blue and green lines) in the presence of $G3$ (solid lines) and $G6$ (dashed lines) for differing values of χ_{PD} and χ_{DS} . Note that the right hand axis corresponds to the cases where $\chi_{PD} = -0.5$, while the left hand axis corresponds to the cases where $\chi_{PD} = -2.0$. (b) Effect of χ_{PD} on dendrimer-drug localization. The inset displays the number of localized drug molecules. (c) Effect of M on the number of encapsulated drug molecules.	101
3.6	Effect of varying l_B (x-axis) and χ_{PD} (y-axis) on $N_{D,excess}$ for (a) $R_D = 0.5a$, $pOH = 4.621$, (b) $R_D = 0.5a$, $pOH = 5.621$, (c) $R_D = 0.5a$, $pOH = 7.621$, (d) $R_D = 2.0a$ and $pOH = 4.621$, (e) $R_D = 2.0a$ and $pOH = 5.621$, and (f) $R_D = 2.0a$ and $pOH = 7.621$. . .	104
3.7	$\Phi_{D,excess}$ observed for $G3$ and $G5$ dendrimers as a function of l_B in the presence of $R_D = 1.0a$ drug molecules in a solution of $pOH = 5.621$, where $\chi_{PD} = -0.5$ and -1.5 . Note that $\Phi_{D,excess}$ is positive for all values of l_B and χ_{PD}	105
4.1	Schematic of a grafted 3^{rd} generation dendrimer having a functionality of 3. The dendrimer portion is represented in black, while the grafted portions are represented in red.	117

4.2	(a) The effect of N_G on the dendrimer monomer (dashed lines) and grafted monomer (solid lines) volume fraction profiles when $\alpha_P = 0.5$ and $pOH = 5.621$. The inset compares the dendrimer graft volume fraction profiles with graft volume fraction profiles of spherical nanoparticles (φ_{NP}) having a radius of R_P . (b) The effect of N_G on the total volume fraction of polymer monomers. The inset displays the effect of grafting length, N_G , on the solvent volume fraction profiles. The conditions correspond to $\alpha_P = 0.5$, $G3$ dendrimers in a solution pOH of 5.621.	128
4.3	(a) The effect of grafting length on the local fraction of charge dissociated monomers. The inset displays the local OH^- concentration. (b) The effect of N_G on the average dendrimer charge for $l_B = 1.0a$	129
4.4	(a) The effect of N_G on the charge fraction carried by $G3$, $\alpha_P = 0.5$ dendrimers for $pOH = 4.621$ (black), 5.621 (red), and 7.621 (green). (b) The dissociation profiles for $G3N_G0$ (solid lines) and $G3N_G60$ dendrimers (dashed lines) for $pOH = 4.621$ (black), 5.621 (red), and 7.621 (green). (c) The OH^- volume fraction profiles corresponding to the $\alpha(r)$ profiles in (b). (d) The effect of pOH on the size of $G3N_G0$ (black), $G3N_G30$ (red), and $G3N_G60$ (green) dendrimers. The inset displays the effect of $\bar{\alpha}$ on R_P	131
4.5	(a) The effect of grafting length on the drug molecule volume fraction density profiles. (b) The effect of N_G on drug encapsulation, $\varphi_{D,excess}$, for $G3$, $n = 5$ dendrimers.	135
4.6	The effect of N_G and l_B on the drug volume fraction profiles and number of drug particles encapsulated when $R_D = 1.0a$ ((a) and (b)), and $2.0a$ ((c) and (d)).	137
4.7	(a) Effect of χ_{PD} and χ_{DS} on $\varphi_{D,excess}$. (b) Drug volume fraction profiles for $N_G = 0$ (black lines) and $N_G = 60$ (blue lines) dendrimers when $\chi_{PD} = -0.5$ (solid lines) and $\chi_{PD} = -2.0$ (dashed lines). (c) Effect of N_G on the $\varphi_{D,excess}$ for varying χ_{PD} and χ_{DS} . Solid lines correspond to the case when $\chi_{GD} = 0$. Dashed lines correspond to the case when $\chi_{GD} = \chi_{PD}$	141
4.8	$\Phi_{D,excess}$ observed for a $G3N_G30$ ((a)-(c) and $G3N_G60$ ((d)-(f)) dendrimers in the presence of $R_D = 1.0a$ drug molecules in a solution of $pOH = 4.621$ ((a) and (d)), 5.621 ((b) and (e)), and 7.621 ((c) and (f)).	145
5.1	(a) Schematic of a grafted 3^{rd} generation dendrimer having a functionality of 3. The dendrimer portion is represented in black, while the grafted portions are represented in red. (b) Schematic visualizing the definition of trains, loops, and tails as measured at the R_{PG} boundary.	156

5.2	(a) Volume fraction profiles of $g = 3$ non-grafted dendrimer monomers complexed with $N_{LPE} = 50$ polyelectrolyte molecules of varying persistence lengths. (b) Effect of persistence length on the monomer volume fraction profiles.	172
5.3	(a) Effect of PL on the fraction of dendriplex loops and tails; (b) Effect of persistence length on the order parameter, $S(r)$	173
5.4	Snapshots of two LPE chains of $\mu = 0.02$ (a) and $\mu = 0.4$ (b) complexed with a $g = 3$ dendrimer (represented as red sphere). The LPEs are color coded such that the monomers residing within the dendrimer sphere are depicted in red while the monomers outside of the dendrimer are indicated in blue.	174
5.5	(a) The effect of PL on the local probability of dendrimer charge dissociation, $\alpha_P\alpha(r)$. The inset displays the corresponding OH^- counterion density profiles. (b) The effect of PL on the effective charge as a function of r	178
5.6	(a) Volume fraction profiles of $g = 3$ dendrimers (solid lines) and their respective grafted monomers (dashed lines) complexed with $\mu = 0.02$, $N_{LPE} = 50$ LPE molecules. The inset displays the R_{PG} values of the dendrimers as a function of N_G (b)-(c) Volume fraction profiles of LPEs having $\mu = 0.02$ (b) and $\mu = 0.4$ (c) complexed with dendrimers of varying N_G	181
5.7	(a)-(b) Effect of N_G on f_{tail} and f_{loop} for $\mu = 0.02$ (a) and $\mu = 0.4$ (b). (c)-(d) Effect of N_G on $\langle N_{tail} \rangle$ and $\langle N_{loop} \rangle$ for $\mu = 0.02$ (c) and $\mu = 0.4$ (d).	183
5.8	Effect of N_G on the integrated charge distributions, $Q(r)$, for $\mu = 0.02$ (a) and $\mu = 0.4$ (b).	185
5.9	Effect of N_G on the potential of mean force profiles for $\mu = 0.02$ (a) and $\mu = 0.4$ (b) LPE molecules.	186
5.10	(a) Density profiles of Charged dendrimer monomers for a $N_G = 30$, $g = 3$ dendrimer complexed with $\mu = 0.02$ LPE molecules. (b) LPE volume fraction profiles (solid lines for $\mu = 0.02$, dotted lines for $\mu = 0.4$) that are complexed with $N_G = 30$, $g = 3$ dendrimers for varying values of $pOH - PK_{B,P}$. Effect of pOH on the PMF profiles of $\mu = 0.02$ (solid lines) $\mu = 0.4$ (dotted lines) LPEs in the presence of $N_G = 0$ (c) and $N_G = 30$ (d) dendrimers.	188
5.11	Effective charge profiles, $Q(r)$, of dendriplexes for varying values of $pOH - PK_{B,P}$. The solid lines correspond to the non-grafted dendrimers and the dotted lines correspond to the case of grafted dendrimers with $N_G = 30$	190

6.1	(a) Schematic of our dendrimer-membrane system wherein the dendrimer is separated by distance z_D from the unperturbed bilayer midplane. (b) Schematic of a grafted 2^{nd} generation dendrimer having a functionality of 3. The dendrimer portion is represented in black, while the grafted portions are represented in red. (c) Schematic of a lipid molecule in our system. The head portion is represented in red, while the tail portions are represented in black.	200
6.2	(a) Volume fraction profiles for the solvent and lipid components of our model membrane under zero surface tension. (b) The membrane surface tension, γ ($k_B T/nm^2$), as a function of the area per lipid head group (nm^{-2}). The inset displays the free energy per lipid head group as a function of the area per lipid.	214
6.3	(a)-(f) Color plots displaying the volume fraction values of $G3$ dendrimers, $\varphi_P(r, z)$, in a $pH = 7$ solution at varying distances from the center of the lipid bilayer, z_D . The lipid bilayer head group volume fraction values are shown through the contour lines, which correspond to values of $\varphi_H = 0.07$ and $\varphi_H = 0.14$	217
6.4	(a) Asphericity of the dendrimer molecules as a function of z_D . The inset displays the ratio, G_{zz}/G_{xx} . (b) The radius of gyration of the dendrimer molecule (normalized to its unperturbed value, R_0) as a function of z_D	220
6.5	(a)-(b) Snapshots of $G3$ PAMAM dendrimers interacting with a DPPC bilayer after initial position of $4nm$ above the bilayer membrane and $500ns$ of simulation time as obtained from the CG MD simulations by Lee and Larson. The black dots represent the dendrimer monomers while the blue groups represent the DPPC headgroups. Reprinted (adapted) with permission from Ref. [73]. Copyright 2006 American Chemical Society.	222
6.6	The relative increase in dendrimer charge for a dendrimer at distance z_D from the bilayer as compared to dendrimers in the absence of an anionic membrane, ΔQ_P , as a function of z_D for $G3$ (black line) and $G4$ (red line) dendrimers.	223
6.7	The dendrimer-membrane potential of mean force, $\Delta\beta F$, for a $G3$ dendrimer (solid black line), $NDG3$ dendrimer (dashed black line), HS representing a $G3$ dendrimer (dotted black line), and $G4$ dendrimer (solid red line) as a function of distance between the dendrimer core monomer and the bilayer midplane.	225
6.8	Color plots displaying the volume fraction values of fixed conformation $NDG3$ dendrimers (a-c) and HS representing $G3$ dendrimers (d-f) in a $pH = 7$ solution at varying distances from the center of the lipid bilayer, z_D . The lipid bilayer head group volume fraction values are shown through the contour lines, which correspond to values of $\varphi_H = 0.07$ and $\varphi_H = 0.14$	228

6.9	The dendrimer asphericity (a and b) and G_{zz}/G_{xx} ratios (b and d) as a function of z_D for $G3$ (a and b) and $G4$ (c and d) dendrimers. The insets quantify the dendrimer radius of gyration values for the $G3$ and $G4$ dendrimers as a function of z_D	232
6.10	Color plots displaying the volume fraction values of $G3$ dendrimer interior (a)-(c) and graft (d)-(f) monomers in a $pH = 7$ solution at varying values of N_G and separation distance $z_D = 0$. The lipid bilayer head group volume fraction values are shown through the contour lines, which correspond to values of $\varphi_H = 0.07$ and $\varphi_H = 0.14$.	233
6.11	The $Q_{Contact}$ values (eq 6.43) between charged $G3$ (a) and $G4$ (b) dendrimer monomers and charged lipid head groups.	235
6.12	The effect of N_G on the dendrimer-membrane potential of mean force, $\Delta\beta F$, as a function of distance between the dendrimer core monomer and the bilayer midplane for $G3$ (a) and $G4$ (b) dendrimers.	237
6.13	The effect of solution pH on the dendrimer-membrane potential of mean force, $\Delta\beta F$, as a function of distance between the dendrimer core monomer and the bilayer midplane for $G3$ (a) and $G4$ (b) dendrimers. The insets quantify the dendrimer charge, Q_{den} for an individual dendrimer in the absence of a membrane.	240
6.14	The effect of membrane tension, grafting length, and pH on the potential of mean, $\Delta\beta F$, between $G3$ dendrimers and an anionic lipid bilayer. Solid lines represent $\gamma = 0.0 k_B T/nm^2$ while dashed lines represent $\gamma = 0.74 k_B T/nm^2$	241
6.15	The effect of pH and neutral grafts on the rupture tension, γ_r , of anionic bilayer membranes.	243

Chapter 1

Introduction

Progress in drug design and understanding of the molecular pathways in disease provide great promise for advances in healthcare. However, realization of the full potential of these fields requires the ability to effectively deliver drug and genetic materials to targeted cells [114]. The need for such delivery vectors has motivated research for the development of polymeric materials in drug and gene therapy systems [88]. In this context, hyper-branched molecules known as dendrimers have exhibited desirable binding and transportive properties in delivery applications [20, 23, 67, 68, 114, 123, 145]. However, outstanding questions remain about how the design of dendrimer molecules affects its drug and genetic material binding affinities and the transport properties of the resulting complexes. In this work, by developing computationally efficient modeling tools, we seek to provide insights to the research community on how varying dendrimer design parameters affect their interactions with drugs, genetic material, and cellular membranes.

1.1 Background and Motivation

Dendrimers are regularly branched polymer molecules, and in fact, their name is derived from the Greek word for “tree”, *dendra* [114]. The highly branched nature of dendrimers can be witnessed in Figure 1.1, which displays the structure of a polyamido amine (PAMAM) dendrimer having a triethanolamine core [56]. The architecture of dendrimers can be characterized through three main quantities: (i) *functionality*, (ii) *generation number*, and (iii) *spacer length*. If we examine the central branch point of the dendrimer (the tertiary amine group located in circle 0), we notice three branches stemming from it, which comprise the “0th” *generation* of the dendrimer. The number of branches stemming from any given branch point is termed as the *functionality*, f , of a dendrimer, and the functionality of the dendrimer in Fig. 1.1 is 2. Moving outward from the core along the branches, we observe a set of branching points which lie on a radial position denoted by circle 0. This set of branch points connect the 0th and 1st *generations* of the dendrimer, and the number of monomers between the two branching points denote the dendrimer *spacer length*, n . Moving further outward, we see the regular addition of *generation* layers until we reach the periphery. The total number of *generation* layers attached to the 0th *generation* denotes the *generation number*, g , of the dendrimer. The regular branching of the dendrimers results in an exponential growth in the number of monomers as g is increased.

Advances in dendrimer synthesis techniques provide the ability to synthesize not only highly monodisperse dendrimer species, but also dendrimers

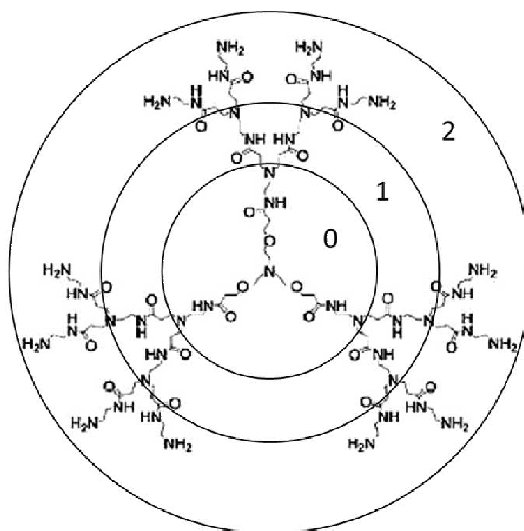


Figure 1.1: A schematic displaying a generation 2 polyamido amine dendrimer having a triethanolamine core. Each of the corresponding generations of the dendrimer are marked by the concentric circles. Reprinted (adapted) with permission from Ref. [56]. Copyright 2012 Wiley.

composed of a wide range of chemical compositions, including hydrophobic/hydrophilic and acidic/basic monomers [3, 23, 162]. For instance, the PAMAM dendrimer in Fig. 1.1 has many weakly basic amine groups, with the primary amine groups residing at the dendrimer periphery and the tertiary amine groups existing at the inner branch points. The hyperbranched structure of dendrimers provides the ability to create nanoscale molecules of very high charge density. Furthermore, functional groups residing in the outermost generations of dendrimers can be tailored to affect their interactions with small molecules [20, 23, 67, 68, 123, 145], polyelectrolytes [24, 69, 94, 131, 147, 187], and biological cells [53, 54, 169]. In order to effectively utilize the large parameter set available to experimentalists, it is beneficial to develop a fundamental understanding on how these parameters affect the dendrimer conformations and resulting properties.

The high monodispersity, small length scales, wide range of chemical compositions, and high charge densities of dendrimers make them desirable candidates for applications in a wide range of fields [9, 114, 117]. However, in the following, we limit our studies to biomedical applications, specifically the use of dendrimers as delivery vectors in drug and gene therapy systems. Successful delivery of drug and genetic materials to targeted cells is met by complex challenges [9, 114, 141]. For instance, around 40% of newly developed pharmaceuticals are not able to be utilized within clinical settings due to their low water solubilities and poor membrane permeabilities [91, 145]. The delivery of genetic materials to cells are hindered by serum nucleases in the

blood, which bind to and degrade the nucleic acid material [9, 114, 141]. Furthermore, the net negative charge of biological membranes creates unfavorable electrostatic interactions between the negatively charged genetic material, and resulting in a decreased membrane permeability [9, 114, 141]. The binding efficacies of dendrimers to drug and genetic materials have been shown to help overcome such challenges [9, 114, 141].

Dendrimers have been shown experimentally to enhance the solubility of poorly soluble drug compounds, which has been hypothesized to occur through three general mechanisms: (i) hydrophobic interactions [22, 55, 70, 115, 122], (ii) electrostatic attractions [5, 21, 130, 184], and (iii) hydrogen bonding [22, 130, 148]. Precise control over dendrimer design allows for the creation of unimicellar, water-soluble dendrimers which have hydrophobic interiors and hydrophilic exteriors [55]. The relatively hydrophobic interiors of these molecules creates a more favorable environment in which hydrophobic molecules may reside. Despite having low water solubility, a large number of drug molecules carry acid and base groups, and the high density of charged monomers carried by dendrimers has been shown to contribute to the increased water solubility of drugs by dendrimers through electrostatic binding [5, 21, 130, 184]. Hydrogen bonding between hydrogen and oxygen groups on both the drug and dendrimer molecules have also been shown through both simulation [148] and experiments [22, 130] to contribute significantly to drug-dendrimer binding. For most dendrimer-drug complexes, binding between dendrimers and drug molecules is likely to result from a combination of these

proposed binding mechanisms. Therefore, it is beneficial to understand how dendrimer architecture and chemical composition affects the various mechanisms through which drugs bind.

The phosphate groups present along the backbone of nucleic acid (NA) materials carry negative charges at all physiologically relevant pH conditions, and the high density of positive charges carried by cationic dendrimers has been shown to drive the complexation between dendrimers and NA materials [18, 69, 187]. The binding of dendrimers to NA materials in turn creates a complex which carries a more positive charge than the corresponding uncomplexed NA material, which creates more favorable interactions between the NA material and the negatively charged cellular membrane [18, 69, 187]. Furthermore, the complexation of dendrimers to NA materials has been shown to the degradation of genetic materials by serum nuclease enzymes [30]. Although there has been progress in understanding the important mechanisms governing the binding between dendrimers and NA materials, a fuller understanding of how dendrimer design can be tailored to maximize binding and transfection ability is needed. Furthermore, there are a number of different types of gene therapy agents including not only large plasmids, but also short single-stranded and double stranded oligomers of varying flexibility. Thus, the role of flexibility of the NA chains on the resulting dendrimer-NA material complexes needs to be understood.

Although cationic dendrimers have been shown to enhance the delivery and cellular internalization of both hydrophobic drugs and genetic materials,

they have a correspondingly high cytotoxicities, which has been speculated to result from non-specific binding between the positively charged dendrimer amines and the negatively charged lipid head groups [47, 59, 81, 110]. Furthermore, these cytotoxic effects increase with increasing generation numbers and dendrimer concentrations [47, 59, 81, 110]. In order to combat high dendrimer cytotoxicities, researchers have performed modification of dendrimer surface amine groups by covalently conjugating poly(ethylene glycol) (PEG) chains to the surfaces [30, 54, 169]. Figure 1.2 displays a schematic for the covalent conjugation of grafts to the dendrimer periphery. The addition of such neutral grafted chains to dendrimers has been shown to reduce dendrimer cytotoxicity [30, 54, 169], and although it has been shown to affect dendrimer complexation with drug molecules and NA materials, the grafted dendrimer counterparts have been proven to still maintain their ability to serve as drug [7, 60, 65] and gene vectors [30, 31, 146, 147]. In order to optimize the design of dendrimers such that they have minimum cytotoxic effect and maximum binding efficacies, a fundamental understanding on how the addition of neutral grafted chains affects dendrimer complexation with drug molecules and NA materials is needed.

A complete understanding for the rational design of dendrimers in drug and gene delivery agents requires insight on many levels, and in Fig. 1.3, we display a schematic which outlines the types of systems examined in this thesis. From each system studied, we seek to address the following issues:(a) *How do the dendrimer design parameters affect dendrimer conformations?* Since their

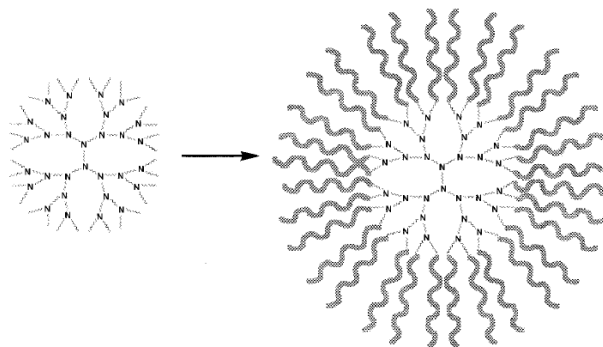


Figure 1.2: A schematic displaying the addition of graft chains to the periphery of a generation 3 dendrimer. Reprinted (adapted) with permission from Ref. [65]. Copyright 2000 American Chemical Society.)

discovery, researchers have had a strong interest in understanding the conformations of dendrimers. Specifically, they were interested in whether or not the dendrimers assume open conformations with internal cavities, or if the dendrimer arms fold back into the interior such that there is little void space inside of the dendrimer. Obtaining such an understanding is relevant for the encapsulation of drug molecules by the dendrimers. (b) *What is the influence of dendrimer architecture and chemical composition on the binding efficacies between dendrimers and drugs?* By varying dendrimer architectural parameters and the chemical properties of both the drug and dendrimer molecules, one can gain physical insight into how dendrimer design can be tailored to enhance encapsulation efficacy of the drug molecules. (c) *How does the dendrimer design and nucleic acid material flexibility affect the complexation between these materials?* The transfection efficiency of dendrimer vectors has been shown to depend upon a number of characteristics including the generation number of the den-

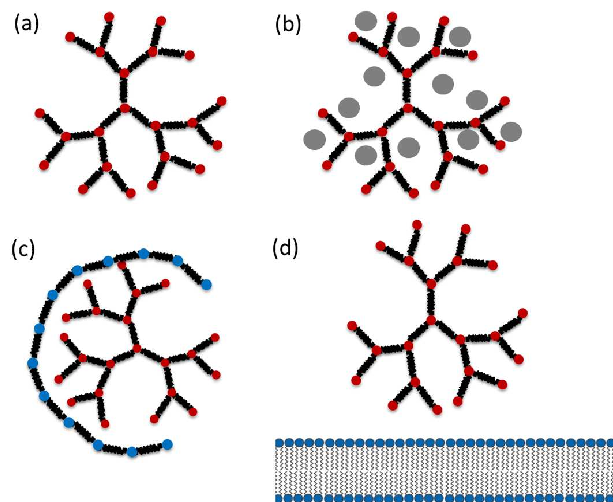


Figure 1.3: A schematic which represents the conformation of polyelectrolyte dendrimer (a), the binding between a dendrimer and model drug molecules (b), the binding between a dendrimer and a linear polyelectrolyte (c), and the interaction of a dendrimer with a bilayer membrane (d).

dendrimer, the presence and length of grafted chains, and the ratio of dendrimers and NA material [18, 24, 30, 31, 69, 94, 131, 146, 147, 150, 164, 187, 188]. By examining the complexation between dendrimers and linear polyelectrolytes, one can gain physical insights which can guide the rational design of dendrimers for their use as delivery vectors. (d) *What is the role dendrimer architecture and solution conditions on the physics of interaction between dendrimers and charged bilayers?* A fundamental understanding on how dendrimers interact with charged bilayer membranes is essential for designing dendrimers which have low cytotoxicities.

Modeling of dendrimer systems began not long after the first dendrimer molecules were synthesized, with the first modeling study being performed by

de Gennes and Hervet [27]. In that model, they applied an analytical self-consistent field theory (SCFT) approach. As computational techniques have become more popular, researchers began to examine dendrimers using methodologies such as Monte Carlo [16, 61, 62, 107–109, 171, 190], molecular dynamics (coarse grained and atomistic) [14, 43, 48, 76, 103–105, 116], dissipative particle dynamics [170, 181], and Brownian dynamics simulations [98, 191]. Furthermore, these techniques have been extended to examine dendrimer interactions with drugs [100, 112, 148], linear polyelectrolytes [63, 64, 71, 72, 96, 99, 101, 120, 166, 172], and bilayer membranes [57, 58, 73–75, 78, 158, 181, 182]. Despite the many useful insights obtained from these studies, two features of experimentally relevant systems that are conspicuously missing: (i) There were no studies which explicitly account for the weakly basic nature of amine containing dendrimers. The probability that a weakly basic monomer exists in a charge dissociated state is dependent upon the chemical potentials of the neutral and charged monomer species and the local concentration of OH^- counterions [86, 121, 174]. Non-homogeneous spatial distributions of weakly acidic and basic monomers resulting from the connectivity of polymer molecules have been shown to influence the spatial distribution of counterions [192], and thus, the local probability that a monomer exists in a charged state [86, 121, 174]. The regular branching within amine containing dendrimer molecules results in a high density of weakly basic monomers, thus, it is pertinent to explicitly account for their weakly basic nature. (ii) There was a lack of computational studies which examined the influence of neutral grafts on dendrimer interac-

tions with drugs, linear polyelectrolytes, and membranes. In this document, we seek to fill in these gaps by performing SCFT calculations for the above discussed systems. Below, we detail our work, which appear as individual chapters.

1.2 Outline of Dissertation

1.2.1 Conformations of Charged Dendrimer Molecules

Using polymer SCFT we study the conformational properties of polyelectrolyte dendrimers. We compare results for three different models of charge distributions on the polyelectrolytes: (i) A smeared, quenched charge distribution characteristic of strong polyelectrolytes; (ii) A smeared, annealed charge distribution characteristic of weak polyelectrolytes; and (iii) An implicit counterion model with Debye-Huckel interactions between the charged groups. Our results indicate that an explicit treatment of counterions is crucial for the accurate characterization of the conformations of polyelectrolyte dendrimers. In comparing the quenched and annealed models of charge distributions, annealed dendrimers were observed to modulate their charges in response to the density of polymer monomers, counterions and salt ions. Such phenomena is not accommodated within the quenched model of dendrimers and is shown to lead to significant differences between the predictions of quenched and annealed model of dendrimers. In this regard, our results indicate that the average dissociated charge, $\bar{\alpha}$, inside the dendrimer serves as a useful parameter to map the effects of different parametric conditions and models onto each other. We also

present comparisons to the scaling results proposed to explain the behavior of polyelectrolyte dendrimers. Inspired by the trends indicated by our results, we develop a strong segregation theory model whose predictions are shown to be in very good agreement with the numerical SCFT calculations.

1.2.2 Encapsulation of Weakly Acidic Molecules by Polyelectrolyte Dendrimers

In order to gain insight into the solubilization of drugs inside dendrimer architectures, we have developed and numerically implemented a SCFT model for the equilibrium characteristics of charged dendrimer molecules in the presence of weakly acidic drug molecules. Using such a model, we examine the relative influence of excluded volume, electrostatic, and local enthalpic interactions upon the solubilization of drugs in dendrimers. When only excluded volume interactions are accounted, there is no driving force for drug solubilization inside the dendrimer and hence depletion of the drug from the dendrimer molecule (relative to the bulk drug concentration) is observed. The inclusion of electrostatic interactions within the model results in solubilization of drugs within the dendrimer. The solubilization of the drugs is shown to increase with increasing drug charge density and increasing dendrimer generation number. We probe the effect of enthalpic interactions and demonstrate that the number of drug molecules encapsulated through enthalpic interaction is dependent upon the number of dendrimer monomers, the enthalpic interaction parameters between the dendrimer and drug (χ_{PD}), and the drug and solvent (χ_{DS}). We also analyze the combined effects of all the preceding interactions to iden-

tify the synergism in their influence and delineate the relative importance of different parameters such as pOH , size of the drugs, and the Bjerrum length of the solution in influencing the encapsulation of drugs by dendrimer molecules.

1.2.3 Effects of Neutral Grafted Chains on the Conformations and Drug Encapsulation Efficacies of Polyelectrolyte Dendrimers

We examine the role of neutral dendrimer grafts upon the conformations and the drug complexation efficacy of weakly basic polyelectrolyte dendrimers by using a SCFT approach. Our results indicate that grafted chains modify the conformations of the dendrimers and lead to a swelling of the dendrimer, the degree of which increases with increasing chain length of the grafts. In turn, such conformational changes leads to a higher charge being carried by the dendrimer molecule. We compare the encapsulation efficacy of grafted and non-grafted dendrimers and find that for strong enough enthalpic and/or electrostatic interactions, the grafted dendrimers are capable of higher amounts of encapsulation than the non-grafted counterparts. By isolating the influences of electrostatic and enthalpic interactions, we clarify the physics behind the observed enhanced encapsulation.

1.2.4 Role of Neutral Grafts and Chain Stiffness on the Binding Between Weakly Basic Dendrimers and Linear Polyelectrolytes

We develop and implement a new hybrid methodology combining SCFT and Monte Carlo simulations to study the complexation between negatively charged semiflexible linear polyelectrolyte (LPE) molecules and a positively

charged dendrimer containing grafts of neutral polymers. We examine the influence of LPE stiffness, length of the dendrimer grafts, and solution pOH upon the characteristics of the resulting complexes. Our results indicate that increasing LPE stiffness reduces the dendrimer-LPE binding affinity and results in an overall higher net charge carried within the dendrimer molecule. When we varied the size of the grafts, the dendrimer-LPE binding strength was seen to decrease with increasing grafting chain length for the flexible LPE chains. In contrast, for stiff LPE chains, the binding strength was not seen to vary significantly with the grafting lengths. Overall, longer grafting lengths were seen to reduce the fraction of exposed LPE molecules, suggesting that grafted dendrimers may better shield nucleic acid material from serum nucleases. Lastly, we found that increasing the solution pOH was seen to enhance both the binding between the dendrimer and LPE molecules and the total positive charge carried by the complex.

1.2.5 Effects of Neutral Grafted Chains and Solution pH on Dendrimer-Membrane Interactions

We use polymer SCFT to study the physics involved in the permeation of charged dendrimer molecules across anionic lipid bilayer membranes. We specifically examine the influence of neutral grafts and pH conditions on the free energies of interactions and the shape deformations of the dendrimer. We observe that the ability of the dendrimer to undergo conformational rearrangements plays a crucial role in influencing the interactions between the dendrimer and the membrane. At neutral pH , we observe that dendrimers with grafted

chains are repelled by the anionic bilayers. However, decreasing the solution pH to endosomal conditions results in attractive dendrimer-membrane interactions under some parametric conditions. We observe that dendrimer insertion into the membrane results in a decreased value in membrane tension at which rupture occurs, and furthermore, that the rupture tension decreasing with the addition of grafts to the dendrimer. Our results suggest that neutral grafts can be utilized to create pH sensitive delivery vectors.

Chapter 2

Conformations of Charged Dendrimer Molecules

2.1 Introduction

Recent advances in polymer synthesis techniques have yielded a variety of new materials that are finding use in a variety of applications [35]. One such context in which polymers are starting to play an important role is in the context of drug delivery applications [88]. However, successful fruition of such applications is still confronted by challenges arising from the drug hydrophobicity and specificity requirements of drug carriers [145]. The use of dendrimers, which are hyper-branched tree-like polymer molecules, has been advanced as an approach to overcome some of the above challenges. Such polymer molecules have been speculated to form complexes with drug molecules that can be delivered to specified targets [20, 23, 67, 68, 123, 145]. For example, Cheng and Xu were able to show that the presence of PAMAM dendrimers increased the aqueous solubility of non-steroidal anti-inflammatory drugs and attributed it to the formation of dendrimer-drug complexes [22].

Maximization of drug encapsulation within a dendrimer requires appropriate conformations wherein the hydrophobic drug molecules can reside.

Motivated by these considerations, there have been a number of theoretical studies aimed at predicting the structure and conformations of dendrimer molecules as a function of different physicochemical parameters. De Gennes and Hervet [27] used scaling theories and predicted a hollow core conformation for neutral dendrimer molecules. However, later studies which used Monte Carlo [16, 82, 109] and molecular dynamics [42] simulations contradicted the preceding results and indicated that the density of polymer segments to be a maximum at the center of the molecule and decrease monotonically in the radially outward direction (*i.e.* a dense core conformation). These results were also validated by Boris and Rubenstein [10], who used self-consistent mean field theory to determine the radial density profile of a dendrimer in a good solvent and demonstrated that their results were indeed consistent with the dense core model suggested by simulations. They pointed out that the results of de Gennes and Hervet arose from an incorrect assumption that the consecutive generation branch points of the dendrimer resided at further radial values relative to the earlier ones. In a later work, Zook and Pickett [194] revisited the model of de Gennes and Hervet and revised it to remove the incorrect assumptions and demonstrated agreement of the refined theory with the dense core model.

Adding charged groups to dendrimers was proposed as a way to achieve open core conformations desired for drug delivery applications. Such considerations have motivated a number of theoretical [8, 38, 40, 43, 48, 79, 90, 98, 102, 106, 108, 157, 171] and experimental [19, 92, 93, 125, 136] studies of charged

dendrimer molecules. For instance, Welch and Muthukumar [171] used Monte Carlo simulations to show that the size and conformations of dendrimers with charged branch and terminal points are strongly dependent on the salt concentration. However, their model for electrostatic effects treated the counterions only at an implicit level and incorporated instead Debye-Huckel interactions between the charged groups. Subsequent work using scaling analysis [11] and computer simulations [8, 38, 40, 43, 48, 90, 102, 106, 108, 135, 157, 176, 178] have shown that counterion localization becomes an important factor for highly branched polymeric structures. Such a phenomenon reduces the electrostatic interactions between the charged monomers and endows nontrivial dependencies for the conformations of the dendrimer as a function of number of dissociable groups, salt concentrations etc.

Broadly speaking, polyelectrolyte molecules can be classified into two categories. *Strong* polyelectrolytes are those which typically achieve full dissociation of the acidic or basic monomers. Modeling such strong acid or base polyelectrolytes is usually simplified by assuming that the effective charge of the polyelectrolyte backbone is independent of the solution conditions [12, 124, 168]. It is also common in modeling efforts to smear this effective charge over the entirety of the polymer backbone (referred to henceforth as the “quenched” model of polyelectrolytes). The second class of polyelectrolytes are termed the *weak* polyelectrolytes. In such cases, the charged monomers are not completely dissociated. Instead, their dissociation, a result of proton exchange with the solvent, is determined as the finite conversion resulting from a chemical equi-

librium condition [12]. In the latter situation, there is usually an interplay between the conformations of the molecule and the resulting dissociated fraction of charges. Such a behavior can lead to nontrivial responses of the polymer molecules to changes in external conditions. For instance, weak polyelectrolyte brushes and star polymers have been shown to undergo dramatic changes in structure upon changes in pH and salt concentrations [121, 139, 174].

Much of the prior theoretical studies of the charged dendrimer molecules have used the quenched model, which is representative of strong polyelectrolytes. In contrast however, many of the commercially available polyelectrolyte dendrimers, such as poly(amidoamine) (PAMAM) dendrimers, have been shown to be weakly basic [126]. Consequently, it is essential to understand the behavior of weakly charged dendrimers and contrast these results with the predictions developed for the strongly charged polyelectrolyte dendrimers. Specifically, we are interested in probing the manner in which pH, salt concentrations and other physical properties of the dendrimer impact upon the overall size and conformational characteristics of the dendrimer. We also seek to compare such results to the predictions of the quenched charge model and models in which the counterions are treated implicitly.

Motivated by the above considerations, in this chapter we develop and numerically analyze a polymer self-consistent field theory (SCFT) [35] model for the structure and conformation of weakly charged PE dendrimers and compare our findings with the results for quenched polyelectrolyte dendrimers. We explicitly study the effect of different system parameters (pOH , charge

fraction, salt concentration, and generation number) and different model assumptions (strong vs weak polyelectrolytes) on the dendrimer conformational characteristics. We also propose a simple extension of the strong stretching theory (SST) which allows for analytical calculations and compare its predictions with the more detailed numerical SCFT calculations.

The rest of the chapter is arranged as follows: In sections 2.2 and 2.3 we discuss the associated terminology and briefly review the scaling arguments proposed to describe the conformations of charged dendrimer molecules. In section 2.4 we describe our self-consistent field theory (SCFT) method and the associated numerical details. In section 2.5 we present the results of the SCFT calculations, and compare them against the predictions for strongly charged dendrimers and models which ignore counterion density distributions. Inspired by the trends seen in our results, we propose a simple extension of the strong stretching theory in section 2.6 to model weakly charged polyelectrolyte dendrimers and compare its results to the numerical results of SCFT. In section 2.7 we conclude with a summary of our results.

2.2 Nomenclature and Terminology

In this section, we define the nomenclature and terminology adopted in our work. Figure 2.1 displays a pictorial representation of a “second generation” dendrimer. At the center of the dendrimer is the core, from which stems three dendrimer spacers, composing the 0^{th} generation. At the end of each spacer is a branch point that connects to two more chains, which constitute

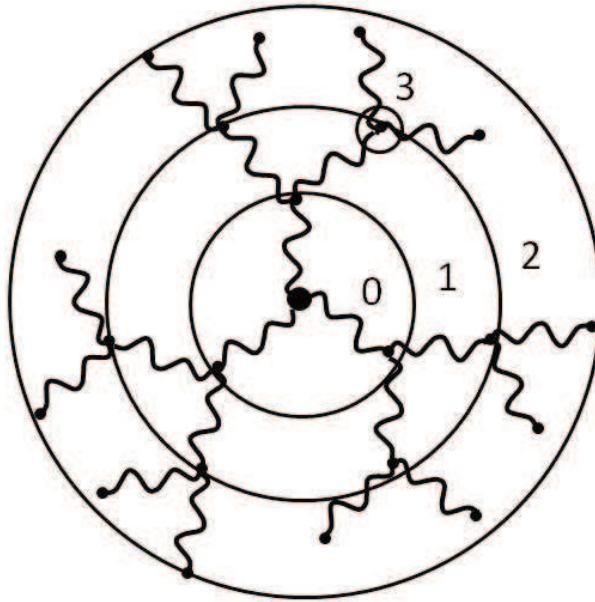


Figure 2.1: Schematic of a 2^{nd} generation dendrimer having a functionality of 3.

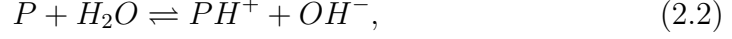
the next generation of spacers. “Functionality” denotes the number of chains stemming from an individual branch point and for all of our calculations we assume a value of 3 for our system. In our framework, each dendrimer is composed of a total of M monomers:

$$M(g) = nf \left((f - 1)^{g+1} - 1 \right) + 1 \quad (2.1)$$

where n is the number of monomers per spacer, f is the branch point functionality, and g is the generation number.

In the subsequent sections, we perform analysis for both weakly and strongly charged dendrimer models. In both models, we assume that the dendrimer is such that every $(1/\alpha_P)^{th}$ ($\alpha_P < 1$) monomer P of the dendrimer can

become charged. For weakly charged systems, we assume that such monomers participate in a charge dissociation reaction of the form



a phenomena which is governed by the law of mass action:

$$K_{b,P} = \frac{[PH^+][OH^-]}{[P]}. \quad (2.3)$$

$K_{b,P}$ denotes the equilibrium constant of the dissociation reaction (Eq. 2.2) and $[A]$ ($A \equiv P, PH^+, OH^-$) refers to the concentration in mol/L of species A . The equilibrium constant $K_{b,P}$ is proportional to $\exp(-\beta\Delta G^o)$, where $\Delta G^o = \xi_{OH^-}^o + \xi_{PH^+}^o - \xi_P^o$ is the free energy of the reaction and ξ_i^o are the standard chemical potentials of the different species involved in the dissociation reaction. Strongly charged dendrimers correspond to the limit of $K_{b,P} \gg 1$, wherein every $(1/\alpha_P)^{th}$ monomer is always dissociated.

To characterize the behavior of the above systems, we adopt models commonly used in previous studies. For strongly charged dendrimers, we adopt a representation commonly referred to as a “quenched” model, in which all the monomers of the dendrimer are assumed to be dissociated, with however an effective (smeared) charge of α_P . For weakly charged dendrimers, we adopt the “annealed” model, in which all the monomers are assumed to be *capable* of dissociation with an effective (smeared) charge of α_P . However, the actual local fraction of dissociated monomers for annealed systems $\alpha(r)$ (where $\alpha(r) < 1$) is dependent on the solution conditions, and is obtained from:

$$K_{b,P} = \frac{\alpha(r)\rho_{OH^-}(r)}{1 - \alpha(r)} \quad (2.4)$$

where $\rho_{OH^-}(r)$ is the local concentration of OH^- counterions. For $K_{b,P} \gg 1$ it can be verified that the annealed dendrimer approaches the limit of a quenched dendrimer with $\alpha(r) = 1$ everywhere. In general however, the $\alpha(r)$ is fixed by the solution conditions represented by pOH and the equilibrium constant $K_{b,P}$ of the base. In the discussions below, we denote the “bulk” value of $\alpha(r)$ (corresponding to a homogeneous solution) for the annealed polymer as α_b . In other words, the dissociated charge of the annealed polyelectrolyte at infinite dilution conditions correspond to $\alpha_P \alpha_b$.

2.3 Scaling regimes for polyelectrolyte dendrimers

Previous analytical works [11, 178] on polyelectrolyte star molecules have shown that the interplay between electrostatic interactions, chain stretching, osmotic pressure of the polymer monomers and entropy of counterions, can result in a variety of scaling regimes for the characteristic size of branched polyelectrolyte molecules [177]. We briefly review these developments below to provide a context for understanding the numerical SCFT results presented in later sections. For branched polyelectrolyte molecules treated within the quenched model, three primary regimes have been distinguished: *polyelectrolyte regime*, *osmotic regime*, and *quasi-neutral regime*.

Polyelectrolyte Regime: The polyelectrolyte regime occurs for parametric conditions such that the local density of charged monomers within the dendrimer is insufficient to induce counterion localization. This is expected to happen for dendrimers of low generation numbers with low values of dissoci-

ated charge [177]. In such a case, a majority of the counterions are located outside the dendrimer, and the size of the dendrimer molecule is determined by a balance between the electrostatic energy (F_{elec}) and conformational entropy (F_{conf}) of the polyelectrolyte molecule. Explicitly, the free energy of the molecule, F , can be estimated as:

$$F = F_{conf} + F_{elec}. \quad (2.5)$$

By using the Flory-like arguments of Wolterink *et al.* [177], we can estimate the conformational free energy of the dendrimer molecules as:

$$\frac{F_{conf}}{k_B T} \cong \frac{9}{2} \frac{R^2}{na^2} [2 - 2^{-g}] \quad (2.6)$$

where R denotes the radius of the dendrimer molecule and a is the Kuhn segment length of the monomers.¹ The electrostatic contribution to the free energy evaluated in the smeared Debye-Huckel approximation is given by:

$$\frac{F_{elec}}{k_B T} \cong \frac{l_B (\alpha_P M)^2 \exp(-\kappa R)}{R} \quad (2.7)$$

where $l_B = e^2/\epsilon k_B T$ is the Bjerrum length (e is the charge of a single electron and ϵ is the dielectric constant of the solvent) and κ is the inverse Debye screening length ($\kappa^2 = 4\pi l_B \sum_i i c_i z_i^2$, where c_i is the concentration and z_i is the valence number of ion species i). When the Debye screening length is large ($\kappa \rightarrow 0$), the screened electrostatic energy is reduced to the Coulombic expression for electrostatic energy. Using the assumption that $\kappa \rightarrow 0$ for the

¹We note that the slight difference in Eq. 2.6 from that derived in Wolterink *et al.* [177] is due to the difference in the architecture assumed for the 0th generation in our model.

polyelectrolyte regime and minimizing the free energy expression in Eq. 2.5 results in the following scaling for the size of the dendrimer:

$$R(g) \cong n^{\frac{1}{3}} \alpha_P^{\frac{2}{3}} M^{\frac{2}{3}} \left(\frac{l_B}{a} \right)^{\frac{1}{3}} a. \quad (2.8)$$

When the above result is reduced for the case of a 0^{th} generation dendrimer, the radius R matches the scaling for the quenched polyelectrolyte star predicted by Borisov and Zhulina [11].

Osmotic Regime; When the degree of branching is large enough to induce counterion localization, free counterions in solution localize within the polyelectrolyte, and reduce the electrostatic energy arising from the charged groups. The polyelectrolyte molecule begins to swell to accommodate the loss of entropy of the counterions, leading to the osmotic regime. In this regime, the size of the polyelectrolyte is assumed to be governed by the stretching energy of the dendritic arms and the osmotic pressure of the localized counterions.

At a scaling level, the local osmotic pressure of the counterions, $\Delta\Pi(r)$, can be estimated to be proportional to the difference between the local ion concentration and its bulk value:

$$\frac{\Delta\Pi}{k_B T} = \sum_i [\rho_i(r) - \rho_{b,i}], \quad (2.9)$$

where the index i accounts for all free ion species and $\rho_{b,i}$ denotes the bulk concentration of the i^{th} free ion. The free ion densities can in turn be obtained from a mean field approximation where the ions can be assumed to interact with the electrostatic field, $\Phi(r)$:

$$\rho_i(r) = \rho_{b,i} \exp(-z_i \Phi(r)) \quad (2.10)$$

where $\Phi(r)$ is the electrostatic potential (normalized by $e/k_B T$), and z_i denotes the valency of the i th free ion. Finally, by assuming that the polymer monomers are completely neutralized by the localized counterions, we can invoke local electroneutrality to relate the concentration of free ions to the density of polymer monomers $\rho_P(r)$ as:

$$\alpha_P \alpha(r) \rho_P(r) + \sum_i z_i \rho_i(r) = 0. \quad (2.11)$$

Using Eqs. 2.10 and 2.11 in Eq. 2.9 yields:

$$\frac{\Delta \Pi}{k_B T} = \sqrt{(\alpha_P \alpha(r) \rho_P(r))^2 + 4\Phi_b^2} - 2\Phi_b. \quad (2.12)$$

where Φ_b denotes the ionic strength of the solution.

Now, two limiting scaling regimes can be deduced within the osmotic regime. For the case of *low salt concentrations* ($\Phi_b \ll 1$), we assume $\alpha_P \alpha(r) \rho_P(r) / (2\Phi_b) \gg 1$. In this case, the osmotic pressure found from Eq. 2.12 can be approximated as:

$$\frac{\Delta \Pi}{k_B T} \sim \frac{\alpha_P \alpha(r) M}{R^3} \quad (2.13)$$

where we assume the monomer density is given by $\rho_P(r) = M/R^3$. For a quenched dendrimer $\alpha(r) \rightarrow 1$, which reduces the osmotic pressure to $\alpha_P M/R^3$. Flory-type scaling of a quenched dendrimer in the low salt osmotic regime can be obtained by balancing the osmotic pressure against the stretching free energy of Eq. 2.6, resulting in the following scaling [177]:

$$R \cong (M n \alpha_P)^{\frac{1}{2}} a \quad (2.14)$$

In the limit of *high salt concentration* ($\alpha_P \alpha(r) \rho_P(r) \ll \Phi_b$), we assume $\alpha(r) \approx \alpha_b$ due to the displacement of OH^- ions by salt counterions which do not participate in acid-base dissociation. The osmotic pressure in Eq. 2.12 can now be approximated for the annealed dendrimer as:

$$\frac{\Delta\Pi}{k_B T} \approx \frac{\alpha_P^2 \alpha^2(r) \rho_P^2(r)}{2\Phi_b} \quad (2.15)$$

Flory-type scaling of a polyelectrolyte dendrimer in the high salt *osmotic regime* can be obtained by balancing the osmotic pressure, which is now given by

$$\frac{R^2 \Delta\Pi}{k_B T} \cong \frac{(\alpha_P \alpha_b M)^2}{\Phi_b R^4} \quad (2.16)$$

against the stretching force of Eq. 2.6, resulting in the following scaling [177]:

$$R \cong M^{2/5} n^{1/5} (\alpha_P \alpha_b)^{2/5} (\Phi_b a^3)^{-1/5} a \quad (2.17)$$

For quenched dendrimers, the $\alpha_P \alpha_b$ term in Eq. 2.17 is replaced with α_P .

Quasi-Neutral Regime: In the quasi-neutral regime, electrostatic and osmotic effects of the localized counterions are much smaller than the steric interactions between the polymer monomers. For charged dendrimers, this situation can be realized at low values of pOH and low fractions of dissociable monomers ($\alpha_P \ll 1$). In such a regime, the size of the molecules determined by balancing the stretching energy of the dendrimer chains and steric interactions of the monomers. In a good solvent, the steric energy of interaction is given by:

$$\frac{F_{int}}{k_B T} \cong \frac{u_0 M}{R^3}, \quad (2.18)$$

where u_0 denotes the excluded volume interaction parameter (in units of a^3). Balancing the steric interaction energy against the stretching energy yields [177]:

$$R \cong M^{\frac{2}{5}} \left(\frac{u_0}{a^3} \right)^{1/5} n^{\frac{1}{5}} a \quad (2.19)$$

As charge effects are assumed to be negligible in this regime, this scaling is expected to describe both quenched and annealed dendrimer models.

2.4 Self-Consistent Field Theory Method

The main focus of this chapter is on the behavior of weakly charged dendrimers represented by the annealed model of polyelectrolytes, and its comparisons to the quenched model of polyelectrolytes and the model in which the counterions are treated implicitly by incorporating Debye-Huckel screened interactions between the charged monomers. In this section we detail the SCFT framework underlying the three models used for characterizing the conformation of charged dendrimer molecules [168]. We note that recently Szleifer *et al.* [121] and Won and coworkers [174] have developed a mean field model for weak polyelectrolyte brushes. Since the SCFT model outlined below shares many common elements with their framework, we restrict our discussion to the most important equations underlying our study. A more descriptive derivation of the model can be found in the above-mentioned articles by Szleifer *et al.* [121] and Won and coworkers [174].

2.4.1 Annealed Charge Model (Explicit Ions)

We consider a system of volume V that contains a single dendrimer molecule of g generations in the presence of H^+ and OH^- ions, and monovalent salt ions which will be denoted (without loss of generality) as Na^+ , and Cl^- ions. The dendrimer is assumed to be spherically symmetric, with their core fixed at the center of the simulation cell.

We employ a semigrand canonical framework within a mean field approximation for our dendrimer model. In this framework, the free energy \mathcal{F} can be identified as:

$$\mathcal{F} = \mathcal{F}_{conf} + \mathcal{F}_{int} + \mathcal{F}_{mix} + \mathcal{F}_{chem} + \mathcal{F}_{elec}. \quad (2.20)$$

Below, we describe each of the above terms in more detail:

(i) The first contribution \mathcal{F}_{conf} accounts for the conformational entropy of the dendrimer and can be written as:

$$\beta\mathcal{F}_{conf} = \ln Q_P + \int d\mathbf{r} w_P(\mathbf{r}) \rho_P(\mathbf{r}) \quad (2.21)$$

where $\beta = 1/k_B T$, $\ln Q_P$ represents the conformational entropy of the dendrimer in the external field $w_P(\mathbf{r})$, and $\rho_P(r)$ denotes the concentration of the polymer monomers. To obtain Q_P we adopt a continuous chain Gaussian model to describe the conformational features of the polymer molecules. We use the symbol “ s ” to index the contour length coordinate along the chain and $\mathbf{r}_{i,j}(s)$ to denote the position in space of the s^{th} segment in the j^{th} branch of

the i^{th} generation. The stretching energy U_0 of the dendrimer chain can then be expressed as:

$$\beta U_0(\{\mathbf{r}\}) = \frac{3}{2a^2} \sum_{i=0}^g \sum_{j=0}^{f(f-1)^i} \int_{s_i}^{s_{i+1}} \left| \frac{d\mathbf{r}_{i,j}(s)}{ds} \right|^2 ds, \quad (2.22)$$

and the partition function Q_P can be obtained as:

$$Q_P = \frac{\int D\mathbf{R} \exp \left[- \sum_{i=0}^g \sum_{j=0}^{f(f-1)^i} \int_{s_i}^{s_{i+1}} ds \left[\frac{3}{2a^2} \left| \frac{d\mathbf{r}_{i,j}(s)}{ds} \right|^2 + w_P(\mathbf{r}_{i,j}(s)) \right] \right]}{\int D\mathbf{R} \exp \left[- \sum_{i=0}^g \sum_{j=0}^{f(f-1)^i} \int_{s_i}^{s_{i+1}} ds \left[\frac{3}{2a^2} \left| \frac{d\mathbf{r}_{i,j}(s)}{ds} \right|^2 \right] \right]} \quad (2.23)$$

(ii) The term \mathcal{F}_{int} of Eq. 2.20 accounts for the nonbonded monomer-monomer interactions, which is quantified using an implicit solvent excluded volume model:

$$\beta \mathcal{F}_{int} = \frac{u_0}{2} \int d\mathbf{r} \rho_P^2(\mathbf{r}) \quad (2.24)$$

where u_0 is the excluded volume parameter that characterizes the size of the dendrimer monomers.

(iii) The entropies of mixing of free ions is accounted in the third term, \mathcal{F}_{mix} and is given as:

$$\beta \mathcal{F}_{mix} = \int d\mathbf{r} \left(\sum_i \rho_i(\mathbf{r}) [\ln \rho_i(\mathbf{r}) v_i - 1 + \beta \xi_i^o] \right). \quad (2.25)$$

In the above, v_i , the volume of the i^{th} species ($i = OH^-, H^+, Cl^-, Na^+$), is equal to a^3 and ξ_i^o is the standard chemical potential of the i^{th} species.

(iv) The fourth term, \mathcal{F}_{chem} , accounts for the free energy contribution from the acid-base equilibrium governed by Eq. 2.3, where the local fraction of

dissociated dendrimer polymer monomers and uncharged monomers are given by $\alpha(\mathbf{r})$ and $1 - \alpha(\mathbf{r})$ respectively. This energy contribution, \mathcal{F}_{chem} , is given as:

$$\beta\mathcal{F}_{chem} = \int d\mathbf{r} \alpha_P \rho_P(\mathbf{r}) [\alpha(\mathbf{r}) (\ln(\alpha(\mathbf{r})) + \beta\xi_{PH^+}^o) + (1 - \alpha(\mathbf{r})) (\ln(1 - \alpha(\mathbf{r})) + \beta\xi_P^o)]. \quad (2.26)$$

(v) The electrostatic interaction between the charged entities are accounted in \mathcal{F}_{elec} :

$$\beta\mathcal{F}_{elec} = \int d\mathbf{r} \left[\rho_e(\mathbf{r})\Phi(\mathbf{r}) - \frac{1}{8\pi l_B} |\nabla\Phi|^2 \right] \quad (2.27)$$

where $\Phi(\mathbf{r})$ is the electrostatic potential which is conjugate to the charge density field, $\rho_e(\mathbf{r})$. The above expression is consistent with electrostatic interactions modeled through a classical Coulombic potential with a spatially homogeneous dielectric constant ϵ . We do note that the inhomogeneities in the density profiles of the ions and polymer monomers are better accounted through a compositionally dependent dielectric constant [121]. However, such a model adds to the numerical and parametric complexity, and so we adopt the simpler model of a spatially uniform dielectric constant.

In order to solve the statistical mechanics of the above model, we employ a mean-field approximation and determine the equilibrium fields, $\rho_P(\mathbf{r})$, $\rho_c(\mathbf{r})$, $\rho_+(\mathbf{r})$, $\rho_-(\mathbf{r})$, $w(\mathbf{r})$, and $\Phi(\mathbf{r})$, as those which minimize the free energy \mathcal{F} of Eq. 2.20. Such a procedure yields the following self-consistent equations [35]:

$$w_P(\mathbf{r}) = u_0 \rho_P(\mathbf{r}) + \alpha_P \ln \left[\frac{1 - \alpha(r)}{1 - \alpha_b} \right] - \alpha_P, \quad (2.28)$$

$$-\frac{1}{4\pi l_B} \nabla^2 \Phi(\mathbf{r}) = \sum_i z_i \rho_i(r) + z_{PH} + \alpha_P \alpha(r) \rho_P(r), \quad (2.29)$$

and

$$\alpha(r) = \frac{1}{1 + \rho_{OH^-}(r)/K_{b,P}}. \quad (2.30)$$

In the above,

$$\rho_i(\mathbf{r}) = \frac{\exp[-\beta \xi_i^o]}{v_i} \exp[-z_i \Phi(\mathbf{r})] \quad (2.31)$$

and

$$\rho_P(\mathbf{r}) = \frac{1}{V_{QP}} \sum_{i=0}^g \Omega_i \int_{s_i}^{s_{i+1}} ds q(\mathbf{r}, s) q^\dagger(\mathbf{r}, s), \quad (2.32)$$

and where Ω_i is the number of branches in the i^{th} generation. The function $q(\mathbf{r}, s)$ represents the probability of finding the s^{th} monomer of the dendrimer at position \mathbf{r} with the condition that the center of dendrimer is fixed at $r = 0$. $q^+(\mathbf{r}, s)$ denotes the complementary probability of finding the $N - s^{th}$ monomer at position \mathbf{r} independent of the location of the monomer at the outer extremity. The functions $q(\mathbf{r}, s)$ and $q^+(\mathbf{r}, s)$ can be found from the following “diffusion-like” equations [35]:

$$\frac{\partial q}{\partial s} = \frac{a^2}{6} \nabla^2 q - [w_P(\mathbf{r})] q; \quad q(\mathbf{r}, s = 0) = \delta(\mathbf{r}). \quad (2.33)$$

where \mathbf{r}_0 is the radius of the dendrimer core at which the branches of the 0^{th} generation are attached. The “initial” condition in Eq. 2.33 constrains the 0^{th} monomer to the dendrimer core at $\mathbf{r} = \mathbf{0}$, which is at the center of the spherical simulation cell. The function $q^\dagger(\mathbf{r}, s)$ that runs from the periphery of the dendrimer is given by

$$-\frac{\partial q^\dagger}{\partial s} = \frac{a^2}{6} \nabla^2 q^\dagger - [w_P(\mathbf{r})] q^\dagger; \quad q^\dagger(\mathbf{r}, s = N) = 1. \quad (2.34)$$

In order to account for the branching within the dendrimer, the above equations are supplemented by the following conditions [41]

$$q^\dagger(\mathbf{r}, s_i^-) = [q^\dagger(\mathbf{r}, s_i^+)]^{f-1} \quad (2.35)$$

$$q(\mathbf{r}, s_i^+) = q(\mathbf{r}, s_i^-) [q^\dagger(\mathbf{r}, s_i^+)]^{f-2} \quad (2.36)$$

where $q^\dagger(\mathbf{r}, s_i^-)$ refers to spatially dependent chain propagator for a monomer at a value of s that is infinitesimally smaller than s_i , the value of s at the i^{th} branching point. The above conditions embody the fact that at the dendrimer branch points, the outer generation chains connect. This is analogous to two independent particles diffusing to the same point in space at the exact same time. Equations 2.35 - 2.36 account for this “time” condition by multiplying these two probabilities [41]. In order to solve for $q(\mathbf{r}, s)$ and $q^\dagger(\mathbf{r}, s)$ we first determine $q^\dagger(\mathbf{r}, s)$ and then subsequently use it via Eq. 2.36 to determine $q(\mathbf{r}, s)$. We assume no flux boundary conditions at the center and periphery of the cell ($\nabla q(\mathbf{r} = 0, s) = \nabla q(\mathbf{r} = \infty, s) = \nabla q^\dagger(\mathbf{r} = 0, s) = \nabla q^\dagger(\mathbf{r} = \infty, s) = 0$). Once $q(\mathbf{r}, s)$ and $q^\dagger(\mathbf{r}, s)$ are known, we can then solve for Q_P using

$$Q_P = \frac{1}{V} \int d\mathbf{r} q^\dagger(\mathbf{r}, s = 0). \quad (2.37)$$

The electrostatic potential $\Phi(\mathbf{r})$ is solved for using the resulting Poisson-Boltzmann (PB) equation (Eq. 2.29). We assume a no flux condition at the center of the cell:

$$\nabla\Phi(\mathbf{r} = 0) = 0 \quad (2.38)$$

At infinitely large radial values, a similar condition is expected to hold. However, computational limitations preclude the use of such large cells. However, on physical considerations, one can argue that the electrostatic potential at the edge of a large but finite sized cell is expected to be small, allowing us to apply the Debye-Huckel approximation to Eq. 2.29. This results in the following boundary condition:

$$\frac{1}{\Phi} \frac{\partial \Phi}{\partial r} \Big|_{r=r_\infty} = -\frac{1}{r_\infty} - \kappa \quad (2.39)$$

where r_∞ is the radial value of outer boundary of the simulation cell and κ is the inverse Debye screening length (see the definition below Eq. 2.7).

2.4.2 Quenched Charge Model (Explicit Ions)

The quenched dendrimer model corresponds to an annealed dendrimer in the limit of full dissociation ($\alpha(r) \rightarrow 1$). The free energy expression of this system is identical to Eq. 2.20, but excludes the entropy of mixing term \mathcal{F}_{chem} associated with the charged and uncharged monomers. Application of the mean-field approximation to such a model yields:

$$w(\mathbf{r}) = u_0 \rho_p(\mathbf{r}) + \alpha_P \Phi(\mathbf{r}) \quad (2.40)$$

$$-\frac{1}{4\pi l_B} \nabla^2 \Phi(\mathbf{r}) = \sum_{m=0} z_m \rho_m(r) + z_{PH} + \alpha_P \rho_P(r) \quad (2.41)$$

where the polymer and free ion densities are given by formulas identical to Eqs. 2.32 and 2.31. The framework outlined in Section 2.4.1 remains applicable to solve for $q(r, s)$, $q^\dagger(r, s)$, and $\Phi(r)$.

2.4.3 Implicit ion model with Debye-Huckel interactions

In an implicit free ion model, the concentration of free ions in the system is assumed to be homogeneous. The latter allows the use of screened Debye-Huckel interactions to represent the electrostatic interactions between the polymer monomers. A dendrimer in the presence of a homogeneous distribution of counterions will have constant dissociation ($\alpha(r) = \alpha_b$), and thus will behave as a quenched dendrimer with each monomer having a charge of $\alpha^* = \alpha_b \alpha_P$. The appropriate mean-field equations in this case are:

$$w(\mathbf{r}) = u_0 \rho_p(\mathbf{r}) + \alpha^* \Phi(\mathbf{r}) \quad (2.42)$$

$$-\frac{1}{4\pi l_B} \nabla^2 \Phi(\mathbf{r}) + \frac{\kappa^2}{4\pi l_B} \Phi(\mathbf{r}) = z_{PH^+} \alpha^* \rho_P(\mathbf{r}) \quad (2.43)$$

where the polymer density is again given by expression Eq. 2.32, and $q(r, s)$, $q^\dagger(r, s)$, and $\Phi(r)$ are solved in the manner outlined in Section 2.4.1.

2.4.4 Numerical Scheme

We employed the Crank-Nicholson finite difference scheme [35, 137] to solve the partial differential equations for $q(r, s)$ and $q^\dagger(r, s)$ in Eqs. 2.33 and 2.34 respectively. We non-dimensionalized our grid by R_g , the radius of gyration of an unperturbed ideal chain that follows the path from the center of the dendrimer to the periphery ($R_g^2 = ((g+1)n)a^2/6$). The contour length of the dendrimer chain was non-dimensionalized by $(g+1)n$. We varied the size of our cell from $50 R_g$ (for the case when $\kappa^{-1} = 3a$) to $150 R_g$ (for the case when $\kappa^{-1} = 100a$) such that the electrostatic potential at the edge of the cell

was less than 0.001, ($\Phi(r = r_{max}) < 0.001$) in order to satisfy the electrostatic potential boundary condition, Eq. 2.39, at the edge of the cell. Random initial guess values for the fields were applied, and the field values were solved via a Picard iteration scheme. We used a convergence criteria which imposed that the largest absolute value of the error in the fields was less than or equal to 0.005.

2.4.5 Parameters

A majority of the results we present are for a third generation ($g = 3$) dendrimer with a spacer length of $n = 5$ monomers. We fix the excluded volume parameter, u_0 , as equal to $0.5a^3$. To reduce the number of parameters, we further set the Bjerrum length to be the same as the Kuhn segment length (which is approximately 0.7 nm in water). The solution screening length, κ^{-1} , was allowed to vary from $3a$ to $50a$ (approximately 2.1nm to 35nm), which in experimental conditions corresponds to salt concentrations from 21.4 mM to 0.077 mM. The pK_b of the annealed dendrimers were chosen to be 5.063, which when converted into units of molecules/ a^{-3} corresponded to a value of 5.685. Except for results depicting the influence of salt concentrations, our studies were effected at a constant value of the screening length. This required us to adjust the salt concentrations appropriately with changes in other physicochemical parameters.

2.5 Results

In the following sections, we present our numerical results for annealed dendrimers within explicit counterion models and compare them to the results for the quenched dendrimer model with explicit ions and quenched dendrimers in implicit ions (Debye-Huckel model). For the sake of brevity, we use the following abbreviations in discussing the results: the model of annealed dendrimers in explicit ions (weak polyelectrolytes) will be designated as AE, quenched dendrimers in implicit ions (with Debye-Huckel interactions) will be denoted as QI, and quenched dendrimers in explicit ions (strong polyelectrolytes) as QE. We note that there are potentially three different parameter choices for effecting the comparisons between AE and QE models:

- (i) The fraction of dissociatable groups on the polymer, α_P , is maintained the same between AE and QE models: This approach ignores the partial dissociation of the AE dendrimers and is hence expected to not be a useful comparison except under conditions which promote a complete dissociation of polyelectrolyte chain. Whence, we did not pursue approach (i) any further in our studies;
- (ii) The fraction of dissociatable groups, α_P , of the quenched model is set to the fraction of dissociated groups at infinite dilution, $\alpha_P\alpha_b$, for the AE model. This approach ensures similar charge conditions for the AE and QE polymers at infinite dilution conditions. We note that if one seeks to model the behavior of weak polyelectrolytes using the QE model, this strategy is the only direct approach which can be implemented *a priori* on the QE model;

(iii) The fraction of dissociatable groups, α_P , of the quenched model is set to the average dissociated charge $\bar{\alpha}$ of the AE dendrimer. The latter can be defined as:

$$\bar{\alpha} = \frac{\alpha_P \int_0^\infty dr r^2 \alpha(r) \rho_P(r)}{\int_0^\infty dr r^2 \rho_P(r)}. \quad (2.44)$$

Comparisons effected under approach (iii) seek to address whether the dissociatable nature of the polymer is relevant beyond determining the total dissociated charge of the dendrimer. However, we note that since this approach requires the dissociation profiles $\alpha(r)$ for the AE model, it is not possible to use this strategy to *a priori* model the behavior of weak polyelectrolytes using the QE model.

Below we discuss results quantifying the influence of pOH , fraction of dissociatable groups α_P and salt concentrations upon the conformations and density profiles of AE dendrimers and compare them with the behavior of QE and QI dendrimers. We specifically adopt approaches (ii) and (iii) in comparing the behaviors at different parametric conditions.

2.5.1 Effects of pOH and the fraction of dissociatable groups α_P on the conformations of AE dendrimers

The influence of the bulk pOH and α_P on the density and charge dissociation profiles of the AE dendrimers are shown in Figs. 2.2a and b. In Fig. 2.2a the density profiles represented by the solid lines correspond to the case where we fix the bulk value of $pOH = 6.185$ (which corresponds to $\alpha_b = 0.76$) and α_P is allowed to vary. The dashed lines represent cases which have a fixed value

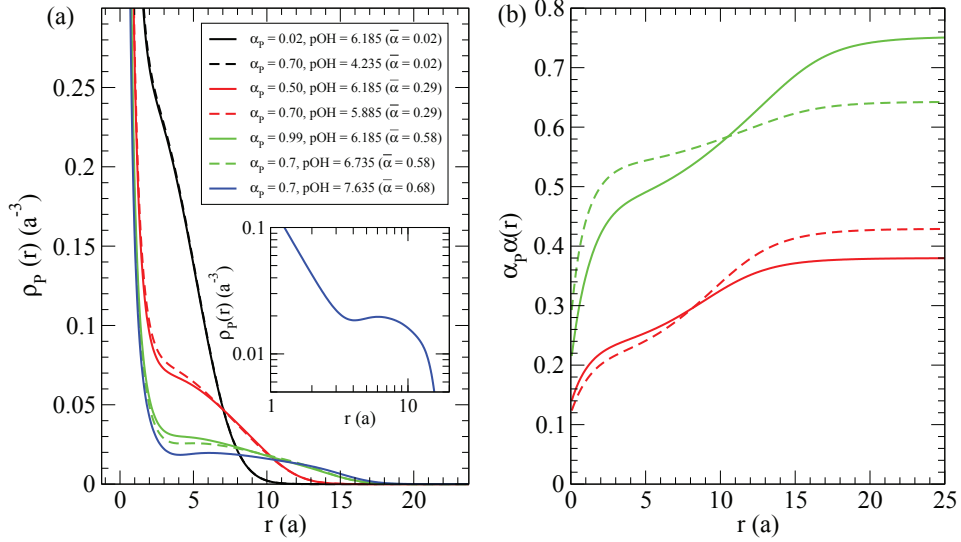


Figure 2.2: Monomer density (a) and charge dissociation $\alpha_P \alpha(r)$ (b) profiles for the $g = 3$, $n = 5$ AE dendrimers with the average dissociated charges indicated in the legend. The solution conditions correspond to a Debye screening length of $3a$. The solid lines represent the case where the bulk $pOH = 6.185$ and α_P is allowed to vary. The dotted lines represent AE dendrimers having $\alpha_P = 0.70$ where the pOH is allowed to vary. The inset in (a) displays the log-log perspective of the $\bar{\alpha} = 0.68$ density plot.

of $\alpha_P = 0.70$, but where the bulk pOH is instead varied. The parameters are chosen such that the average dissociated charge $\bar{\alpha}$ is kept the same between pairs of α_P and pOH conditions (the solid and dotted lines). To reduce clutter, in Fig. 2.2b we display the charge fraction dissociation profiles only for two sets of parameters.

Overall, in Fig. 2.2 we observe that at low α_P and pOH , the AE dendrimers have a dense core profile (the singularity-like behavior of the density profile as $r \rightarrow 0$ is a result of the grafting boundary condition embodied in

Eq. 2.33). Upon increasing α_P or pOH we observe an “expansion” of the dendrimer which manifests through a decrease in the monomer density values near the center and a corresponding increase of density at the periphery. At even higher values of pOH (and α_P , the latter not explicitly displayed) we observe that the dendrimer density profiles become non-monotonic (*c.f.* the blue line in Fig. 2.2a and the corresponding log-log density plot in the inset). Interestingly, we observe that despite the significant differences in the charge dissociation profiles (Fig. 2.2b) at different conditions, the monomer density profiles predicted for different parameters match semiquantitatively when the average dissociated charge $\bar{\alpha}$ is rendered the same.

To rationalize the trends observed in Fig. 2.2, we first note that increasing either α_P or pOH results in the same qualitative effect, *viz.*, an enhanced dissociation of the monomers. The latter is reflected in the results displayed in Fig. 2.2b as well as in the $\bar{\alpha}$ values displayed in the legend. The influence of α_P upon the overall charge can be understood as being the outcome of increasing the number of dissociatable groups. On the other hand, increasing pOH lowers the concentration of OH^- ions. Due to the reaction equilibrium condition Eq. 2.3, there is a corresponding increase in the number of dissociated charges. Using this framework, the dense core profile seen at low α_P or pOH can be rationalized as the characteristic behavior expected for dendrimers with low charge fractions under which conditions they resemble neutral dendrimers [10, 16, 42, 82, 109]. With increasing α_P and pOH however there is an increase in the charge density inside the dendrimer due to the enhanced dissociation

(see Fig. 2.2b). The electrostatic interactions accompanying this increased charge density leads to the observed expansion of the dendrimer.

The nonmonotonicity noted at high $pOHs$ in Fig. 2.2, can be rationalized as a consequence of two competing effects. We first note that the monotonically *decreasing* density profiles which are characteristic of neutral dendrimers can be attributed to the backfolding of dendrimer arms which allows them to maximize their conformational entropy [10]. Introduction of charged monomers is expected to create electrostatic repulsion which forces the dendrimer branch points and terminal groups to reside at further radial values. In Figure 2.3, we corroborate this hypothesis by displaying the density profiles of the branch points for AE dendrimers with bulk pOH values 4.235 and 7.635 (the dotted green and blue lines of Fig. 2.2). As the dendrimer becomes more charged we observe that the maxima of the branch point number densities become more segregated and pushed to radially further distances. As shown previously in the theory of DeGennes and Hervet [27], dendrimers which are restricted to having subsequent generations be located at larger radial values are expected to lead to monotonically growing density profiles. The non-monotonic variations in the density profiles in Fig. 2.2a can then be rationalized as characteristic of the transition from the monotonically decreasing density profiles representative of low charge fractions to the monotonically increasing density profiles expected at very high charge fractions.

Despite the close agreement noted in Fig. 2.2 between the different parametric conditions at a fixed $\bar{\alpha}$, there are some noticeable quantitative dif-

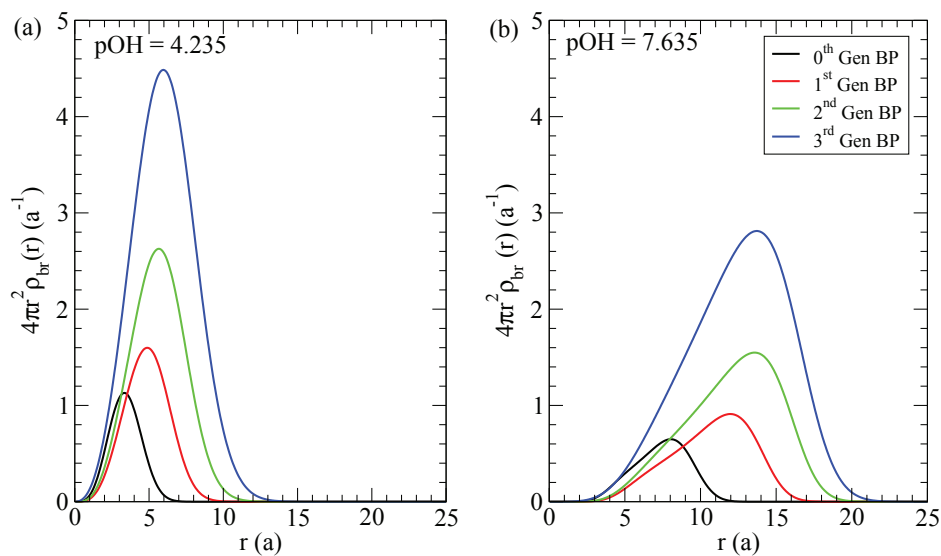


Figure 2.3: Density profiles for the branch points of the $g = 3$, $n = 5$, $\kappa^{-1} = 3a$ AE dendrimer with $pOH = 4.235$ (a) and $pOH = 7.635$ (b). Increasing the charge fraction results in a higher electrostatic force acting on the dendrimer monomers, forcing the shell density maxima to reside at further radial values.

ferences between the results at different parametric conditions. Explicitly, we observe that at a specified $\bar{\alpha}$, conditions corresponding to higher pOH have a slightly more “open” configuration relative to the situation with a lower pOH . For instance, when $\bar{\alpha} = 0.58$, we see that the AE dendrimer at conditions $pOH = 6.735$ and $\alpha_p = 0.70$ (dotted green line in Fig. 2.2) has a lower density near the center and correspondingly a larger value at the extremity in comparison to the case where $pOH = 6.185$ and $\alpha_p = 0.99$ (solid green line). Similar considerations are also seen to apply when $\bar{\alpha} = 0.29$. These results can be rationalized by considering the charge dissociation profile of the dendrimer which is displayed in Fig. 2.2b. Explicitly, we observe that conditions corresponding to larger pOH s have smaller α_p 's and correspondingly a lower dissociation of charge at the bulk conditions. However, since $\bar{\alpha}$ is maintained the same between pairs of conditions corresponding to higher and lower pOH , there has to necessarily be larger amounts of dissociated charge in the interior of the dendrimers at conditions corresponding to larger pOH . The more open configurations in such systems can then be rationalized as arising from the enhanced electrostatic repulsions accompanying the enhanced charge density in the interior of the dendrimer.

In sum, the above results indicate that charging the dendrimer results endows them with more open configurations and nonmonotonic density profiles due to the resulting electrostatic interactions. While the actual density and charge dissociation profiles are seen to exhibit an interplay between the pOH and α_p effects, the parameter $\bar{\alpha}$ is seen to serve as an excellent quantitative

measure to map the different parameters and characterize their influence upon the dendrimer configurations. These considerations point to the hypothesis that not only the influence of different parameters, but that the partially dissociatable nature of the dendrimer can be subsumed within the average dissociated charge fraction $\bar{\alpha}$. We test this hypothesis critically below by considering the behaviors of QE and QI models which do not allow for partial dissociation of the charges.

2.5.2 Comparing the charge fraction effects of AE, QE and QI Models

As noted in the introduction to this section, there are at least two parametric choices for comparing the behavior of AE dendrimers to the corresponding results for QE and QI dendrimers. In the strategy we termed approach (ii), the fraction of dissociatable groups of the QE and QI models α_P is chosen to match with the bulk value of the fraction of dissociatable groups for the AE model. For specified conditions (pOH and α_P) of the AE model, the latter can be deduced directly from Eq. 2.3.

In Fig. 2.4a and b we display a comparison of the density profiles and the corresponding charge fractions for the AE and QE dendrimers based on the above-discussed parametric choice. We observe that the density profiles of the QE dendrimers are significantly different compared to the AE dendrimers. Explicitly, the QE dendrimers are seen to possess a much more open configuration with a less dense core and an outer region which extends to significantly

further distances compared to the AE dendrimers. These differences can be rationalized by considering the charge density profiles displayed in Fig. 2.4b. It is seen that while the bulk dissociations in the AE and QE dendrimers match, the dissociated charge fractions in the interior of the dendrimer are strikingly different. Explicitly, since the AE dendrimers can modulate their charges, they exhibit less dissociation in the interior regions corresponding to the dense core. As a result, the AE dendrimers minimize the electrostatic interactions resulting from the core region and are thus able to maintain a compact configuration. In contrast, QE dendrimers exhibit a spatially homogeneous charge dissociation and cannot modulate their charge fractions in response to monomer densities. In such situations, compact configurations lead to significant electrostatic repulsions. To minimize such an effect, the QE dendrimers adopt a more open configuration which allows for a lower monomer density throughout its volume.

The above results provide a striking demonstration of the importance of including the partially dissociatable nature of the charged groups in predictions of the conformations of the weakly charged polyelectrolyte dendrimer. Indeed, the use of a quenched model for such systems would overestimate the “openness” of the dendrimer and its potential ability to accommodate drug and penetrant molecules. In contrast, we observe that a correct treatment of the dissociation indicates a much more compact configuration similar to the case of neutral dendrimers.

A more fundamental comparison between the AE and QE models can be

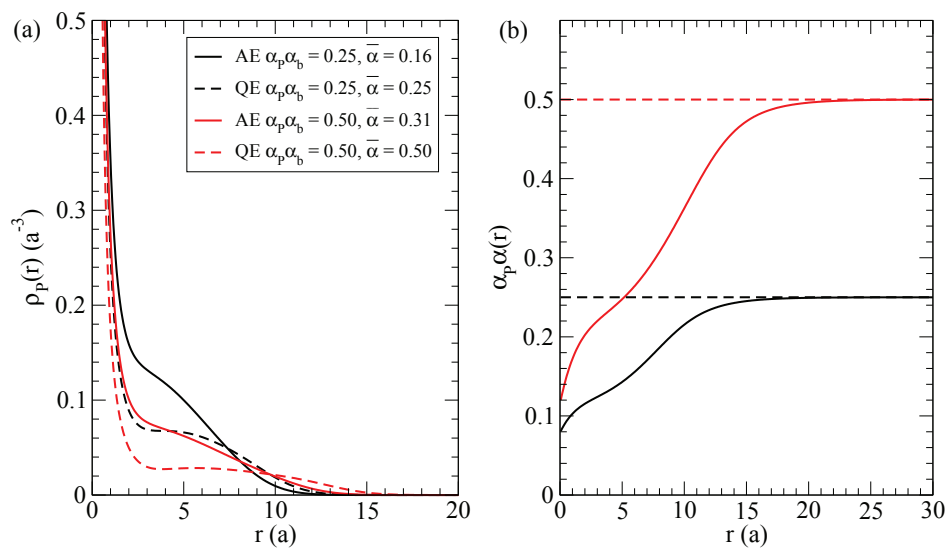


Figure 2.4: Monomer density (a) and $\alpha_P \alpha(r)$ dissociation (b) profiles for $g = 3$, $n = 5$, $\kappa^{-1} = 3a$ AE (solid lines) and QE (dashed lines) dendrimers with $\alpha_P \alpha(r)$ values of 0.25 (black) and 0.50 (red).

achieved by adopting the strategy termed in the introduction as approach (iii). In this situation, we ensure that the average charge fraction $\bar{\alpha}$ is maintained the same between the AE and QE models. Since this approach was also shown to be effective in mapping the trends occurring in the AE model at different parametric conditions, it is natural to enquire if such a mapping also transcends the specific model used. To implement this approach, we note that since the QE model exhibits no spatial variations in the charge dissociation, this requires us to fix the fraction of dissociatable groups α_P in the QE model to match with the $\bar{\alpha}$ for the AE model. However, since the latter depends explicitly on $\alpha(r)$ of the AE model, implementation of this approach requires as input the solution of the corresponding SCFT model for AE dendrimers.

Figure 2.5 compares the density profiles of AE, QE and QI models for two different parametric conditions of average charge fraction $\bar{\alpha}$. At low values of $\bar{\alpha}$, the density profiles of the different models are seen to be essentially identical and conform to the characteristics expected for neutral polymers. At higher values of the average charge, we observe that the QE and QI dendrimers exhibit a more open core conformation embodying the electrostatic repulsions which arise from the increased charge density within the dendrimer. More interestingly, it can be seen that at the same average charge $\bar{\alpha}$, the behaviors of the QE and QI dendrimers match semi-quantitatively with the results for the AE dendrimers. The latter observation confirms that while the dissociatable nature of the polymer proves important for determining the overall dissociated charge in the dendrimer $\bar{\alpha}$, the conformations of the dendrimer as reflected

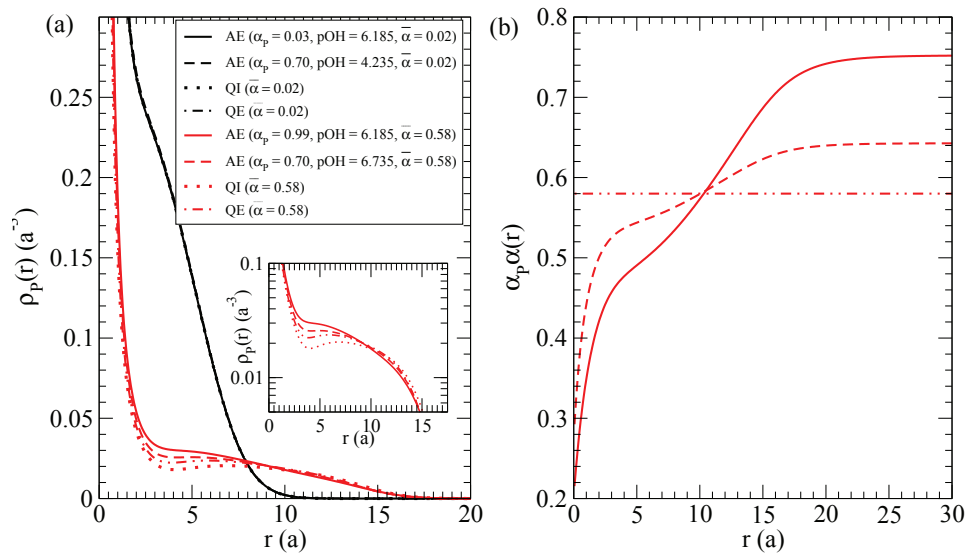


Figure 2.5: Monomer density (a) and charge dissociation (b) profiles for $g = 3$, $n = 5$, $\kappa^{-1} = 3a$ AE, QI, and QE dendrimers with charge fraction values of $\bar{\alpha} = 0.02$ (black) and 0.58 (green). The inset in (a) displays a logarithmic plot of the density profiles for the $\bar{\alpha} = 0.58$ dendrimers.

in the monomer density profiles appear to be slaved only to $\bar{\alpha}$ and not the dissociatable nature of the polyelectrolyte.

Despite the excellent agreement seen in Fig. 2.5 between the density profiles of AE, QE and QI dendrimers, we do note that minor quantitative differences exist. Explicitly, the QE and QI dendrimers are both seen to have lower density values near the center as compared to the AE dendrimers, with the QI dendrimers being the least dense near the center. At approximately $r = 10a$, the density profiles begin to cross, with the QI dendrimers having the highest density values at the periphery. These deviations are more clearly evident in the inset of Fig. 2.5 which displays the logarithm of the density values to emphasize the deviations in dendrimer conformations. These results point to a trend of open configurations, with the degree of openness increasing in the order of AE, QE and QI dendrimers. Such trends can be rationalized by considering the charge fractions displayed in Fig. 2.5b wherein it is seen that since the QE and QI dendrimers have a constant degree of charge dissociation ($\alpha(r) \rightarrow 1$), the QE dendrimer dissociation value near the center, α_P , is larger than that of the corresponding AE dendrimer, $\alpha_P\alpha(r)$. To minimize the resulting electrostatic interactions, the QE dendrimers adopt lower density values near the center than the corresponding AE dendrimers. Moreover, since counterion localization is not possible in the implicit ion model of QI dendrimers, for a given charge density the electrostatic repulsions are also higher for the QI dendrimer than for the AE or QE dendrimers. The latter explains the relatively more open configurations seen in the QI model.

In sum, the results presented in this section indicate significant differences in the conformations and density profiles exhibited by the models of strong and weak polyelectrolytes when compared at conditions corresponding to the same bulk charge fractions. Such results indicate the importance of an explicit inclusion of the dissociatable nature of the charged groups accompanying weak polyelectrolytes. However, when the models were compared at a specified total charge dissociated within the dendrimer, the density profiles were in excellent agreement with each other.

2.5.3 Effect of salt concentration on the conformation and sizes of dendrimers

In this section, we present results illustrating the effect of salt concentration upon the size and conformations of AE and QE dendrimer molecules. We quantify our results in terms of the size of the dendrimer, R , defined in terms of the second moment of the density profile:

$$R^2 = \frac{\int_0^\infty dr r^4 \rho_P(r)}{\int_0^\infty dr r^2 \rho_P(r)}. \quad (2.45)$$

In comparing the results of AE and QE dendrimers, we revert to the approach (ii) where the parameters are chosen to ensure that bulk charge dissociations match between the models.

In Figure 2.6 we display the effect of increasing salt concentration for QE ($\alpha_P = 0.53$) and AE ($\alpha_P \alpha_b = 0.53$) dendrimers, with the inset displaying a log-log representation of the same behavior. We observe strikingly different characteristics for the behaviors of QE and AE dendrimers. Explicitly, we

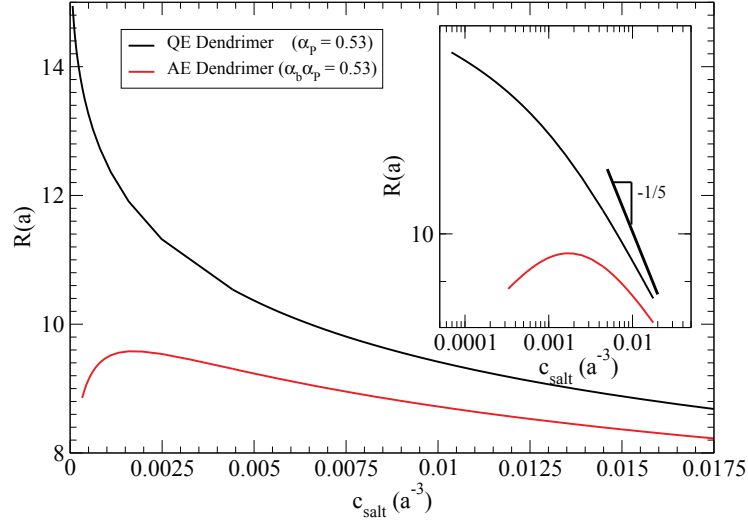


Figure 2.6: The effect of salt concentration on the size of $g = 3$, $n = 5$ AE ($\alpha_P \alpha_b = 0.53$) and QE ($\alpha_P = 0.53$) dendrimers.

see that the size of the dendrimer predicted by the QE model monotonically decreases with increasing salt concentration. In contrast, the results for the AE dendrimers are seen to exhibit a non-monotonic trend, where the size of the dendrimer initially increases with increasing salt concentration, but however, decreases with further increase in the salt concentrations. At large salt concentrations, both the QE and AE dendrimers are seen to exhibit a qualitatively similar behavior and scale in a manner consistent with the prediction (Eq. 2.17) of the high salt *osmotic regime* [177].

The above results for AE dendrimers are qualitatively similar to the nonmonotonic height variations seen in the context of weak polyelectrolyte brushes [121, 174], and arise as a result of an interplay between the presence of

the salt ions and the charge dissociation of the polymers. To see this explicitly, in Figure 2.7a we display the manner in which OH^- and salt ion profiles change with salt concentration. We see that as the salt concentration is increased, the density of the OH^- ions inside the dendrimer decreases, whereas, the concentration of the salt ions increases. As a result of the acid-base equilibrium condition (Eq. 2.4), we expect the fraction of monomers that dissociate to also correspondingly increase (see Fig. 2.7b). The latter leads to an enhancement of the electrostatic repulsions, which is responsible for the swelling of the dendrimer noted upon addition of salt. Further addition of salt leads to increased electrostatic screening, which diminishes the electrostatic interactions between charged monomers. The latter reduces the repulsive interactions between the polymer monomers and facilitates the compact conformations seen at larger salt concentrations. In contrast, for QE dendrimers, since the charge dissociation is a fixed quantity, increasing salt concentrations can only enhance the screening of the electrostatic interactions and hence there is no mechanism for salt-induced expansion in their sizes. Interestingly, as a result of the competing effects of the salt on the conformations of AE dendrimers, we observe that the quantitative influence of salt is much more mitigated in the context of AE dendrimers when compared to the QE dendrimers.

2.5.4 Scaling Behavior of AE, QE and QI Models

In this section, we compare the scaling behavior of the size of the dendrimers with the predictions outlined in section 2.3. Specifically, we consider

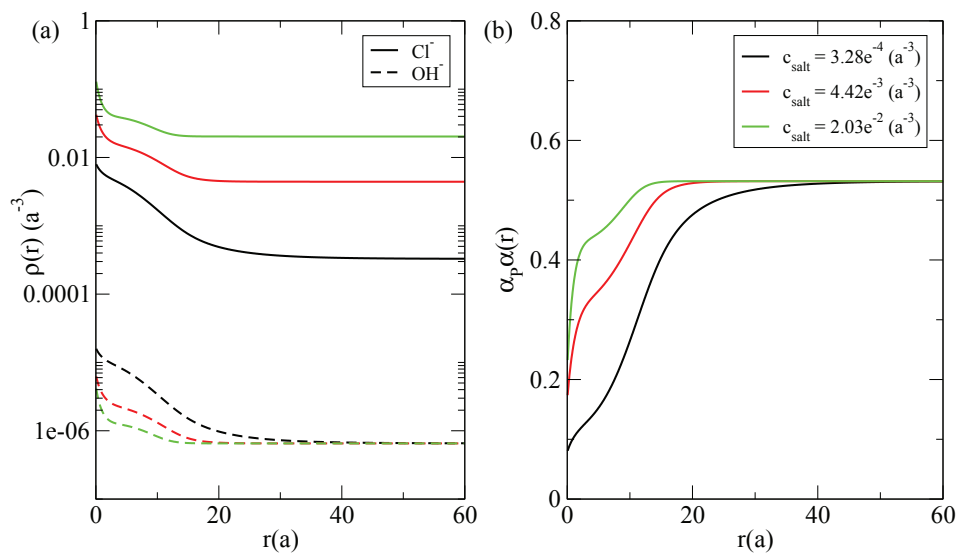


Figure 2.7: (a) The effect of salt concentration on the Cl^- (solid) and OH^- (dotted) density profiles inside AE dendrimers; (b) Charge dissociation profiles in the AE dendrimers as a function of salt concentrations.

the regimes of low and high salt concentrations and compare the scalings of the sizes of AE, QE and QI dendrimers with the charge dissociation and the generation number (quantified through the number of monomers $M(g)$, Eq. 2.1). We note that the results presented in the preceding sections have clearly demonstrated that the bulk charge fraction of the AE dendrimers does not serve as a good measure for comparing their conformational characteristics at different pOH and α_P conditions or to the results for QE dendrimers. In contrast, the average charge fraction $\bar{\alpha}$ in the AE dendrimer was shown to be a parameter which quantitatively captures the charge effects of AE dendrimers. Consequently, we use the parameter $\bar{\alpha}$ to probe the scaling behavior of AE dendrimers.

The effect of charge fraction and the generation numbers on the sizes of AE, QI, and QE dendrimers in the regimes corresponding to *high salt concentrations* are displayed in Figure 2.8a and b. We again observe that except for small differences, the radii of the QE and AE dendrimers, and that of the AE dendrimers at different parametric conditions are virtually identical when considered at the same $\bar{\alpha}$. Overall, we observe that for a given $\bar{\alpha}$ that the sizes of the dendrimers consistently follow the order $QI > QE > AE$, trends which are consistent with the behaviors seen and explained in the context of Fig. 2.5. At low values of average charge we see that the dendrimer size is only weakly dependent on the charge fraction. This result is consistent with the predictions of the scaling in the quasi-neutral regime (Eq. 2.19). As the charge fraction is increased, the size behavior of the dendrimer is seen to approach the *high salt*

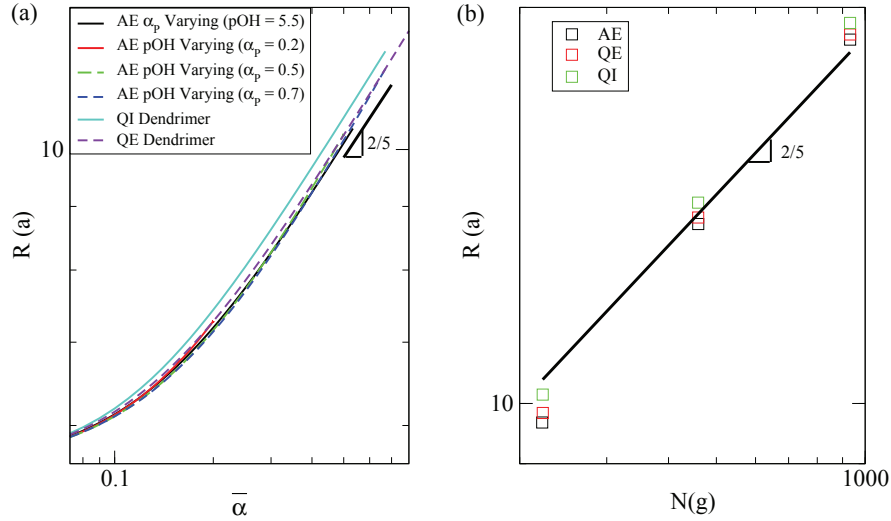


Figure 2.8: (a) Scaling of dendrimer size of the $g = 3$, $n = 5$, $\kappa^{-1} = 3a$ AE, QI, and QE dendrimers with respect to charge fraction. (b) Scaling of dendrimer size of the $\bar{\alpha} = 0.45$, $n = 5$, $\kappa^{-1} = 3a$ AE, QI, and QE dendrimers with respect to the number of monomers.

osmotic regime scaling (Eq. 2.17). The results displayed in Fig. 2.8b are also consistent with the results expected for such a regime (Eq. 2.17).

The fact that the above scaling behaviors indicate a correspondence to the osmotic regime is somewhat surprising in light of the fact that electroneutrality is not strictly satisfied for the parameters considered. To see this more explicitly, we consider a quantity which embodies the effective charge carried in the dendrimer and is defined as:

$$Q = 4\pi \int_0^R r^2 \rho_e(r) dr. \quad (2.46)$$

In Fig. 2.9a we display Q for different parametric conditions, wherein it is

seen that the dendrimers have a finite effective charge which increases with increasing $\bar{\alpha}$. To reconcile the results of Fig. 2.9a with the scaling observed in Fig. 2.8, we recall that the osmotic scaling regime invokes the mechanism of counterion localization to arrive at its predictions. Consequently, we consider a measure for the overall degree of counterion localization, ϕ_{resid} defined as:

$$\phi_{resid} = \frac{\int_0^R r^2 \rho_e(r) dr}{\int_0^\infty r^2 \alpha_P \alpha(r) \rho_P(r) dr}, \quad (2.47)$$

representing the uncompensated charge inside the dendrimer relative to the total charge carried by the dendrimer. Small values of ϕ_{resid} represent significant counterion localization effects and viceversa. In Fig. 2.9b we display $\phi_{resid}(\bar{\alpha})$ for the $\kappa^{-1} = 3a$ AE and QE dendrimers. As the charge fraction is increased we see that $\phi_{resid} \ll 1$ at large $\bar{\alpha}$. The latter trends are consistent with an increased degree of counterion localization at larger $\bar{\alpha}$ and rationalizes the osmotic regime scaling observed in Fig. 2.8.

Decreasing the salt concentration of the dendrimer solution is expected to increase the solution screening length, and render the electrostatic interactions more important. Figures 2.10a and b displays the effects of charge fraction and the generation numbers on the sizes of QI and QE dendrimers for solution screening lengths of $\kappa^{-1} = 3a, 25a$, and $50a$. Due to numerical constraints associated with the large simulation cells needed to accommodate the screening lengths for AE dendrimers, we could not perform such simulations for AE dendrimers. However, based on the results presented in Fig. 2.5, we expect that the trends exhibited by AE dendrimers to match almost quantitatively with the results for QE dendrimers (with the QE dendrimers being

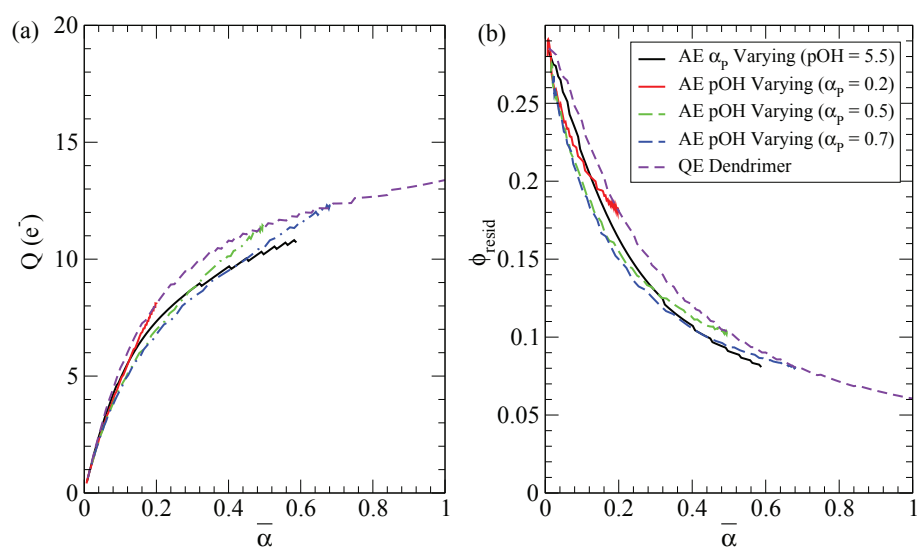


Figure 2.9: (a) Effective charge in the dendrimer Q ; and (b) The fraction of uncompensated charge (ϕ_{resid}) for the $g = 3$, $n = 5$, $\kappa^{-1} = 3a$ AE, QI, and QE dendrimers as a function of $\bar{\alpha}$.

slightly larger). In Fig. 2.10, the QI dendrimers are seen to be consistently larger than the corresponding QE dendrimers at a specified charge fraction. As κ^{-1} increases, we observe that the scaling dependencies (as a function of charge and the generation number) of the QI dendrimers start to approach the behavior predicted for the *polyelectrolyte regime* (Eq. 2.8). In contrast, the scaling dependence of the QE dendrimers with respect to $\bar{\alpha}$ is seen to approach the low salt concentration *osmotic regime* scaling (Eq. 2.14). However, the scaling dependence of QE dendrimers with respect to the number of monomers exhibits an exponent which is slightly larger than behavior expected in *osmotic regime* scaling (0.58 instead of 0.5).

The trends observed in Fig. 2.10 can be rationalized as follows: the osmotic scaling regime seen for the QE dendrimers is justified yet again by considering the function $\phi_{resid}(\bar{\alpha})$ displayed in Fig. 2.11. As κ^{-1} increases, we see that the absolute values of $\phi_{resid}(\bar{\alpha})$ of the QE dendrimers increase, which indicates higher amounts of unscreened charge. However, it is seen that at large values of $\bar{\alpha}$, $\phi_{resid}(\bar{\alpha})$ still falls to small values. Thus, even at large screening lengths we see that counterion localization is prevalent in the QE dendrimers and accounts for the low salt osmotic scaling regime seen in QE dendrimers. In contrast, due to the lack of a mechanism for counterion localization within the QI model, the scaling behavior of the sizes in the latter model is seen to approach the result predicted for the polyelectrolyte scaling regime (Eq. 2.8).

In summary, the above scaling trends indicate that counterion local-

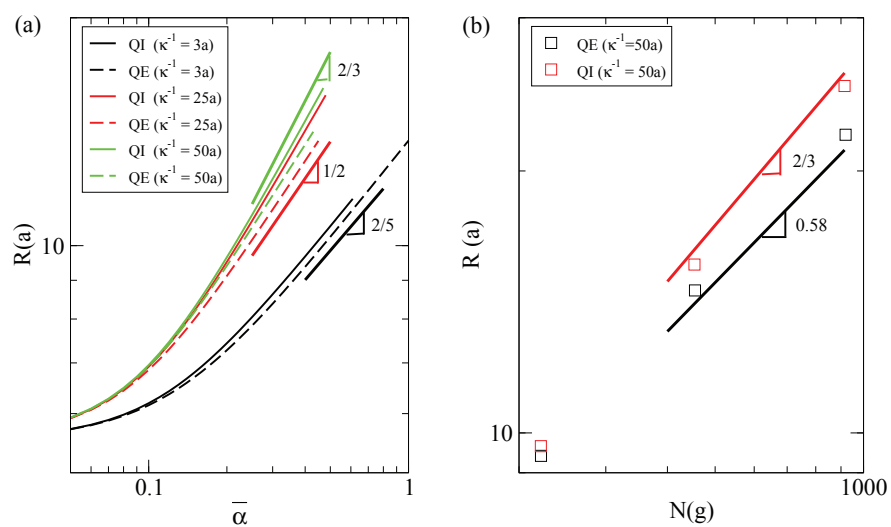


Figure 2.10: (a) Dendrimer size scaling of the $g = 3$, $n = 5$ QI and QE dendrimers with respect to charge fraction for $\kappa^{-1} = 3a$, $25a$, $50a$. (b) Dendrimer size scaling of the $\bar{\alpha} = 0.20$, $n = 5$, $\kappa^{-1} = 50a$ QI and QE dendrimers with respect to monomer number.

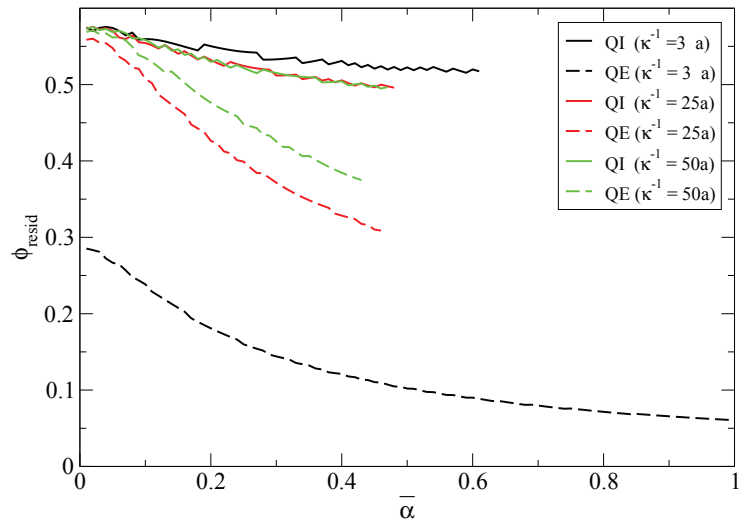


Figure 2.11: The fraction of uncompensated charge (ϕ_{resid}) for the $g = 3$, $n = 5$ QI and QE dendrimers as a function of $\bar{\alpha}$ for $\kappa^{-1} = 3a, 25a, 50a$. We see that increasing κ^{-1} results in higher values of ϕ_{resid} , with ϕ_{resid} decreasing with increasing $\bar{\alpha}$ for a fixed value of κ^{-1} .

ization plays a crucial role in influencing the conformational characteristics of polyelectrolyte dendrimers. Since such a phenomena is absent in the QI models, the results of the latter are seen to consistently overpredict the size of the dendrimer. Moreover, at low salt concentrations, the results of the QI model are seen to be qualitatively different from that of the QE model. Such observations highlight the importance of an explicit treatment of counterions in models for predicting the conformational features of polyelectrolyte dendrimer.

2.6 Strong Stretching Theory for Weak Polyelectrolyte Dendrimers

The numerical SCFT results presented in the preceding section indicated the importance of counterion localization and the dominance of the osmotic scaling regimes in the conformational characteristics of dendrimer molecules. In such a regime, the charge inside the dendrimer volume is assumed to be neutralized by localized counterions, and thus one can use the approximation of local electroneutrality [11, 95, 177]. Moreover, as a first approximation, the excluded volume interactions of the polymer monomers can be neglected in favor of accounting for the osmotic pressure of the localized counterions. Inspired by such trends, in this section, we propose a strong stretching theory (SST) based analytical approximation to determine the density of the free ions, polymer monomers, and the dissociation profiles for weakly charged polyelectrolytes.

The SST approximation was initially developed to describe the charac-

teristics of diblock copolymer phases [140] and polymer brushes grafted to flat surfaces [113, 193]. Subsequent work has extended the formalism to describe a number of situations, including, phase behavior of multiblock copolymers [128, 133], self-assembly of polymer-nanoparticle mixtures [138] etc. Pertinent to the present work, Pickett and coworkers developed a SST to describe conformations of neutral dendrimers [134, 194]. In the following, we use the results of Pickett and account for electrostatic interactions to extend the SST formalism to describe polyelectrolyte dendrimers.

The framework of SST begins with a representation in which the intermolecular interactions between the polymer chains are accounted by considering noninteracting polymer chains in a spatially varying chemical potential field. The latter, denoted $P(r)$ below, is determined self-consistently by imposing the constraint that the statistics of the polymer chains in the potential field match with the monomer density profile. In the limit when the grafted chains are strongly stretched, random walk fluctuations about their classical chain paths can be ignored and an analytical form for the self-consistent potential can be determined by employing an “equal time” constraint. The latter constitutes the main assumption underlying SST and results in a parabolic potential profile for planar polymer brush systems [113, 193]:

$$P(r) = \Lambda - k^2 r^2 \tag{2.48}$$

where Λ is a constant determined by application of the appropriate boundary condition and k is the spring constant of the polymer chain. In modifying the

above theory to neutral dendrimer molecules, Pickett showed that the form of the potential $P(r)$ remained intact [134], but found that the spring constant k depends on the parameters of the dendrimer molecule. Specifically, for the case of $g = 3$ considered in this chapter, $k = \arccos \left[1/3\sqrt{5 + \sqrt{13}} \right] / 4$.

To extend the above model to the case of polyelectrolyte dendrimers, we combine the above SST framework with the assumption of local electroneutrality (Eq. 2.11) to obtain expressions for the local dissociation and monomer density profiles [95]. When electroneutrality holds, the free energy of the system F is given as:

$$F = F_{stretch} + F_{polye}, \quad (2.49)$$

where $F_{stretch}$ is the stretching energy of the polymer chain and F_{polye} is the free energy associated with the charged species and is given by:

$$\begin{aligned} \frac{\beta F_{polye}(r)}{V} = & \alpha_P \rho_P(r) [\alpha(r) \ln \alpha(r) + (1 - \alpha(r)) \ln(1 - \alpha(r))] \\ & + \alpha(r) \xi_{PH^+}^o + (1 - \alpha(r)) \xi_P^o + \sum_i \rho_i [\ln \rho_i(r) v_i + \xi_i^o - 1] + \sum_i \rho_{i,b}, \end{aligned} \quad (2.50)$$

where V is the system volume and ξ_i^o is the standard chemical potential of the i^{th} species participating in the acid-base dissociation reaction. The first four terms in Eq. 2.50 account for the mixing entropy and chemical potential energy of the charged and uncharged monomers on the dendrimer molecule backbone. The fifth term accounts for the entropy of mixing and chemical potential energy of the i free species in the system. The osmotic pressure of free counterions in the bulk solution is in the last term on the right hand side of Eq. 2.50. Consistent with assumptions underlying the osmotic scaling

regime, we have neglected polymer excluded volume interactions. Inclusion of the latter into the analysis below is straightforward, but in such a case the final result cannot be expressed in an analytical form.

Minimization of the polyelectrolyte free energy components in Eq. 2.50 with respect to the monomer density ($\rho_P(r)$) yields the potential field that acts on the monomers. Upon setting it equal to the parabolic potential of Eq. 2.50 we obtain:

$$\alpha_P \ln[1 - \alpha(r)] = \Lambda' - k^2 r^2, \quad (2.51)$$

where Λ' is a constant. The latter can be determined by applying the boundary condition $\alpha(r = R) = \alpha_b$ which requires the dissociation profile to match with its bulk value at the edge of the dendrimer $r = R$. Using such a constraint, we obtain

$$\alpha(r) = 1 - (1 - \alpha_b) \exp\left(\frac{k^2 R^2 - k^2 r^2}{\alpha_P}\right). \quad (2.52)$$

The above equation for $\alpha(r)$ can be combined with the local electroneutrality approximation (Eq. 2.11) to obtain the local polymer density, $\rho_P(r)$ as

$$\rho_P(r) = \frac{\Phi_b}{\alpha_P} \left(\frac{\alpha_b}{1 - \alpha_b} \frac{1 - \alpha(r)}{\alpha^2(r)} - \frac{1 - \alpha_b}{\alpha_b} \frac{1}{1 - \alpha(r)} \right) \quad (2.53)$$

where Φ_b denotes the ionic strength of the bulk solution.

The main predictions of SST are embodied in Eqs. 2.52 and 2.53, which quantify the polymer monomer density and dissociation profiles. The dendrimer monomer density profiles from SST and SCFT approaches are compared in Figure 2.12(a). At low values of charge fraction (black lines), the SST density profiles are seen to have very high density values near the center

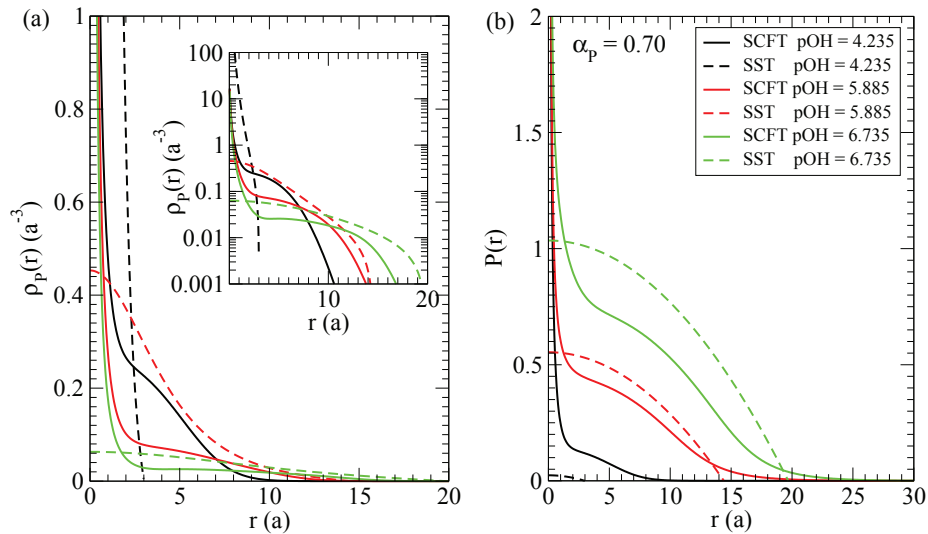


Figure 2.12: (a) Comparison of the AE dendrimer monomer density profiles from SST and the SCFT simulations. (b) Comparison of the SST parabolic potential profiles with the results of the SCFT simulations for $g = 3$, $n = 5$, $\kappa^{-1} = 3a$ AE dendrimers.

(see inset) but lack the decaying tail seen in the SCFT results. As the charge fraction (pOH) is increased, we observe that the SST density profiles achieve more open configurations and begins to more accurately capture the tail features of the SCFT density profiles. However, even at high charge fractions, we observe that the SST profiles lack the high densities near the dendrimer center seen in the SCFT profiles.

The comparisons between SST and SCFT density profiles can be better understood through an examination of the corresponding potential profiles which are displayed in Fig. 2.12b. In general we notice that the SCFT profiles exhibit a singularity-like behavior near the center. The latter can be rational-

ized by considering the distribution of the 0^{th} generation branch points, which were displayed in Fig. 2.3 (black lines). The narrow distribution of the 0^{th} branch point indicates a high degree of stretching near the center and results in dead zones for the branch and terminal points (see Fig. 2.3b) [4, 140]. The SST model in contrast assumes that the end point distribution is positive and non-zero for $0 < r < R$ and hence cannot capture such features, and explains the discrepancies between SST and SCFT results for the density profiles near the core.²

At low charge fraction (black lines) we observe that the SST potential is much smaller than the corresponding SCFT potential. In this case, the low concentration of charged monomers results in a very small osmotic energy contribution to the SST potential. However, in contrast, the SCFT potential is almost entirely accounted by the monomer-monomer excluded volume interactions which were neglected in our SST framework. Not surprisingly, the SST predictions are in disagreement with the SCFT results. However, as the charge fraction is increased we witness that the potential profile predicted by SST to match very well (beyond the region of the center of the dendrimer) with the SCFT predictions. Small quantitative discrepancies do exist and can

²Under these conditions, a more appropriate model for the density profiles near the center is the Daoud and Cotton model for a spherical brush, which assumes that all brush free ends are equally far from the grafting surface. This accommodates the more segregated branch and terminal point distributions in Fig. 2.3b. For instance, Wijmans and Zhulina [173] used a hybrid approach for spherical brushes, combining the scaling model for spherical brushes proposed by Daoud and Cotton [25] near the curved surface and SST at larger radial values. This approach allowed them to achieve more accurate analytical predictions for curved polymer brush density profiles.

be attributed to the assumption of local electroneutrality condition and the neglect of polymer monomer excluded volume interactions. Notwithstanding such differences, the analytical formulae embodied in Eqs. 2.52 and 2.53 are seen to provide an excellent quantitative representation of the conformational characteristics of weak polyelectrolyte dendrimers.

2.7 Summary

In this chapter, we presented results for the behavior of quenched and annealed dendrimers under varying charge fraction, pOH , and salt conditions. Our results indicated that counterion localization plays an important role in influencing the conformations of polyelectrolyte dendrimers and thereby reinforced the importance of treating the free ions explicitly. For the annealed dendrimers we observed that the charge fraction of the dendrimer was always less than the fraction of dissociable monomers. Moreover, the annealed dendrimers were able to modulate their charges in response to the density of polymer monomers, counterions and salt ions. Such features were not capture-able in the quenched model of dendrimers and led to significant discrepancies between the predictions of quenched and annealed model of the dendrimers. Our results also indicated that the average charge fraction $\bar{\alpha}$ serves as a useful parameter to map the effects of different conditions and models onto each other.

We also presented comparisons to the scaling results proposed to explain the behavior of polyelectrolyte dendrimers. Inspired by the trends indi-

cated by our results, we developed a strong segregation theory model which provided analytical expressions for the density profiles and the dissociation characteristics of the annealed dendrimers. The predictions of the latter was shown to be in very good agreement with the numerical SCFT calculations.

Chapter 3

Encapsulation of Weakly Acidic Molecules by Polyelectrolyte Dendrimers

3.1 Introduction

Approximately forty percent of newly developed pharmaceuticals prove to be ineffective at a therapeutical level because of poor water solubility and low membrane permeabilities [145]. This has motivated the pursuit of a number of approaches, many of which involves the use of polymeric materials to increase the bioavailability of hydrophobic drugs [88]. In this context, some researchers have proposed the use of dendrimers, which are hyperbranched tree-like polymer molecules, to encapsulate and deliver hydrophobic drug molecules [20, 23, 67, 68, 123, 145]. Synthesis techniques of dendrimer molecules have advanced to a sufficient degree to allow the formulation of monodisperse molecules with precise control over their charge, flexibility, and solubility [3, 23, 162]. Control over these characteristics have allowed researchers to create uni-micellar water-soluble dendrimers that have interiors favorable for hosting hydrophobic molecules [20, 23, 67, 68, 123, 145]. Subsequent experimental researches have demonstrated the ability of such dendrimers to successfully encapsulate non-steroidal anti-inflammatory drugs (NSAIDs), which typically exhibit low water solubility [22].

A number of mechanisms have been proposed to explain the efficacy of dendrimers to solubilize and encapsulate drug molecules. These have included hydrophobic interactions between the non-polar portions of drug molecules and dendrimer interiors [22, 55, 70, 115, 122], electrostatic attractions between the charged groups of the dendrimer and the drug molecules [5, 21, 130, 184], and hydrogen bonding interactions between drug molecules and the amine/amide hydrogen atoms of the dendrimer monomers [22, 130, 148]. For instance, recent studies by Kannaiyan and Imae examined the effects of hydrophobic interactions between hybrid poly(propyleneimine) (PPI)-poly(amidoamine) (PAMAM) dendrimers and pyrene molecules [55]. Their study found that the aqueous solubility of hydrophobic pyrene molecules increases when hybrid dendrimers (hydrophobic PPI core, with hydrophilic PAMAM shell) were used as opposed to either the pure PPI or PAMAM species. Beezer and co-workers found that hydroxyl terminated PAMAM dendrimers formed stable complexes with benzoic acid at pH values above 7, where the inner tertiary amine groups have a high probability of being protonated and the acid groups have a high probability of being deprotonated [5]. They attributed the complex formation to ion-pairing between the carboxylic acid groups and charged dendrimer tertiary amine groups. Cheng and Xu examined the effect of PAMAM dendrimers on the solubility of NSAIDs [22]. Their studies found that increasing both the generation number and concentration of dendrimers increased NSAID solubility, which was hypothesized to occur through electrostatic and hydrogen bonding interactions. They also observed an increase in ketoprofen solubil-

ity as the solution pH was increased from pH 3 to pH 6 and speculated that the increase in encapsulation was due to electrostatic attraction between the charged acidic ibuprofen molecules and the primary amine terminal groups. From the preceding discussion, it is clear that a number of mechanisms manifest in influencing the solubilization of drugs by dendrimers. However, the relative roles and importance of the different mechanisms have not been clarified in a systematic manner.

There have also been some theoretical studies on the complexation between dendrimers and host molecules [17, 29, 50, 70, 100, 112, 144, 148, 153, 154]. The role of hydrogen bond formation in NSAID-dendrimer complexation was examined through atomistic molecular dynamics (MD) simulations by Tanis and Karatasos [148]. Their studies revealed that hydrogen bonding occurs between hydrogen atoms of the primary and tertiary amine groups and oxygen groups of the hydroxyl and carbonyl groups of the ibuprofen molecules. Although their study shed important insights on the role of hydrogen bonding formation for their system, it did not account for electrostatic interactions between protonated amine groups and deprotonated ibuprofen molecules. Motivated by NMR studies of dendrimer-drug complexes studied by Zhao *et al.* [189], Maiti and coworkers recently used MD to characterize the potentials of mean force (PMF) between free and bound Salicylic acid (Sal), L-Alanine (Ala), Phenylbutazone (Pbz) and Primidone (Prim) drug molecules in the presence of unprotonated ($pH \sim 10$) and partially protonated ($pH \sim 7$) PAMAM dendrimers [100]. They witnessed a lower free energy barrier for escape

of encapsulated drugs when the drugs were more soluble. Furthermore, they witnessed large increases in the free energy barriers for the negatively charged Pbz and Sal drugs when the dendrimers became protonated. In a different line of work, Sun and Crooks used a mean field approximation and a surface adsorption model to predict the binding of protons and metal ions to dendrimers. Their model approximated the dendrimer binding sites as concentrically charged shells and did not allow for conformational changes that have been witnessed under varying solution conditions [144].

Although some computational studies do exist that shed light on the complexation between dendrimers and molecules [17, 29, 50, 70, 100, 112, 144, 148, 153, 154], to our knowledge there are no existing studies that simultaneously incorporate the effects of dendrimer conformations and charge dissociation (for both weakly acidic molecules and weakly basic dendrimer groups) on the dendrimer-molecule complexation. In the previous chapter, we developed polymer self-consistent field theory (SCFT) [35] model for charged dendrimer molecules and used it to enumerate the conformational characteristics of dendrimer molecules [86]. Using such a framework, we showed that even the charge carried by a weakly basic dendrimer could not be known *a priori* for a given set of solution and architectural parameters. Rather, the latter was determined by an interplay between the electrostatic localization of free ions within the dendrimer molecule and the osmotic energy costs of such localization. In the present chapter we extend our previous model to include the presence of weakly acidic drug molecules in solution and use such a represen-

tation to study the solubilization of the drug molecules inside the dendrimer. In order to gain insight into the physics behind the various mechanisms underlying complexation, we individually examine the effects of excluded volume interactions, electrostatic attractions, and enthalpic interactions (used as a means to model the hydrophobic nature and hydrogen-bonding interactions) between the dendrimer monomers and the drug molecules. We then combine these different interactions and explore the parameter space in order to gain insights into the synergistic effects of the different interactions upon the overall encapsulation. The parameters that we choose to investigate include the dendrimer generation numbers, drug molecule sizes, solution pOH , solution Bjerrum length, the strength of enthalpic interactions between the dendrimer monomers and drug molecules, and the drug hydrophobicity.

The rest of the chapter is arranged as follows. In Section 3.2 we discuss the associated terminology, our SCFT model, and the associated numerical details. In Sec. 3.3 we display results for the encapsulation of drug particles by charged dendrimers when only excluded volume interactions are incorporated (3.3.1); both electrostatic and excluded volume interactions are incorporated (3.3.2); both enthalpic and excluded volume interactions are incorporated (3.3.3); and when electrostatic, enthalpic, and excluded volume interactions are all simultaneously incorporated (3.3.4). In Section 3.4 we conclude with a summary of our results.

3.2 Self-Consistent Field Theory Method

The focus of this chapter is to characterize the complexation phenomena between acidic drug molecules and charged annealed polyelectrolyte (PE) dendrimers. In this section we detail the model and the SCFT framework we used to study the equilibrium conformations of the drug-dendrimer complexes.

In our framework, we consider a spherically symmetric system of volume V that contains a single weakly basic dendrimer molecule fixed at the center of the cell and in the presence of solvent molecules (denoted as S), H^+ and OH^- ions, monovalent salt ions (which will be denoted without loss of generality as Na^+ and Cl^-), and weakly acidic drug molecules denoted as D . The main ingredients of our model are the following:

(i) We adopt a flexible, continuous Gaussian chain model in order to model the dendrimer spacers. Such a model has also been used in prior studies to examine the phase behavior of dendritic block copolymers [41] and scaling behaviors of neutral and charged dendrimer molecules [86, 177]. In reality, the flexibility of the dendrimer spacer units are determined by the monomeric unit underlying the dendrimer architecture [162]. There have also been some simulation studies which have examined the effects of rigidity on dendrimer conformations. For instance, Carbone *et al.* have shown using coarse-grained simulations that more rigid polyphenylene dendrimers display significantly decreased backfolding of the dendrimer arms as compared to that observed for more flexible PAMAM dendrimers [14, 15]. Blaack and coworkers [48] observed that the stiffer dendrimer molecules resulted in more shell-like conformations,

while the softer bonded dendrimers resulted in a more homogeneous monomer distribution. However, to maintain simplicity, in this work we use the continuous Gaussian chain model which does not accommodate the influence of spacer rigidity.

(ii) We assume that the hydrophobic nature of the drug and hydrogen bonding interactions between the drug and polymer monomers can both be represented by simple forms of enthalpic interactions. Specifically, we model the hydrophobicity of the drug through a local pairwise energy contribution which depends on the product of the local densities of the solvent and drug. In a similar manner, the drug and dendrimer hydrogen bonding interactions are modeled through local pairwise energy which depends on the product of the densities of the drug and dendrimers. To this objective, we employ a Flory-Huggins χ -parameter to quantify the strengths of the enthalpic interactions between the drug, polymer, and solvent molecules [33]. The parameter χ_{ij} can be considered as the average enthalpy of mixing between the i^{th} and j^{th} species. For our work, we set $\chi_{PD} \leq 0$ and $\chi_{DS} \geq 0$ to model the favorable interactions between the dendrimer-drug species and the unfavorable (hydrophobic) interactions between the drug and solvent molecules.

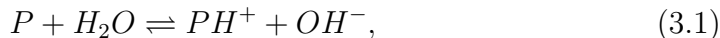
(iii) The electrostatic interactions arising between the dissociated charges are modeled using a classical Coulombic potential with a spatially homogeneous dielectric constant, ϵ .

(iv) We adopt a point-like representation for the drug (see Section 3.2.2 for a discussion of the validity of this assumption), solvent, and ion molecules.

We retain the volume of the drug molecule, v_D , as a parameter probed, but assume that the volumes of each polymer monomer and solvent molecule are identical and equals ρ_0^{-1} . We neglect the volume occupied by the ions.

(v) Fluctuations in the local sum of polymer, solvent, and drug densities from the average bulk density, ρ_0 , are minimized by the inclusion of a harmonic compressibility penalty [13, 119, 180]. Since the drug molecule densities are dilute, we assume that a harmonic compressibility penalty is sufficient for modeling the overall incompressibility of the system and excluded volume interactions between the drug molecules. Thus we do not include any non-quadratic (non-ideal) density functional theory (DFT) steric interaction terms for the interactions of drug molecules [155].

In our model, we assume that every $(1/\alpha_P)^{th}$ monomer P of the dendrimer portion of the molecule *is capable* of undergoing charge dissociation through an equilibrium reaction of the form



a phenomena which is governed by the law of mass action:

$$K_{b,P} = \frac{[PH^+][OH^-]}{[P]} = \frac{\alpha_b \rho_0 \varphi_{OH^-,b}}{1 - \alpha_b}, \quad (3.2)$$

where $K_{b,P}$ denotes the equilibrium constant of the dissociation reaction (Eq. 3.1), $[A]$ ($A \equiv P, PH^+, OH^-$) refers to the concentration in mol/L of species A , α_b is the fraction of polymer monomers in bulk solution that are charged, and $\varphi_{OH^-,b}$ is the bulk volume fraction of OH^- ions. The equilibrium constant

$K_{b,P}$ is proportional to $\exp(-\beta\Delta G^o)$, where $\Delta G^o = \xi_{OH^-}^o + \xi_{PH^+}^o - \xi_P^o$ is the free energy of the reaction and ξ_i^o are the standard chemical potentials of the different species involved in the dissociation reaction. We note that the framework of our model for the dendrimers shares many similarities to recent mean field studies of weak polyelectrolyte brushes by Szeifer *et al.* [121] and Won and coworkers [174]. We model the dissociation of the acidic drug molecules, D , also as an equilibrium reaction of the form



where

$$K_a = \frac{[D^-][H^+]}{[DH]} = \frac{\alpha_{D,b}\rho_0\varphi_{H^+,b}}{1 - \alpha_{D,b}}, \quad (3.4)$$

$\alpha_{D,b}$ is the fraction of drug molecules in bulk solution that are charged, $\varphi_{H^+,b}$ is the bulk volume fraction of H^+ ions, and the equilibrium constant, $K_{a,D}$, is proportional to $\exp(-\beta(\xi_{D^-}^o + \xi_{H^+}^o - \xi_{DH}^o))$.

We employ a semigrand canonical framework to describe the equilibrium characteristics of the dendrimer, salt, drug, solvent, and ion mixture and solve it within a mean field approximation to deduce the density profiles of the different components [35]. In this framework, the free energy \mathcal{F} can be identified as:

$$\mathcal{F} = \mathcal{F}_{conf} + \mathcal{F}_{int} + \mathcal{F}_{comp} + \mathcal{F}_{mix} + \mathcal{F}_{chem} + \mathcal{F}_{elec}. \quad (3.5)$$

(i) The first contribution, \mathcal{F}_{conf} , accounts for the conformational entropy of the PE dendrimer, which can be written as:

$$\beta\mathcal{F}_{conf} = \ln Q_P + \rho_0 \int d\mathbf{r} w_P(\mathbf{r}) \varphi_P(\mathbf{r}), \quad (3.6)$$

where $\beta = 1/k_B T$, Q_P is the partition function for a single noninteracting grafted dendrimer molecule subject to the external field $w_P(\mathbf{r})$ and is given by Eq. 2.37. $\varphi_P(\mathbf{r})$ denotes the volume fraction of the dendrimer chain monomers (in general, we use $\varphi_i(\mathbf{r})$ to denote the concentration of the i^{th} species).

(ii) The term \mathcal{F}_{int} of Eq. 3.5 accounts for the pairwise steric interactions between the monomers of the dendrimer, drug molecules, and solvent molecules and is given by:

$$\beta\mathcal{F}_{int} = \rho_0 \int d\mathbf{r} \sum_{i \neq j} \chi_{ij} \varphi_i(\mathbf{r}) \varphi_j(\mathbf{r}), \quad (3.7)$$

where χ_{ij} is the Flory-Huggins interaction parameter between the i^{th} and j^{th} species.

(iii) The term \mathcal{F}_{comp} of Eq. 3.5 accounts for the fluctuations in overall average density from the bulk density and is given as

$$\beta\mathcal{F}_{comp} = \frac{\zeta\rho_0}{2} \int d\mathbf{r} [\varphi_P(\mathbf{r}) + \varphi_S(\mathbf{r}) + \varphi_D(\mathbf{r}) - 1]^2, \quad (3.8)$$

where ζ is a dimensionless parameter that quantifies the magnitude of the harmonic energy penalty for local density fluctuations away from the average bulk density, ρ_0 . The above contribution, \mathcal{F}_{comp} , is used to replace a delta function incompressibility constraint, which constrains the average local density to equal ρ_0 . We note that the above model assures incompressibility in the limit $\zeta \rightarrow \infty$. However, in order to reduce the numerical difficulties associated with the high densities of our dendrimers near their cores, we include this energetic term with a large but finite ζ , which, while not capable of enforcing perfect incompressibility, still proves effective in constraining the total average density to be

close to ρ_0 . We note that approaches similar to Eq. 3.8 have previously been used in the case of confined polymer melts [180], spherical polymer brushes [13], and triblock copolymers [119] to enforce the incompressibility constraint.

(iv) The entropies of mixing of free ions are accounted in the fourth term, \mathcal{F}_{mix} and is given as:

$$\begin{aligned} \beta\mathcal{F}_{mix} = \rho_0 \int d\mathbf{r} \left\{ \sum_i \varphi_i(\mathbf{r}) [\ln \varphi_i(\mathbf{r}) - 1 + \beta\xi_i^o] + \varphi_S(\mathbf{r}) [\ln \varphi_S(\mathbf{r}) - 1 + \beta\xi_S^o] \right. \\ \left. + (1 - \alpha_D(\mathbf{r})) \varphi_D(\mathbf{r}) [\ln (1 - \alpha_D(\mathbf{r})) \varphi_D(\mathbf{r}) - 1 + \beta\xi_{DH}^o] + \right. \\ \left. \alpha_D(\mathbf{r}) \varphi_D(\mathbf{r}) [\ln \alpha_D(\mathbf{r}) \varphi_D(\mathbf{r}) - 1 + \beta\xi_{D-}^o] \right\}, \end{aligned} \quad (3.9)$$

where $i = OH^-, H^+, Cl^-, Na^+$, $\alpha_D(\mathbf{r})$ is the local probability of a drug molecule being in the charged state, and ξ_j^o is the standard chemical potential of the j^{th} species.

(v) The fifth term, \mathcal{F}_{chem} , accounts for the free energy contribution from the dendrimer acid-base equilibrium governed by Eq. 3.2. We use a notation in which the local fraction of dissociated dendrimer polymer monomers and uncharged monomers are denoted as $\alpha(\mathbf{r})$ and $1 - \alpha(\mathbf{r})$ respectively. This energy contribution, \mathcal{F}_{chem} , is then given as:

$$\begin{aligned} \beta\mathcal{F}_{chem} = \rho_0 \int d\mathbf{r} [\alpha_P \varphi_P(\mathbf{r}) [\alpha(\mathbf{r}) (\ln(\alpha(\mathbf{r})) + \beta\xi_{PH^+}^o) \\ + (1 - \alpha(\mathbf{r})) (\ln(1 - \alpha(\mathbf{r})) + \beta\xi_P^o)]]. \end{aligned} \quad (3.10)$$

(vi) The electrostatic interactions between the charged entities are accounted within \mathcal{F}_{elec} :

$$\beta\mathcal{F}_{elec} = \int d\mathbf{r} \left[\rho_0 \varphi_e(\mathbf{r}) \Phi(\mathbf{r}) - \frac{1}{8\pi l_B} |\nabla \Phi|^2 \right], \quad (3.11)$$

where $\Phi(r)$ is the electrostatic potential (normalized by $e/k_B T$) conjugate to the charge density field, $\rho_0 \varphi_e(\mathbf{r})$. The above expression is consistent with electrostatic interactions modeled through a classical Coulombic potential with a spatially homogeneous dielectric constant ϵ . We note that the inhomogeneities in the density profiles of the ions, ionized drug molecules, and polymer monomers are in principal better accounted through a dielectric constant which varies with composition [121, 168]. However, such a model adds to the numerical and parametric complexity, and hence we adopt the simpler model of a spatially uniform dielectric constant.

In order to solve the statistical mechanics of the above model, we employ a mean-field approximation and determine the equilibrium fields, $\varphi_P(\mathbf{r})$, $\varphi_i(\mathbf{r})$ [$i = Na^+, Cl^-, H^+, OH^-$], $\varphi_D(\mathbf{r})$, $\varphi_S(\mathbf{r})$, $w_P(\mathbf{r})$, $w_D(\mathbf{r})$, $w_S(\mathbf{r})$, $\alpha_P(r)$, $\alpha_D(r)$, and $\Phi(\mathbf{r})$, as those which minimize $\beta\mathcal{F}/\rho_0$. Such a procedure yields the following set of self-consistent equations [35]:

$$w_P(\mathbf{r}) = \chi_{PD}\varphi_D(\mathbf{r}) + \chi_{PS}\varphi_S(\mathbf{r}) + \zeta [\varphi_P(\mathbf{r}) + \varphi_D(\mathbf{r}) + \varphi_S(\mathbf{r}) - 1] + \alpha_P \ln \left[\frac{1 - \alpha(r)}{1 - \alpha_b} \right] - \alpha_P, \quad (3.12)$$

$$w_D(\mathbf{r}) = \chi_{PD}\varphi_P(\mathbf{r}) + \chi_{DS}\varphi_S(\mathbf{r}) + \zeta [\varphi_P(\mathbf{r}) + \varphi_D(\mathbf{r}) + \varphi_S(\mathbf{r}) - 1] - \ln [\varphi_{D,b} (\alpha_{D,b} \exp(-z_{D-}\Phi(\mathbf{r})))], \quad (3.13)$$

$$w_S(\mathbf{r}) = \chi_{PS}\varphi_P(\mathbf{r}) + \chi_{DS}\varphi_D(\mathbf{r}) + \zeta [\varphi_P(\mathbf{r}) + \varphi_D(\mathbf{r}) + \varphi_S(\mathbf{r}) - 1], \quad (3.14)$$

$$-\frac{1}{4\pi l_B} \nabla^2 \Phi(\mathbf{r}) = \rho_0 \left[\sum_{ions} z_i \varphi_i(\mathbf{r}) \right. \quad (3.15)$$

$$\left. + z_{PH} + \alpha_P \alpha(r) \varphi_P(\mathbf{r}) + z_{D-} \alpha_D(r) \varphi_D(\mathbf{r}) \right],$$

$$\alpha_D(r) = \frac{1}{1 + \rho_0 \varphi_{H^+}(r) / K_{a,D}}, \quad (3.16)$$

and

$$\alpha(r) = \frac{1}{1 + \rho_0 \varphi_{OH^-}(r)/K_{b,P}}. \quad (3.17)$$

In the above,

$$\varphi_P(\mathbf{r}) = \frac{\eta_P}{Q_P} \sum_{i=0}^g \Omega_i \int_{s_i}^{s_{i+1}} ds q(\mathbf{r}, s) q^\dagger(\mathbf{r}, s), \quad (3.18)$$

$$\varphi_D(\mathbf{r}) = \eta_D \exp[-\beta \xi_{DH}^o - \beta \xi_{D-}^o] \exp[-w_D(\mathbf{r})], \quad (3.19)$$

and

$$\varphi_i(\mathbf{r}) = \eta_i \exp[-\beta \xi_i^o] \exp[-z_i \Phi(\mathbf{r})], \quad (3.20)$$

where z_j denotes the charge valency of the j th species, $\eta_j = v_j \rho_0$, with v_j being the volume of a molecule or the j^{th} type, and Ω_i is the number of branches in the i^{th} generation. The function $q(\mathbf{r}, s)$ represents the probability of finding the s^{th} monomer of the dendrimer at position \mathbf{r} with the condition that the center of dendrimer is fixed at $r = 0$. $q^+(\mathbf{r}, s)$ denotes the complementary probability of finding the $N - s^{th}$ monomer at position \mathbf{r} independent of the location of the monomer at the outer extremity. See Sec. 2.4.1 for a detailed discussion of $q(\mathbf{r}, s)$ and $q^+(\mathbf{r}, s)$. The electrostatic potential, $\Phi(\mathbf{r})$, is solved using the resulting Poisson-Boltzmann (PB) equation (Eq. 3.15). We refer the reader to Sec. 2.4.1 for the corresponding PB equation boundary conditions.

3.2.1 Potential of Mean Force for Drug Insertion

Recent MD simulations of Maiti and coworkers used the potential of mean-force (PMF) as a quantitative measure to characterize the propensity for complexation between dendrimers and drug molecules [100]. PMFs characterize the “local” free energy of insertion of the drug and was obtained through

the average force experienced by the drug at a given location, when sampled over the configurations of other molecules. Although we do not perform such rigorous PMF calculations in our studies, we note that at dilute concentrations of the drug, the density profiles of the drug, $\varphi_D(r)$, is expected to be related to the potential of mean-force $w_{PMF}(r)$ as

$$w_{PMF}(r) \simeq -k_B T \ln [\varphi_D(r)]. \quad (3.21)$$

Based on this perspective, in discussing our results for the density profiles of the drug molecules, we recast them into a PMF (denoted as $w_D(r)$) and discuss the qualitative features exhibited by such a measure.

3.2.2 Justification of the Model of a “Point-Like” Drug Molecule

Typically the sizes of the drug molecules are of the order of the size of dendrimer spacers. For instance, the molecular weight of ibuprofen is 206 while the molecular weight of a PAMAM dendrimer spacer is 83. Thus, an appropriate model for the drug particles would account for the finite size of the drug particles. In our preliminary studies, we considered two potential models for the drug molecules: (i) A point-like representation of the drug, albeit with a finite drug volume, v_D ; and (ii) A model in which the drug molecule is modeled as a sphere of radius R_D (and an equivalent volume, v_D). For a spherically symmetric system, the density values for the sphere model cannot be calculated when $r < R_D$, and hence we used the approximation that $\varphi_D(r) = \varphi_D(R_D)$ for $0 < r < R_D$.

Fig. 3.1 displays a comparison of the volume fraction profiles for the two models, where $R_D = 1.0a$ and $R_D = 2.0a$ drug molecules are in the presence of $G3$ dendrimers in a solution of $pOH = 5.621$ and $\chi_{PD} = -\chi_{DS} = -2.0$. We see that gradients in the drug molecule volume fractions are steepest near the dendrimer center ($r \leq R_D$) and display a sharp decline for $r > R_D$. When we compare the results of the two models, we see disagreement between the $\varphi_D(r)$ profiles near the center, arising from our approximation for $r < R_D$. However, there is seen to be excellent agreement between the density profiles predicted by the two models for $r > R_D$ (see insert of Fig. 3.1). We also compared the results of the above models for other parameters, and confirmed that similar agreement holds for a number of other parameters. Based on such comparisons, in order to reduce the computational costs, we adopted a point-like model for our drug molecules, and the results presented in Section 3.3 correspond to such a representation.

3.2.3 Numerical Scheme

We employed a Crank-Nicholson finite difference scheme [35, 137] to solve the partial differential equations for $q(r, s)$ and $q^\dagger(r, s)$. We non-dimensionalized our grid by $R_g = \sqrt{Na^2/6}$, where $N = (g + 1)n$ is the contour length from the center of the dendrimer to the edge of the grafted chain. We used a cell size of $75R_g$ such that the electrostatic potential at the edge of the cell was less than 0.001, ($\Phi(r = r_{max}) < 0.001$) in order to satisfy the electrostatic potential boundary condition, Eq. 2.39. Random initial values for the fields

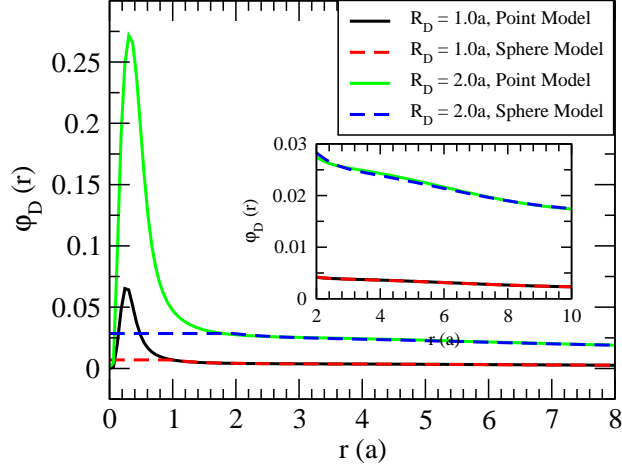


Figure 3.1: Comparison of the density profiles for the point-like and sphere-like drug models. The inset displays a comparison of the $\varphi_D(r)$ for the region $r \geq R_D$.

were applied, and the field values were solved via a Picard iteration scheme. We used a convergence criteria which imposed that the largest absolute value of the error in the fields from their self-consistent values was less than or equal to 0.0001.

3.2.4 Parameters

A majority of the results we present are for a third generation ($g = 3$) dendrimer with a dendrimer spacer length of $n = 5$ monomers. The average dendrimer monomer fraction, $\bar{\varphi}_P$, is defined as:

$$\bar{\varphi}_P = \frac{Mv_0}{V}, \quad (3.22)$$

where v_0 is the monomer volume, equal to $a^3 = \rho_0^{-1}$, and V is the simulation volume. We choose $\bar{\varphi}_P = 2.09 \times 10^{-5}$ to be the value corresponding to a

single $g = 3$, $n = 5$ dendrimer in a simulation cell of $75R_g$. When R_g and M were modified to study changes in dendrimer architectures, we adjusted $\bar{\varphi}_P$ appropriately. In all the simulation studies, we fixed the fraction of monomers that can participate in the charge dissociation reaction of Eq. 3.1 to be $\alpha_P = 0.5$. We note that α_P does influence the charge carried by the dendrimer molecule, and we have shown previously that the average dissociated charge of the annealed dendrimer, given by:

$$\bar{\alpha} = \frac{\alpha_P \int_0^\infty dr r^2 \alpha(r) \rho_P(r)}{\int_0^\infty dr r^2 \rho_P(r)}, \quad (3.23)$$

cannot be known *a priori* and is always less than the fraction of monomers that can participate in the charge dissociation reaction ($\bar{\alpha} < \alpha_P \alpha_b$) [86]. Drug molecules examined in the literature are capable of carrying multiple acid groups. However, in our simulations we assume that each drug molecule is capable of carrying one e^- of charge. Since we vary the drug molecule volume, v_D , in our simulations, we set the normalized (volumetric) charge density of the drug molecules to be $z_{D^-} = -1.0/\eta_D$.

We made the dendrimer monomers slightly hydrophobic by setting $\chi_{PS} = 0.05$. In order to reduce the number of parameters in our simulations we also set $-\chi_{PD} = \chi_{DS}$. We fixed the bulk drug number density by setting $\exp[-\beta\xi_{DH}^o - \beta\xi_{D^-}^o + \chi_{DS}\varphi_{S,b}]$ at a constant value of 5.0×10^{-4} . We choose this value in order to witness encapsulation of multiple drug molecules within the dendrimer, which corresponds to experimental observations. The solution screening length, κ^{-1} , was fixed to $3a$ (approximately 2.1nm). The

pK_b of the annealed dendrimers and pK_a of the drug molecules were chosen to be 5.0, which when converted into units of molecules/ a^{-3} corresponded to a value of 5.621. Our studies were effected at a constant value of the screening length, which required us to adjust the salt concentrations appropriately with changes in other physicochemical parameters. In order to probe the effect of electrostatic interactions on drug encapsulation, we allow the Bjerrum lengths to vary in the range of $1a$ to $6a$, where a is the Kuhn segment length and is assumed to be 0.7 nm, the Bjerrum length of water. To satisfy the constraint of the solution screening length, κ^{-1} , the corresponding bulk salt concentration was chosen to satisfy $\kappa^2 = 4\pi l_B \sum i c_i z_i^2$. At a physical level, changing the Bjerrum lengths require changing the dielectric constant of the solvent. Such changes can be expected to modify the dissociation constants of the different components. However, we treat l_B mainly as a parameter to vary the strength of the electrostatic interactions and ignore the other effects which may arise as a consequence of changing l_B .

3.3 Results

In the following sections we present results which examine the effect of pairwise enthalpic and electrostatic interactions on the encapsulation ability of charged drug molecules within PE dendrimers for a variety of parameter values for the generation numbers, pOH , drug size, drug concentration, and drug-polymer interaction. In addition to examining the local drug density and potential profiles, we quantify encapsulation ability of the dendrimers through

an “excess adsorption” like quality:

$$\varphi_{D,excess} = 4\pi \int_0^{\infty} dr [\varphi_D(r) - \varphi_{D,b}] r^2, \quad (3.24)$$

where $\varphi_D(r)$ represents the equilibrium volume fraction profile of the drug molecule and $\varphi_{D,b}$ represents the bulk volume fraction of the drug. The number of encapsulated drug molecules is then found as $N_{D,excess} = \varphi_{D,excess}/v_D$. In order to quantify the effects of the different interactions, we first examine the case where neither electrostatic interactions ($z_{D-} = 0$) nor enthalpic interactions ($\chi_{PD} = \chi_{DS} = 0$) are incorporated. We then individually incorporate the electrostatic interactions and enthalpic interactions respectively to clarify their influence upon the encapsulation efficacy. Subsequently, we examine the effect of simultaneously incorporating electrostatic and enthalpic interactions on the overall encapsulation ability of the dendrimers.

3.3.1 Non-Interacting Drug Molecules

In this section we consider the case where the drug molecules only interact with the dendrimer by excluded volume interactions accounted through Eq. 3.8. This case corresponds to a scenario where the drug molecules are *completely soluble* in the solvent ($\chi_{DS} = 0.0$). We examine this scenario mainly as a base case to quantify the relative influences of the other interactions in the solubilization of drugs.

Figure 3.2a displays the volume fraction profiles for drug particles in the presence of dendrimers of different generations, with the inset showing

the corresponding dendrimer density profiles. For all cases, we observe that the drug volume fraction profiles increase monotonically as we move from the center to the periphery of the dendrimer. These results can be rationalized by noting that since the dendrimer is fixed at the center of the cell, the density of dendrimer segments is maximum near $r = 0$, and falls monotonically with increasing distance from the center (*c.f.* inset of Fig. 3.2a). Since only excluded volume interactions are present between the drug and dendrimer segments (Eq. 3.8), the drug density profiles correspondingly exhibit gradients which are proportional and opposite to those observed for the dendrimer segment densities.

The effect of the excluded volume interactions on the drug encapsulation, $\varphi_{D,excess}$, is displayed in Figure 3.2b. It is seen that $\varphi_{D,excess}$ is negative for all drug sizes and dendrimer generation numbers, indicating a depletion of the drugs from the dendrimer. Furthermore, increasing the size of the drug R_D is seen to result in even lower $\varphi_{D,excess}$ values. These trends can be explained by noting that with increasing R_D , the excluded volume interactions between the drug and the dendrimer segments become more pronounced and therefore leads to enhanced depletion of the drugs from the dendrimer. Interestingly, the quantity N_D obtained by normalizing $\varphi_{D,excess}$ through the volume of the drugs (v_D) is seen to be independent of v_D , suggesting that the number of drugs depleted is relatively independent of its size in these dilute drug concentration regimes.

Lastly, we examine the effect of increasing dendrimer generation num-

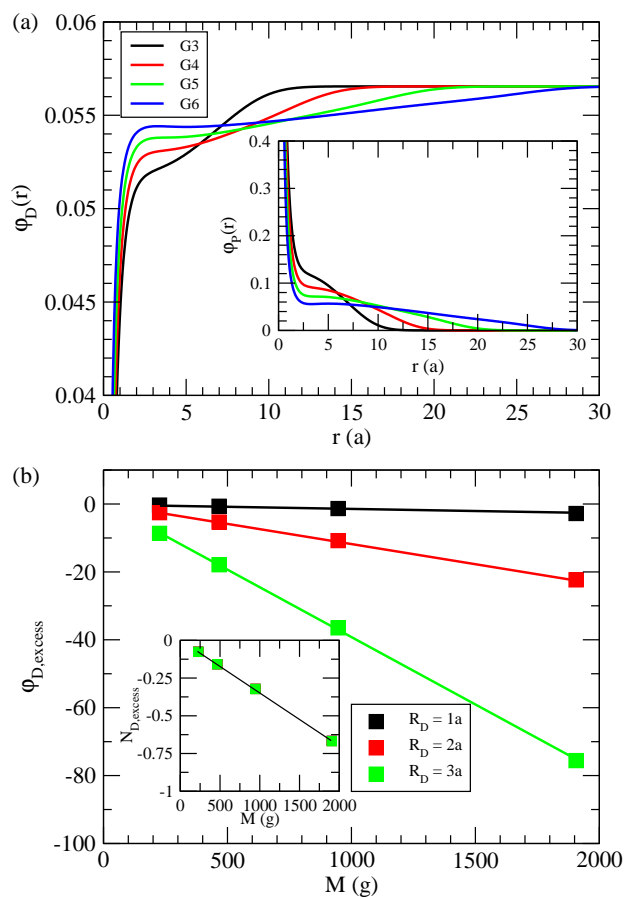


Figure 3.2: (a) The effect of generation number on the volume fraction profiles of drug molecules, $\varphi_D(r)$ (the size of the drug molecule $R_D = 3a$). The inset displays the dendrimer volume fraction profile, $\varphi_P(r)$. (b) The effect of generation number and R_D on drug molecule encapsulation, $\varphi_{D,excess}$, which is seen to have negative values for all cases. The inset displays the number of drug molecules encapsulated.

bers upon the drug depletion. The inset of Figure 3.2a shows that increasing generation number results in lower dendrimer density near the core, with however a longer tail. Such behavior has previously been shown to be a result of increased stretching of the dendrimer backbones, which in turn has been attributed to the increased number of monomers in the dendrimers and the corresponding enhancement in steric repulsion between them [177]. This effect manifests itself in the drug density profiles through an increased drug density near the core with increasing generation numbers. However, the preceding effects are offset by the fact that increasing the number of monomers carried by the dendrimer results in a larger volume overall occupied by the dendrimer monomers. As a consequence, the total dendrimer volume fraction, $\bar{\varphi}_P$, increases linearly with M , which correspondingly causes a depletion of both the solvent and drug molecules with a linear M dependence as seen in the results displayed in Fig. 3.2b.

The above results indicate that depletion of the drug molecules from the dendrimer center is expected to occur when only excluded volume interactions are accounted. The excluded volume interactions create a monotonically increasing drug PMF (or equivalently, a decreasing volume fraction profile) as the center of the drug molecule approaches the core of the dendrimer molecule.

3.3.2 Electrostatic Interaction Effects

In this section, we present results elucidating the effects of electrostatic interactions on drug molecule encapsulation. Specifically, we quantify the

influences of the solution pOH (or α_b), Bjerrum length (l_B), and charge density of the drug molecules (z_D , which is assumed to be inversely proportional to the volume of the drug) on dendrimer-drug complexation.

Figure 3.3a displays the PMF experienced by the drug, $w_D(r)$ (Eq. 3.21), for $R_D = 0.5a$ and $2.0a$ drugs in the presence of $G3$ and $G6$ dendrimers for different Bjerrum lengths. All the $w_D(r)$ profiles are seen to display a non-monotonic behavior with varying distance from the center of the dendrimer, r . Near the center of the dendrimer ($r = 0$) the dendrimer density is high, and hence the PMF exhibits a large positive value arising from the influence of excluded volume interactions. However, moving outward from the center, we see the PMF decreases and becomes negative as a consequence of the increased importance of electrostatic interactions between the monomers and drugs. Subsequently the PMF reaches a local minimum due to the reduction in the density of the dendrimer monomers and monotonically increases to the bulk value.

Qualitatively, we see that the depth of the potential wells increase with increasing Bjerrum length, l_B . These trends can be rationalized by noting that increasing l_B has the effect of enhancing the electrostatic attractions between the charged monomers and drug molecules (Eq. 3.11). Moreover, since the solution screening length is fixed, increasing the Bjerrum length correspondingly decreases the salt concentration, which results in enhanced attraction between the drug and dendrimer. As a consequence, we also observe an increased encapsulation of drug molecules with increasing l_B in Figure 3.3b.

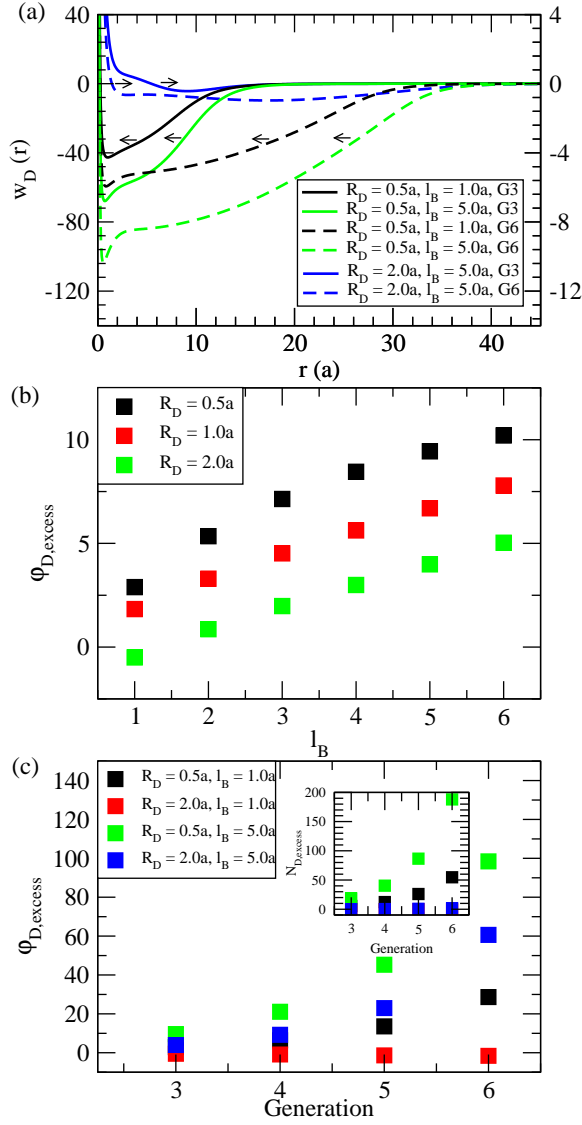


Figure 3.3: (a) The PMFs, $w_D(r)$, experienced by the drug $R_D = 0.5a$ (green and black lines) and $R_D = 2.0a$ (blue lines) in the presence of $G3$ (solid lines) and $G6$ (dashed lines) dendrimers for differing values of l_B . Note that the left hand axis corresponds to the cases where $R_D = 0.5a$, while the right hand axis corresponds to the cases where $R_D = 2.0a$. (b) The effect of l_B on the encapsulation ability of a $G3$ dendrimer in a solution of $pOH = 5.621$. (c) Effect of dendrimer generation on encapsulation ability for small ($R_D = 0.5a$) and large ($R_D = 2.0a$) drug molecules in solution with short ($l_B = 0.5a$) and long ($l_B = 5.0a$) Bjerrum lengths.

The effect of the drug size on the PMFs can be seen by comparing the blue and green curves in Fig. 3.3a. We witness a large decrease in both the depth and width of the potential as the drug size is increased from $R_D = 0.5a$ to $2.0a$, with the corresponding minima residing at larger radial values for the larger drugs. This effect on $w_D(r)$ can be attributed to the enhanced repulsions arising from increased influence of the excluded volume interactions that accompanies the increase in the size of the drug molecules. Moreover, by our assumption of fixed drug charge, increasing the drug size decreases the magnitude of the charge density in the drugs. This in turn reduces the electrostatic attraction between the drug molecules and charged monomers and correspondingly lowers the density of drugs within the dendrimer. As seen in Fig. 3.3b, this reduction in the depth of the potential well with increasing R_D in turn causes the amount of encapsulation, $\varphi_{D,excess}$, to also decrease. The main conclusion we derive from the results of Figures 3.3a and b is that, in order for electrostatic encapsulation of drugs by dendrimers to manifest as a positive value of $\varphi_{D,excess}$, the electrostatic attractions must be strong enough to overcome the excluded volume interactions. Such a positive encapsulation condition is seen typically for small enough particles and/or large l_B .

Studies by Cheng and Xu showed that higher generation PAMAM dendrimers display an increased ability of drug solubilization as compared to their lower generation counterparts, an effect which in part can be attributed to the larger number of primary and tertiary amine groups that accompany the higher generation dendrimers. In Fig. 3.3a, the effect of generation number on $w_D(r)$

can be seen by comparing the solid and dashed lines for a given color. The larger dendrimers are seen to create potential wells that are both deeper and wider. The increased depth can be attributed to not only the increase in the total number of charged monomers, but also the decrease in the monomer density near the dendrimer center that is seen to occur with increasing generation number (see inset of Fig. 3.2a), which reduces the local steric repulsion felt by the drugs inside of the dendrimer. The increased width of the potential well is attributed to the increase in the dendrimer monomer density tail, which results in charged monomers residing at further radial values than the lower generation counterparts. Thus the increase in both the total number of charged monomers and their corresponding range of influence causes the attractive potential well to widen. The influence of the preceding effects on the net drug encapsulation is displayed in Fig. 3.3c. For all cases but one ($l_B = 1.0a$ and $R_D = 2.0a$, parameters for which excluded volume interactions are more influential), we observe that the encapsulation increases with increasing generation numbers. However, we see that for the cases where electrostatic interactions are the weakest ($l_B = 1.0a$ and $R_D = 2.0a$), encapsulation decreases with increasing generation number. In the inset of Fig. 3.3c, we display the number of drug molecules encapsulated as a function of generation numbers and drug sizes. Consistent with the trends seen for $\varphi_{D,excess}$, we observe that $N_{D,excess}$ also increases with increasing generation numbers. However, we see a higher dependency of N_D on the drug molecule size, with the smaller drug molecules being able to achieve much larger levels of complexation resulting from their

correspondingly higher charge densities.

The fraction of monomers and drug molecules that are charged can also be varied through manipulation of the solution pOH . Figure 3.4a displays the effect of bulk solution pOH on $\varphi_{D,excess}$ when $pK_{a,D}$ and $pK_{b,P}$ are varied. We see a non-monotonic dependence on the encapsulation efficacy with increasing pOH . Moreover, the height and breadth of $\varphi_{D,excess}$ is also seen to decrease as $pK_{a,D}$ (set equal to $pK_{b,P}$ in our model) is increased. These trends can be understood by noting that as pOH is increased, the basic dendrimer monomers become more dissociated, whereas the acidic drug molecules become correspondingly less dissociated. When the pOH is low, the drug molecules are highly dissociated, but are however not able to form electrostatic complexes with the uncharged dendrimer monomers. Upon increasing the pOH , the dendrimers become more highly charged and encapsulation is enhanced. At even higher pOH conditions, the dendrimer charge fraction approaches its maximum value of α_P , but the dissociation of the drug molecules is low due to the high H^+ ion concentration. This effect serves to decrease the electrostatic complexation and is responsible for the observed decrease in $\varphi_{D,excess}$ at high pOH .

To explain the effect of $pK_{a,D}$ and $pK_{b,P}$ upon the above trends, we first note that the pK_b and pK_a values determine the influence of solution pOH on the range over which the dendrimer and drug molecules are charged. To demonstrate this, the effect of $pK_{b,P}$ and $pK_{a,D}$ values on charge dissociation of the dendrimer and drug molecules are displayed in the data of Fig. 3.4b.

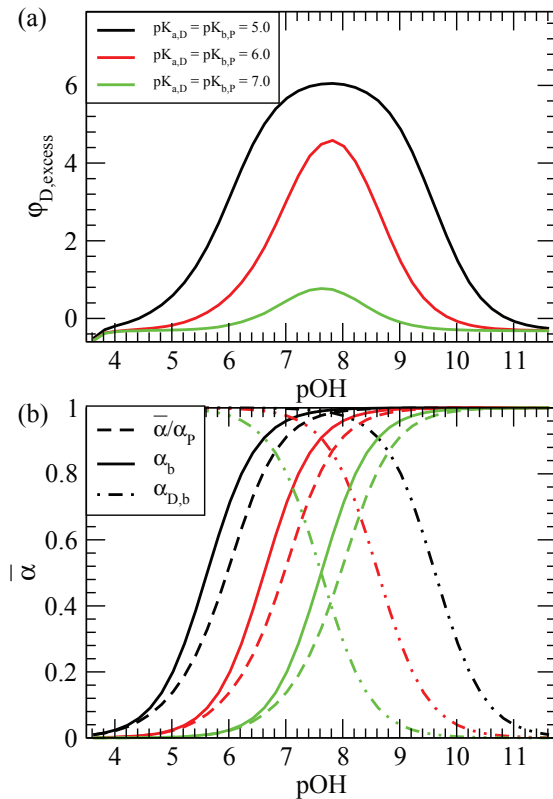


Figure 3.4: (a) The effect of pOH , $pK_{a,D}$, and $pK_{b,P}$ on the encapsulation ability of a $G3$ dendrimers, where $l_B = 1.0a$ and $R_D = 1.0a$. Encapsulation is seen to non-monotonic with respect to pOH . (b) Effect of pOH on the charge fraction ($\bar{\alpha}_P$), bulk polymer probability of dissociation ($\bar{\alpha}_{P,b}$), and bulk drug dissociation ($\bar{\alpha}_{D,b}$) for the cases where $pK_{a,D} = pK_{b,P} = 5.0$ (black), $pK_{a,D} = pK_{b,P} = 6.0$ (red), and $pK_{a,D} = pK_{b,P} = 7.0$ (green).

As the dendrimer pK_b is increased, the range over which $\bar{\alpha}_P/\alpha_P$ increases is seen to be shifted to higher pOH values. Similarly, increasing pK_a is seen to shift the variation in $\alpha_{D,b}$ to lower pOH . Hence, decreasing pK_b and pK_a of the dendrimer monomers and drug molecules respectively results in a broader range of pOH solution conditions wherein both the dendrimer monomers and drug molecules are charged, allowing them to participate in electrostatic complexation and broadens the curves displayed in Fig. 3.4a. Overall, the results of Fig. 3.4 suggest that the magnitudes of electrostatic driven encapsulation can be finely tuned by varying the pK_a and pK_b values of the chosen acids and polybases respectively.

In sum, from the above results (Figs. 3.3 and 3.4) we see that the electrostatic attraction between dendrimers and drug molecules can create an attractive well in the PMF for the drugs that is capable of resulting in drug encapsulation. This attraction is enhanced through increasing Bjerrum length and increased charge density of the drug. Our results are consistent with the findings of Maiti and coworkers, wherein they showed that the negatively charged hydrophobic drug Pbz displayed higher amounts of encapsulation than the neutrally charged Prim hydrophobic drug [100]. They attributed such a behavior to the increased attraction between the PAMAM dendrimer and Pbz drug resulting from electrostatic interactions. Our results also indicate that increasing the dendrimer generation number results in higher charge being carried by the dendrimer molecule, which in turn increases the electrostatic attraction between the dendrimers and the drug molecules. In our calculations,

enhanced encapsulation with increasing dendrimer generation number is seen if the increase in electrostatic attractions are stronger than the enhanced steric repulsion that occurs with increasing dendrimer generation number. Finally, we also observed that the electrostatic complexation between dendrimers and drugs can be tuned through variation of the pK_a and pK_b values of the chosen acids and polybases respectively.

3.3.3 Enthalpic Interaction Effects

In this section, we present results which examine the effects of the hydrogen bonding attractions between drug and dendrimers and the hydrophobic nature of the drug upon the drug PMF profiles and their encapsulation. To isolate the preceding effects, for the results presented in this section we exclude electrostatic interactions by setting $z_D = 0$. Moreover, in order to reduce the number of parameters to be probed, we assume $\chi_{PD} = -\chi_{DS}$.

The effect of χ_{PD} on the PMF, $w_D(r)$, is displayed in Fig. 3.5a for $R_D = 0.5a$ and $2.0a$ drug molecules in the presence of $G3$ and $G6$ dendrimers. Qualitatively, we notice that the $w_D(r)$ profiles exhibit similar non-monotonic trends as observed in Fig. 3.3a. However, the widths of the potential wells resulting from the enthalpic attraction effects are seen to be smaller than the potential wells from electrostatic attraction. We believe that this difference arises from the fact that electrostatic interactions are non-local with respect to densities of the different components, whereas the enthalpic interactions were modeled to be local in nature. We also observe that the depth of the

potential wells increase with increasing attraction (larger negative χ_{PD}) for both $R_D = 0.5a$ and $2.0a$ drug molecules (note the difference in scale between the $\chi_{PD} = -0.5$ and -2.0 results). The increased attraction that arises for large negative χ_{PD} results in increased values of $\varphi_{D,excess}$ and $N_{D,excess}$ for a given R_D , an effect which is displayed in Fig. 3.5b.

In examining the role of the size of the drug R_D for fixed χ_{PD} , we observe that little to no variations are observed in $w_D(r)$ when the size of the drug is varied (compare solid red and blue lines). Furthermore, $\varphi_{D,excess}$ is seen to increase with increasing R_D when is fixed. We rationalize these trends by noting that the driving force for the drug encapsulation increases with an increase in the local dendrimer monomer concentrations, $\varphi_P(r)$, and a decrease in the local solvent concentration, $\varphi_S(r)$. Our results indicate (not displayed) that when the size of the drug, R_D , is varied at fixed values of χ_{PD} and χ_{DS} , there is practically no variance in the solvent depletion profiles or the dendrimer conformations. Since the local attraction of the drug to the dendrimer does not vary significantly with variation in the size of the drug, $\varphi_{D,excess}$ is expected to be proportional to only the volume of the drug, and as a consequence, $N_{D,excess}$ can be expected to be independent of R_D . Both these expectations are seen to borne out in the results displayed in Fig. 3.5b.

In Figure 3.3a, increasing the generation number is seen to increase both the depth and width of the drug PMFs for the values of χ_{PD} probed. These results can be easily explained as a consequence of the fact that the number of hydrogen bonding sites of the dendrimer increases with increas-

ing generation dendrimers. Furthermore, larger dendrimers will exclude more solvent molecules from their interior through excluded volume interactions, which increases the encapsulation of drugs through hydrophobic interactions. We quantify the effect of generation number on drug encapsulation in Fig. 3.5c, wherein we observe that, consistent with the preceding observations, the number of drug molecules encapsulated, $N_{D,excess}$, grows with $M(g)$.

In sum, the above results display that increasing enthalpic attractive interactions causes an increase in the depth of the drug PMFs. However, the drug PMFs were not seen to vary significantly with the dendrimer size, and the number of drugs encapsulated by the dendrimers was seen to only be a function of χ_{PD} , χ_{DS} , and dendrimer generation number. In qualitative agreement with our findings, Maiti and coworkers saw that the non-soluble drugs Pbz and Prim had higher free energy barriers than the water soluble Ala and Sal drugs [100]. In the Maiti study however, the larger hydrophobic drug, Pbz, was found to have a deeper potential well than the smaller Prim molecule. However, the increased energy barrier for the Pbz molecule can possibly be attributed to its negative charge, which causes complexation with the positively charged amine groups. Although electrostatic interactions were neglected in the present section, the increased PMF well seen for Pbz is consistent with the findings of Sec. 3.3.2.

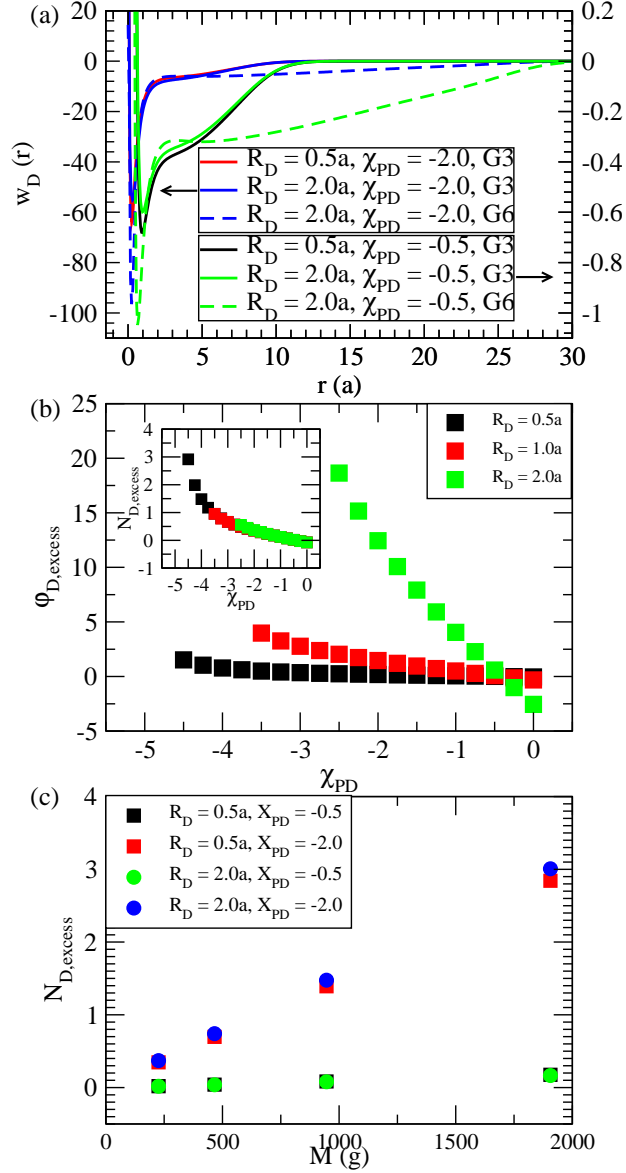


Figure 3.5: (a) The drug PMFs for $R_D = 0.5a$ (black and red lines) and $R_D = 2.0a$ (blue and green lines) in the presence of $G3$ (solid lines) and $G6$ (dashed lines) for differing values of χ_{PD} and χ_{DS} . Note that the right hand axis corresponds to the cases where $\chi_{PD} = -0.5$, while the left hand axis corresponds to the cases where $\chi_{PD} = -2.0$. (b) Effect of χ_{PD} on dendrimer-drug localization. The inset displays the number of localized drug molecules. (c) Effect of M on the number of encapsulated drug molecules.

3.3.4 Electrostatic Interaction and Enthalpic Effects

In the previous sections we examined the individual effects of excluded volume, electrostatic, and hydrophobic interactions on drug-dendrimer complexation. By individually examining these effects, we were able to show that:

- Depletion and encapsulation of drugs by dendrimers are seen to be independent of the drug volume when either only excluded volume or enthalpic interaction effects are accounted.
- Electrostatic encapsulation of drugs by dendrimers is dependent on the drug charge density, which is controlled through the total charge carried by the drug and the drug volume. Electrostatic encapsulation only occurs when the drug molecules charge to volume ratio is high enough to overcome steric repulsion.
- When only excluded volume interactions are accounted, increasing generation number results in higher depletion. When either enthalpic or electrostatic interactions are accounted (in addition to excluded volume interactions), increasing generation number will result in increased encapsulation if the respective enthalpic and electrostatic parameters are strong enough to overcome the increased steric repulsion that accompanies the larger generation dendrimers.

In this section we consider the model in which all the three effects are combined and examine their influence on drug complexation.

Figure 3.6 displays color-coded representations of drug encapsulation (as quantified by $N_{D,excess}$) of drug molecules of two different sizes ($R_D = 0.5a$ and $R_D = 2.0a$) by $G3$ dendrimers in solutions of different pOH when χ_{PD} , χ_{DS} , and l_B are varied. We notice that as we increase the pOH (Fig. 3.6a-c, and Fig. 3.6d-f) for any χ_{PD} , the number of encapsulated drug molecules also correspondingly increases (as seen in the color gradients of the plots), a trend which can be rationalized as a result of enhanced electrostatic attraction between the drug molecules and dendrimer monomers resulting from the increased dendrimer monomer dissociation. At low pOH , (Figs. 3.6a and d) the relative gradient in color for the individual plots is seen to be strong in the negative χ_{PD} (vertical) direction as compared to the higher pOH results. Under the low pOH conditions, the dendrimer monomers have a very low probability of dissociation, and the electrostatic interactions play only a weak role as compared to the enthalpic interactions, especially for the larger drugs. As the pOH of the solution increases, the dissociated charge of the dendrimer increases and electrostatic attractions begin to play a more influential role over encapsulation, and hence the color gradients in the χ_{PD} direction are seen to become relatively weaker.

Qualitatively, our results are in agreement with recent MD work by Maiti and coworkers. They observed that the non-soluble drugs (Pbz and Prim), which have a high χ_{DS} value, have deeper PMF wells than the soluble drugs (Ala and Sal). A deeper PMF well physically corresponds to a situation where higher amounts of drug are encapsulated. Furthermore, the depth of

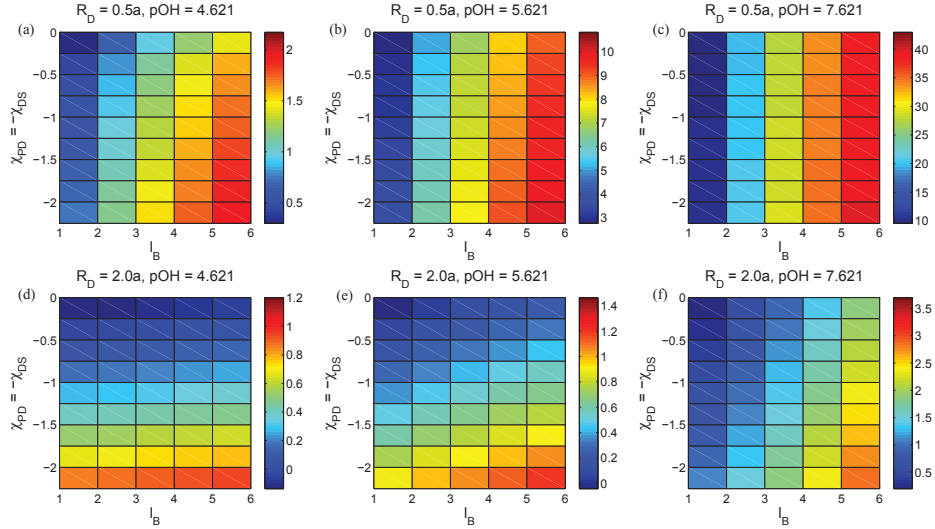


Figure 3.6: Effect of varying l_B (x-axis) and χ_{PD} (y-axis) on $N_{D,excess}$ for (a) $R_D = 0.5a$, $pOH = 4.621$, (b) $R_D = 0.5a$, $pOH = 5.621$, (c) $R_D = 0.5a$, $pOH = 7.621$, (d) $R_D = 2.0a$ and $pOH = 4.621$, (e) $R_D = 2.0a$ and $pOH = 5.621$, and (f) $R_D = 2.0a$ and $pOH = 7.621$

the well was seen to increase significantly (from $9kcal/mol$ to $42kcal/mol$) in Ref. [100] when the dendrimers go from being unprotonated (pH 10) to protonated (pH 7), which would correspond to a large increase in the number of encapsulated drugs upon increasing the charge carried by the dendrimer. We qualitatively witness these effects upon increasing both the solution pOH and the Bjerrum length, l_B .

Although we see in Fig. 3.6 that the general complexation trends observed in Secs. 3.3.2 and 3.3.3 are upheld when we incorporate both electrostatic and enthalpic interactions, an interesting question is whether there is any synergism among the interactions in influencing the encapsulation behav-

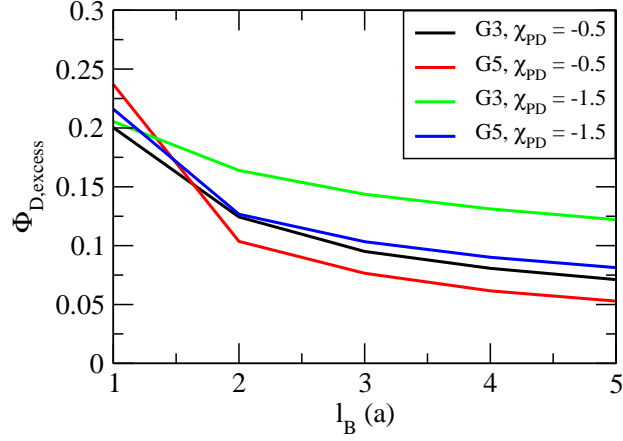


Figure 3.7: $\Phi_{D,excess}$ observed for $G3$ and $G5$ dendrimers as a function of l_B in the presence of $R_D = 1.0a$ drug molecules in a solution of $pOH = 5.621$, where $\chi_{PD} = -0.5$ and -1.5 . Note that $\Phi_{D,excess}$ is positive for all values of l_B and χ_{PD} .

ior. To discern this, we quantify the “enhanced” encapsulation arising from the synergistic effects by defining a quantity, $\Phi_{D,excess}$, which is given by:

$$\Phi_{D,excess} = \frac{\varphi_{D,excess,int+elec} - (\varphi_{D,excess,elec} + \varphi_{D,excess,int})}{\varphi_{D,excess,elec} + \varphi_{D,excess,int}}, \quad (3.25)$$

where $\varphi_{D,excess,int+elec}$ is the encapsulation that occurs when excluded volume, electrostatic, and enthalpic interactions are simultaneously accounted, whereas $\varphi_{D,excess,elec}$ is the encapsulation that occurs when only excluded volume and electrostatic interactions are accounted, and $\varphi_{D,excess,int}$ is the encapsulation that occurs when only excluded volume and enthalpic pairwise interactions are accounted.

Figure 3.7 displays $\Phi_{D,excess}$ for $G3$ and $G5$ dendrimers for a drug with $R_D = 1.0a$ in a solution of $pOH = 5.621$, where $\chi_{PD} = -0.5$ and -1.5 . We witness positive values of $\Phi_{D,excess}$ for all l_B , χ_{PD} and generation numbers

indicating synergy between the different interactions when the electrostatic and enthalpic contributions are considered together. The monotonic decrease in $\Phi_{D,excess}$ with increasing Bjerrum length, l_B , indicates that this synergism is most prominent when the electrostatic interactions are weaker. For small negative χ_{PD} and high Bjerrum lengths, the electrostatic interactions are very strong compared to the enthalpic interactions, and the corresponding depth of the drug PMFs are dominated by electrostatic contributions. At larger (negative) χ_{PD} , the enthalpic attractions between the dendrimer and drug becomes more significant, causing $\Phi_{D,excess}$ to increase at larger l_B . The quantitative manifestation of the synergism is seen to depend on the generation numbers in Fig. 3.7. At low Bjerrum lengths ($l_B = 1.0a$), the $G5$ dendrimers display larger $\varphi_{D,excess}$. However, $\varphi_{D,excess}$ of the $G5$ dendrimers is seen to decrease more rapidly with increasing l_B than that of the $G3$ dendrimers, and we attribute this trend to the enhancement of electrostatic attraction for the higher generation dendrimers as compared to the lower generation dendrimers. Overall, these non-additive trends highlight the simultaneous influence of multiple binding mechanisms between dendrimers and drug molecules.

3.4 Summary

In this chapter, we presented results for the encapsulation of charged drug molecules by electrostatic and hydrophobic interaction between and charged dendrimers for dilute concentrations of drugs. By isolating the effects of excluded volume interactions, electrostatic attractions, and hydrophobic inter-

actions we were able to delineate the different parameters and their relative importance in influencing the encapsulation of drugs by dendrimer molecules. When only excluded volume interactions are accounted, we witnessed a depletion of drug molecules inside the dendrimer molecule relative to that of the bulk concentration. Incorporation of electrostatic attractions resulted in localization of drug molecules, with the smallest drug molecules seeing the most localization within the dendrimer. This effect is due to the fact that the smaller drug molecules carry more charge per volume (in our framework, we kept the charge carried by the drug a constant). Higher generation dendrimers, which carry more charge per dendrimer molecule than lower generation dendrimers, were seen to also promote drug encapsulation. Complexation due to enthalpic interaction effects in our studies were seen to be dependent only upon the interaction parameters χ_{PD} , χ_{PS} , and the number of monomers carried by the dendrimer, M . Lastly, when electrostatic and enthalpic attractive interactions were combined in our simulations, a synergy is observed between the interactions in promoting the encapsulation.

Chapter 4

Effects of Neutral Grafted Chains on the Conformations and Drug Encapsulation Efficacies of Polyelectrolyte Dendrimers

4.1 Introduction

High hydrophobicities and low membrane permeabilities limit almost forty percent of newly developed pharmaceuticals from being used in practice [91, 145]. The need to increase the availability of hydrophobic drugs in physiological conditions has motivated the investigation of different kinds of polymeric materials as drug carriers and delivery vehicles [88]. One such avenue pursued by researchers involves the use of hyper-branched tree-like molecules known as dendrimers [20, 23, 67, 68, 123, 145]. Due to advances in synthesis techniques, researchers are presently able to create monodisperse dendrimer molecules with precise control over their flexibility, solubility, and charge [3, 23]. This has led to the development of water-soluble dendrimer molecules that are capable of hosting and controllably releasing weakly soluble drug molecules [20, 23, 67, 68, 123, 145]. Many weakly soluble drugs, including non-steroidal anti-inflammatory drugs (NSAIDs) and anti-cancer drugs, have been shown to form complexes with basic dendrimer molecules, such as poly(amidoamine) (PAMAM) dendrimers [22, 186]. Different interaction

mechanisms have been proposed to rationalize the complexation, which include the hydrophobic nature of the drugs [22, 55, 70, 115, 122], electrostatic attractions between the drugs and dendrimers [5, 21, 130, 184], and hydrogen bonding interactions [22, 130, 148].

The ability of dendrimers to solubilize weakly acidic drug molecules has been shown to increase with increasing generation number and has been attributed to the exponential increase (with generation number) in the number of dendrimer monomers that partake in dendrimer-drug complexation [22]. Unfortunately, dendrimers bearing primary amino group termini also induce hole-formation in the cell membrane due to electrostatic interactions between the anionic lipid head groups and cationic dendrimer surface amines. Such an effect has also been shown to intensify with increasing generation number [47, 51, 110]. Thus, increasing dendrimer size has the unintended consequence of increasing their cell cytotoxicity. To combat this effect, experimentalists have covalently conjugated poly(ethylene glycol) (PEG) chains to dendrimer terminal groups [60, 65]. This has resulted in reduced cytotoxicity of cationic dendrimers [60, 169], while simultaneously decreasing their immunogenicity and increasing their blood circulation time [66]. Along with decreasing dendrimer cytotoxicity, the addition of PEG grafts has also been shown to increase the encapsulation of hydrophobic drugs as compared to non-grafted dendrimers [65]. For instance, experiments by Kojima *et al.* demonstrated increased solubility for the anti-cancer drugs methotrexate (MTX, which is weakly acidic) and adriamycin (ADR, which is weakly basic) in solution with

PAMAM dendrimers grafted with polyethylene glycol (PEG) as compared to ungrafted PAMAM dendrimers [65]. The authors hypothesized that the increase in complexation of the grafted dendrimers could be a result of the more open dendrimer conformations resulting from the steric interactions between the added PEG grafts. In a different work, Bhadra *et al.* [7] also found that PEGylation of PAMAM dendrimers not only increased encapsulation but also significantly reduced the release rates of the anti-cancer drug 5-fluorouracil compared to non-grafted PAMAM dendrimers. The effect of PEG grafting length on pyrene encapsulation by PAMAM dendrimers was studied by Yang *et al.*, wherein they observed a non-monotonic relationship between the PEG grafting length and the number of encapsulated pyrene molecules ($M_w = 2000 > M_w = 5000 > M_w = 750$) [183]. They hypothesized that this non-monotonic behavior could be a result of increased aggregation of the PEGylated dendrimers, which they predicted would increase with increasing PEG molecular weight.

In a different context of application, dendrimers conjugated with PEG have also been applied in nanoparticle templating and synthesis [44, 46]. Such techniques make use of the physics that transition metals tend to segregate within the dendrimer interior due to electrostatic interactions and/or coordination with amine and amide groups. Subsequent reduction of metallic species results in dendrimer encapsulated nanoparticles, which can be stabilized through intermolecular steric repulsion between dendrimers. The addition of PEG grafts to dendrimers have been shown to provide a wider range

of solvents and polymers with which such nanotemplates could be fabricated [46].

There have been some theoretical studies of the role of neutral grafts on the conformation, dynamics, and interparticle interactions of dendrimer molecules [76–78, 190, 191]. Monte Carlo (MC) studies by Zhou and Chen found that the grafting of neutral polymer chains to *neutral* dendrimers results in a reduction of the backfolding of the terminal groups and a subsequent decrease in monomer density near the dendrimer center [190]. This effect was seen to increase with increasing grafted chain length and was attributed to the steric effect of the grafted chains. Interactions between poly(ethylene oxide) (PEO) chains and PAMAM dendrimers were studied by Tanis and Karatasos [149]. Although their simulations were not for conjugated dendrimers, they were able to shed insight into how the presence of PEO affects the intradendrimer hydrogen bonding between PAMAM carbonyl oxygens, primary amine hydrogens, PEO ether oxygens, water hydrogens, and water oxygens. In a different line of study, Lee and Larson used the MARTINI coarse grained (CG) force field to examine the structure [76–78], interparticle interactions [76, 78], and membrane interactions [78] of PEGylated PAMAM dendrimers. In their studies, they accurately reproduced experimentally measured sizes of PEGylated dendrimers, and observed brushlike behavior of the dendrimer grafts at high grafting densities [76–78].

In this work, we report the results of coarse-grained modeling of the influence of neutral grafts upon the conformations of polyelectrolyte dendrimers

and their subsequent influence on the complexation between weakly acidic drug molecules and polybasic dendrimers. The present work was motivated by our recent article which developed a self-consistent field theory (SCFT) model to study the complexation between weakly basic *non-grafted* dendrimers and weakly acidic drug molecules [84]. In that study, we delineated the effects of excluded volume interactions, electrostatic attractions, and enthalpic interactions (used in our work to model the hydrophobic nature of the drugs and hydrogen-bonding interactions between the drugs and polymer) on the encapsulation of drug molecules by non-grafted dendrimers. Moreover, our coarse-grained results were qualitatively consistent with the reported results of atomistically detailed simulations [100] and were able to furnish insights into the mechanisms underlying the complexation between dendrimers and drugs.

In this chapter we extend our previous work [84] to include the presence of neutral polymer grafts attached to the dendrimer periphery and examine the effect of such grafts on the equilibrium conformations of charged dendrimers and the drug encapsulation ability of the dendrimers. The parameters that we choose to investigate include the drug molecule sizes, solution pOH , solution Bjerrum length, the strength of enthalpic interactions between the dendrimer monomers and drug molecules, and the drug hydrophobicity.

The rest of the chapter is arranged as follows. In Section 4.2 we discuss our model and the associated terminology. In Section 4.3, we first investigate the effect of grafting length on neutral and charged dendrimers in the absence of any drug molecules (Sec. 4.3.1). We then incorporate drug molecules in the

presence of dendrimers and study their complexation. To isolate the different mechanisms, we individually consider the case where we incorporate (i) only excluded volume interactions (Sec. 4.3.3); (ii) electrostatic and excluded volume interactions (Sec. 4.3.4); (iii) enthalpic and excluded volume interactions (Sec. 4.3.5). Finally, we consider the phenomena resulting when we incorporate electrostatic, enthalpic, and excluded volume interactions (Sec. 4.3.6) simultaneously. In Section 4.4 we conclude with a summary of our results.

4.2 Model and Self-Consistent Field Theory

Our model considers a system comprised of a single weakly grafted dendrimer molecule positioned with its core at the center of a spherically symmetric cell of volume V . The dendrimer (P) and its grafts (G) are in the presence of solvent molecules (S), H^+ and OH^- ions, monovalent salt ions (which we denote as Na^+ and Cl^-), and weakly acidic drug molecules denoted as D . The physics included in our model is based on the following assumptions:

(i) To model the dendrimer spacers and neutral grafts, we use a flexible, continuous Gaussian chain model [41, 86, 177]. In reality, dendrimer spacer flexibility depends on the chemical nature of the dendrimer monomeric units [162]. In a previous work [84], we examined the role of spacer length upon the conformations and drug encapsulation ability of dendrimers. Although we observed quantitative changes in the dendrimer conformations upon varying the spacer length [14, 15, 48], we did not witness any differences in the qualitative

mechanisms underlying drug encapsulation in dendrimers. As a consequence, in order to reduce the number of parameters probed, in the present work we do not undertake a study of the dendrimer spacer lengths. Moreover, we also assume that the Kuhn segment lengths of the dendrimer and graft monomers are identical.

(ii) In this work, we treat the dendrimer monomers as weak bases and the drug particles as weak acids by explicitly incorporating the acid-base equilibrium reaction into our framework. We model the charge dissociation of the dendrimer monomers using an approach similar to that adopted in the recent mean field studies for weak PE brushes by Szleifer *et al.* [39, 121, 165] and Won and coworkers [49, 174]. We assume that a fraction, α_P , of the dendrimer monomers carry dissociable charge groups and are capable of becoming charged through the equilibrium reaction given in Eq. 3.1. In a similar fashion, dissociation of the acidic drug molecules, D , is modeled as an equilibrium reaction which is given by Eq. 3.3. The equilibrium constants of the former and latter equilibrium reactions are given by Eqs. 3.2 and 3.4 respectively.

(iii) The hydrophobic nature and hydrogen bonding interactions between the drug molecules and polymer monomers are assumed to be representable through energetic terms which depend on the local concentrations of the drug, solvent, and dendrimer monomers. We use a simple quadratic density functional and Flory-Huggins χ -parameters [33] to model such interactions. Specifically, the parameter, χ_{ij} , accounts for the strength of the average

enthalpy of mixing between the i^{th} and j^{th} species. In this study, we restrict $\chi_{DS} \geq 0$ and $\chi_{PD} \leq 0$ to model the drug hydrophobicity and the hydrogen bonding interactions between the drugs and dendrimer respectively.

(iv) The electrostatic interactions between charged molecules are modeled using a classical Coulomb potential [35].

(v) The drug, solvent, and ion molecules are modeled as point-like particles. We refer the reader to our previous work for the justification of this assumption for the drug molecules [84]. We assume that the volume of the polymer monomers and solvent molecules are identical and we set them to ρ_0^{-1} . The volume of the drug molecule, v_D (in units of ρ_0^{-1}), is left as a parameter that we vary, while the ion volume is neglected.

(vi) We use a harmonic compressibility penalty [13, 119, 180] to minimize fluctuations in the local sum of the densities of different components (polymer, solvent, and drug) from the average bulk density, ρ_0 . Since the drug molecules are present in dilute concentrations, we do not include any higher order drug-drug steric interaction terms [151].

A schematic representation of a “third generation” dendrimer (black) with grafted chains (red) attached at the periphery is displayed in Fig. 4.1. The center monomer and the three branches stemming from it compose the 0^{th} generation of the dendrimer. The next generation of dendrimer branches connect to the end of the spacer, and the number of branches stemming from an individual branch point is termed as the “functionality” of the dendrimer.

In this notation, the number of monomers comprising a non-conjugated dendrimer molecule, M , is given by:

$$M(g) = nf \left((f - 1)^{g+1} - 1 \right) + 1 \quad (4.1)$$

where n is the number of monomers per spacer, f is the branch point functionality, and g is the generation number. We assume that every terminal group of the dendrimer molecule is grafted with a polymer of length N_G such that the number of monomers in the graft portion of the dendrimer molecule is given as:

$$M_G(g) = N_G f (f - 1)^g. \quad (4.2)$$

Based on the above assumptions, we develop a thermodynamic model for the free energy of the system containing the dendrimer, grafts, solvent, salt and drug molecules. We employ a semi-grand canonical framework to describe the free energy of our system, and we solve it within a mean field approximation [35]. In this framework, the free energy, \mathcal{F} , can be identified as [121]:

$$\mathcal{F} = \mathcal{F}_{conf} + \mathcal{F}_{int} + \mathcal{F}_{comp} + \mathcal{F}_{mix} + \mathcal{F}_{chem} + \mathcal{F}_{elec}. \quad (4.3)$$

The terms \mathcal{F}_{int} , \mathcal{F}_{comp} , \mathcal{F}_{mix} , \mathcal{F}_{chem} , and \mathcal{F}_{elec} are equivalent to Eqs. 3.7, 3.8, 3.9, 3.10, and 3.11 respectively. Because the dendrimers in this work have grafted chains, the term \mathcal{F}_{conf} must be modified to account for such changes to the chain architecture and is given by:

$$\beta \mathcal{F}_{conf} = \ln Q_{PG} + \rho_0 \int d\mathbf{r} w_P(\mathbf{r}) \varphi_P(\mathbf{r}) + \rho_0 \int d\mathbf{r} w_G(\mathbf{r}) \varphi_G(\mathbf{r}). \quad (4.4)$$

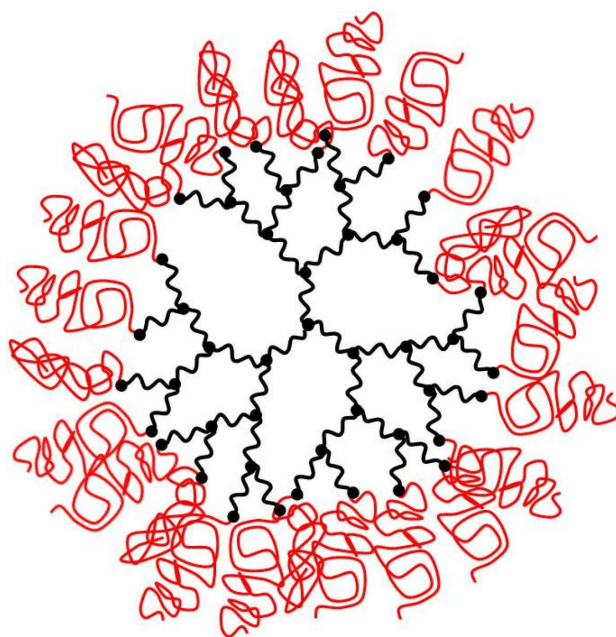


Figure 4.1: Schematic of a grafted 3^{rd} generation dendrimer having a functionality of 3. The dendrimer portion is represented in black, while the grafted portions are represented in red.

In the above, Q_{PG} represents the partition function of the grafted dendrimer in the external fields $w_P(\mathbf{r})$ and $w_G(\mathbf{r})$. To obtain Q_{PG} , we assume that the conformations of the dendrimer and grafts can be described using a continuous Gaussian chain model [35]. We use the symbol, “ s ” to index the segments along the chain contour, $\mathbf{r}_{i,j}(s)$, to denote the position in space of the s^{th} segment in the j^{th} ($j = 1 \dots f(f-1)^i$) branch of the i^{th} ($i = 1 \dots g$) generation on the dendrimer molecule, and $\mathbf{r}_k(s)$ to denote the position of the s^{th} segment on the k^{th} ($k = 1 \dots f(f-1)^g$) grafted chain. The stretching energy U_0 of the dendrimer chain is then given as:

$$\begin{aligned} \beta U_0(\mathbf{r}) = & \frac{3}{2a^2} \sum_{i=0}^g \sum_{j=0}^{f(f-1)^i} \int_{s_i}^{s_{i+1}} |\dot{\mathbf{r}}_{i,j}(s)|^2 ds \\ & + \frac{3}{2a^2} \sum_{k=0}^{f(f-1)^g} \int_{s_{g+1}}^{s_{end}} |\dot{\mathbf{r}}_k(s)|^2 ds. \end{aligned} \quad (4.5)$$

The partition function, Q_{PG} , can be determined from the spatial probability distribution of each of the monomers within the dendrimer molecule. We calculate both the probability of finding the s^{th} monomer of the dendrimer at position \mathbf{r} , $q(\mathbf{r}, s)$, with the condition that the center of the dendrimer is fixed at $r = 0$, and the complementary probability of finding the $N - s^{th}$ monomer at position \mathbf{r} , $q^\dagger(\mathbf{r}, s)$, independent of the location of the monomer at the outer extremity. The partition function, Q_{PG} , is obtained from:

$$Q_{PG} = \frac{1}{V} \int d\mathbf{r} q^\dagger(\mathbf{r}, s = 0), \quad (4.6)$$

The functions $q(\mathbf{r}, s)$ and $q^\dagger(\mathbf{r}, s)$ can be found from the following “diffusion-

like” equations [35]:

$$\begin{aligned} \frac{\partial q}{\partial s} &= \frac{a^2}{6} \nabla^2 q - [\gamma(s)w_P(\mathbf{r}) + (1 - \gamma(s))w_G(\mathbf{r})]q; \\ q(\mathbf{r}, s = 0) &= \delta(\mathbf{r}). \end{aligned} \quad (4.7)$$

where $\gamma(s) = 1 \forall s \leq s_g, \gamma(s) = 0 \forall s > s_g$. The “initial” condition in Eq. 4.7 forces the central (0^{th}) monomer to reside at $\mathbf{r} = 0$ (the center of the spherical simulation cell). The function $q^\dagger(\mathbf{r}, s)$ that runs from the periphery of the dendrimer is given by

$$\begin{aligned} -\frac{\partial q^\dagger}{\partial s} &= \frac{a^2}{6} \nabla^2 q^\dagger - [\gamma(s)w_P(\mathbf{r}) + (1 - \gamma(s))w_G(\mathbf{r})]q^\dagger; \\ q^\dagger(\mathbf{r}, s = N) &= 1. \end{aligned} \quad (4.8)$$

In order to account for the branching within the dendrimer, we apply the following conditions [41]

$$q^\dagger(\mathbf{r}, s_i^-) = [q^\dagger(\mathbf{r}, s_i^+)]^{f-1}; \quad i \leq g \quad (4.9)$$

$$q(\mathbf{r}, s_i^+) = q(\mathbf{r}, s_i^-) [q^\dagger(\mathbf{r}, s_i^+)]^{f-2}; \quad i \leq g \quad (4.10)$$

where $q^\dagger(\mathbf{r}, s_i^-)$ refers to spatially dependent chain propagator for a monomer at a value of s that is infinitesimally smaller than s_i , the value of s at the i^{th} branching point. The above conditions (Eqs. 4.9 - 4.10) embody the fact that at the dendrimer branch points, the $f - 1$ outer generation chains connect. This is analogous to $f - 1$ independent particles diffusing to the same point in space at the exact same time [41]. In order to solve for $q(\mathbf{r}, s)$ and $q^\dagger(\mathbf{r}, s)$ we first determine $q^\dagger(\mathbf{r}, s)$ and then subsequently use it via Eq. 4.10 to determine $q(\mathbf{r}, s)$. We assume no flux boundary conditions at the center and periphery of the cell ($\nabla q(\mathbf{r} = 0, s) = \nabla q(\mathbf{r} = \infty, s) = \nabla q^\dagger(\mathbf{r} = 0, s) = \nabla q^\dagger(\mathbf{r} = \infty, s) = 0$).

The self-consistent equations are found as the saddle point of Eq. 4.3 with respect to the fields $\varphi_P(\mathbf{r})$, $\varphi_G(\mathbf{r})$, $\varphi_{Na^+}(\mathbf{r})$, $\varphi_{Cl^-}(\mathbf{r})$, $\varphi_{H^+}(\mathbf{r})$, $\varphi_{OH^-}(\mathbf{r})$, $\varphi_S(\mathbf{r})$, $w_P(\mathbf{r})$, $w_G(\mathbf{r})$, $w_{Na^+}(\mathbf{r})$, $w_{Cl^-}(\mathbf{r})$, $w_{H^+}(\mathbf{r})$, $w_{OH^-}(\mathbf{r})$, $w_D(\mathbf{r})$, $w_S(\mathbf{r})$, and $\Phi(\mathbf{r})$. Such a procedure yields [35]:

$$\begin{aligned} w_P(\mathbf{r}) = & \chi_{PG}\varphi_G(\mathbf{r}) + \chi_{PD}\varphi_D(\mathbf{r}) + \chi_{PS}\varphi_S(\mathbf{r}) \\ & + \zeta (\varphi_P(\mathbf{r}) + \varphi_G(\mathbf{r}) + \varphi_D(\mathbf{r}) + \varphi_S(\mathbf{r}) - 1) \\ & + \alpha_P \ln \left[\frac{1 - \alpha(r)}{1 - \alpha_b} \right] - \alpha_P, \end{aligned} \quad (4.11)$$

$$\begin{aligned} w_G(\mathbf{r}) = & \chi_{PG}\varphi_P(\mathbf{r}) + \chi_{GD}\varphi_D(\mathbf{r}) + \chi_{GS}\varphi_S(\mathbf{r}) \\ & + \zeta (\varphi_P(\mathbf{r}) + \varphi_G(\mathbf{r}) + \varphi_D(\mathbf{r}) + \varphi_S(\mathbf{r}) - 1), \end{aligned} \quad (4.12)$$

$$\begin{aligned} w_D(\mathbf{r}) = & \chi_{PD}\varphi_P(\mathbf{r}) + \chi_{GD}\varphi_G(\mathbf{r}) + \chi_{DS}\varphi_S(\mathbf{r}) \\ & + \zeta (\varphi_P(\mathbf{r}) + \varphi_G(\mathbf{r}) + \varphi_D(\mathbf{r}) + \varphi_S(\mathbf{r}) - 1) \\ & + \ln \left[\frac{1 - \alpha_D(r)}{1 - \alpha_{b,D}} \right] - 1.0, \end{aligned} \quad (4.13)$$

$$\begin{aligned} w_S(\mathbf{r}) = & \chi_{PS}\varphi_P(\mathbf{r}) + \chi_{GS}\varphi_G(\mathbf{r}) + \chi_{DS}\varphi_D(\mathbf{r}) \\ & + \zeta (\varphi_P(\mathbf{r}) + \varphi_G(\mathbf{r}) + \varphi_D(\mathbf{r}) + \varphi_S(\mathbf{r}) - 1), \end{aligned} \quad (4.14)$$

$$\begin{aligned} -\frac{1}{4\pi l_B} \nabla^2 \Phi(\mathbf{r}) = & \rho_0 \left[\sum_i z_i \varphi_i(\mathbf{r}) \right. \\ & \left. + z_{PH} + \alpha_P \alpha(\mathbf{r}) \varphi_P(\mathbf{r}) + z_D - \alpha_D(\mathbf{r}) \varphi_D(\mathbf{r}) \right], \end{aligned} \quad (4.15)$$

$$\alpha_D(r) = \frac{1}{1 + \rho_0 \varphi_{H^+}(r) / K_{a,D}}, \quad (4.16)$$

and

$$\alpha(r) = \frac{1}{1 + \rho_0 \varphi_{OH^-}(r) / K_{b,P}}. \quad (4.17)$$

In the above,

$$\varphi_P(\mathbf{r}) = \frac{\eta_P \bar{\varphi}_P N}{M(g) Q_{PG}} \sum_{i=0}^g \Omega_i \int_{s_i}^{s_{i+1}} ds q(\mathbf{r}, s) q^\dagger(\mathbf{r}, s), \quad (4.18)$$

$$\varphi_G(\mathbf{r}) = \frac{\eta_G \bar{\varphi}_G N}{M_G(g) Q_{PG}} \Omega_g \int_{s_{g+1}}^{s_{end}} ds q(\mathbf{r}, s) q^\dagger(\mathbf{r}, s), \quad (4.19)$$

$$\varphi_D(\mathbf{r}) = \frac{\varphi_{D,b}}{\exp(-\chi_{DS} \varphi_{S,b})} \exp[-w_D(\mathbf{r})/N], \quad (4.20)$$

where $N = (g + 1)n + N_G$ is the contour length from the center of the dendrimer to the edge of the grafted chain, $\eta_j = v_j \rho_0$, with v_j being the volume of a j^{th} molecule of the j^{th} type, and Ω_i is the number of branches in the i^{th} generation. The electrostatic potential, $\Phi(\mathbf{r})$, is solved using the resulting Poisson-Boltzmann (PB) equation (Eq. 4.15). We refer the reader to Sec.2.4.1 for the corresponding PB equation boundary conditions.

We employed the Crank-Nicholson finite difference scheme [35,137] to solve the partial differential equations for $q(r, s)$ and $q^\dagger(r, s)$ in Eqs. 4.7 and 4.8 respectively. We solve these equations on a lattice, which is non-dimensionalized by $R_g = \sqrt{Na^2/6}$. We used a cell size of $75R_g$ such that the electrostatic potential at the edge of the cell was less than 0.001, ($\Phi(r = r_{max}) < 0.001$) in order to satisfy the electrostatic potential boundary condition, Eq. 2.39. Random initial values for the fields were applied, and the field values were solved via a Picard iteration scheme [34]. We used a convergence criteria which imposed that the largest absolute value of the error in the fields from their self-consistent values was less than or equal to 0.0001.

4.2.1 Parameters

In all our parametric studies, we modeled the dendrimers as having a functionality of $f = 3$ and a spacer length of $n = 5$ monomers. Our results are

for third generation ($g = 3$) dendrimers, and the grafting lengths were varied from $N_G = 0$ to $N_G = 60$. In each of our calculations, we fixed the average dendrimer monomer fraction, represented as:

$$\bar{\varphi}_P = \frac{Mv_0}{V}, \quad (4.21)$$

where v_0 is the monomer volume (equal to $a^3 = \rho_0^{-1}$, where a is the Kuhn segment length). The fraction of monomers that are capable of charge dissociation is fixed to be $\alpha_P = 0.5$. However, we note that the local fraction of dissociated monomers in the dendrimer, denoted as $\alpha(r)$, varies in space and is a function of the local OH^- concentration and monomer $pK_{b,P}$. The actual fraction of dissociated monomers, $\bar{\alpha}$, is then given as:

$$\bar{\alpha} = \frac{\alpha_P \int_0^\infty dr r^2 \alpha(r) \rho_P(r)}{\int_0^\infty dr r^2 \rho_P(r)}. \quad (4.22)$$

The high degree of branching associated with polyelectrolyte dendrimers results in a high density of charged monomers within the dendrimer and makes localization of the OH^- counterions energetically favorable at equilibrium. Increasing the local concentration of OH^- ions results in a decreased probability of monomer dissociation (through Eq. 3.2). Thus, $\bar{\alpha}$ is always less than the fraction of monomers that can participate in the charge dissociation reaction ($\bar{\alpha} < \alpha_P \alpha_b$) [86].

Although there have been experimental studies on the encapsulation of multivalent drug molecules [65, 152, 184], in the present model we assume that each drug molecule is monovalent and is capable of carrying one e^- of charge.

When we vary the size of the drug molecules, the normalized valency of the drug molecule varies as $z_{D^-} = -1.0/(\rho_0 v_D)$. Hence in our model, larger drug molecules have lower normalized charge densities.

We made the dendrimer monomers slightly hydrophobic and the grafted monomers slightly hydrophilic by setting $\chi_{PS} = -\chi_{GS} = 0.05$. In all our simulations we set $-\chi_{PD} = \chi_{DS}$ to reduce the number of parameters probed. Furthermore, we account only for excluded volume interactions between the drugs and dendrimer grafts by setting $\chi_{GD} = 0.0$. We fixed the number density of drugs in the bulk (molarity) by setting $\varphi_{D,b}\rho_0/(\exp(-\chi_{DS}\varphi_{S,b})v_D)$ at a constant value of 5.0×10^{-4} . This value was chosen to be of the order of the values requisite to witness drug encapsulation comparable to that observed under experimental conditions [55, 65, 68, 115, 152]. The solution screening length, κ^{-1} , is given by $\kappa^2 = 4\pi l_B \sum_i c_i z_i^2$ (where c_i is the concentration of ion species i) and was fixed to be $3a$ (where a is the Kuhn segment length and is assumed to be 0.7 nm, the Bjerrum length of water). The $pK_{b,P}$ of the annealed dendrimers and $pK_{a,D}$ of the drug molecules were fixed at 5.0, which when converted into units of molecules/ a^{-3} corresponds to a value of 5.621. Since our studies were performed at constant screening length conditions, we adjusted the bulk salt concentration appropriately with changes in other physicochemical parameters as to keep κ^{-1} a constant. The effect of electrostatic interactions on the drug encapsulation was probed by varying the solution Bjerrum length from $1a$ to $6a$. Changing the Bjerrum lengths require changing the dielectric constant of the solvent and can be expected to modify the dissociation constants of the

different components. However, we ignored such effects and treat l_B only as a parameter to vary the strength of the electrostatic interactions.

4.3 Results and Discussion

In this section, we display results which elucidate the influence of neutral grafts on the complexation between polybasic dendrimers and drug molecules. Preliminary to examining drug encapsulation, in Section 4.3.1 we first quantify the effect of the grafts on the conformations of the dendrimers in the absence of drugs. While this issue has been studied by other researchers and reported in earlier publications [76, 77, 190, 191], we still undertake this study to examine the correspondence between the results of the coarse-grained model (used in our study) and the earlier results. Moreover, many characteristics of the drug encapsulation results presented in the subsequent sections are shown to be a consequence of the influence of the grafts upon the conformations of the dendrimers themselves. Therefore, cataloging such conformational changes provides a means for us to understand the mechanisms underlying drug encapsulation.

4.3.1 Conformations of Grafted Polyelectrolyte Dendrimers

In Fig. 4.2a, we display the radial variation of the volume fraction profiles of the dendrimer and grafted monomers as a function of the grafting length N_G for charged dendrimers. For all values of N_G , we see that the volume fraction profiles of the dendrimer monomers monotonically decrease from

the center to its periphery. However, as N_G is increased, the volume fraction near the center of the dendrimer is seen to decrease, whereas the corresponding volume fractions at large r are seen to increase. These results suggest that upon increasing the grafting length, the dendrimer profiles transition from a dense core conformation (with a high density near the center) to a shell-like conformation (where more of the dendrimer monomers are located close to the periphery). Similar trends have been previously reported in the MC simulation study for neutral dendrimers by Zhou and Chen [190] and the CG MD simulations of charged PEGylated dendrimers by Lee and Larson [77]. In both studies, the authors attributed such conformational changes to the increased tension in the polymer backbone arising from the steric repulsions involving the additional monomers in the grafted chains. Consistent with above changes in the dendrimer density profiles, the density of grafted monomers near the core of the dendrimer is seen to decrease while the tail of its density profile increases with N_G . These trends also agree with the previous simulations [77, 190], and are again attributed to the increased tension along the backbone of the grafts, which increases with N_G .

Since dendrimers have very high curvature, it is of interest to examine how the density profiles of the dendrimer grafts compare to neutral polymer chains grafted to nanoparticles of comparable size. A quantitative measure of the size of the *dendrimer portion* of the molecule can be obtained by using the second moment of the monomer distribution given as:

$$R_P^2 = \frac{\int_0^\infty dr r^4 \varphi_P(r)}{\int_0^\infty dr r^2 \varphi_P(r)}. \quad (4.23)$$

Using the methodology of Trombly and Ganesan [163], we compare the volume fraction profiles of the dendrimer grafts with spherical nanoparticle graft volume profiles, $\varphi_{NP}(r)$, for nanoparticles having a radius R_P , a grafting density $\sigma = f(f - 1)^g / (4\pi R_P^2)$, and a grafting length of N_G . We observe that the dendrimers with longer grafts more closely mimic the behavior of spherical nanoparticles as compared to the shorter grafting lengths. The differences in the two models can be attributed to backfolding of the dendrimer terminal groups, which in turn results in higher graft penetration within the dendrimer molecule. Although this behavior is even observed for the longest grafts, the tail portion of the dendrimer grafts are observed to approach that seen for the spherical nanoparticles as N_G is increased.

In the context of drug encapsulation discussed in the subsequent sections, the excluded volume steric interactions experienced by the drug molecules are influenced by the total volume fraction of polymer monomers $\varphi_P(r) + \varphi_G(r)$ (displayed explicitly in Fig. 4.2b). It is seen that increasing N_G leads to a slight decrease in the total concentration of polymer monomers near the core of the dendrimer. Such trends can be attributed to a near compensating effect of the decreased dendrimer monomer densities by a corresponding increase in the PEG monomer concentrations near the center of the dendrimer (*c.f.* Fig. 4.2a). However, due to the presence of the graft monomers, the addition of grafts is seen to lead to a much larger radial region over which the polymer monomers are present. Hence, we expect that the steric interactions experienced by the drug molecules will be significantly enhanced with an increase in

N_G .

A related quantity of interest for drug encapsulation is the solvent density profile, $\varphi_S(r)$. Indeed, due to the hydrophobic nature of the drug and the attraction between the drug and dendrimer monomers, drug molecules added to the system can be expected to replace the solvent molecules from the interior of the dendrimer. In the inset of Fig. 4.2b, we display $\varphi_S(r)$ as a function of grafting length. We observe that with increasing N_G there is an enhancement of solvent near the core of the dendrimer, but however such an increase is much less significant compared to the changes in the dendrimer monomer volume fraction profiles. On the other hand, in the shell region of the dendrimer and the region occupied by the grafted molecules, it can be seen that the solvent densities are less than the bulk value. In other words, addition of grafts to the dendrimer leads to a significant enlargement of the regions which are more favorable to hosting the solvophobic drug molecules.

Since drug encapsulation can also be driven by electrostatic interactions, the second property we consider is the influence of grafting upon the effective charge of the dendrimer. In our previous work, we demonstrated that incorporating explicit counterions and polyacid-base dissociation leads to an interplay between gradients in the dissociation profiles of the monomers and the conformations of the dendrimers [86]. To characterize the influence of grafts on such phenomena, in Fig. 4.3a, we display the local probability of dissociation, $\alpha(r)$ (Eq. 4.17), (when $\alpha_P = 0.5$) for a $G3$ dendrimer in a solution of $pOH = pK_{b,P} = 5.621$. In all cases, we notice the effective dissociation,

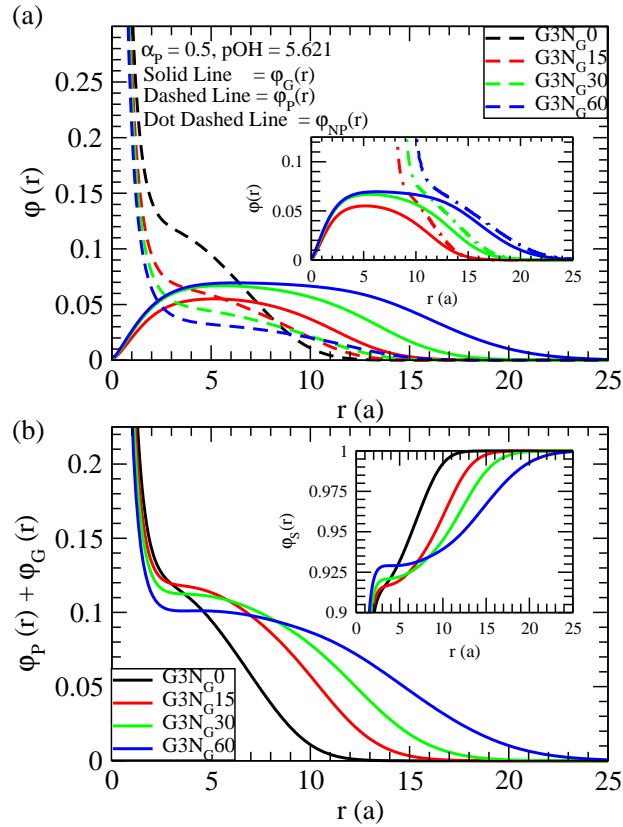


Figure 4.2: (a) The effect of N_G on the dendrimer monomer (dashed lines) and grafted monomer (solid lines) volume fraction profiles when $\alpha_P = 0.5$ and $pOH = 5.621$. The inset compares the dendrimer graft volume fraction profiles with graft volume fraction profiles of spherical nanoparticles (ϕ_{NP}) having a radius of R_P . (b) The effect of N_G on the total volume fraction of polymer monomers. The inset displays the effect of grafting length, N_G , on the solvent volume fraction profiles. The conditions correspond to $\alpha_P = 0.5$, G3 dendrimers in a solution pOH of 5.621.

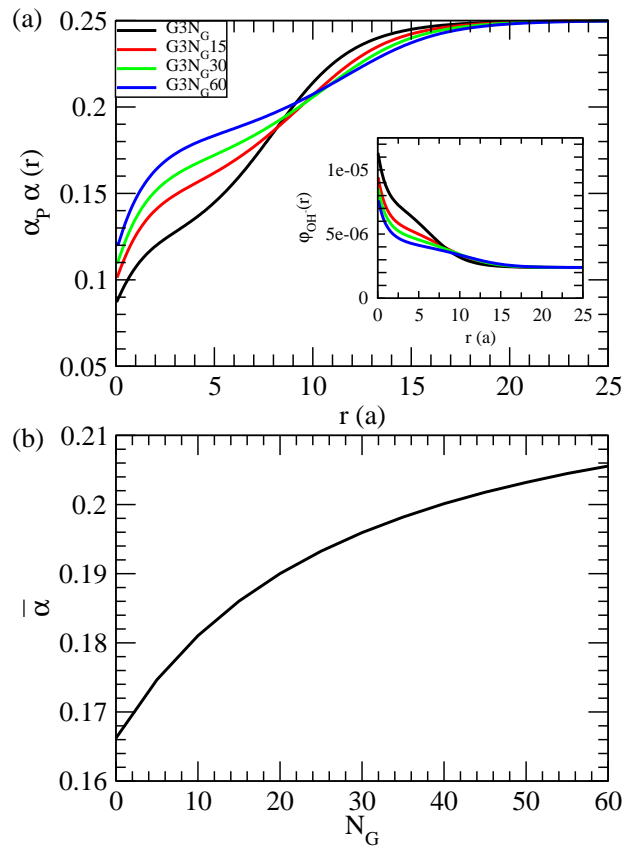


Figure 4.3: (a) The effect of grafting length on the local fraction of charge dissociated monomers. The inset displays the local OH^- concentration. (b) The effect of N_G on the average dendrimer charge for $l_B = 1.0a$.

$\alpha(r)$, increases from the dendrimer center to its periphery. This behavior of $\alpha(r)$ can be understood by noting that the central region of the dendrimer possesses a significant density of charged monomers. Correspondingly, there is also significant OH^- localization (see inset of Fig. 4.3a) as a result of the attraction between the high density of charged dendrimer monomers and the negatively charged OH^- counterions. Hence the effective charge is lowest at the center. Increasing N_G is seen to result in higher monomer charge dissociation near the center of the dendrimer, whereas the tail of the dissociation profile is seen to become reduced. However, the overall effective charge fraction carried by the dendrimers, $\bar{\alpha}$, is seen to increase with increasing N_G (*c.f.* Fig. 4.3b). These results can be explained by recalling that as N_G is increased, the local monomer density (and hence the charge density) near the center of the dendrimer decreases (Fig. 4.2a). As a consequence, the local OH^- ion densities can also be expected to decrease, thereby resulting in a higher effective dissociation near the center of the dendrimer.

Since dendrimers used for drug delivery applications are expected to be exposed to conditions of varying pOH [141], it is of interest to examine how the solution pOH affects the dependence of the net effective dissociation, $\bar{\alpha}$, on N_G . In Fig. 4.4a we display $\bar{\alpha}(N_G)$ for solution conditions corresponding to $pOH = 4.621, 5.621, \text{ and } 7.621$. Qualitatively consistent with the results of Fig. 4.3b, $\bar{\alpha}$ monotonically increases with increasing N_G for all values of pOH . However, the steepness in the variation of $\bar{\alpha}$ (with respect to N_G) is seen to be largest for the case when $pOH = pK_{b,P} = 5.5621$. These results can

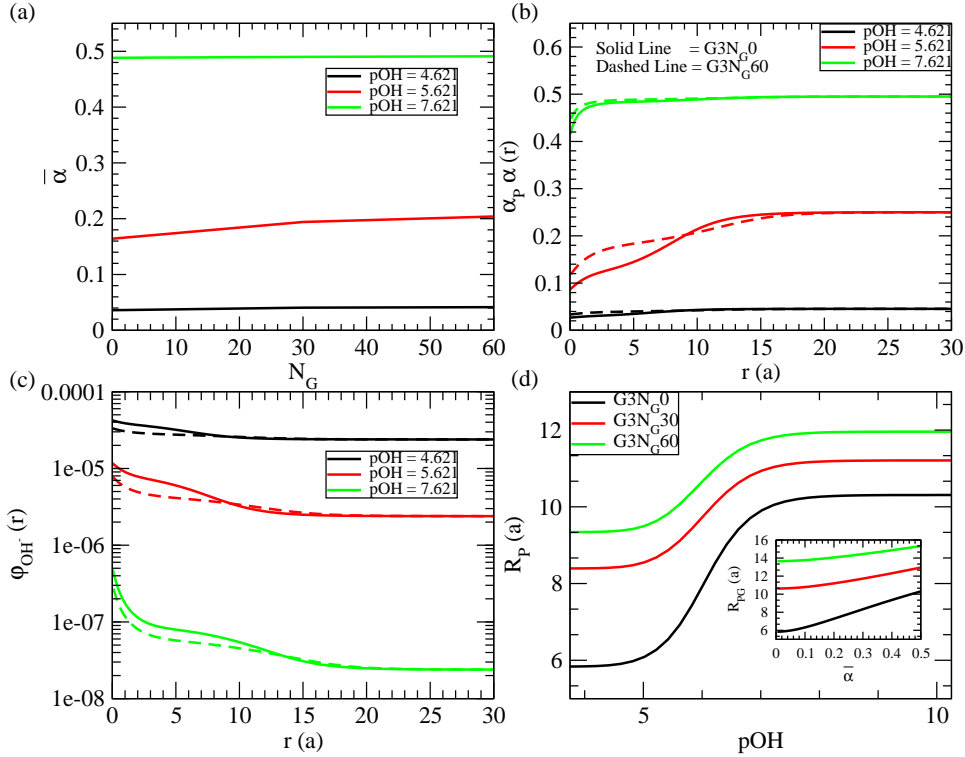


Figure 4.4: (a) The effect of N_G on the charge fraction carried by $G3$, $\alpha_P = 0.5$ dendrimers for $pOH = 4.621$ (black), 5.621 (red), and 7.621 (green). (b) The dissociation profiles for $G3N_G0$ (solid lines) and $G3N_G60$ dendrimers (dashed lines) for $pOH = 4.621$ (black), 5.621 (red), and 7.621 (green). (c) The OH^- volume fraction profiles corresponding to the $\alpha(r)$ profiles in (b). (d) The effect of pOH on the size of $G3N_G0$ (black), $G3N_G30$ (red), and $G3N_G60$ (green) dendrimers. The inset displays the effect of $\bar{\alpha}$ on R_p .

be rationalized by examining the dissociation profiles for the grafted and non-grafted dendrimers at different pOH values, which is displayed in Fig. 4.4b. At low pOH (red lines) we observe that there are not much differences in $\alpha(r)$ between grafted and non-grafted dendrimers. This can be rationalized through the OH^- volume fraction profiles displayed in Fig. 4.4c. For lower

pOH ($pOH = 4.621$), the bulk concentration of OH^- ions is large, and hence, there is significant localization of OH^- ions near the center of the dendrimer, causing $\bar{\alpha}$ to be low. In this situation, increasing the length of the grafts only slightly influences the total charge carried by the dendrimers, and hence $\bar{\alpha}$ exhibits only little sensitivity to N_G . However, when the pOH is comparable to $pK_{b,P}$ (corresponding to the case where $pOH = 5.621$), we observe that $\alpha(r)$ exhibits significant differences between grafted and non-grafted cases. When the $pOH = pK_{b,P}$, slight changes in the local OH^- concentration can result in significant changes in $\alpha(r)$. Since OH^- concentrations are in turn related to the local dendrimer monomer concentrations, the variations induced in the latter through the presence of grafts, acquire more significance. Finally, when the solution $pOH > pK_b$ ($pOH = 7.621$), the bulk OH^- ion concentration is low (see green curves in Fig. 4.4c) and allows for a substantial amount of charge dissociation. Although the local OH^- concentrations within the dendrimer increases with increasing N_G , its effect on α is seen in Fig. 4.4b to be relatively weak due to the relatively large difference in pOH and $pK_{b,P}$. Thus, the effect of N_G on $\bar{\alpha}$ is also seen to be much weaker when $pOH > pK_b$.

In our previous work [84], we observed that increasing the solution pOH of *non-grafted* weakly basic dendrimers resulted in larger dendrimer sizes due to the enhanced electrostatic repulsions. In Fig. 4.4d, we depict the results for the dependence of R_P on $\bar{\alpha}$ and compare the results for the grafted and non-grafted dendrimers. While qualitatively the behavior of the grafted and non-grafted dendrimers is similar, we notice that the size of the non-grafted

dendrimers is more sensitive to changes in pOH and $\bar{\alpha}$ as compared to the grafted dendrimers. The reduced sensitivity of grafted dendrimers to pOH and electrostatic effects can be attributed to the more dominant role of steric repulsions that accompanies the presence of grafted chains.

The inset of Fig. 4.4d displays the root second moment values for the dendrimer and graft portions of the conjugates, R_{PG} , as a function of the dendrimer charge fraction. Similar to the trends observed for R_P , we observe a decreased dependence of R_{PG} with respect to $\bar{\alpha}$ with increasing N_G . In the experiments performed by Kojima *et al.* [65], the hydrodynamic radii of the dendrimer conjugates were measured and were found to increase from 3.5 nm to 6.4 nm (1 : 1.83 ratio) upon the conjugation of PEG (550) chains to the dendrimer periphery. For our system, a grafted chain of $N_G = 25$ corresponds to a molecular weight of 560. When $\bar{\alpha} = 0$, we observe that increasing grafting length from $N_G = 0$ to $N_G = 25$ causes R_{PG} to increase from $5.8a$ to $10.0a$ (1 : 1.71 ratio, data not shown), which is in good agreement both with the experiments of Kojima *et al.* [65] and previous simulations by Zhou and Chen [190].

In sum, we observe that the addition of grafted chains to the dendrimer results in a stretching on the dendrimer backbone, which arises from the steric repulsions from the grafted monomers. However, the density profiles of the polymer monomers were seen to be practically unchanged near the core of the dendrimer, which suggested that the decreased density of the dendrimers monomers are compensated by the grafts. However, addition of grafts was

seen to result in a larger extent of polymer monomers as well as an enlarged regions favorable for hosting solvophobic molecules. Our results also indicated that increasing the graft length results in a slightly higher charge carried by the dendrimer. However, the sensitivity of $\bar{\alpha}$ with respect to N_G was seen to be highest when the solution pOH is close to the $pK_{b,P}$ of the dendrimer monomers, but became much more reduced at lower and higher $pOHs$.

4.3.2 Encapsulation of Drugs in Dendrimers: Quantities of Interest

In the following sections we quantify the influence of polymer grafts on the encapsulation efficacy of dendrimer molecules in the presence of drugs. Our SCFT calculations yield the equilibrium volume fraction profiles of the drug molecules, $\varphi_D(r)$. We also quantify the encapsulation efficacy of the dendrimers through an “excess adsorption” measure, given as:

$$\varphi_{D,excess} = 4\pi \int_0^{\infty} dr [\varphi_D(r) - \varphi_{D,b}] r^2. \quad (4.24)$$

In turn, the *number* of encapsulated drug particles $N_{D,excess}$ can be found as:

$$N_{D,excess} = \varphi_{D,excess}/v_D. \quad (4.25)$$

In the present work, we investigate the influence of grafting length on the encapsulation efficacy ($\varphi_{D,excess}$ or equivalently $N_{D,excess}$) of the polybasic dendrimers and elucidate the physics in terms of the dendrimer conformations discussed in Sec. 4.3.1. We first examine the case where neither electrostatic nor enthalpic interactions are present ($z_{D^-} = 0.0$; $\chi_{PD} = \chi_{DS} = 0$). We then

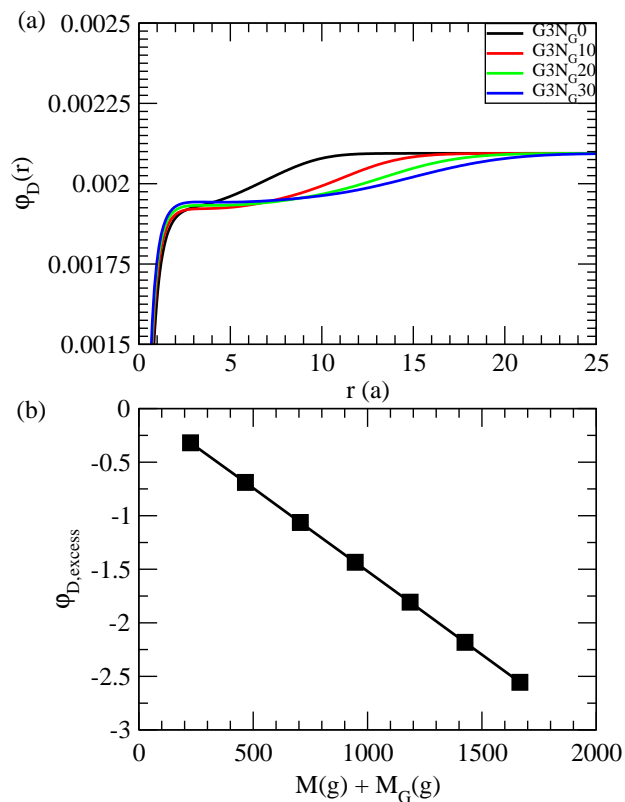


Figure 4.5: (a) The effect of grafting length on the drug molecule volume fraction density profiles. (b) The effect of N_G on drug encapsulation, $\phi_{D,excess}$, for $G3$, $n = 5$ dendrimers.

individually incorporate electrostatic interactions and enthalpic interactions individually to clarify their influence upon the drug encapsulation efficacy of the grafted dendrimers. Finally, we examine the effect of combining both electrostatic and enthalpic interactions and compare the encapsulation efficacy of the grafted dendrimers against the non-grafted counterparts.

4.3.3 Influence of Excluded Volume Interactions

In this section we consider the case for which the only interactions between the drugs and the dendrimer molecules are the excluded volume interactions accounted through Eq. 3.8. This situation corresponds to a scenario where the drug molecules are *soluble* in the solvent ($\chi_{DS} = 0.0$) and will be excluded from the dendrimer due to steric excluded volume interactions. We examine this (admittedly) academic scenario mainly as a base case to quantify the relative influences of the electrostatic and enthalpic interactions on the solubilization of drugs. In our earlier work [84], we observed that inclusion of just excluded volume interactions between the dendrimer and drugs resulted in depletion of the drugs (negative values of $\varphi_{D,excess}$) for all parametric conditions of drug sizes and generation numbers. In this section, we quantify the influence of grafting chain length on the depletion of the drugs.

Figure 4.5a displays the effect of increasing N_G on the volume fraction profiles of the drug molecules, in which we witness depletion of drug molecules for all N_G . As N_G increases, the local concentration of drug particles near the center of the dendrimer slightly increases, but the tail of the depletion profile of $\varphi_D(r)$ is seen to extend to longer radial distances. This behavior, which can be rationalized as a consequence of the steric interactions between the drug and the dendrimer (and graft) molecules, is seen to qualitatively mirror the behavior of polymer monomer volume fractions profiles ($\varphi_P(r) + \varphi_G(r)$) displayed in Fig. 4.2b. Despite the slight enhancement of the drug concentrations in the core region with increasing N_G , the depletion arising

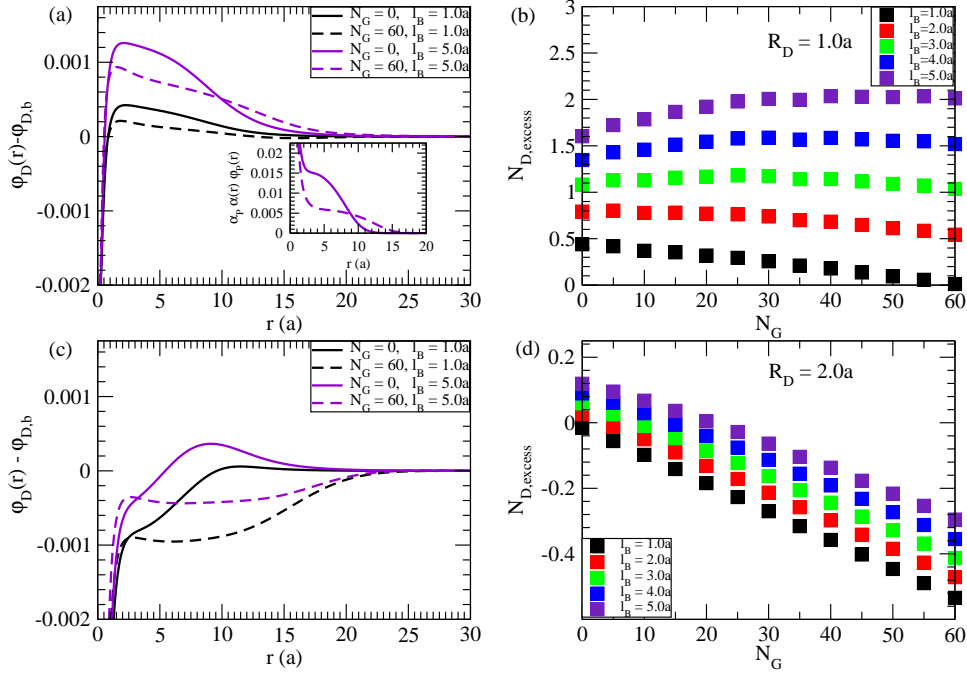


Figure 4.6: The effect of N_G and l_B on the drug volume fraction profiles and number of drug particles encapsulated when $R_D = 1.0a$ ((a) and (b)), and $2.0a$ ((c) and (d)).

from total volume occupied by dendrimer and graft monomers is much more significant and increases with N_G . Therefore, we can expect that the total amount of depleted drugs will increase with increasing N_G — an expectation which is confirmed by the results displayed in Fig. 4.5b.

4.3.4 Influence of Electrostatic Interactions

Electrostatic interactions between basic groups on the dendrimer and acidic drug molecules have been reported to be a significant factor in drug-dendrimer complexation [5, 21, 130, 184]. In Fig. 4.6a, four examples of drug

volume fraction profiles of the $R_D = 1.0a$ drugs are displayed. Not surprisingly, we see that there is an enhancement of the volume fractions of the drugs with increasing l_B , which can be attributed to the increase in the strength of electrostatic interactions. For the cases where $l_B = 1.0a$, we notice that the densities of the drugs in the both the core and the periphery regions of the dendrimer decreases as N_G is increased. In contrast, when l_B is large ($l_B = 5.0a$), we see that while the drug volume fraction profiles near the dendrimer center still decreases with increasing N_G , the drug volume fractions in the periphery of the dendrimer increase with increasing N_G .

To understand the above results, we note that (in the present section) the drug encapsulation tendencies are determined by an interplay between the steric interactions experienced by the drug molecules and the electrostatic attractions between the dendrimer monomers and the drug molecules. Increasing N_G results in a decrease in the density of charged monomers in the core region and a segregation to further radial values (see inset of Fig. 4.6a). As a consequence, the densities of the drug molecules in the core region also decreases. The behavior of the density of the drugs in the periphery region is determined by an interplay between the enhanced steric repulsions arising from the grafted chains (Fig. 4.2b) and the enhanced electrostatic interactions arising from the presence of a larger concentration of charged monomers (see the inset of Fig. 4.6a). For weak electrostatic interactions ($l_B = 1.0a$) and longer grafts, steric interactions are expected to dominate, and therefore addition of grafts decreases the density of drugs at the periphery. In contrast, for

strong electrostatic interactions and smaller grafts, electrostatic interactions lead to an enhancement in drug concentrations in the periphery relative to the ungrafted cases.

In Fig. 4.6b, we display the corresponding $N_{D,excess}$ values as l_B is varied. Consistent with the above discussion, at low l_B , the encapsulation efficacy of the drug molecules is seen to decrease with increasing N_G . However, at higher l_B values, $N_{D,excess}$ is seen to increase at lower N_G due to electrostatic interactions but then decreases at larger N_G due to the increased importance of steric interactions.

In our previous study [84], we observed that drug encapsulation through electrostatic complexation was a strong function of the volumetric charge density of the drug. Recall that the normalized valency of the drug molecule varies as $z_{D^-} = -1.0/(\rho_0 v_D)$. Hence in our model, larger drug molecules have lower normalized charge densities, and correspondingly weaker electrostatic interactions. In Fig. 4.6c we display the effect of changing N_G and l_B on the volume fraction profiles of larger ($R_D = 2.0a$) drugs. Consistent with our previous results [84] and the above discussion in the context of $R_D = 1.0a$, we observe that for the larger drugs, addition of grafts leads to a reduction in the density of the drugs both near the center and the periphery region of the dendrimer. Figure 4.6d displays $N_{D,excess}$ as a function of l_B and N_G . Consistent with the behavior of the density profiles, we observe a monotonic decrease in the encapsulation efficacy of the dendrimers for all N_G .

In sum, the results of Fig. 4.6 indicate that the drugs will be encap-

sulated within the dendrimer only if the charge density of the drugs and the solution l_B is high enough to overcome the excluded volume interactions. If the drug charge density is high enough, drug loading is seen to initially increase with increasing N_G , but then subsequently decreases with further lengthening of the grafts. In all the other cases, encapsulation was seen to monotonically decrease with increasing N_G . We note that the results presented here correspond to the case where the $pOH = pK_{b,P}$, for which we demonstrated in Fig. 4.4a that the electrostatic effects are most sensitive to N_G . However, if the solution pOH is much different from the dendrimer $pK_{b,P}$, then the increase of charge with increasing N_G will likely not be sufficient to overcome the enhancement in the steric interactions, and we expect to see only a small regime for which $N_{D,excess}$ is positive.

4.3.5 Effects of Enthalpic Interactions on Drug Encapsulation

In this section we present results which model the influence of hydrogen bonding and hydrophobic interactions (in conjunction with the excluded volume steric interactions) upon encapsulation of drugs.

The effects of χ_{PD} and χ_{DS} (in our model, we set $\chi_{PD} = -\chi_{DS}$) on encapsulation efficacy for $G3$ dendrimers of various N_G are displayed in Fig. 4.7a. Not surprisingly, we observe increased encapsulation with an increase in the magnitude of the attraction between the drug and the polymer (χ_{PD}). More pertinently, this trend is seen to hold for all N_G . We notice three interesting general trends in the data presented in Fig. 4.7a. When the dendrimer-drug

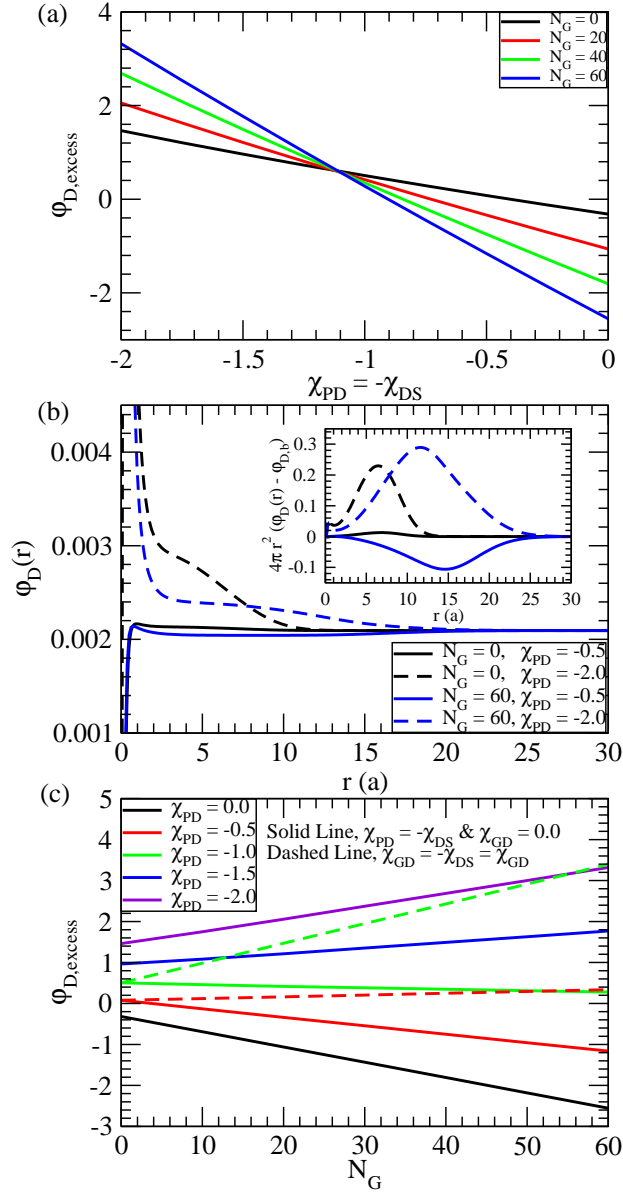


Figure 4.7: (a) Effect of χ_{PD} and χ_{DS} on $\phi_{D,excess}$. (b) Drug volume fraction profiles for $N_G = 0$ (black lines) and $N_G = 60$ (blue lines) dendrimers when $\chi_{PD} = -0.5$ (solid lines) and $\chi_{PD} = -2.0$ (dashed lines). (c) Effect of N_G on the $\phi_{D,excess}$ for varying χ_{PD} and χ_{DS} . Solid lines correspond to the case when $\chi_{GD} = 0$. Dashed lines correspond to the case when $\chi_{GD} = \chi_{PD}$.

attraction is low, net depletion of the drug (as reflected in the negative value for $\varphi_{D,excess}$) from the dendrimer occurs, with a larger depletion occurring for larger values of N_G . When the magnitude of χ_{DS} is increased, net encapsulation begins to occur (positive values of $\varphi_{D,excess}$), with an intermediate regime of χ_{DS} in which highest encapsulation efficacy occurs for the non-grafted dendrimers. However, when χ_{DS} becomes greater than a critical value, increasing N_G is seen to monotonically increase the $\varphi_{D,excess}$.

The above trends can be rationalized by noting that the encapsulation efficiencies (in this section) are determined by an interplay of three factors: (i) steric interactions of the drug molecules with the polymer monomers (Fig. 4.2b); (ii) presence of a more favorable environment for solvophobic molecules inside the dendrimers (inset of Fig. 4.2b); and (iii) enthalpic attractions between the drug molecules and the dendrimer monomers (Fig. 4.2a). Increasing N_G serves to increase the steric interactions (factor (i)), but also enhances the solvophobic region (factor (ii)) and the extent of the density profiles of the dendrimer monomers (factor (iii)).

When the drug molecules are only weakly hydrophobic (which also corresponds to weaker attraction between the dendrimer and drugs, since $\chi_{PD} = -\chi_{DS}$), the driving forces from attractions are not strong enough to overcome the steric interactions, and hence there is depletion of the drug from the dendrimer. In such a case, increasing N_G leads to a larger depletion due to the enhancement in the steric interactions. Such trends are clearly borne out in Fig. 4.7b (when $\chi_{PD} = -0.5$), wherein we compare the $\varphi_D(r)$ profiles

(also displayed as $4\pi r^2[\varphi_D(r) - \varphi_{D,b}]$ in the inset) for $N_G = 0$ (black lines) and $N_G = 60$ (blue lines) dendrimers. These considerations lead to a negative slope of $\varphi_{D,excess}$ with respect to N_G at small negative χ_{PD} as displayed in Fig. 4.7c.

For stronger drug-dendrimer attractions ($\chi_{PD} = -2.0$), we see that both $N_G = 0$ and $N_G = 30$ dendrimers are capable of encapsulating drugs (reflected in the enhanced local drug volume fraction values over the bulk values in Fig. 4.7b), and the total amount of encapsulation is seen to increase with N_G (see Fig. 4.7c). Under these conditions, the presence of a larger solvophobic region inside the dendrimer and the hydrogen bonding attractions between the drugs and dendrimer monomers are able to overcome the enhanced steric interactions arising from increased N_G .

We note that in our study, the interaction between the drug and grafts was assumed to be zero ($\chi_{GD} = 0.0$) in order to simplify our parameter studies. However, we expect the encapsulation efficacy of the grafted dendrimers to be larger if strong enough enthalpic attractions between the grafts and drug are present. To verify this hypothesis, we modified our model to include an attraction between the drug molecules and the grafts, and quantified its strength through a Flory-Huggins like interaction parameter χ_{GD} . Further, to reduce the number of parametric choices, we adopted $\chi_{GD} = \chi_{PD}$. The corresponding results are displayed in Fig. 4.7b (dashed lines), wherein it is seen that the grafted dendrimer system displays positive values of encapsulation for all the N_G probed. Moreover, $\varphi_{D,excess}$ exhibits a positive slope with N_G , suggesting

that encapsulation increases with increasing with increasing graft lengths.

In sum, we observe that encapsulation of hydrophobic drugs is expected to be higher for grafted dendrimers only if the enthalpic attractions between the dendrimer and drug are sufficiently high. If the enthalpic interactions are not strong enough, the less grafted dendrimers display higher encapsulation efficacy. However, inclusion of enthalpic attractions between the drugs and the grafts was seen to enlarge the regime of graft lengths over which positive encapsulation is observed. Although we cannot make a quantitative comparison, our results qualitatively agree with the experiments of Kojima *et al.*, which displayed that increasing PEG lengths resulted in higher encapsulation values for the hydrophobic adriamycin drug molecules.

4.3.6 Combined Influence of Electrostatic and Enthalpic Interactions

In this section we address the combined effects of electrostatic and enthalpic interactions by presenting results for the situation when all the interactions are simultaneously present. In our previous study [84], we observed that when electrostatic and enthalpic attractive interactions were combined, a synergy was observed between the interactions in promoting the encapsulation to levels beyond the sum of the individual contributions. Here we examine the effect of N_G on encapsulation efficacy of the grafted dendrimers and compare it to that of the non-grafted dendrimers. To facilitate this comparison we

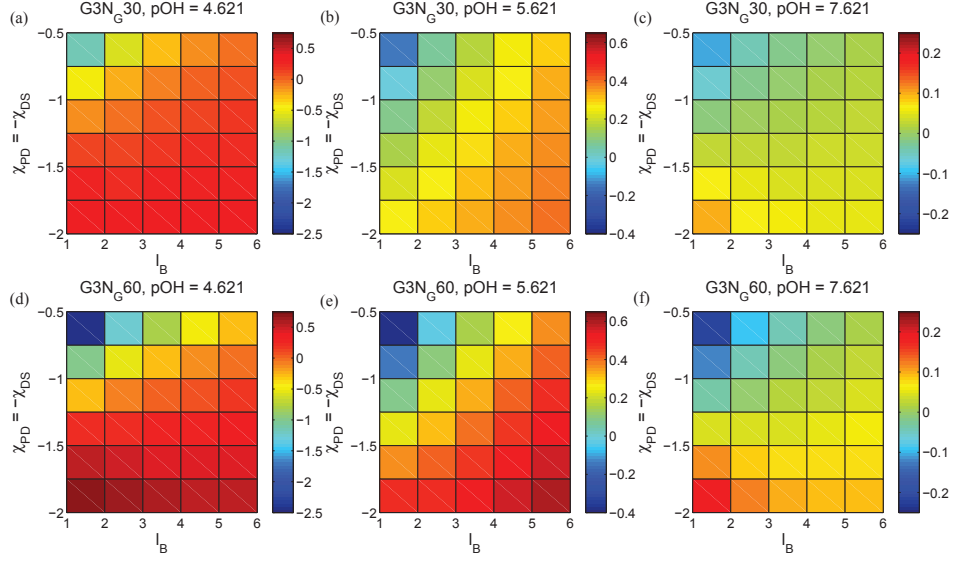


Figure 4.8: $\Phi_{D,excess}$ observed for a $G3N_G30$ ((a)-(c)) and $G3N_G60$ ((d)-(f)) dendrimers in the presence of $R_D = 1.0a$ drug molecules in a solution of $pOH = 4.621$ ((a) and (d)), 5.621 ((b) and (e)), and 7.621 ((c) and (f)).

consider a quantity:

$$\Phi_{D,excess} = \frac{\varphi_{D,excess,grafted} - \varphi_{D,excess,non-grafted}}{\varphi_{D,excess,non-grafted}}. \quad (4.26)$$

Figure 4.8 displays color plots of the $\Phi_{D,excess}$ values for $N_G = 30$ and $N_G = 60$ dendrimers under varying solution pOH conditions, l_B , and χ_{PD} ($= -\chi_{DS}$) values. It is seen that for both $N_G = 30$ and $N_G = 60$, $\Phi_{D,excess}$ values are only positive for sufficiently strong enthalpic and electrostatic conditions. At small l_B and χ_{PD} values, the non-grafted dendrimers are seen to encapsulate more drugs, with the encapsulation of the $N_G = 60$ dendrimers being the lowest. For $\chi_{PD} < -1.25$ we observe enhanced encapsulation by the grafted dendrimers for all values of l_B . When $\chi_{PD} > -1.25$, we see some positive

$\Phi_{D,excess}$ values for the relatively high l_B scenarios. Under these conditions, the higher charge carried by the dendrimer and the resulting electrostatic interactions results in higher encapsulation efficacy by the grafted dendrimers.

Interestingly, the $N_G = 60$, $pOH = 5.621$ ($= pK_{b,P}$) case provides the largest parameter space with positive values of $\Phi_{D,excess}$. This result can be understood in the context of the discussion accompanying Fig. 4.4a. Therein we witnessed that $\bar{\alpha}$ is most sensitive to N_G when the solution $pOH = pK_{b,P}$. Thus, the influence of grafting is expected to be most significant when $pOH = pK_{b,P}$. In contrast, when there are significant differences in solution pOH and dendrimer $pK_{b,P}$, we expect the increase in local hydrophobicity (*i.e.* the enthalpic interactions) created by the dendrimer grafts to be the more influential mechanism driving the complexation of the grafted dendrimers over the non-grafted counterparts, and hence higher encapsulation is observed only in grafted dendrimers at large χ_{PD} values.

4.4 Summary

In this chapter, we have examined the influence of neutral dendrimer grafts upon the conformations of weakly basic polyelectrolyte dendrimers and the encapsulation of weakly acidic drug molecules. With increasing dendrimer grafting length, the dendrimers were shown to transition from a dense core-like conformation to a dense shell-like conformation. The swelling caused by increasing grafting length in turn resulted in an increase in charge carried by the dendrimer. The dendrimer conformations of the grafted dendrimers were

seen to be less sensitive to changes in solution pOH conditions as compared to non-grafted counterparts, which makes the former less “tunable” with respect to salt concentration and pOH than non-grafted dendrimers.

We also presented results which quantified the effect of grafting length on the encapsulation of drugs by dendrimer molecules. We observed that increasing the strength of the enthalpic interactions resulted in a relative increase in the encapsulation efficacy of the grafted dendrimers as compared to the non-grafted dendrimers. The more highly grafted dendrimers were seen to exhibit better electrostatic encapsulation ability than non-grafted dendrimers, which was attributed to the fact that they carry more charge due to increased swelling that accompanies the more highly grafted dendrimers. However, at large N_G , the steric interactions were seen to become dominant and result in a decrease in encapsulation with an increase in N_G . Isolation of the enthalpic effects showed that the non-grafted dendrimers were better at drug encapsulation at lower values of the enthalpic attraction parameters, but however, the encapsulation efficacy was seen to increase with grafting length for stronger enthalpic attractions. The results presented in the work serve to highlight the complex physics involved in the drug encapsulation by grafted dendrimers and suggest that a careful tuning of the parameter space may be necessary to achieve higher complexation relative to the non-grafted counterparts.

Chapter 5

Role of Neutral Grafts and Chain Stiffness on the Binding Between Weakly Basic Dendrimers and Linear Polyelectrolytes

5.1 Introduction

Gene therapy involves the application of therapeutic nucleic acid (NA) materials to manipulate gene expression of targeted cells. Advances in biomedical research have yielded effective gene therapy agents that not only include large plasmids, but also shorter single and double stranded oligomers (*e.g.* antisense oligonucleotides, siRNA, and DNAzymes) of varying flexibility [18, 24, 30, 31, 69, 94, 131, 146, 147, 150, 164, 187, 188]. Successful gene therapy requires the transport of genetic material to targeted cells, permeation of the cell membrane, and endosomal escape before the onset of lysosomal degradation. Serum nucleases in the blood stream rapidly degrade unshielded genetic material, and the negative charge of the NAs hinders their ability to permeate the negatively charged cell membrane. To overcome these challenges, researchers have proposed the use of cationic polymer molecules as gene delivery vectors for NA material. Dendrimers, regularly branched tree-like polymer molecules, which carry amine groups have shown great promise as efficient gene vectors [18, 24, 30, 31, 69, 94, 131, 146, 147, 150, 164, 187, 188], and

advances in their synthesis techniques have allowed researchers to produce highly monodisperse molecules, with precise control over their size, solubility, flexibility, charge, and functionality [3, 23, 162]. Concomitantly, a number of experiments have demonstrated that by controlling one or more of such synthesis parameters, the transfection ability of dendrimers can potentially be optimized against their cytotoxicity [18, 24, 30, 69, 94, 131, 146, 147, 150, 164, 188]. As a result, there is presently an active interest in developing a fundamental understanding on the influence of design characteristics of dendrimer molecules upon their transfection efficiencies.

As a consequence of the vast parameter space available for synthetic chemists, theoretical models and computer simulations have emerged as an attractive means to study complexation phenomena involving dendrimers and model NA materials [159]. The most detailed studies in this regard have used atomistic simulations to study the phenomenology of dendrimer-DNA binding [52, 56, 101, 120, 129, 166]. While such studies have provided valuable insights the binding between dendrimers and NA materials, identification of the physical principles underlying complexation phenomena over a broad parameter space is very computationally expensive in such methodologies. Motivated by these limitations, a number of coarse-grained simulations have modeled the NA material as either a flexible or a semiflexible linear polyelectrolyte (LPE) and studied the physics of their binding with dendrimers [63, 64, 71, 72, 96, 97, 156, 172]. For instance, Welch and Muthukumar used a Monte Carlo (MC) methodology to study the complexes formed between dendrimers and a LPE

[172]. They observed different possibilities for complexation such as the complete encapsulation of the LPE, partial interpenetration between LPE and the dendrimer, etc. Lyulin and coworkers performed a series of Brownian dynamics simulation studies on the influence of the dendrimer/NA charge ratio upon the overall charge of the dendrimer-LPE complexes [71, 72, 96, 97]. They observed that when the charge carried by the LPE molecule exceeded that of the dendrimer molecule, an excess of charged LPE molecules were adsorbed by the dendrimer (overcharging).

More recent studies have examined the effect of LPE rigidities upon the relevant physics of binding. For example, Tian and Ma [156] used coarse-grained MD simulations and observed a decrease in dendrimer-LPE contacts as LPE stiffness increased. Klos and Sommer applied MC simulations to examine the effects of LPE rigidity and chain length on the complexation with non-grafted charged dendrimers under a wide variety of bending energies and electrostatic parameters [64]. Their work demonstrated that dendrimer-LPE complexes (dendriplexes) could be stable even for very stiff chains if the electrostatic interactions are strong enough.

Despite the vast number of theoretical and simulation studies which have studied the binding between dendrimers and linear polyelectrolytes, a few outstanding issues remain which motivated the work we report in this chapter:

(i) *Influence of polymer grafts on the dendrimer-LPE complexation:* A number of experimental studies have shown that the transfection efficiency of

dendrimers is enhanced with increasing dendrimer generation, an effect which has been attributed to the increase in charge carried by the larger generation dendrimers [18, 69, 187]. However, an enhancement of the positive charges carried by the dendrimers also leads to the formation of holes in the anionic cellular membrane, an effect which is cytotoxic [47, 51, 110]. To combat this phenomena, researchers have pursued modification of the dendrimers by covalent conjugation of poly(ethylene glycol) (PEG) chains to the periphery of the dendrimer molecules [30, 31, 146, 147, 150]. For instance, Tack *et al.* examined the effect of PEGylation of the peripheral amines upon the transfection of PPI dendrimer-DNAzyme complexes, and observed that PEGylated dendrimers exhibited high transfection efficiencies [146]. Later studies by Fant *et al.* demonstrated that PEGylation of poly(amidoamine) (PAMAM) dendrimers decreased the binding affinity between the PEGylated dendrimers and the plasmid DNA [30, 31]. The latter has been suggested to be beneficial for the dissociation of the dendrimer complex once inside of the cellular cytoplasm, a necessary step for successful gene transfection [30, 31, 94]. While a number of works have elucidated the effect of neutral and grafts on the structure and dynamics of both charge and uncharged dendrimer molecules [77, 190, 191], there is still a lack of understanding on how dendrimer grafts influence the complexation of dendrimers with LPEs. Some outstanding questions in this regard are: How does the grafting length affect the LPE-dendrimer binding strength? How do grafts affect the shielding/exposure of the LPE molecules? What is the role of grafts upon the resulting dendriplex charges?

(ii) *The role of solution pH on dendrimer-LPE complexation:* In the course of transfection, dendriplexes are exposed to a variety of pH environments. For instance, dendriplexes within the endosome face a low pH environment, leading to the adsorption of H^+ ions by the dendrimer and creating an osmotic pressure which results in the rupture of the membrane [143, 188]. While previous LPE-dendrimer simulations have studied the influence of pH changes upon the properties of dendriplexes by modulating the number of charged monomers [56, 72, 101, 129], an accurate model for weak polyelectrolytes needs to account for acid-base equilibrium effects and their simultaneous influence on LPE binding and conformations. For instance, in a recent work we compared the conformations of weak and strong polyelectrolyte dendrimers and noted several differences arising from the capability of the former to tune the dissociation of charges in response to their conformation and interactions [86]. To our knowledge, there have not been any studies which have examined the influence of such acid-base equilibrium considerations in the context of pH changes to delineate their influence upon the binding between dendrimers and linear polyelectrolytes.

Motivated by the above shortcomings, we report results from coarse-grained modeling of grafted weakly basic dendrimer molecules and charged LPE molecules. In order to elucidate the effect of design parameters on dendriplex formation, we develop a new hybrid approach which combines self-consistent field theory (SCFT) and Monte Carlo simulation. In contrast to an explicit MC or MD simulation simulation of the dendrimer, the LPE, and

counterion species, the methodology we propose provides an expedited approach to access the equilibrium thermodynamics of the system as well as the conformational features of the LPEs. Using such a framework, we examine the effects of dendrimer grafting length, polyelectrolyte chain stiffness, and solution pOH on the dendriplex and LPE chain conformations. The rest of the chapter is arranged as follows. In Section 5.2 we discuss our hybrid SCFT-MC model and the associated terminology. In Section 5.3, we present results that examine the effect of LPE stiffness (Sec. 5.3.1), grafting length (Sec. 5.3.2), and solution pOH (Sec. 5.3.3). In Section 5.4 we conclude with a summary of our results.

5.2 Hybrid Self-Consistent Field Theory and Monte Carlo Approach

As mentioned in the introduction, we develop and apply a hybrid SCFT-MC methodology to study the characteristics of dendrimer-LPE complexes. In a nutshell, the framework of polymer SCFT enumerates the statistical features of an interacting system of polymer chains by considering an equivalent system of noninteracting chains in the presence of pseudo chemical potential fields [35]. These chemical potential fields are further determined in a self-consistent manner to impose the inhomogeneous densities of the appropriate components. Using such a methodology, a density functional theory for the system free energy can be constructed which allows one to deduce the equilibrium composition profiles (i.e. morphologies).

Polymer SCFT allows us to determine the equilibrium density profiles of the dendrimer, LPE, counterions and salt components for specified conditions of dendrimer architecture, LPE stiffness, and solution pOH . However, SCFT by itself is incapable of providing information on certain quantities of interest (*e.g.* conformational features such radius of gyration and the COM distributions of the LPE chains). As a means to access such features, we use the SCFT chemical potential fields as input to MC simulations of non-interacting LPE chains. From the MC simulations, we determine the conformational properties of the LPE chains, specifically, the LPE COM densities and the loop/tail distributions of the complexed LPEs. In our MC simulations, we significantly reduce the system degrees of freedom and the associated computational costs by only considering interactions between individual chains and the SCFT fields. This approach allows us to obtain as much information about the LPEs as would be available by using a much more computationally intensive MC or MD simulation involving all the species in the system. Below we present a more detailed description of the SCFT model and the MC simulation approach.

5.2.1 Self-Consistent Field Theory Model

Our model system is composed of a dendrimer (P) and its grafts (G) in the presence of linear polyelectrolyte molecules (LPE), solvent molecules (S), H^+ and OH^- ions, and monovalent salt ions (denoted as Na^+ and Cl^-). Figure 5.1a presents a schematic representation of a “third generation” dendrimer

(black) with neutral grafted chains (red) attached at the periphery. The 0^{th} generation is comprised of the core monomer and the three stemming branches, and the next generation of dendrimers is comprised of the spacers attached at the end groups of the 0^{th} generation. The “functionality” of the branches denote the number of branches stemming from an individual branch point, and in this notation, the number of monomers, M , comprising a non-conjugated dendrimer molecule is given by:

$$M(g) = nf \left((f - 1)^{g+1} - 1 \right) + 1 \quad (5.1)$$

where n is the number of monomers per spacer, f is the branch point functionality, and g is the generation number. We assume that every terminal group of the dendrimer molecule is grafted with a polymer of length N_G such that the number of monomers in the graft portion of the dendrimer molecule is given as:

$$M_G(g) = N_G f (f - 1)^g. \quad (5.2)$$

We note that during PEGylated dendrimer synthesis, complete PEGylation of the dendrimer primary amines is unlikely to occur due to the steric interactions resulting from PEGylation [45, 94]. However, to simplify our SCFT framework and the number of parameters involved, we assume that every end group of the dendrimer is PEGylated.

Our system is spherically symmetric, with the core dendrimer monomer constrained to the center. In modeling our system, we make the following assumptions:

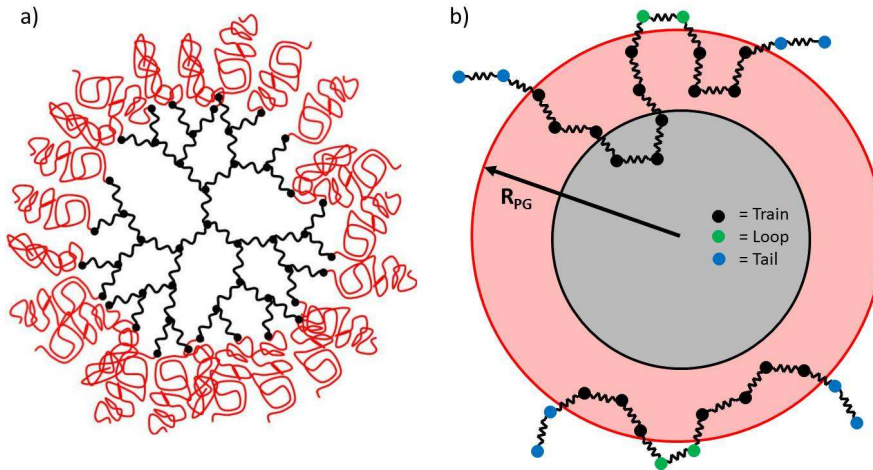


Figure 5.1: (a) Schematic of a grafted 3^{rd} generation dendrimer having a functionality of 3. The dendrimer portion is represented in black, while the grafted portions are represented in red. (b) Schematic visualizing the definition of trains, loops, and tails as measured at the R_{PG} boundary.

(i) We model the dendrimer spacers and neutral grafts as flexible continuous Gaussian chains. We note that in reality, the flexibility of dendrimer spacers is dependent upon the chemistry of the dendrimer monomers [162]. Although previous studies have found that the flexibility of dendrimer molecules affects their conformations [14, 15, 48] and binding affinities with genetic material [132], we treat the spacers as flexible chains in this study to simplify our model and parameter sweep.

(ii) The flexibility of the LPE molecules has been shown to affect dendrimer/LPE complexation [64, 156]. In this study, we assume that the chain is semiflexible and use the wormlike chain model to describe their conformations [35]. To account for the conformations of the LPE molecules in a spherically

symmetric cell, we use a recently developed SCFT framework to access the information of semiflexible polymers in a spherically symmetric system [36].

(iii) We assume that electrostatic interactions are the main attractive forces driving the complexation between the dendrimer and LPE molecules. Thus, we do not include any other enthalpic terms that account for hydrophobic interaction or hydrogen bonding between the dendrimers and LPE. The electrostatic interactions between charged molecules and ions in our system are modeled using a classical Coulomb potential [35], with a spatially constant dielectric value.

(iv) We model the total density of the overall system as almost uniform by including a harmonic compressibility penalty for deviations of the local density from the average density, ρ_0 [13, 119, 180]. Such a penalty reduces the magnitude of the density fluctuations relative to the bulk density, ρ_0 (we assume that only the dendrimer monomers (P), grafted monomers (G), LPE molecules (LPE), and solvent molecules (S) possess volume) [35].

(v) In this work, we treat the dendrimer monomers as weak bases and the drug particles as weak acids by explicitly incorporating the acid-base equilibrium reaction into our framework. We model the charge dissociation of the dendrimer monomers using an approach similar to that adopted in the recent mean field studies for weak PE brushes by Szleifer *et al.* [39, 121, 165] and Won and coworkers [49, 175]. We assume that a fraction, α_P , of the dendrimer monomers carry dissociable charge groups and are capable of becoming charged through the equilibrium reaction given in Eq. 3.1. The equilibrium

constant for the acid-base equilibrium reaction is given by Eq. 3.2. To reduce parametric complexity, we assume that α_P does not change when comparing grafted and non-grafted dendrimers. However, in reality the addition a PEG chain to a dendrimer converts a primary surface amine to an amide bond, which strongly reduces its ability to absorb a hydrogen ion. Thus, our results that compare grafted and non-grafted dendrimers are equivalent to comparing PEGylated and acetylated dendrimers that have the same number of reacted terminal monomers.

(vi) We model the charge on the LPE by using a fixed charge model, where every monomer along the chain carries a charge of $z_{LPE} = -1.0$. This is expected to be reasonable since the phosphate groups present in phosphate-ribose/deoxyribose backbones of RNA and DNA have pK_a values near 0. Thus they are strong acids and will be almost completely charged at physiological conditions.

Using the above assumptions, we develop an equilibrium thermodynamic model for the free energy of the system containing the dendrimer, grafts, solvent, ions, and LPE molecules. We employ a semi-grand canonical framework to describe the free energy of our system, and we solve it within a mean field approximation [35]. In this framework, the free energy \mathcal{F} can be identified as [121]:

$$\mathcal{F} = \mathcal{F}_{conf} + \mathcal{F}_{int} + \mathcal{F}_{comp} + \mathcal{F}_{mix} + \mathcal{F}_{chem} + \mathcal{F}_{elec}. \quad (5.3)$$

The terms \mathcal{F}_{int} , \mathcal{F}_{comp} , \mathcal{F}_{mix} , \mathcal{F}_{chem} , and \mathcal{F}_{elec} are equivalent to Eqs. 3.7, 3.8, 3.9, 3.10, and 3.11 respectively. However, the presence of semi-flexible LPE

molecules in our system requires us to modify the \mathcal{F}_{conf} term. The conformational entropy contribution to the free energy is given by

$$\begin{aligned} \beta\mathcal{F}_{conf} = & \ln Q_{PG} + Q_{LPE} + \rho_0 \int d\mathbf{r} w_P(\mathbf{r}) \varphi_P(\mathbf{r}) \\ & + \rho_0 \int d\mathbf{r} w_G(\mathbf{r}) \varphi_G(\mathbf{r}) + \rho_0 \int d\mathbf{r} w_{LPE}(\mathbf{r}) \varphi_{LPE}(\mathbf{r}), \end{aligned} \quad (5.4)$$

which quantifies the conformational entropy of the grafted dendrimer and linear polyelectrolyte molecules in the external fields $w_P(\mathbf{r})$, $w_G(\mathbf{r})$, and $w_{LPE}(\mathbf{r})$. In the above, Q_{PG} and Q_{LPE} represent the partition functions of the grafted dendrimer and LPE molecules respectively. To obtain these partition functions, we assume that the conformations of the grafted dendrimers can be described using a continuous Gaussian chain model, while the conformations of the LPE molecules can be described using the the Kratky-Porod (KP) model [35].

In the KP model, the bonded interactions are quantified through the elastic bending energy term [35]

$$\beta U_{0,KP} = \frac{\lambda}{2} \sum_{i=0}^{n_{LPE}} \int_0^{N_{LPE}} ds \left| \frac{d\mathbf{u}_i(s)}{ds} \right|^2, \quad (5.5)$$

where $\mathbf{u}_i(s) \equiv \mathbf{r}_i(s)/ds$ represents the tangent vector to the chain at the contour location s and is constrained to be a unit vector. The term λ represents the bending elasticity of the polymer and is directly proportional to the persistence length of the polymer. In a similar fashion to Q_{PG} , the partition function of the LPE chains, Q_{LPE} , can be calculated from

$$Q_{LPE} = \int d\mathbf{r} \int d\mathbf{u} q_{LPE}(\mathbf{r}, \mathbf{u}, N_{LPE}), \quad (5.6)$$

where the field $q_{LPE}(\mathbf{r}, \mathbf{u}, s)$ satisfies the equation

$$\begin{aligned} \frac{\partial q_{LPE}(\mathbf{r}, s)}{\partial s} &= -\mathbf{u} \cdot \nabla_{\mathbf{r}} q_{LPE} + \frac{1}{2\lambda} \nabla_{\mathbf{u}}^2 q_{LPE}(\mathbf{r}, s) - w_{LPE}(r) q_{LPE}. \\ q_{LPE}(\mathbf{r}, \mathbf{u}, s = 0) &= 1. \end{aligned} \quad (5.7)$$

The term $q_{LPE}(\mathbf{r}, \mathbf{u}, s)$ represents the statistical weight that a wormlike chain experiencing a potential $w_{LPE}(\mathbf{r})$ has its segment s at position \mathbf{r} with orientation \mathbf{u} . For LPE molecules, we assume no flux boundary conditions at the center and periphery of the cell ($\nabla q_{LPE}(\mathbf{r} = 0, \mathbf{u}, s) = \nabla q_{LPE}(\mathbf{r} = \infty, \mathbf{u}, s) = 0$).

Because the system is spherically symmetric, we can exploit the property that

$$q_{LPE}(\mathbf{r}, \mathbf{u}, s) \equiv q_{LPE}(\mathbf{r}, \mathbf{u} \cdot \mathbf{e}_r, s) \quad (5.8)$$

where r denotes the radial distance from the center of the dendrimer and \mathbf{e}_r represents the unit radial vector (relative to an origin placed at the center of the dendrimer) at the location \mathbf{r} . We adopt a local coordinate system centered on \mathbf{r} , with \mathbf{e}_r representing the z axis and $\mathbf{u} \cdot \mathbf{e}_r = \cos \theta$, so that Eq. 5.7 can be represented as

$$\begin{aligned} \frac{\partial q_{LPE}(\mathbf{r}, \theta, s)}{\partial s} &= -\cos \theta \frac{\partial q_{LPE}}{\partial r} + \frac{\sin \theta}{r} \frac{\partial q_{LPE}}{\partial \theta} \\ &+ \frac{1}{2\lambda} \frac{1}{\sin \theta} \frac{\partial}{\partial \theta} \left(\sin \theta \frac{\partial q_{LPE}}{\partial \theta} \right) - w_{LPE}(r) q_{LPE}. \\ q_{LPE}(\mathbf{r}, \theta, s = 0) &= 1. \end{aligned} \quad (5.9)$$

Equation 5.9 forms the starting point for analyzing the configurations of semi-flexible polymers in spherically symmetric situations. A convenient way to solve Eq. 5.9 is by expanding $q_{LPE}(\mathbf{r}, \theta, s)$ and $q_{LPE}^\dagger(\mathbf{r}, \theta, s)$ in terms of Legen-

Legendre polynomials

$$q_{LPE}(\mathbf{r}, \theta, s) = \sum_l q_{LPE,l}(r, s) P_l(\cos \theta), \quad (5.10)$$

where P_l represents the l^{th} order Legendre polynomial. By using the properties of Legendre polynomials, Eq. 5.9 can be transformed into

$$\begin{aligned} \frac{\partial q_{LPE,l}}{\partial s} = & -\frac{l+1}{2l+3} \frac{\partial q_{LPE,l+1}}{\partial r} - \frac{l}{2l-1} \frac{\partial q_{LPE,l-1}}{\partial r} \\ & - \frac{(l+1)(l+2)}{2l+3} \frac{q_{LPE,l+1}}{r} + \frac{l(l-1)}{2l-1} \frac{q_{LPE,l-1}}{r} \\ & - \frac{l(l+1)}{2\lambda} q_{LPE,l} - w_{LPE}(r) q_{LPE,l}, \end{aligned} \quad (5.11)$$

subject to the conditions

$$\nabla q_{LPE,l}(r=0, s) = 0; \quad q_{LPE,l}(r, s=0) = \delta_{l,0}. \quad (5.12)$$

The self-consistent equations are found as the saddle point of Eq. 5.3 (multiplied by β/ρ_0) with respect to the fields $\varphi_i(\mathbf{r})$ (where $i = P, G, LPE, Na^+, Cl^-, H^+, OH^-,$ and S), $w_i(\mathbf{r})$, and $\Phi(\mathbf{r})$. Such a procedure yields [35]:

$$\begin{aligned} w_P(\mathbf{r}) = & \zeta (\varphi_P(\mathbf{r}) + \varphi_G(\mathbf{r}) + \varphi_{LPE}(\mathbf{r}) + \varphi_S(\mathbf{r}) - 1) \\ & + \alpha_P \ln \left[\frac{1 - \alpha(r)}{1 - \alpha_b} \right] - \alpha_P, \end{aligned} \quad (5.13)$$

$$w_G(\mathbf{r}) = \zeta (\varphi_P(\mathbf{r}) + \varphi_G(\mathbf{r}) + \varphi_{LPE}(\mathbf{r}) + \varphi_S(\mathbf{r}) - 1), \quad (5.14)$$

$$\begin{aligned} w_{LPE}(\mathbf{r}) = & \zeta (\varphi_P(\mathbf{r}) + \varphi_G(\mathbf{r}) + \varphi_{LPE}(\mathbf{r}) + \varphi_S(\mathbf{r}) - 1) \\ & + z_{LPE} \alpha_{LPE} \Phi(\mathbf{r}), \end{aligned} \quad (5.15)$$

$$w_S(\mathbf{r}) = \zeta (\varphi_P(\mathbf{r}) + \varphi_G(\mathbf{r}) + \varphi_{LPE}(\mathbf{r}) + \varphi_S(\mathbf{r}) - 1), \quad (5.16)$$

$$\begin{aligned} -\frac{1}{4\pi l_B \rho_0} \nabla^2 \Phi(\mathbf{r}) = & \sum_{i=\text{ions}} z_i \varphi_i(\mathbf{r}) + z_{PH^+} \alpha_P \alpha(\mathbf{r}) \varphi_P(\mathbf{r}) \\ & + z_{LPE} \alpha_{LPE} \varphi_{LPE}(\mathbf{r}), \end{aligned} \quad (5.17)$$

and

$$\alpha(\mathbf{r}) = \frac{1}{1 + 10^{pK_b, P-pOH} \exp(-z_{OH} \Phi(r))}. \quad (5.18)$$

In the above, z_i represents the charge valency of the i^{th} species and

$$\varphi_P(\mathbf{r}) = \frac{\eta_P \bar{\varphi}_P}{M(g) Q_{PG}} \sum_{i=0}^g \Omega_i \int_{s_i}^{s_{i+1}} ds q_{PG}(\mathbf{r}, s) q_{PG}^\dagger(\mathbf{r}, s), \quad (5.19)$$

$$\varphi_G(\mathbf{r}) = \frac{\eta_G \bar{\varphi}_G}{M_G(g) Q_{PG}} \Omega_g \int_{s_{g+1}}^{s_{end}} ds q_{PG}(\mathbf{r}, s) q_{PG}^\dagger(\mathbf{r}, s), \quad (5.20)$$

$$\varphi_{LPE}(\mathbf{r}) = \eta_{LPE} \varphi_{LPE,b} \int_0^{N_{LPE}} ds \sum_l \frac{q_{LPE,l}(r, s) q_{LPE,l}(r, N_{LPE} - s)}{2l + 1}, \quad (5.21)$$

$$\varphi_S(\mathbf{r}) = \varphi_{S,b} \exp[-w_S(\mathbf{r})], \quad (5.22)$$

and

$$\varphi_{ion}(\mathbf{r}) = \exp[-\beta \xi_{ion}^o] \exp[-z_{ion} \Phi(\mathbf{r})], \quad (5.23)$$

where $N = (g + 1)n + N_G$ is contour length from the center of the dendrimer to the edge of the grafted chain, $\eta_j = v_j \rho_0$, with v_j being the volume of a j^{th} molecule, and Ω_i is the number of branches in the i^{th} generation. See Sec. 4.2 for a detailed discussion of $q_{PG}(\mathbf{r}, s)$ and $q_{PG}^\dagger(\mathbf{r}, s)$.

We solve the Poisson-Boltzmann (PB) equation (Eq. 5.17) in order to obtain $\Phi(\mathbf{r})$, and we assume a no flux condition at the center of the cell:

$$\nabla \Phi(\mathbf{r} = 0) = 0. \quad (5.24)$$

At infinitely large radial values, gradients in $\Phi(\mathbf{r})$ are expected to approach zero. However, computational limitations preclude the use of such large cells, and we instead assume that the electrostatic potential decays to zero at the

edge of our simulation cell. We used a cell size of $75R_g$ such that the electrostatic potential could smoothly decay to 0.

We employed the Crank-Nicholson finite difference scheme [35, 137] to solve the partial differential equations for $q_{PG}(r, s)$ and $q_{PG}^\dagger(r, s)$ in Eqs. 4.7 and 4.8 respectively. We solve these equations on a lattice which is non-dimensionalized by $R_g = \sqrt{Na^2/6}$. To obtain the numerical solution for $q_{LPE,i}(r, s)$, we employ a two-step Lax-Wenderoff (LW) method similar to that suggested by Daoulas and co-workers. Truncation of the Legendre polynomial expansion (Eq. 5.10) to $l = 6$ was found to ensure sufficient convergence of the density profiles. The presence of large positive w_{LPE} values near the dendrimer core led to oscillations in the density profiles near the dendrimer core, which were more pronounced for increased LPE rigidity. In order to remove oscillations from our system, we used a one step Lax method close to the dendrimer center and transitioned into the two step LW method away from the dendrimer core. The equations were solved by using discretizations in the range of $dr = 1/30$ and $ds = 1/2000$. Random initial values for the fields were applied, and the field values were solved via a Picard iteration scheme [34]. We used a convergence criteria which imposed that the largest absolute value of the error in the fields from their self-consistent values was less than or equal to 0.005.

In addition to determining $\varphi_i(r)$, we also characterize the conformations

of the LPE chains through an orientational order parameter, $S(r)$ defined as

$$S(r) = \left\langle \frac{3 \cos^2 \theta(r) - 1}{2} \right\rangle, \quad (5.25)$$

where $\theta(r)$ denotes the angles formed between the radial vector emanating from the dendrimer center and the LPE bond vectors, and $\langle \dots \rangle$ denotes an average over the LPE conformations. In the SCFT framework, this order parameter is defined as the largest eigen value of the tensorial field

$$\mathbf{S}(\mathbf{r}) = \frac{\int ds \int d\mathbf{u} q_{LPE,i}(r, \mathbf{u}, s) \frac{1}{2} (3\mathbf{u}\mathbf{u} - \mathbf{I}) q_{LPE,i}(r, \mathbf{u}, N_{LPE} - s)}{\int ds \int d\mathbf{u} q_{LPE,i}(r, \mathbf{u}, s) q_{LPE,i}(r, \mathbf{u}, N_{LPE} - s)}. \quad (5.26)$$

By applying Eq. 5.8 and performing a Legendre polynomial expansion of q_{LPE} and q_{LPE}^\dagger , one may obtain a scalar value of S as a function of r . Complete ordering of the LPE bonds in a tangential orientation (along the θ axis) corresponds to the case where $S(r) = -0.5$, whereas complete alignment with the radial axis corresponds to the case where $S(r) = 1.0$. The SCFT potentials corresponding to the LPE monomers, $w_{LPE}(r)$, are used to effect Monte Carlo simulations of semi-flexible chains as described in the next section.

5.2.2 Monte Carlo Simulation of the LPE Chains

As discussed earlier, Monte Carlo simulations are used in our work as a means to access the conformational features of the LPE chains. In our MC simulations, we simulate worm-like chains (Kratky-Porod model) [35] that interact only with the field, $w_{LPE}(r)$ (obtained from SCFT calculations). The latter incorporates the effects of the electrostatic and steric interactions of the LPEs with the dendrimer. The semi-flexible chain consists of $N_{LPE} + 1$

monomers connected by N_{LPE} bonds of fixed length b , and the energy of the system is given by:

$$\frac{\mathcal{F}}{k_B T} = \sum_{i=1}^{n_{LPE}} \sum_{s=1}^{N_{LPE}} \left[\frac{\lambda}{b} (1 - \cos(\theta_{i,s})) + b w_{LPE}(\mathbf{r}_i(s)) \right], \quad (5.27)$$

where λ is the persistence length of chain, $\mathbf{r}_i(s)$ denotes the position of s^{th} monomer in the i^{th} chain, $\theta_{i,s}$ is the angle between bonds sharing a vertex at $\mathbf{r}_i(s)$, n_{LPE} is the total number of polyelectrolyte chains in the system, k_B is Boltzmanns constant, and T is temperature. The MC simulations are performed in canonical ensemble of 1000 chains ($n_{LPE} = 1000$). The polyelectrolyte chains are placed at random in a simulation box of length equal to 100 (in bond length units). The radial field, $w_{LPE}(r)$ (with the dendrimer at $r = 0$), from the SCFT simulations is superimposed onto the center of the simulation box. The chain conformations are sampled by employing a combination of crank-shaft rotation, slithering snake, and pivoting moves [26]. Metropolis criterion based on the energetic differences is used to accept or reject the proposed conformations [111]. Each MC cycle consists of one attempt of crank-shaft rotation per monomer and an attempt of both a pivot and slithering snake move per chain. The pivot and slithering snake steps are global moves, which help to enhance the diffusion of the LPE chains.

In the MC simulations, the system is first equilibrated for 3×10^6 MC cycles and then various structural quantities are averaged each 100 MC cycles for 3×10^6 more MC cycles. The averaged quantities include radially averaged radius of gyration, the center of mass density of polyelectrolyte chains, and

loop/tail distributions (*c.f.* Fig. 5.1b for the definitions of loops, tails, and trains).

5.2.3 Parameters

In this study, we fixed the generation number, functionality, and spacer length of the dendrimer to be $g = 3$, $f = 3$, and $n = 5$ respectively. In order to examine the effects of grafting length, we varied the grafting length from $N_G = 0$ to $N_G = 30$. In each of our calculations, we fixed the average dendrimer monomer fraction, $\bar{\varphi}_P \equiv M/(V\rho_0)$, to be 2.09×10^{-5} , which corresponds to a single non-grafted ($N_G = 0$) dendrimer in a simulation cell of $75 R_g$ (where $R_g = \sqrt{Na^2/6}$ and $N = (g + 1)n + N_G$ is the contour length from the center of the dendrimer to the edge of the grafted chain). We fixed the fraction of dendrimer monomers that are capable of charge dissociation at $\alpha_P = 0.5$. For our simulations, we choose an arbitrary value of $pK_{b,P} = 5.0$, but express our results in terms of $pOH - pK_{b,P}$. Unless otherwise noted, the $pK_{b,P}$ of the dendrimer monomers matches the solution pOH in our simulations.

We note that fixing α_P does not necessarily fix the total charge carried by the dendrimer. Indeed, the local fraction of dissociated monomers in the dendrimer, $\alpha(r)$, is inhomogeneous and given by

$$\alpha(r) = \frac{1}{1 + 10^{pK_{b,P} - pOH} \exp(-z_{OH^-} \Phi(r))}, \quad (5.28)$$

where z_{OH^-} is the valency of the OH^- ions and $\Phi(r)$ is the non-dimensional electrostatic potential. From Eq. 5.28, we see that the local dissociation depends on the local electrostatic potential, $\Phi(r)$, and the difference in dendrimer

$pK_{b,P}$ and solution pOH . The high degree of branching associated with polyelectrolyte dendrimers results in a high density of charged monomers within the dendrimer and makes localization of the OH^- counterions energetically favorable at equilibrium [39, 49, 83, 84, 86, 121, 165, 174]. Increasing the local concentration of OH^- ions results in a decreased probability of monomer dissociation (through Eq. 3.1). Since the local probability of monomer dissociation varies in space, we also calculate the average dissociated fraction of the dendrimer, $\bar{\alpha}$, which is given as:

$$\bar{\alpha} = \frac{\alpha_P \int_0^\infty dr r^2 \alpha(r) \rho_P(r)}{\int_0^\infty dr r^2 \rho_P(r)}. \quad (5.29)$$

Based on the above discussion, we expect the average dissociation ($\bar{\alpha}$) to be always less than the fraction of monomers that can participate in the charge dissociation reaction ($\alpha_P \alpha_b$) [83, 84, 86].

We fix the LPE chain length to be $N_{LPE} = 50$ and the fraction of charged LPE monomers, α_{LPE} , to be 1.0. The non-dimensional persistence length (PL) of the LPE chains, $\mu = PL/N_{LPE}a$ (where a is the Kuhn segment length and is assumed to be 0.7 nm, the Bjerrum length of water), is varied from $\mu = 0.02$ to $\mu = 0.4$. We modeled the LPE molecules in a grand canonical framework and fixed their bulk density to be $\varphi_{LPE,b} = 0.0001$. The solution screening length, κ^{-1} , is given by $\kappa^2 = 4\pi l_B \sum_i c_i z_i^2$ (where c_i is the concentration of the free ion and LPE species) and was fixed to be $3a$. To maintain a fixed screening length under varying pOH conditions, we adjusted the bulk salt concentration of the solution appropriately with changes in pOH .

5.3 Results

Below we discuss results displaying the effects of neutral dendrimer grafts, LPE stiffness, and solution pOH on the conformations and structure of dendrimer-LPE complexes. Specifically, we seek to identify the influence of different parameters upon the following characteristics:

(i) *The amount and conformations of complexed LPEs*: A key quantity characterizing the efficacy of dendrimers in gene therapy applications is the exposure of the complexed LPEs to solvent medium and the degradative enzymes present therein. To quantify such features, we first define the radius of the grafted dendrimer, R_{PG} as:

$$R_{PG} = \frac{\int_0^\infty dr r^4 (\varphi_P(r) + \varphi_G(r))}{\int_0^\infty dr r^2 (\varphi_P(r) + \varphi_G(r))}, \quad (5.30)$$

where $\varphi_P(r)$ and $\varphi_G(r)$ are the respective volume fraction profiles of the dendrimer and graft portions of the grafted dendrimer. Subsequently, we identify *complexed* LPEs as those having at least one of their monomers residing within R_{PG} .

For complexed chains, we quantify their “exposure” through the distribution of loops and tails. Loops and tails refer to segments of adsorbed LPE chains which lie outside R_{PG} . For loops, *both* ends of the loop connect to monomers which lie within R_{PG} . In contrast for a tail, *only one* of the tail monomers is attached to a LPE monomer residing within R_{PG} (*c.f.* Fig. 5.1b for a pictorial representation of loops, tails, and trains). Using our MC simulations, we quantify the fraction of adsorbed chains that reside in loops and

tails (denoted as f_{loop} and f_{tail} respectively) and the average length of loops and tails (denoted as $\langle N_{loop} \rangle$ and $\langle N_{tail} \rangle$ respectively).

(ii) *Charge of the resulting dendriplex:* Typically, the positive charge carried by the cationic delivery vectors leads to their binding with negatively charged genetic material. The expectation is that the complex will possess a net positive charge which will facilitate an energetically favorable interaction with the negatively charged cell membranes. In this context, it is of immense interest to understand the influence of different physical parameters upon the overall charge of the complex. In our work, we quantify the effective charge of the dendrimer complex through a local quantity, $Q(r)$, defined as:

$$Q(r) = \int_0^r dr' 4\pi\rho_0 r'^2 \varphi_e(r'), \quad (5.31)$$

where $\rho_0\varphi_e(r')$ is the local density of charge. Eq. 5.31 quantifies the total charge contained in a sphere of radius r , with the center of the sphere fixed at $r = 0$. We use the behavior of $Q(r)$ to understand the effects of dendrimer and LPE parameters on the resulting charge of the complex.

(iii) *Binding strength between the dendrimer and LPE molecules:* After successful delivery of genetic material to the cell has occurred, the dendrimer and NA material must dissociate. To quantify the role of different physical parameters upon the ease of dissociation, we quantify the binding strength through the potential of mean force (PMF), $w_{PMF}(r)$, for the interactions between the LPE and dendrimer. The potential of mean force quantifies the difference in free energy of a dendrimer and LPE whose COMs are separated by

a distance r relative to infinite dendrimer-LPE separation. Strictly speaking, $w_{PMF}(r)$ requires calculation of free energies for a dendrimer and LPE at a fixed distance r from the core of the dendrimer. However, we use a more approximate framework wherein the center of mass density of LPEs obtained from our MC simulations, $\rho_{COM}(r)$, is used to deduce $w_{PMF}(r)$ through:

$$w_{PMF}(r) \simeq -k_B T (\ln[\rho_{COM}(r)] - \ln[\rho_{COM,b}]), \quad (5.32)$$

where $\rho_{COM}(r)$ and $\rho_{COM,b}$ are the local COM and bulk concentration COM densities respectively. The above expression is expected to be valid for dilute concentrations of LPE and does not account for the deformation of the dendrimer arising from fixing the LPE at a distance r .

In presenting our results, we first present the SCFT results characterizing the influence of the different parameters upon the local volume fractions of the dendrimer and LPE molecules and the orientational order of the LPE molecules. We then discuss the results for the above quantities of interest, *viz.* (i) loop and tail distributions, (ii) charge of the dendriplex, and (iii) dendrimer-LPE potential of mean force.

5.3.1 Effect of Persistence Length on LPE Complexation

The binding mechanism between charged dendrimers and linear polyelectrolytes has been largely attributed to the electrostatic attraction between the charged dendrimer monomers and LPE molecules [101, 120, 166]. Since dendrimers have been shown to effectively bind to both single and double

stranded DNA and RNA molecules [18, 30, 31, 146, 147, 150], it is of interest to gain fundamental insight into the effect of LPE stiffness upon dendrimer-LPE binding affinities. Previous works by both Tian and Ma [156] and Klos and Sommer [64] have addressed the effects of LPE stiffness upon the properties of complexed dendrimers. Below we present results which complement the results presented in their works, and also make comparisons where appropriate.

Dendrimer-LPE Conformations: We first consider the situation of a non-grafted $g = 3$ dendrimer with LPEs of different persistence lengths (μ). Figure 5.2a displays the volume fraction profiles of the dendrimer monomers not in the presence of LPE molecules (dashed violet line) and in the presence of LPEs having persistence lengths of $\mu = 0.02, 0.1, 0.2,$ and 0.4 . Consistent with results of earlier works [83, 84, 86, 177], the dendrimer displays a dense core conformation, with a maximum in the monomer density near the center followed by a monotonic decay with increasing r . Interestingly, we observe in Fig. 5.2a that the dendrimers participating in complexation with the stiffer LPE molecules have more open conformations as compared to the case involving more flexible LPE chains. Furthermore, we observe that the dendrimers not in the presence of LPEs have the most open conformations. Such a behavior can be rationalized through examination of the corresponding LPE volume fraction profiles, which are displayed in Fig. 5.2b. There we observe that the local density of LPE monomers within the dendrimer decreases with increasing μ , whereas the extent of the LPE density tails increases with μ . Such a lowering of the LPE monomer density within the dendrimer molecule results

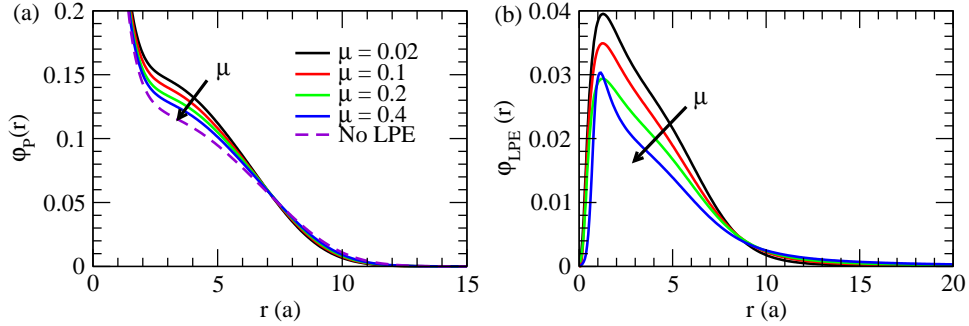


Figure 5.2: (a) Volume fraction profiles of $g = 3$ non-grafted dendrimer monomers complexed with $N_{LPE} = 50$ polyelectrolyte molecules of varying persistence lengths. (b) Effect of persistence length on the monomer volume fraction profiles.

in a higher net positive charge density and consequently results in a more open conformation of the dendrimer due to the resulting electrostatic repulsions.

Loop and Tail Statistics: To further understand the behavior of LPE density profiles, in Fig. 5.3 we display the effect of persistence length on the statistics of the loops and tails. Explicitly, Fig. 5.3a displays the fraction of complexed LPE chain monomers which exist as loops (f_{loop}) and tails (f_{tail}). We observe that f_{loop} decreases with increasing μ , whereas f_{tail} is seen to increase with μ . Further, we see that f_{tail} is much more sensitive to μ than f_{loop} , suggesting that increasing the persistence lengths of the LPE results in a large fraction of the LPE monomers being pushed outside of the dendrimer as tails. These results serve to explain our observations from Fig. 5.2b, which displayed a decrease in local LPE volume fraction within the dendrimer with increasing μ .

To provide a more pictorial depiction of the trends displayed in Fig. 5.3a,

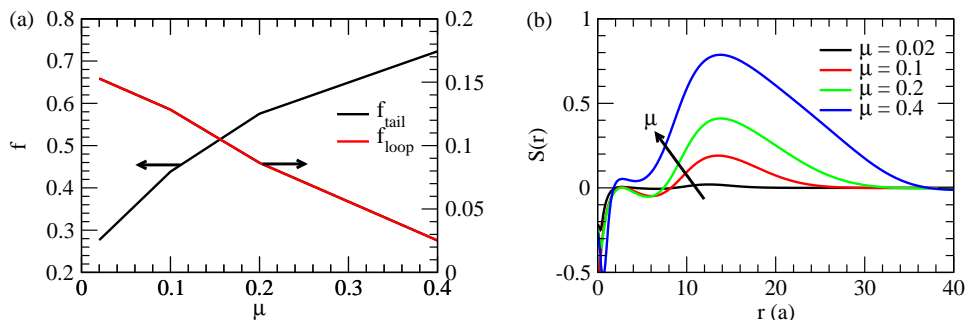


Figure 5.3: (a) Effect of PL on the fraction of dendriplex loops and tails; (b) Effect of persistence length on the order parameter, $S(r)$.

we display snapshots of $\mu = 0.02$ and $\mu = 0.4$ LPE molecules complexed with non-grafted $g = 3$ dendrimers in Figures 5.4a and b respectively. The flexible chains (Fig. 5.4a) are seen to exhibit short tails and a significant number of loops, with a large number of monomers residing within the dendrimer due to the coiled conformations of the LPE chains. In contrast, the stiff LPE chains (Fig. 5.4b) have long protruding tails (with no loops observed in the displayed snapshots). Furthermore, the flexible chains have a high number of monomers residing within the dendrimer (Fig. 5.2b), while the stiff chains have only a relatively straight train of monomers residing within the dendrimer.

To clarify further the above-noted differences in the conformations of the stiff and flexible LPEs within the LPE-dendrimer complex, we display the spatially dependent order parameter, $S(r)$, for different values of μ in Figure 5.3b. For all cases, we observe a non-monotonic behavior of the order parameter as a function of distance from the center of the dendrimer. We note that the negative values of $S(r)$ correspond to situations where the LPE

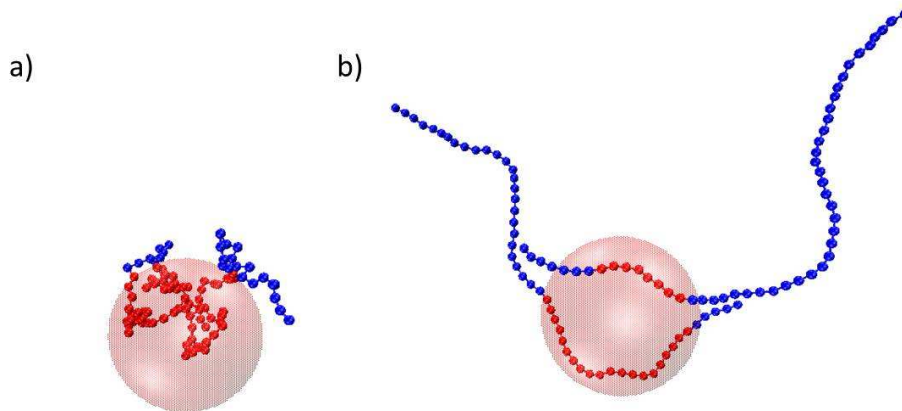


Figure 5.4: Snapshots of two LPE chains of $\mu = 0.02$ (a) and $\mu = 0.4$ (b) complexed with a $g = 3$ dendrimer (represented as red sphere). The LPEs are color coded such that the monomers residing within the dendrimer sphere are depicted in red while the monomers outside of the dendrimer are indicated in blue.

molecules adopt conformations which are perpendicularly oriented to the radial vector, whereas positive order parameter values correspond to the situation wherein the axes of the LPE molecule is aligned on an average with the radial vector. We generally notice negative or small positive values for the order parameter near the core of the dendrimer molecule, which can be explained by noting that near the dendrimer core, there is a high density of dendrimer monomers, which creates steric repulsion between the dendrimer and LPE monomers. Since the LPE monomers are not able to penetrate the center of the dendrimer core, they reside near and bend around the core, resulting in a perpendicular orientation of the LPE to the radial vector. Moving outward from the core, we notice a rather steep increase in the order parameter until it reaches a maximum value, consistent with the radial alignment of the LPE

monomers. As μ increases, we begin to notice an increase in the maxima and distribution widths of $S(r)$, which is indicative of the protrusion of long tails outward from the dendrimer center for stiff chains, in agreement with the snapshot of Fig. 5.4b. In contrast, the results of Fig. 5.3b suggest that the flexible chains reside in conformations that have little ordering ($S \approx 0$), corresponding to an almost globular conformation (*c.f.* Fig. 5.4a).

In sum, the above results for the volume fraction, loop and tail, and order parameter data display that increasing LPE stiffness results in the enhancement of exposed LPE material. Physically, this phenomena results from the competition between electrostatic and bending energies [64, 156]. Indeed, on the one hand, electrostatic interaction favor the chains to maximize their contact with the dendrimer monomers. However, due to the spherical shape and small spatial dimensions of the dendrimers, assuming a LPE conformation which maximizes contact with the dendrimer requires a highly coiled LPE conformation. Increasing the LPE persistence length results in a higher bending energy, which suppresses the chain's ability to assume a highly coiled conformations. This in turn results in longer tail formation and reduced LPE localization within the dendrimer.

Dendriplex Charge: As discussed previously, the overall charge of the dendrimer complex is hypothesized to play an important role in the cellular internalization of dendriplexes [18, 24, 30, 31, 52, 69, 131, 147, 164, 187, 188]. Thus, it is of interest to examine the effect of persistence length of the LPE on the charge of the resulting complex. We note that dendrimers are often

composed of weakly basic amine groups, in which the local charge dissociation is sensitive to the local concentration of counterions [83, 84, 86, 174]. In the absence of LPEs, the high density of charged monomers carried by the dendrimer molecules correspondingly results in significant counterion localization. In the presence of LPE molecules, which by themselves also carry a large number of negatively charged monomers, we expect that complexation with the dendrimer would affect the local density of counterions and thereby modulate the dissociation of the dendrimer monomers.

In Fig. 5.5a, we display the effect of LPE persistence length on the local dendrimer charge dissociation profiles, $\alpha(r)$, and the OH^- volume fraction profiles, φ_{OH^-} (inset). Consistent with our above expectations, we observe that the addition of LPE molecules to the system results in a significant reduction in the amount of OH^- ions within the dendrimer, which in turn enhances the local probability of charge dissociation in the dendrimer monomers. More quantitatively, we found that the bare dendrimers (in the absence of LPE molecules) carried charge fractions of $\alpha = \bar{0}.166$ (Eq. 5.29), whereas, dendrimers in the presence of $\mu = 0.4$ LPE molecules carried a charge fraction of $\bar{\alpha} = 0.211$. We note that the reduction in counterion localization within dendrimers upon dendrimer-LPE complexation has been observed previously in the simulations of Tian and Ma [156]. However, their study did not consider the weakly basic nature of dendrimer molecules and hence could not account for changes in the dissociation of the dendrimer monomers. Thus, the inclusion of LPE molecules is seen to have a significant effect upon the overall dissociation of weakly basic

dendrimers.

Relative to the effects arising from the addition of LPE chains to the system, we notice that modulating the LPE stiffness has a much smaller impact on the charge dissociation of the dendrimer. In general, we observe that the amount of counterion localization within the dendrimer decreases with decreasing μ , which in turn enhances the local probability of monomer dissociation. Physically, such results can be understood to be a consequence of the decreased localization of stiff LPEs within the dendrimer as compared to the flexible LPE chains. Interestingly, we notice a slight depletion of OH^- ions just outside of the dendrimer periphery for the $\mu = 0.4$ LPEs. We attribute this phenomena to the presence of the long negative tails of LPE protruding from the dendriplex, which act to locally deplete negatively charged ions.

In order to examine the effect of persistence length of the LPEs upon the charge of the resulting complex, we present $Q(r)$ (Eq. 5.31) in Fig. 5.5b. Overall, as we move out from the core of the dendrimer, we observe an increase in $Q(r)$ until it reaches a maxima around $r = 9a$ (which corresponds to $1.4R_{PG}$). Subsequently, $Q(r)$ is seen to drop and become negative at larger r before becoming zero (*i.e.* neutral) for large r . To understand these results, we note that the core of the dendrimer-LPE complex is primarily populated by the positively charged dendrimer monomers (*c.f.* Fig. 5.2a), and hence the core region of the dendrimer-LPE complex is expected to be positively charged. The negatively charged LPE monomers are seen to reside in the region exterior to the dense core. The latter neutralizes the charges of the

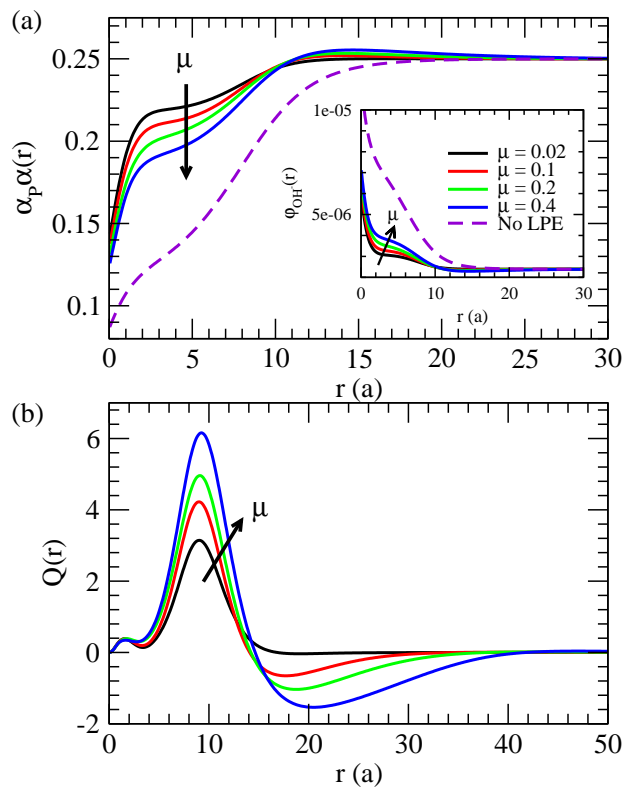


Figure 5.5: (a) The effect of PL on the local probability of dendrimer charge dissociation, $\alpha_p \alpha(r)$. The inset displays the corresponding OH^- counterion density profiles. (b) The effect of PL on the effective charge as a function of r .

dendrimer monomers and leads to the decrease in $Q(r)$. The outer fringes of the complex are primarily populated by the tails of the negatively charged LPE monomers, which explains the dip in $Q(r)$ to negative values. Interestingly, we notice that the magnitudes of both the maxima within the dendrimer and the minima outside of the dendrimer increases with increasing μ . These dependencies on μ can be rationalized through the $\varphi_{LPE}(r)$ plots in Fig. 5.2b, which show a decrease in local LPE concentration within the dendrimer and a correspondingly longer tail.

In their recent work, Tian and Ma noticed a positive gain in dendriplex charge as LPE stiffness was increased [156], a trend which qualitatively matches our above results. Likewise, Klos and Sommer noticed a decrease in the number of condensed LPE monomers as the stiffness was increased, which would correspond to a higher positive charge within the dendrimer [64].

5.3.2 Effect of Grafting Length on LPE Complexation

In the previous section, we witnessed that increasing the LPE stiffness resulted in an increased LPE exposure through the presence of long tails. Correspondingly, we witnessed the presence of a negatively charged region outside of the dendrimer molecule, which might affect interaction with the negatively charged cellular membrane. Because the use of grafted dendrimers has been proposed as an alternative to non-grafted dendrimers, below we presents results illustrating the influence of grafts on LPE exposure, dendriplex charge, and dendrimer-LPE binding strengths.

Dendrimer-LPE Conformations: We begin by discussing the influence of grafts upon the dendrimer conformations. Figure 5.6a displays the density profiles of grafted dendrimers for varying values of N_G in the presence of flexible LPEs ($\mu = 0.02$). We observe that increasing N_G lowers the dendrimer monomer densities near the core and results in an extended tail. Correspondingly, the penetration of grafted chains within the dendrimer and the overall extent of the grafts are seen to increase with N_G . As a result, the size of the dendrimer molecule (R_{PG}) increases with N_G (displayed as a function of N_G in the inset) [83]. Since adding grafts to the dendrimer is seen to result in significant conformational changes of the dendrimers, it can be expected that such changes would also affect the way the LPE molecules complex with the dendrimer. Figures 5.6b and c show the effect of N_G on the local concentration of LPE monomers within the dendrimer for the cases of LPEs with $\mu = 0.02$ and 0.4 respectively. The general behavior of the LPE volume fraction profiles mirrors the non-monotonic trends of the LPE volume fraction profiles observed in Fig. 5.2b. For both types of LPE molecules, we observe that increasing N_G results in a local decrease in the density of LPE monomers near the dendrimer core. The N_G dependence of the LPE density profiles and conformations can be attributed to two factors: (i) The increased segregation of the charged dendrimer monomers towards the periphery seen in Fig. 5.6a, which results in an attraction of negatively charged LPEs to such regions, and (ii) The enhanced steric repulsions arising from the presence of grafted polymer monomers near the dendrimer center.

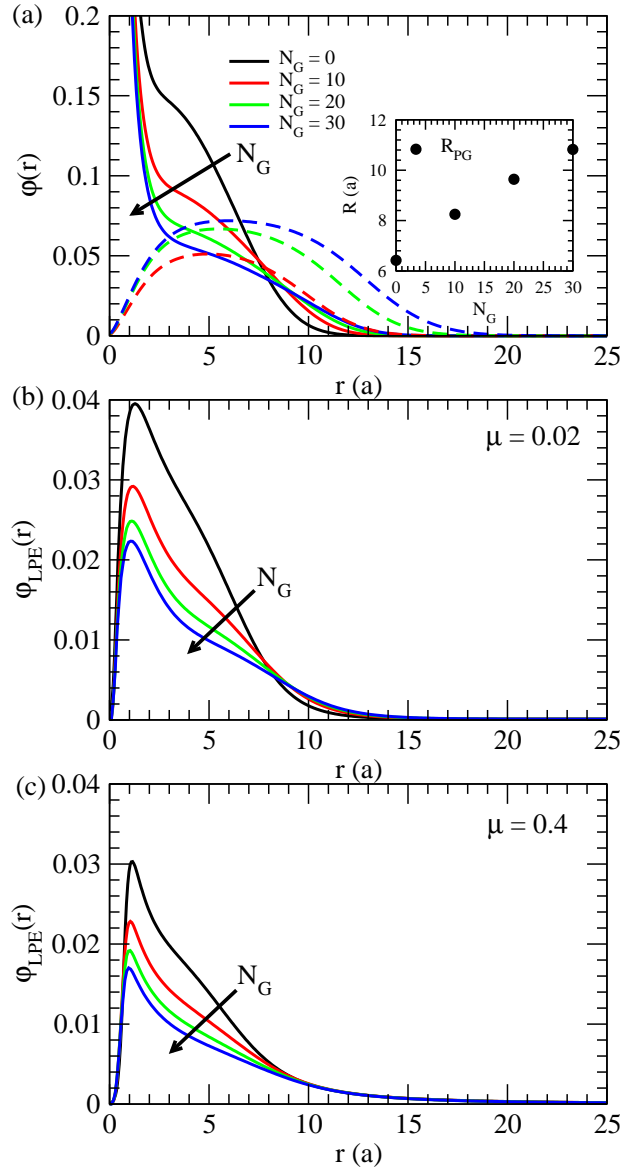


Figure 5.6: (a) Volume fraction profiles of $g = 3$ dendrimers (solid lines) and their respective grafted monomers (dashed lines) complexed with $\mu = 0.02$, $N_{LPE} = 50$ LPE molecules. The inset displays the R_{PG} values of the dendrimers as a function of N_G (b)-(c) Volume fraction profiles of LPEs having $\mu = 0.02$ (b) and $\mu = 0.4$ (c) complexed with dendrimers of varying N_G .

Loop and Tail Formation: In order to quantify the exposure of the LPE molecules in the complexes with grafted dendrimers, Figures 5.7a-d display both the fraction and average lengths of loops and tails of the complexed LPEs. Both Figs. 5.7a and b show that the fraction of material existing in loops and tails decreases with increasing grafting length, suggesting that the grafted dendrimers are better capable of shielding the LPE molecules from the surrounding medium. Correspondingly, in Figs. 5.7c and d we observe a monotonic decrease in the average lengths of loops and tails as N_G increases. The relative decrease in the amount of material existing in loops and tails is seen to be much higher for the flexible chains. Flexible chains have highly coiled conformations, allowing them to more easily reside within the dendrimer. The presence of grafts provides a larger *volume* in which the flexible LPEs may reside, which in turn reduces the probability that portions of adsorbed chain monomers may be exposed. On the other hand, the stiff LPE chains have much more linear conformations, and thus the increase in the size of the dendrimer only provides a larger *radius* over which the LPEs can be located. Hence, the changes in f_{loop} and f_{tail} are relatively smaller for persistent chains. In support of the preceding argument, we observe that f_{tail} in Fig. 5.7b decreases linearly with N_G , which mirrors the near linear increase in R_{PG} with respect to N_G displayed in the inset of Fig. 5.6a. Overall, the above results suggest that the addition of grafts to the dendrimer results in a significant impact on the exposure of complexed LPEs. Such results are consistent with recent observations reported in Fant *et al.*, where PEGylated PAMAM dendrimers

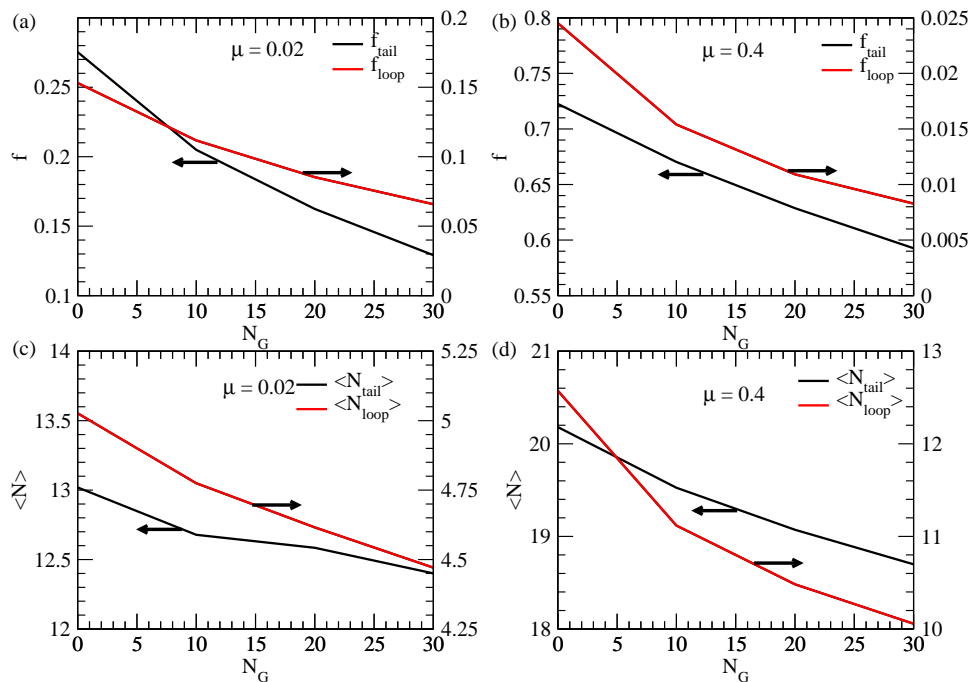


Figure 5.7: (a)-(b) Effect of N_G on f_{tail} and f_{loop} for $\mu = 0.02$ (a) and $\mu = 0.4$ (b). (c)-(d) Effect of N_G on $\langle N_{tail} \rangle$ and $\langle N_{loop} \rangle$ for $\mu = 0.02$ (c) and $\mu = 0.4$ (d).

were seen to better protect plasmid DNA from degradative serum nucleases than corresponding acetylated PAMAM dendrimers [30].

Dendriplex Charge: As observed in the previous section, the presence of LPE molecules, especially the case of stiff LPEs, resulted in significant modulation in overall charge of the dendrimer molecules (*c.f.* Fig. 5.5). The influence of grafts on such characteristics are displayed in Figure 5.8. Overall, the qualitative shape of the profiles is seen to match those from Fig. 5.5b. However, we do notice that increasing N_G has the overall effect of shifting the global $Q(r)$ maxima to further radial values, an effect which can be attributed

to the graft-induced outward segregation of the charged dendrimer monomers. Interestingly, the maximum values of $Q(r)$ are seen to increase with N_G for complexes with flexible LPE chains. Such trends can be rationalized from the results displayed in Fig. 5.6, wherein it is seen that the addition of grafts to the dendrimer reduces the extent to which the LPE chains penetrate inside of the dendrimer. In contrast, we observe that for stiff LPEs, increasing N_G results in a slight reduction in the $Q(r)$ maxima. Since the addition of grafts moves the charged dendrimer monomers outwards, increasing N_G enhances contact between the stiff LPEs and charged dendrimer monomers, thus allowing LPE chains to better compensate the charge of the dendrimer monomers. Due to such compensation effects, we observe that the valley in $Q(r)$ becomes less significant with an increase in N_G . We note that in the gene silencing studies of Tang *et al.* [147], the addition of grafts to $g = 5$ and $g = 6$ dendrimers was shown to reduce the corresponding zeta potentials (from 34.5 to 26.9 for $g = 5$ dendrimers, and from 33.6 to 27.9 for $g = 6$ dendrimers), suggesting an overall reduction the effective charge of the dendrimers. This trend is in qualitative agreement with the results from Fig. 5.8b.

Dendrimer-LPE PMF: To quantify the influence of grafts upon the binding strength between LPEs and dendrimers, in Figures 5.9a and b we display the PMFs for LPE molecules ($\mu = 0.02$ (a) and 0.4 (b)) interacting with dendrimers of varying N_G values. In general, we notice that the more flexible chains exhibit a deeper potential well and hence a strong binding to dendrimers of a given grafting length. For the flexible chains, we notice that

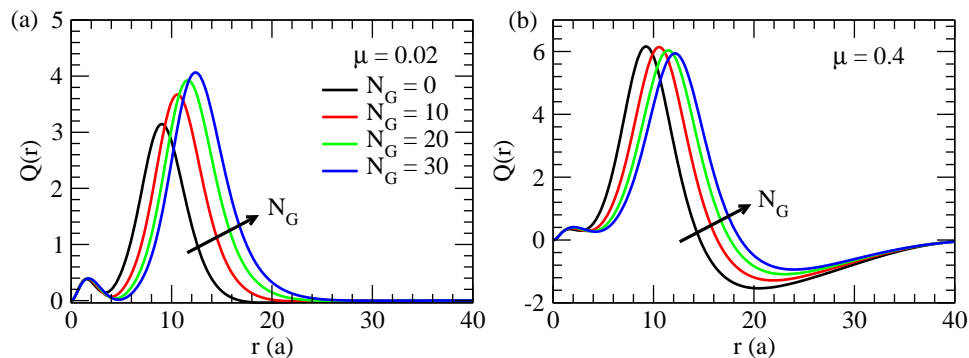


Figure 5.8: Effect of N_G on the integrated charge distributions, $Q(r)$, for $\mu = 0.02$ (a) and $\mu = 0.4$ (b).

increasing grafting length reduces the magnitude of the potential well depth while increasing its width. Physically, we attribute this phenomena to both the enhancement of steric repulsions between the conjugated dendrimer and LPE monomers and the accompanying localization of charged dendrimer monomers to further radial values. Interestingly for the stiff chains, the effect of N_G on the dendrimer-LPE PMF profiles are seen to be minimal, suggesting that the binding between the dendrimer and stiff LPE molecules is not affected by the addition of grafts. As discussed in the context of $Q(r)$ profiles, increasing N_G of the stiff LPE dendriplexes results in two competing effects, viz., the steric interactions induced reduced localization of LPE monomers and the enhanced number of electrostatically favorable contacts resulting from the increase in the radius of the dendrimer. We speculate that two preceding effects compensate to lead to a weak LPE-dendrimer binding strength dependence on dendrimer grafting length for stiffer chains.

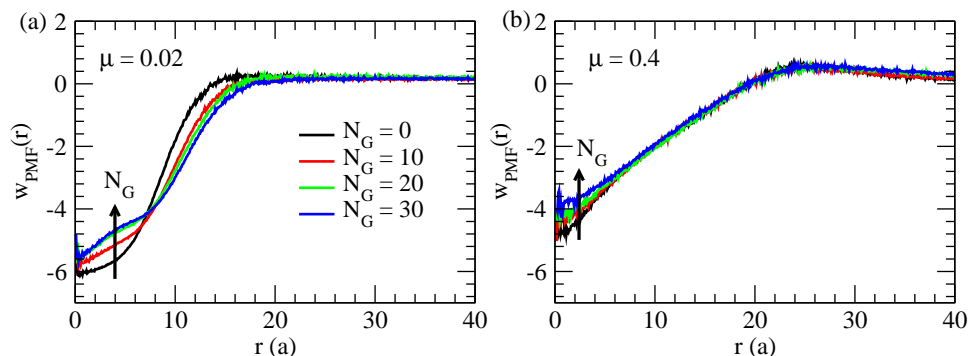


Figure 5.9: Effect of N_G on the potential of mean force profiles for $\mu = 0.02$ (a) and $\mu = 0.4$ (b) LPE molecules.

In conclusion, we have shown that the addition of grafts to dendriplexes reduces the amount of exposed LPE material, an effect which likely which is beneficial from the perspective of trying to reduce degradation of genetic material by serum nucleases. For stiff LPE molecules, we notice that the addition of grafts reduces the amount of overcharging (negative $Q(r)$ values), while not having a strong affect on the strength of binding between the dendrimer. In contrast, increasing the grafting length of dendriplexes comprised of flexible LPEs results in a reduction in the binding strength, with no overcharging observed.

5.3.3 Effect of pOH on Complexation

Transport of the dendriplex through the cellular membrane requires endosomal escape, a process triggered through a decrease in pH within the endosome. Below, we present results quantifying the effect of solution pOH

on the dendrimer-LPE binding strengths and the overall dendriplex charge. The former quantifies the influence of changing solution conditions on the ease of release of LPEs, whereas the latter is expected to have implications for the interaction of the dendriplexes with the endosomal membrane.

Dendrimer-LPE PMF: Since electrostatic interactions have been shown to be the main mechanism through which dendrimers bind to LPEs [101, 120, 166], in Fig. 5.10a we first present results illustrating the influence of pOH upon the charged monomers of the dendrimers. Explicitly, Fig. 5.10a depicts the volume fraction profiles of the $N_G = 30$ charged dendrimer monomers ($\alpha_P \alpha(r) \varphi_{LPE}(r)$), for different pOH conditions. Consistent with physical expectations (Eq. 3.1), we observe that increasing the solution pOH results in higher densities of charged monomers, which extend over a larger region of space.

It is expected that the above pOH induced enhancement on the dendrimer charge will have a significant effect on the conformation and binding of the LPE molecules. In Figure 5.10b, we display LPE density profiles for varying values of pOH . The LPE profiles are seen to maintain the general shapes discussed in the context of Figs. 5.2b, 5.6b, and 5.6c. However, we observe that increasing the pOH of the solution results in an enhancement of LPE monomers inside the dendrimer core and in the outer shell. These effects can be attributed to the enhancement of dendrimer monomer charge dissociation seen in Fig. 5.10a. Moreover, in agreement with our previous observations, we see that increasing the stiffness of the LPE chains decreases the overall density

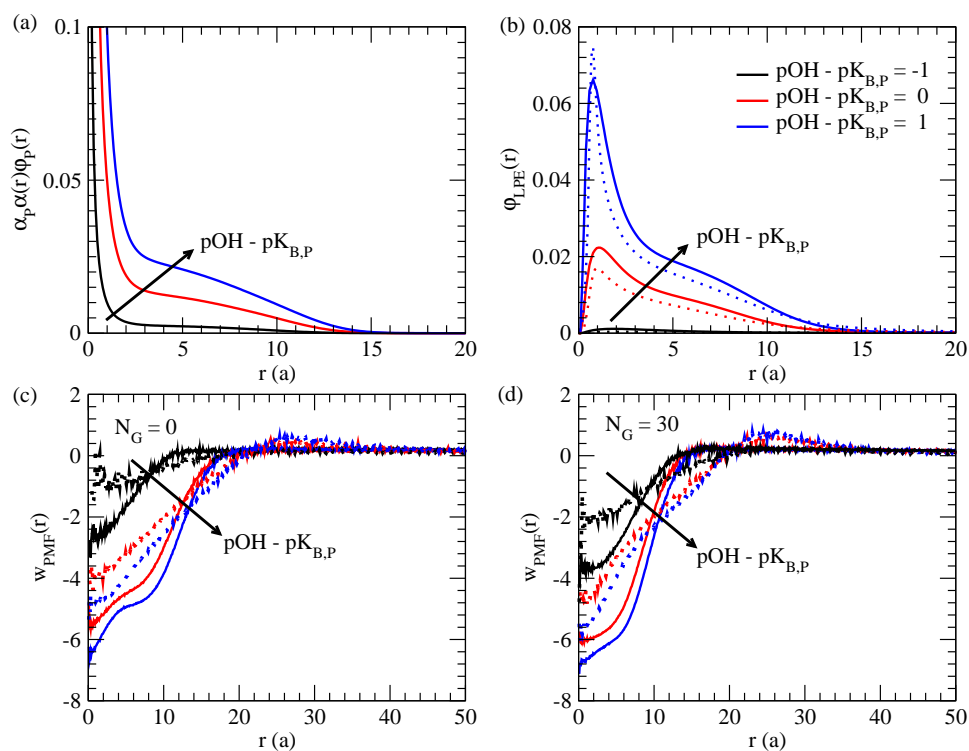


Figure 5.10: (a) Density profiles of Charged dendrimer monomers for a $N_G = 30$, $g = 3$ dendrimer complexed with $\mu = 0.02$ LPE molecules. (b) LPE volume fraction profiles (solid lines for $\mu = 0.02$, dotted lines for $\mu = 0.4$) that are complexed with $N_G = 30$, $g = 3$ dendrimers for varying values of $pOH - PK_{B,P}$. Effect of pOH on the PMF profiles of $\mu = 0.02$ (solid lines) $\mu = 0.4$ (dotted lines) LPEs in the presence of $N_G = 0$ (c) and $N_G = 30$ (d) dendrimers.

of the LPE chains, but in turn extends the LPE density tail.

In Fig. 5.10c we display the effect of pOH upon PMFs for non-grafted dendrimer-LPE systems. We observe that increasing the solution pOH results in an increase in the magnitude of the strength of interaction between the dendrimer and the LPEs. In comparing flexible and stiff chains we observe that the stiffer chains display lower strengths of association, which is consistent with our discussion in the previous section. In comparing the grafted and non-grafted complexes (*c.f.* Fig. 5.10d), we again observe (see Figs. 5.8) that the grafts influence the binding of flexible chains compared to stiff LPEs. Overall, the above results indicate that a low pH environment, *e.g.* inside the lysosome, is expected to lead to strong binding between dendrimer and DNA molecules. Hence, dissociation of the dendrimer-LPE complexes are more likely to occur within the cytoplasm as compared to the endosome.

Dendriplex Charge: In Fig. 5.11, we display $Q(r)$ of the dendriplexes for varying solution pOH conditions. We observe that increasing the solution pOH results in a higher net charge carried by the dendrimers and a higher level of overcharging of the dendrimer for the stiff LPEs. The increase in the maxima in $Q(r)$ can be attributed to the increase in dendrimer charge that accompanies the increase in solution pOH . In qualitative agreement with the results in Fig. 5.5b (and the discussions therein), we observe that for a given pOH increasing μ results in an enhancement of the maxima in $Q(r)$. Likewise, we observe that increasing the dendrimer grafting length reduces the amount of “overcharging” witnessed for the stiff LPEs (*c.f.* Fig. 5.8). For both the

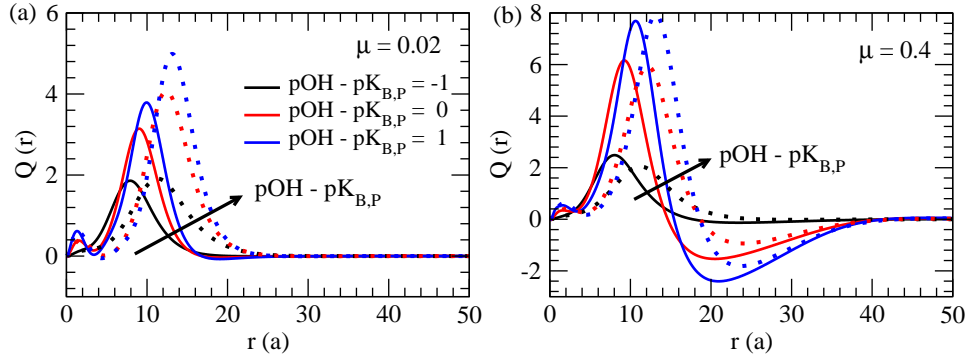


Figure 5.11: Effective charge profiles, $Q(r)$, of dendriplexes for varying values of $pOH - PK_{B,P}$. The solid lines correspond to the non-grafted dendrimers and the dotted lines correspond to the case of grafted dendrimers with $N_G = 30$.

stiff and flexible LPE complexes, we observe that an increase in pOH not only enhances the binding between the dendrimer and LPE molecules, but also increases the overall positive charge of dendriplex. The latter may prove beneficial for disruption of the endosome capsule, a process which needs to occur before the onset of lysosomal degradation.

5.4 Summary

In this work, we presented results of a study using a hybrid methodology of SCFT calculations and MC simulations to understand the influence of chain stiffness, neutral dendrimer grafts, and solution pOH upon the complexation between weakly basic polyelectrolyte dendrimers and linear polyelectrolyte molecules. We observed that an increase in the LPE stiffness resulted in a reduction in the localization of LPE chains within the dendrimer molecule, and

in turn an increased positive charge within the dendrimer. The complexation stiff LPEs results in the protrusion of long tails and a negatively charged shell outside the dendrimer. The presence of LPE molecules within the system was also seen to result in a significant decrease in the amount of condensed counterions, which in turn enhanced the amount of dendrimer monomers that were charged, a synergistic effect which enhanced the binding between the dendrimer and LPE. This phenomena was seen to be most prominent for the highly flexible LPE chains. From our MC simulations, we are able to quantify the PMF between the dendrimer and LPE molecules, and observed that increasing LPE stiffness resulted in a decrease in binding strength.

The addition of grafts to the dendrimer was seen to not only affect the dendrimer conformations, but also the binding between the dendrimer and LPE molecules. Increasing dendrimer grafting length resulted in decreased localization within the dendrimer for both flexible and stiff chains. For the flexible LPEs, we observed that increasing the grafting length resulted in more positive charge being carried within the dendrimer molecule, an effect which was attributed to the increase in exclusion of LPE monomers from the dendrimer due to steric repulsions. In contrast, for the stiffer LPE chains, we noticed a slight decrease in the positive charge within the dendrimer with increasing grafting length. Although increasing grafting length resulted in a reduction in LPE monomer density near the dendrimer center, the increased stretching of the dendrimer branches in turn enhances the contact between the charged dendrimer and LPE monomers. These two competing effects ul-

mately led to a reduction in the positive charge carried within the dendrimer and the negative charge in the shell outside of the dendrimer. Lastly, we studied the effect of solution pOH on the binding between the dendrimer and LPE molecules. Here we observed that increasing pOH (decreasing pH) results in enhanced binding between the LPE and dendrimer molecules.

This paper, along with previous works [56, 63, 64, 71, 72, 96, 97, 101, 120, 129, 156, 159, 166, 172], has provided insights on physics relevant to dendrimer-LPE complexation in the framework of a single dendrimer in the presence of LPE molecules. Although it is valuable to understand how dendrimer and LPE parameters affect the resulting dendriplex charge, physically relevant dendriplexes have length scales that exceed the dimensions of a single dendrimer and DNA/RNA molecule [18, 147, 150]. Indeed, simulations have examined the binding between a single LPE molecule and multiple dendrimers [71, 166]. In future works, we plan to extend the present framework to understand the role of multi-body dendrimer LPE interactions on the formation of dendrimer-LPE complexes to obtain a physically accurate picture.

Chapter 6

Effects of Neutral Grafted Chains and Solution pH on Dendrimer-Membrane Interactions

6.1 Introduction

Cationic dendrimers have shown great promise in drug and gene therapy applications. For instance, water-soluble dendrimers have been shown to effectively bind to many hydrophobic drug molecules, thus increasing the aqueous solubility of the latter [114]. Cationic dendrimers have also been demonstrated to bind to negatively charged genetic material, which serves the dual purpose of shielding the latter from degradative enzymes in the blood and creating more favorable electrostatic interactions between the nucleic acid material and the negatively charged cellular membrane [30, 69].

Despite the advantages realized through positively charged dendrimers, a number of studies have noted that the non-specific electrostatic binding to charged lipid head groups of cellular membranes may contribute to dendrimer cytotoxicity, and such effects have been noted to increase with dendrimer size, charge density, and concentration [47, 59, 81, 110]. In order to reduce the cytotoxicities of dendrimers, researchers have pursued the strategy of lowering the dendrimer surface charges by replacing the surface primary amine groups

with non-charged moieties, such as acetyl groups or polyethylene glycol (PEG) chains [30, 54, 169]. These modifications have been shown to reduce the formation of membrane pores and dendrimer cytotoxicity [30, 54, 169].

Despite a number of efforts [1, 30, 47, 54, 57–59, 73–75, 78, 81, 89, 110, 158, 169, 181, 182], there is still not full clarity on the physics and parameters governing dendrimer-membrane interactions and the role of grafts in modulating such interactions. Many of the previous theoretical and simulation works have used the model of nanoparticles interacting with membranes to deduce conclusions regarding the dendrimers [28, 37, 87, 160, 161]. For instance, Ginzburg and Balijepalli used self-consistent field theory (SCFT) to model the non-specific interactions between spherical nanoparticles and bilayers and found that the resulting morphology was strongly dependent on the nanoparticle-lipid interaction energies [37]. Recent works by Ting and Wang have extended such methodologies to include electrostatic interactions and also have studied the influence of bilayer surface tensions [160, 161]. Their work found that it is energetically favorable for tensionless membranes to partially wrap spherical nanoparticles rather than form pores in the bilayer. Furthermore, they observed that the presence of nanoparticles reduces the rupture tension of the membranes. Coarse-grained (CG) molecular dynamics (MD) simulations by Li and Gu examined the adsorption of surface charged nanoparticles on zwitterionic membranes and were able to show that the driving force for the wrapping of the nanoparticle by the membrane was determined by the interplay of electrostatic attractions and bending rigidity of the mem-

brane [87]. A recent dissipative particle dynamics (DPD) study by Ding *et al.*, demonstrated that asymmetry in nanoparticle shape and surface modification of nanoparticles can strongly influence their ability to penetrate bilayer membranes [28].

While the above studies have provided valuable insights into the interactions between nanoparticles and bilayer systems, such models are not capable of explicitly accounting for all the characteristics of dendrimer molecules. Indeed, our own previous studies (and others) have shown that (i) the distribution of monomers within the dendrimer is nonuniform, with the interior region of the dendrimers possessing a significant amount of void space [120], and that (ii) the dendrimers may exhibit some flexibility and deform to modulate their interactions [1, 57–59, 73–75, 78, 83–86, 89, 120, 158, 179, 181, 182]. Motivated by such considerations, recently there have been a number of MD and DPD studies which have explicitly modeled the dendrimer to study their interactions with charged bilayers [1, 57–59, 73–75, 78, 89, 158, 181, 182]. For instance, atomistic MD simulations by Kelly *et al.* showed that 3rd generation polyamidoamine (PAMAM) dendrimers deformed significantly as they approached and contacted zwitterionic dimyristoylphosphatidylcholine (DMPC) bilayers [57–59]. Coarse-grained MD studies by Lee and Larson showed that dendrimer molecules are capable of inserting themselves into the hydrophobic portion of the bilayer so that the charged terminal amine groups can make contact with the charged head groups of both leaflets [73]. A recent study by Tian and Ma used CG MD to examine the interactions between dendrimers

and bilayers of varying compositions [158]. They observed that when cationic dendrimers interacted with asymmetric bilayers (neutral upper leaflet and negatively charged lower leaflet), the dendrimers were able to move some of the negatively charged lipids to the neutral leaflet. Using a DPD simulation approach, Yan and Yu were able to show that increasing bilayer surface tension resulted in enhanced permeation of charged dendrimers [181,182]. Furthermore, they were able to demonstrate that the insertion of dendrimer molecules into bilayer membranes reduced the surface tension at which the membrane ruptures. These results have highlighted the importance of explicitly accounting for the dendrimer conformational degrees of freedom in examining their interactions with bilayers.

Although there have been a few computational studies which have considered non-grafted dendrimer-membrane interactions, we are aware of only one simulation study which has examined the role of polymer grafts on the dendrimer membrane interactions [78]. Specifically, Lee and Larson observed that adding neutral grafts to the surfaces of dendrimers reduced their membrane permeability by an extent which was correlated to the length of the grafts. While their study clarified some of the mechanisms underlying the reduced cytotoxicity of grafted dendrimers, their results were based upon specific physicochemical conditions and membrane properties. Hence, the interplay of parameters such as solution pH and membrane tension with the influence of grafts remains unresolved.

Motivated by the above considerations, in this study we develop a

coarse-grained model of grafted, charged dendrimers interacting with anionic membranes. We use such a model to study the following issues:

(i) *How do the dendrimer conformational degrees of freedom influence its interactions with and permeation through membranes?* Since a number of earlier works have shown that dendrimers are capable of deforming in the presence of bilayer membranes [1, 57–59, 73–75, 78, 89, 158, 181, 182], we undertake a systematic study to clarify the specific influences of dendrimer flexibility and internal voids on the mechanistic pathways underlying dendrimer penetration through membranes;

(ii) *How does the addition of neutral grafts affect the interactions between dendrimers and charged bilayers?* We quantify the free energy of interaction between the dendrimer and membrane as a function of distance between them, and using such a framework, we examine the influence of dendrimer architecture, such as generation number and graft length, upon the dendrimer-membrane interactions.

(iii) *How does solution pH and membrane surface tension affect the interactions between dendrimers and charged bilayers?* A dendrimer which is outside of the cell and approaching the plasma membrane is exposed to a neutral pH environment, with the bilayer membrane existing in a low tension state. However, once inside the endosome, the pH environment experienced by the dendrimer changes, and the surface tension of the endosomal membrane is speculated to be enhanced through the proton sponge effect [6, 143, 185]. Hence, understanding the physicochemical mechanisms underly-

ing the dendrimer-membrane interactions requires knowledge of such features under a variety of membrane tension and pH conditions. Motivated by such issues, we adopt a model which explicitly accounts for acid-base equilibrium effects (a feature lacking in previous works), and thereby quantify the influence of pH conditions. We also examine the influence of membrane tension on the interactions between grafted and non-grafted dendrimers and membranes.

The rest of the article is arranged as follows. In Section 6.2, we discuss our SCFT model and the associated terminology. In Section 6.3, we present our results, and we conclude with a summary of our findings in Section 6.4.

6.2 Model

6.2.1 Self-Consistent Field Theory Model

We consider a single (weakly basic) dendrimer (P) and its grafts (G) in a system containing a lipid bilayer membrane, solvent molecules (S), H^+ and OH^- ions, and monovalent salt ions (denoted as Na^+ and Cl^-). We model the lipids in our system as graft copolymers consisting of a hydrophilic head segment (H) of N_H head monomers which are attached to two hydrophobic tail segments (T) of N_T tails. Figure 6.1a presents schematic representations for the lipid and dendrimer molecules in our system. Figure 6.1b displays a dendrimer (black) with neutral grafted chains (red) attached at the periphery. The 0^{th} generation of the dendrimer is comprised of the core monomer and the three stemming branches, and the next generation of dendrimers is comprised of the spacers attached at the end groups of the 0^{th} generation. There are

two generational layers attached to the 0^{th} generation, thus, the generation number, g , of the dendrimer in Fig. 6.1b is $g = 2$. The “functionality,” f , of the branches denote the number of branches stemming from an individual branch point, and in Fig. 6.1b, $f = 3$. In our notation, the number of interior dendrimer monomers, M , comprising the dendrimer molecule is given by

$$M(g) = nf \left((f - 1)^{g+1} - 1 \right) + 1 \quad (6.1)$$

where n is the number of monomers per spacer. PAMAM dendrimers are composed both primary amines (NH_2), which reside in the outermost generation, and tertiary amines (NH), which belong to the inner generations [114]. Therefore, the total number of tertiary amine groups in our dendrimer molecules is given by

$$M_{NH}(g) = f (f - 1)^g \quad (6.2)$$

and the number of tertiary amine groups is given by:

$$M_{NH_2}(g) = f \left((f - 1)^g - 1 \right) + 1 \quad (6.3)$$

We assume that every terminal group of the dendrimer molecule is grafted with a polymer of length N_G such that the number of monomers in the graft portion of the dendrimer molecule is given as:

$$M_G(g) = N_G f (f - 1)^g. \quad (6.4)$$

We note that during synthesis of PEG grafted dendrimers, complete PEGylation of the dendrimer primary amines is unlikely to occur [45, 94]. Moreover,

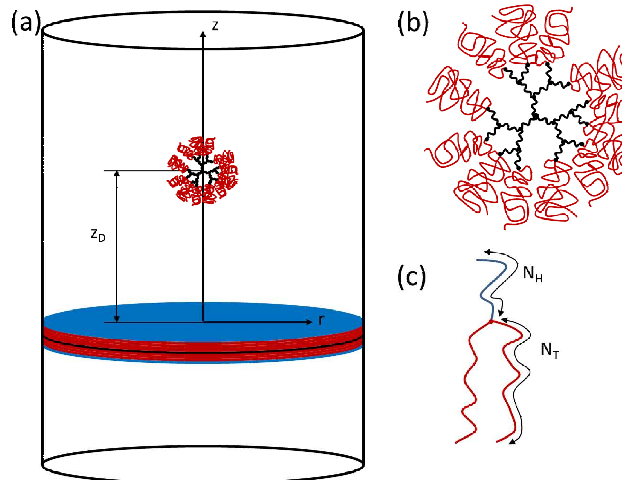


Figure 6.1: (a) Schematic of our dendrimer-membrane system wherein the dendrimer is separated by distance z_D from the unperturbed bilayer midplane. (b) Schematic of a grafted 2^{nd} generation dendrimer having a functionality of 3. The dendrimer portion is represented in black, while the grafted portions are represented in red. (c) Schematic of a lipid molecule in our system. The head portion is represented in red, while the tail portions are represented in black.

the addition a PEG chain to a dendrimer converts a primary surface amine to an amide bond, which strongly reduces its ability to absorb a hydrogen ion and thus carry a positive charge. However, to simplify our SCFT framework and the number of parameters involved, we assume that every end group of the dendrimer is PEGylated (*c.f.* Fig. 6.1b) and also allow our surface amine groups to be charged. Another important point is that our results compare grafted and non-grafted dendrimers capable of carrying the same amounts of charge. Therefore, our results more closely represent comparisons between PEGylated and acetylated dendrimers that have the same number of reacted terminal monomers.

Below we discuss the assumptions utilized in the derivation of the SCFT equations and present the final expression for the system free energy.

(i) We model the dendrimer, neutral grafts, and lipid molecules as flexible continuous Gaussian chains. In reality, the flexibility of these components is dependent upon the chemistry of the monomers [162]. Although previous works have studied the influence of finite dendrimer flexibility and have found it to affect their conformations and density profiles [14, 15, 48], treating both dendrimer and lipid monomers as flexible chains has been shown to still yield qualitatively accurate results [83–86, 177]. Therefore, to simplify our model and parameter space, we treat the dendrimer, graft, and lipid molecules as flexible chains.

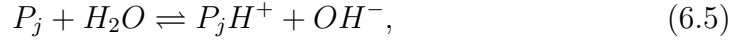
(ii) We assume that electrostatic interactions are the main *attractive* forces driving the complexation between the dendrimer and membrane molecules. While some simulations have shown that hydrophobic interactions between the dendrimer interior and lipid tail groups may have an important influence on the binding strength between dendrimers and lipid bilayers [57, 58, 181], we neglect such effects in our model to maintain parametric simplicity. The electrostatic interactions in our system are modeled using a classical Coulomb potential [35] with a spatially varying dielectric value, which is assumed to depend linearly on the local component density and dielectric values (see Eq. 6.13 below).

(iii) We assume that there are no enthalpic interactions between the dendrimer and its grafts. Some studies have shown that hydrogen bonding between graft chains and dendrimers may occur [149]. However, to reduce

the number of parameters, we set the Flory-Huggins interaction parameter between the dendrimer and grafted monomers, χ_{PG} , to be 0.

(iv) We model the total local density of the solvent, dendrimer, graft, and lipid monomers as almost uniform by including a harmonic compressibility penalty for deviations away from the average system density, ρ_0 [35].

(v) We model the charge dissociation of the primary and tertiary amine dendrimer monomers using an approach similar to that adopted by Szleifer *et al.* [39, 121, 165] and Won and co-workers [49, 174]. Explicitly, we assume that fractions $\alpha_{P_{NH}}$ and $\alpha_{P_{NH_2}}$ of the inner and outermost generation monomers respectively carry dissociable charge groups and are capable of becoming charged through the equilibrium reaction:



where j represents the NH and NH_2 groups. In a dilute solution containing unconnected dendrimer monomers, the equilibrium fraction of charged monomers, f_b , can be determined through the law of mass action:

$$K_{b,P_j} = \frac{[P_jH^+][OH^-]}{[P_j]} = \frac{f_b\rho_0\varphi_{OH^-,b}}{1-f_b}, \quad (6.6)$$

where K_{b,P_j} denotes the equilibrium constant of the dissociation reaction (Eq. 6.5), $[X]$ ($X \equiv P_j, P_jH^+, OH^-$) refers to the concentration in mol/L of species X , ρ_0 is the density of a single monomer, and $\varphi_{OH^-,b}$ is the bulk volume fraction of OH^- ions. The equilibrium constant, K_{b,P_j} , is proportional to $\exp(-\beta\Delta G^o)$, where $\Delta G^o = \xi_{OH^-} + \xi_{P_jH^+} - \xi_{P_j}$ is the free energy of the reaction and ξ_i^o

are the standard chemical potentials of the different species involved in the dissociation reaction. In our calculations, we use different pK_b values for the outermost and inner amine groups [126]. To reduce parametric complexity, we assume that α_{P_j} does not change when comparing grafted and non-grafted dendrimers.

(vi) The lipids used in our system are composed of negatively charged, hydrophilic head groups that are attached to two hydrophobic tail groups. Following the model of Ting and Wang [160, 161], we capture the non-electrostatic energetic interactions of the lipids through the use of both local Flory-Huggins χ -parameters and non-local interactions proportional to the square of the local density gradient of the lipid components. As we discuss later in Section 6.2.2, we choose the corresponding parameters so that the properties of the bilayers in our system mimic those of experimentally relevant amphiphilic bilayers [118]. We control the surface tension of the lipid bilayers by varying the lipid molecule chemical potentials, ξ_L , in addition to the energetic interaction parameters.

Using the above assumptions within a semi-grand canonical ensemble framework (open with respect to the lipid, solvent, and ion species, and closed with respect to the number of dendrimer monomers), we can write the system free energy (within an additive constant) as a functional of the local densities, $\varphi_i(r)$, of the i components ($i = S, H^+, OH^-, Na^+, Cl^-, H, T, P_{NH}, P_{NH_2}$,

and G components) as:

$$\begin{aligned}
\frac{\beta\mathcal{F}}{\rho_0} = & \int d\mathbf{r} \left[\sum_{j \neq k} \left(\chi_{jk} \varphi_j \varphi_k + \frac{\kappa_j}{2} [\nabla \varphi_j]^2 \right) + \sum_{i=ions,S} \varphi_i (\ln \varphi_i - 1 + \beta \xi_i) \right. \\
& + \frac{\zeta}{2} \left(\sum_l \varphi_l - 1 \right)^2 + \sum_{j=NH,NH_2} \alpha_{P_j} \varphi_{P_j} [f_j (\ln(f_j) - 1 + \beta \xi_{P_j H^+}) \\
& + (1 - f_j) (\ln(1 - f_j) - 1 + \beta \xi_{P_j})] \\
& + \left(\sum_{j=NH,NH_2} z_{P_j H^+} \alpha_{P_j} f_j \varphi_{P_j} + z_H \alpha_H \varphi_H + \sum_{i=ions} z_i \varphi_i \right) \Phi - \frac{\epsilon}{2\rho_0} |\nabla \Phi|^2 \Big] \\
& - \frac{V \bar{\varphi}_P}{M} \ln Q_{PG} - \exp(-\beta \xi_L) Q_L \\
& - \int d\mathbf{r} \left(\sum_{j=NH,NH_2} w_{P_j} \varphi_{P_j} + w_G \varphi_G + w_H \varphi_H + w_T \varphi_T \right).
\end{aligned} \tag{6.7}$$

The first term,

$$\sum_{j \neq k} \int d\mathbf{r} \chi_{jk} \varphi_j \varphi_k, \tag{6.8}$$

accounts for non-specific, pairwise enthalpic interactions, quantified in this work through Flory-Huggins χ parameters [35]. The second term,

$$\sum_j \int d\mathbf{r} \frac{\kappa_j}{2} [\nabla \varphi_j]^2, \tag{6.9}$$

reduces the sharpness of the lipid head tail interface and provides an additional parameter, κ , through which we can control the properties of our bilayer mem-

brane [160]. The terms,

$$\int d\mathbf{r} \left(\sum_{j=NH, NH_2} \alpha_{P_j} \varphi_{P_j} [f_j (\ln(f_j) - 1 + \beta \xi_{P_j H^+}) + (1 - f_j) (\ln(1 - f_j) - 1 + \beta \xi_{P_j})] + \sum_{i=ions, S} \varphi_i (\ln \varphi_i - 1 + \beta \xi_i) \right), \quad (6.10)$$

account for the chemical potential, mixing, and translational entropies of the ions, solvent, and the charged/uncharged dendrimer monomers [121]. The variables, f_j , represent the local probability that the primary ($j = NH_2$) and tertiary ($j = NH$) amine groups exist in a charged state. We reduce fluctuations in our system density through the term [35]

$$\int d\mathbf{r} \frac{\zeta}{2} \left(\sum_i \varphi_i - 1 \right)^2, \quad (6.11)$$

where ζ quantifies the strength of the harmonic energy penalty, which is incorporated to reduce total density fluctuations (we consider only volume contributions from the $l = P_{NH}, P_{NH_2}, G, S, H,$ and T species), and represents a measure of the compressibility of the system. We treat all ions in our system explicitly and calculate the electrostatic energy [35] from

$$\int d\mathbf{r} \left[\left(\sum_{j=NH, NH_2} z_{P_j H^+} \alpha_{P_j} f_j \varphi_{P_j H^+} + z_H \alpha_H \varphi_H + \sum_{i=ions} z_i \varphi_i \right) \Phi - \frac{\epsilon}{2\rho_0} |\nabla \Phi|^2 \right], \quad (6.12)$$

where z_i denotes the valencies of the i^{th} charged species and α_H representing the fraction of lipid head monomers that carry charge. Φ denotes the electrostatic potential field (normalized by $k_B T$), with ϵ representing the local

dielectric constant (given in units of $\epsilon_0 = 8.85 \times 10^{-12}(A \cdot s)^2/(J \cdot m)$, the permittivity of vacuum), which is assumed to be given as [160]

$$\epsilon(r) = \epsilon_P \varphi_P(r) + \epsilon_G \varphi_G(r) + \epsilon_H \varphi_H(r) + \epsilon_T \varphi_T(r) + \epsilon_S \varphi_S(r), \quad (6.13)$$

where ϵ_l represents the dielectric constant of the pure component l . The last terms,

$$-\frac{V\bar{\varphi}_P}{M} \ln Q_{PG} - \exp(-\beta\xi_L) Q_L - \int d\mathbf{r} \left(\sum_{j=NH, NH_2} w_{P_j} \varphi_{P_j} + w_G \varphi_G + w_H \varphi_H + w_T \varphi_T \right), \quad (6.14)$$

account for the conformational entropy of the dendrimer and lipid chains [35]. The potential fields, w_i , are Lagrange multipliers conjugate to the respective density fields, $\varphi_i(\mathbf{r})$ ($i = P_{NH}, P_{NH_2}, G, H$, and T). The terms Q_{PG} and Q_L represent the single chain partition functions of the dendrimer and lipid chains. To obtain these partition functions, we assume that the conformations of the grafted dendrimers and lipid molecules can be described using a continuous Gaussian chain model. In such a model, the chain is represented by the continuous contour path, $\mathbf{r}_i(s)$, and the corresponding stretching energy of the chain is given by the general expression [35],

$$\beta U_0(\mathbf{r}) = \frac{3}{2a^2} \sum_{i=0}^{n_{branch}} \int_{s_{i,0}}^{s_{i,f}} \left| \frac{\mathbf{r}_i(s)}{ds} \right|^2 ds, \quad (6.15)$$

where a is the Kuhn segment length of the polymers, n_{branch} is the total number of the respective dendrimer and lipid branches, and $s_{i,0}$ and $s_{i,f}$ are locations of the beginning and ending monomers for the i^{th} branch.

The partition functions, Q_j ($j = PG, L$), can be determined by calculating the statistical weights of a chain diffusing along its trajectory to a point

in space, which are given by $q_i(\mathbf{r}, s)$ and $q_i^\dagger(\mathbf{r}, s)$. The functions $q_i(\mathbf{r}, s)$ are calculated by first starting from $s = 0$ (center of the dendrimer ($j = PG$) or lipid head group ($j = L$)) and then moving forward in s . In a similar fashion, $q_i^\dagger(\mathbf{r}, s)$ describes the statistical weight of the chain diffusing backward in s , starting from the $s_{j,end}$ (edge of the grafted dendrimer ($j = PG$) or free end of the lipid tail group ($j = L$)). The partition function of grafted dendrimer and lipid chains can then be calculated from [35]:

$$Q_j = \frac{1}{V} \int d\mathbf{r} q_i^\dagger(\mathbf{r}, s = 0), \quad (6.16)$$

The functions $q_j(\mathbf{r}, s)$ and $q_j^\dagger(\mathbf{r}, s)$ can be found from the following “diffusion-like” equations [35]:

$$\frac{\partial q_j}{\partial s} = \frac{a^2}{6} \nabla^2 q_j - W_j(\mathbf{r}, s) q_j. \quad (6.17)$$

The $W_j(\mathbf{r}, s)$ functions are given by

$$W_{PG}(\mathbf{r}, s) = \begin{cases} w_{P,NH}(r), & 0 \leq s_{PG} < n(g-1) \\ w_{P,NH_2}(r), & n(g-1) \leq s_{PG} < ng \\ w_G(r), & ng \leq s_{PG} < ng + N_G \end{cases} \quad (6.18)$$

and

$$W_L(\mathbf{r}, s) = \begin{cases} w_H(r), & 0 \leq s_L < N_H \\ w_T(r), & N_H \leq s_L < N_T \end{cases} \quad (6.19)$$

for the dendrimer and lipid molecules respectively. In order to fix the position of the dendrimer center at $\mathbf{r} = (r = 0, z = z_D)$, we apply use a Gaussian constraining potential (variance = $0.05R_g$, where $R_g = \sqrt{(N_H + N_T)a^2/6}$), for the “initial” condition, $q_{PG}(\mathbf{r}, s = 0)$. For the lipid chains, we apply $q_L(\mathbf{r}, s = 0) = 1$. The function $q_i^\dagger(\mathbf{r}, s)$ that runs from the periphery of the dendrimer

is given by

$$-\frac{\partial q_j^\dagger}{\partial s} = \frac{a^2}{6} \nabla^2 q_j^\dagger - W_j(\mathbf{r}, s) q_j^\dagger; \quad (6.20)$$

$$q_j^\dagger(\mathbf{r}, s = s_{end}) = 1.$$

In order to account for the branching within the dendrimer, we apply the following conditions [41]

$$q_{PG}^\dagger(\mathbf{r}, s_i^-) = \left[q_{PG}^\dagger(\mathbf{r}, s_i^+) \right]^{f-1}; \quad s \leq ng \quad (6.21)$$

$$q_{PG}(\mathbf{r}, s_i^+) = q_{PG}(\mathbf{r}, s_i^-) \left[q_{PG}^\dagger(\mathbf{r}, s_i^+) \right]^{f-2}; \quad s \leq ng \quad (6.22)$$

where $q_{PG}^\dagger(\mathbf{r}, s_i^-)$ refers to spatially dependent chain propagator for a monomer at a value of s that is infinitesimally smaller than s_i , the value of s at the i^{th} branching point. The above conditions (Eqs. 6.21 - 6.22) embody the fact that at the dendrimer branch points, the $f - 1$ outer generation chains connect. This is analogous to $f - 1$ independent particles diffusing to the same point in space at the exact same time [41]. In a similar fashion, for the lipid molecules, we apply

$$q_L^\dagger(\mathbf{r}, s = N_T^-) = \left[q_L^\dagger(\mathbf{r}, s = N_T^+) \right]^2; \quad s \leq ng \quad (6.23)$$

$$q_L(\mathbf{r}, s = N_T^+) = q_L(\mathbf{r}, s = N_T^-) \left[q_L^\dagger(\mathbf{r}, s = N_T^+) \right]; \quad s \leq ng \quad (6.24)$$

The self-consistent equations are found as the saddle point of Eq. 6.7 with respect to the fields $\varphi_i(\mathbf{r})$ (where $i = P_{NH}, P_{NH_2}, G, H, T, Na^+, Cl^-, H^+, OH^-$, and S), $f(\mathbf{r})$, $w_i(\mathbf{r})$, and $\Phi(\mathbf{r})$. Such a procedure yields [35].

$$w_{P_j} = \zeta \left(\sum_{k=P,G,L,S} \varphi_k - 1 \right) - \frac{\epsilon_{PG}}{2\rho_0} |\nabla\Phi|^2 + \alpha_{P_j} \ln \left[\frac{1 - f_j}{1 - f_{b,j}} \right] - \alpha_{P_j}, \quad (6.25)$$

$$w_G(\mathbf{r}) = \zeta \left(\sum_{k=P,G,L,S}^{max} \varphi_k - 1 \right) - \frac{\epsilon_{PG}}{2\rho_0} |\nabla\Phi|^2, \quad (6.26)$$

$$w_H(\mathbf{r}) = \chi_{HT}\varphi_T + \chi_{HS}\varphi_S + \zeta \left(\sum_{k=P,G,L,S}^{max} \varphi_k - 1 \right) + \kappa_H \nabla^2 \varphi_H - \frac{\epsilon_H}{2\rho_0} |\nabla\Phi|^2 + z_H \alpha_H \Phi, \quad (6.27)$$

$$w_T(\mathbf{r}) = \chi_{HT}\varphi_H + \chi_{TS}\varphi_S + \zeta \left(\sum_{k=P,G,L,S}^{max} \varphi_k - 1 \right) + \kappa_T \nabla^2 \varphi_T - \frac{\epsilon_T}{2\rho_0} |\nabla\Phi|^2, \quad (6.28)$$

$$w_S(\mathbf{r}) = \chi_{HS}\varphi_H + \chi_{TS}\varphi_T + \zeta \left(\sum_{k=P,G,L,S}^{max} \varphi_k - 1 \right) - \frac{\epsilon_S}{2\rho_0} |\nabla\Phi|^2, \quad (6.29)$$

$$-\nabla(\epsilon\nabla\Phi) = \rho_0 \sum_{j=NH,NH_2} z_{P_jH} + \alpha_{P_j} f_j \varphi_{P_jH} + z_H \alpha_H \varphi_H + \sum_{i=ions} z_i \varphi_i \quad (6.30)$$

and

$$f_j = \frac{1}{1 + 10^{pK_b, P_j - pOH} \exp(-z_{OH} \Phi)}. \quad (6.31)$$

In the above, z_i represents the charge valency of the i^{th} species and

$$\varphi_{PNH} = \frac{1}{VQ_{PG}} \sum_{i=0}^{g-1} \Omega_i \int_{n_i}^{n(i+1)} ds q_{PG}(s) q_{PG}^\dagger(s), \quad (6.32)$$

$$\varphi_{PNH_2} = \frac{1}{VQ_{PG}} \Omega_g \int_{n(g-1)}^{ng} ds q_{PG}(s) q_{PG}^\dagger(s), \quad (6.33)$$

$$\varphi_G = \frac{1}{VQ_{PG}} \Omega_g \int_{ng}^{ng+N_G} ds q_{PG}(s) q_{PG}^\dagger(s), \quad (6.34)$$

$$\varphi_H = \int_0^{N_H} ds q_L(s) q_L^\dagger(s), \quad (6.35)$$

$$\varphi_L = \int_{N_H}^{N_T+N_H} ds q_L(s) q_L^\dagger(s), \quad (6.36)$$

$$\varphi_S = \exp[-\beta\xi_S] \exp[-w_S], \quad (6.37)$$

and

$$\varphi_{ion} = \exp[-\beta\xi_{ion}^o] \exp[-z_{ion}\Phi], \quad (6.38)$$

where v_j is the volume of a j^{th} molecule and Ω_i is the number of branches in the i^{th} generation.

To numerically solve the equations resulting from the above minimization procedure, we employ a cylindrical coordinate system wherein the z -axis of the cylinder is chosen to pass through the center of the dendrimer and is oriented normally to the bilayer membrane (see Fig. 6.1a). We fix the distance between the central dendrimer monomer and the midplane between the two lipid bilayers by enforcing an attractive Gaussian potential on the central dendrimer monomer. We use the lipid and solvent density profiles obtained in the absence of a dendrimer to fix the lipid density profiles at the edge of the cell.

To obtain $\Phi(\mathbf{r})$, we solve the Poisson-Boltzmann (PB) equation (Eq. 6.30) assuming no flux in the radial directions at $r = 0$ and $r = r_\infty$ ($\nabla\Phi = 0$) and periodic boundary conditions in the z -direction. For our simulation cell, we used a size of $15R_g$ for the cylinder radius and $40R_g$ for the cylinder height. In order to solve for $q_j(\mathbf{r}, s)$ and $q_j^\dagger(\mathbf{r}, s)$, we first determine $q_j^\dagger(\mathbf{r}, s)$ and then

subsequently use it via Eqs. 6.22 and 6.24 to determine $q_j(\mathbf{r}, s)$. We assume no flux boundary conditions at the $r = 0$ and $r = r_\infty$ ($\nabla q_j = 0$) while we use periodic boundary conditions in the z -direction. We employed an alternating-direction implicit scheme [137] to solve the partial differential equations for $q_j(r, s)$ and $q_j^\dagger(r, s)$ in Eqs. 6.17 and 6.20 respectively. The spatial dimensions of our system are resolved on a mesh size of $\Delta r = \Delta z = 1/8R_g$ and the contour coordinate, s , is resolved on a mesh size of $\Delta s = (N_H + N_T)/64$.

The potential of mean force (PMF) between the dendrimer and membrane quantifies the energy required to move the dendrimer and a membrane to a specified distance from an initial state of infinite separation. By examining the free energy of the dendrimer-membrane system at varying values of the distance between the dendrimer and membrane, we determine how the dendrimer, solution, and membrane tension parameters affect the potentials of mean force (PMFs) between the dendrimer and membrane. A positive PMF value corresponds to a repulsive dendrimer-membrane interaction, while a negative PMF value corresponds to attraction between the dendrimer and membrane.

As discussed in the introduction, there is strong motivation to consider the influence of membrane tensions on the dendrimer-membrane interactions. The tension of a membrane, γ , can be calculated by examining the manner by which the system's equilibrium free energy changes with membrane area for a fixed number of lipid molecules, $\gamma = \partial\mathcal{F}/\partial A|_{n_L}$ (where A is the total area of the membrane bilayer). In order to calculate the surface tension for our

system, we calculate the free energy for a $1D$ canonical ensemble simulation of the lipid components (in the absence of a dendrimer), where the volume fraction of the lipids, $\bar{\varphi}_L$, are fixed and the size of the simulation cell is varied to change the area per lipid head group, a_L . We use such results to map the influence of lipid head group area on the resulting surface tension. In turn, by relating the chemical potentials of the lipids, ξ_L , to the area per lipid head group, we can perform grand canonical ensemble simulations at specified membrane tensions.

6.2.2 Parameters

We fix the functionality and spacer length of the dendrimers to be $f = 3$ and $n = 2$ respectively. The dendrimer generation number and grafting lengths in our simulation are varied from $g = 3$ to $g = 4$ and $N_G = 0$ to $N_G = 12$ respectively. When comparing the results of grafted and non-grafted dendrimers, we use the notation, GXN_GY , to denote a dendrimer having a generation number of X and a grafting length of Y . In line with assumption (ii) discussed in the previous section, we assume that the Flory-Huggins parameters between the grafted dendrimer (P_{NH} , P_{NH_2} , and G species) and the solvent, lipid components (H and T) are identically zero (*i.e.* $\chi_{P_jG} = \chi_{P_jH} = \chi_{P_jT} = \chi_{P_jS} = \chi_{GH} = \chi_{GT} = \chi_{GS} = 0$). Furthermore, we set the non-local interaction coefficients, κ , for the dendrimer, graft, ion, and solvent species to be 0.

Titration experiments by Niu *et al.* determined the binding constants

for the primary and tertiary amine groups of PAMAM dendrimers [126], and following their findings, we use $pK_{b,P_{NH_2}} = 4.8$ for the primary and $pK_{b,P_{NH}} = 7.7$ for the tertiary amine groups respectively. We assume that $\alpha_{P_{NH}} = \alpha_{P_{NH_2}} = 0.5$ for the dendrimer monomers such that only a single monomer per dendrimer branch may be charged. All the solvent and monomer species in our system have a volume of $b^3 = \rho_0^{-1}$, where $b = 0.4\text{nm}$ is the Kuhn segment length of both the dendrimer and lipid species.

We fix the number of lipid head monomers to be $N_H = 2$ and the number of lipid tail groups per chain to be $N_T = 8$. Using these architectural parameters, the total volume of a single lipid is found to be 1.152nm^3 , which agrees with previous observations of hydrated bilayers [118]. The surface charge density of lipid bilayers is a function of their composition, and for biologically relevant membranes, there is a net negative charge in the membrane bilayer. Following the model of Ting and Wang [160], we fix the fraction of lipid head groups that carry charge, α_H , to be 0.25. The lipid Flory-Huggins and non-local square gradient interaction parameters were chosen to be $\chi_{HT} = 6.0$, $\chi_{TS} = 2.0$, $\chi_{HS} = 0.0$, and $\kappa_H = \kappa_T = 0.5$ respectively. In order to mimic biologically relevant conditions, we fix the salt concentration in the system to be 150mM . Following the work of Ting and Wang [160], we choose the dielectric constants for our various components to be $\epsilon_S = 80$, $\epsilon_H = \epsilon_P = \epsilon_G = 50$, and $\epsilon_T = 2$.

Using the above parameters, we observe tensionless bilayer formation with a corresponding area per lipid molecule, a , equal to 0.67nm^{-2} and bi-

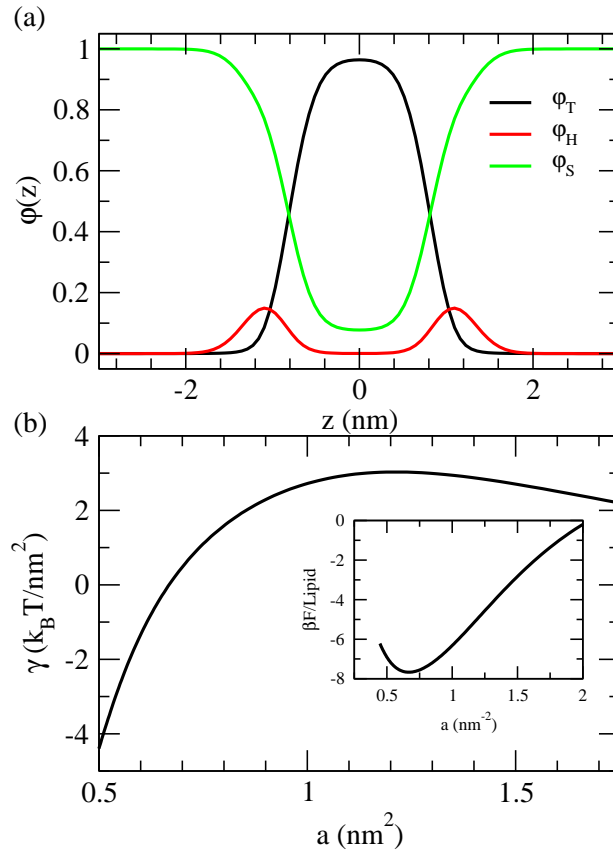


Figure 6.2: (a) Volume fraction profiles for the solvent and lipid components of our model membrane under zero surface tension. (b) The membrane surface tension, γ ($k_B T/nm^2$), as a function of the area per lipid head group (nm^{-2}). The inset displays the free energy per lipid head group as a function of the area per lipid.

layer width of approximately $3.1nm$ (*c.f.* Fig. 6.2a), which is in reasonable agreement with previous observations [118]. The surface tension of our membrane as a function of a and the corresponding free energy per lipid are shown Fig. 6.2b and its inset respectively. We observe that at low a , the membrane has negative surface tension values, and under these conditions, an unconstrained membrane would increase its area until a state of zero surface tension is realized. The *rupture tension*, γ_r , of a membrane is the maximum tension a membrane can sustain, beyond which the membrane experiences mechanical failure and the membrane surface tension decreases with increasing a . Here we see that our membrane has a rupture tension of $3.03k_B T/nm^2$ at $a = 1.21nm^2$. Quantitatively, we observe that our membrane system mimics the area per lipid head group ($0.72nm^{-2}$) and rupture tension values ($0.75 - 2.75k_B T/nm^2$) as seen in experiments [118, 127].

6.3 Results

We begin by examining the interactions between *non-grafted* $G3$ and $G4$ dendrimers and a tensionless membrane and compare our results to previous works. Moreover, by using simple variants of our model, we specifically clarify the roles of flexibility and porosity of the dendrimers in influencing their interactions with membranes. Subsequently, we present results which clarify the influence of neutral grafted chains on the interactions between weakly basic dendrimers and charged bilayer membranes. Lastly, we quantify the influence of solution pH and membrane surface tension on the potentials of mean force

between the grafted dendrimers and the lipid bilayers.

6.3.1 Dendrimer-Membrane Interaction

As a first step to understanding the role of dendrimer architecture and solution conditions upon the dendrimer-membrane interactions, we present some general qualitative features of the dendrimer-membrane interactions seen in our model. In Figures 6.3a-f, we display the conformations of non-grafted $G3$ dendrimers in a $pH = 7$ solution for varying distances, z_D , between the dendrimer and a tensionless membrane. As the dendrimer approaches the lipid membrane, it is seen to elongate in the z direction and initiate contact with the negatively charged lipid head group monomers (represented through the solid contour lines). Interestingly, we observe only minor deformations in the shape of the bilayer membranes during the approach of the dendrimer. After initiating contact with the membrane, the dendrimer is seen to spread over the bilayer, and in Fig. 6.3e, we explicitly see a branch of the dendrimer reach across the bilayer to initiate contact with the bottom leaflet of the bilayer. Finally, when the dendrimer center is placed at the center of the membrane, we observe a symmetric conformation, wherein the dendrimer initiates contact with both leaflets so that it can maximize the contact between the negatively charged head groups and the positively charged terminal amine groups.

While Fig. 6.3 presents a qualitative picture of the density profiles, in the following we quantify the shape and nature of the distortions undergone by a dendrimer. For this purpose, we use the gyration tensor, \mathbf{G} , whose elements

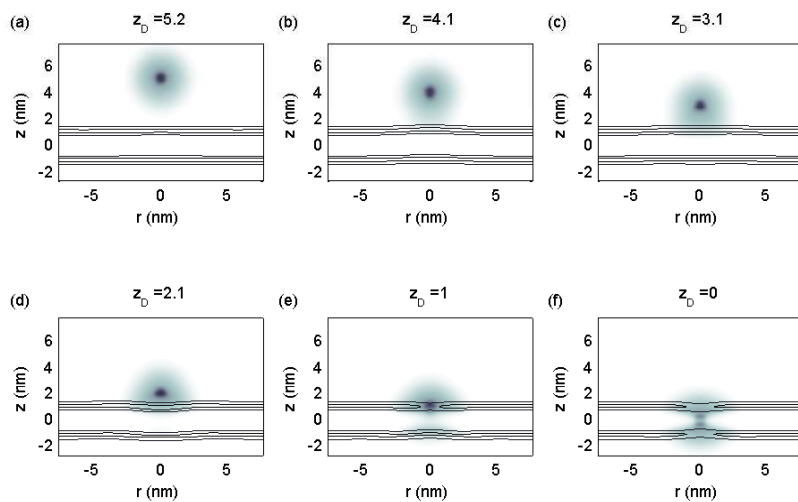


Figure 6.3: (a)-(f) Color plots displaying the volume fraction values of $G3$ dendrimers, $\varphi_P(r, z)$, in a $pH = 7$ solution at varying distances from the center of the lipid bilayer, z_D . The lipid bilayer head group volume fraction values are shown through the contour lines, which correspond to values of $\varphi_H = 0.07$ and $\varphi_H = 0.14$.

are given by

$$G_{ij} = \frac{\int dV(\varphi_{P_{NH}}(\mathbf{r}) + \varphi_{P_{NH_2}}(\mathbf{r}))r_i r_j}{\int dV(\varphi_{P_{NH}}(\mathbf{r}) + \varphi_{P_{NH_2}}(\mathbf{r}))}, \quad (6.39)$$

where r_i is the i^{th} Cartesian coordinate of the position vector, \mathbf{r} , the origin of which is chosen to be the dendrimer center of mass. Since we operate in a cylindrical system with angular symmetry, the non-diagonal elements of \mathbf{G} are zero, and $G_{xx} = G_{yy}$. To quantify the nature and magnitude of the dendrimer deformations, we utilize the asphericity parameter,

$$A_s = 1 - 3 \frac{G_{xx}G_{yy} + G_{xx}G_{zz} + G_{yy}G_{zz}}{(G_{xx} + G_{yy} + G_{zz})^2} \quad (6.40)$$

and the dendrimer radius of gyration, R ,

$$R^2 = G_{xx} + G_{yy} + G_{zz}. \quad (6.41)$$

In Figs. 6.4a and b, we display the dendrimer asphericity and radius of gyration for $G3$ and $G4$ dendrimers as a function of the distance between the dendrimer and membrane, z_D . For both $G3$ and $G4$ dendrimers, we notice that as the dendrimer approaches a distance of approximately $2R_0$ from the membrane (where R_0 represents the unperturbed size of the dendrimer and corresponds to $4.1nm$ for $G3$ dendrimers, and $5nm$ for $G4$ dendrimers), distortions begin to manifest. If we examine the ratio, G_{zz}/G_{xx} (inset of Fig. 6.4a), we see $G_{zz}/G_{xx} > 1$ before the dendrimer initiates contact with the membrane, which is consistent with the prolate spheroidal shapes seen in Fig. 6.3b. Upon initial contact with the membrane (at approximately $3.1nm$ for $G3$ dendrimers, and $3.6nm$ for $G4$ dendrimers), we see that the elongation of the dendrimer

along the z -axis ceases, and the dendrimer returns to having a nearly spherical shape *c.f.* Fig. 6.3c), corresponding to $A_s \simeq 0$. During dendrimer insertion into the membrane, we notice that the conformational changes depend on the generation of the dendrimer. For the $G3$ dendrimer, upon insertion into the membrane (at $2.1nm$), the dendrimer asphericity increases to its maximal value, and the conformation assumes a highly oblate shape (*c.f.* inset of Fig. 6.4a). Interestingly, as the dendrimer moves further into the membrane, we observe a reduction in asphericity, which we attribute to elongations along both the z -axis and the radial direction. As a corroboration of the latter, in Fig. 6.4b, we observe that the size R of the $G3$ dendrimer does indeed increase when it is inserted inside of the membrane. On the other hand, we notice a different behavior in the A_S and G_{zz}/G_{xx} values for the $G4$ dendrimers as they penetrate the membrane. Specifically, we see that the asphericity of the $G4$ dendrimer monotonically increases towards the center of the bilayer membrane, which is consistent with the dendrimer assuming a more oblate shape as it penetrates more deeply in the membrane. These differences between the behaviors of $G3$ and $G4$ dendrimers can be attributed to the larger diameter of the latter, as a consequence of which they assume more oblate conformations and maximize contact with the bilayer. Correspondingly, the $G4$ dendrimer radius of gyration is seen to increase as seen in Fig. 6.4b.

The above-discussed results of our model agree with the qualitative features reported in previous MD simulations and experimental observations [57–59, 73, 142]. In the atomistic MD simulations by Kelly *et al.* [57–59], they

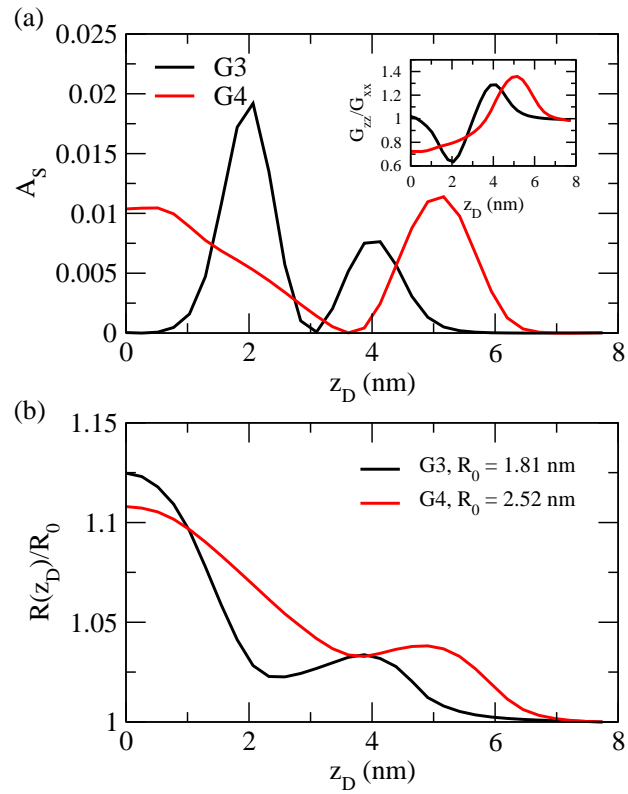


Figure 6.4: (a) Asphericity of the dendrimer molecules as a function of z_D . The inset displays the ratio, G_{zz}/G_{xx} . (b) The radius of gyration of the dendrimer molecule (normalized to its unperturbed value, R_0) as a function of z_D .

observed elongation of $G3$ dendrimers as the latter approached DMPC bilayers. Furthermore, contact between a single dendrimer and leaflet bilayers has been previously witnessed in the CG MD simulations by Lee and Larson [73], and we display some snapshots from their work in Fig. 6.5 to demonstrate qualitative similarities between their work and our results (compare Figs. 6.5a and b and our results in Figs. 6.3d and e). Solid-state NMR studies by Smith *et al.* have also confirmed the contact between the dendrimer interior components and lipid tail groups [142]. From their findings, they proposed that the dendrimer molecules contact both leaflets of the bilayer in the transfer of the dendrimer across the bilayer. The obtained density profiles in our work support this proposed behavior.

A unique feature of our model is the explicit accounting for the weakly basic nature of the amine groups along our dendrimer backbone and the resulting modulation of dendrimer charges based on the local density of OH^- ions. For instance, in an earlier study, we found that such effects can significantly influence the interactions and complexation of dendrimers with polyelectrolyte molecules [85]. To probe the magnitude of similar effects on our model, we use the quantity ΔQ_P , which is defined as

$$\Delta Q_P = \frac{Q_P(z_D) - Q_{P,0}}{Q_{P,0}}, \quad (6.42)$$

in which $Q_P(z_D)$ is the total charge carried by a dendrimer whose central monomer is at z_D , and $Q_{P,0}$ is the corresponding charge of the dendrimer far from the membrane. In a nutshell, ΔQ_P quantifies the change in total charge

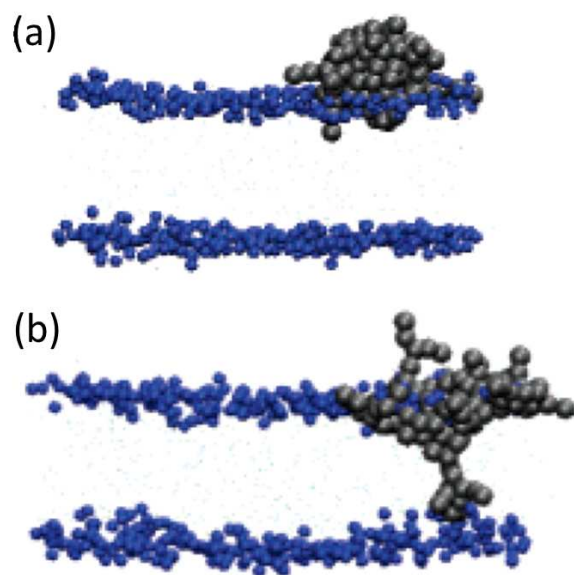


Figure 6.5: (a)-(b) Snapshots of *G3* PAMAM dendrimers interacting with a DPPC bilayer after initial position of $4nm$ above the bilayer membrane and $500ns$ of simulation time as obtained from the CG MD simulations by Lee and Larson. The black dots represent the dendrimer monomers while the blue groups represent the DPPC headgroups. Reprinted (adapted) with permission from Ref. [73]. Copyright 2006 American Chemical Society.

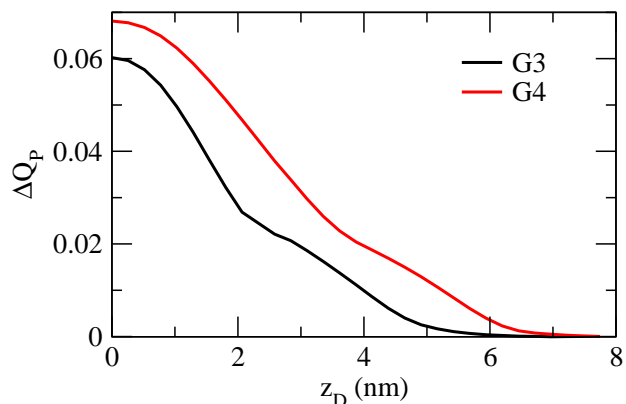


Figure 6.6: The relative increase in dendrimer charge for a dendrimer at distance z_D from the bilayer as compared to dendrimers in the absence of an anionic membrane, ΔQ_P , as a function of z_D for $G3$ (black line) and $G4$ (red line) dendrimers.

carried by the dendrimer as it approaches the membrane. In Fig. 6.6, we display the results for ΔQ_P , wherein we observe a 6 – 7% increase in the total charge carried by the $G3$ and $G4$ dendrimers as they approach the anionic membrane. The negative charge of the lipid head groups of the membranes results in a local depletion of OH^- ions near the lipid head groups, and this in turn *increases* the local dissociation probability, f , for the weakly basic dendrimer monomers, thereby increasing the charge carried by the dendrimer. These results suggest that even when the solution pH is kept a constant, the overall charge of the dendrimer can increase by almost 10% to account for the changes in the local ion concentrations. Since previous works have not treated the acid-base equilibrium reaction explicitly, such effects have not been reported in earlier studies.

While the results of Figs. 6.3 and 6.4 help identify the mechanisms

of dendrimer transport through membranes, in order to better quantify the interactions between dendrimers and cells, it is useful to consider the potentials of mean force (PMFs) between the dendrimers and lipid membrane. In Fig. 6.7, we display the PMFs corresponding to non-grafted $G3$ and $G4$ dendrimers as a function of z_D . We observe that the system free energy decreases as the dendrimers approach the lipid bilayer, signifying an attractive interaction between the dendrimer and lipid bilayer. In comparing $G3$ and $G4$ dendrimers, we observe that the latter exhibits a deeper and a longer ranged potential well. Such features can be respectively rationalized as a consequence of the larger number of charges and the size of the $G4$ dendrimers. In physical units, we observe binding strengths of approximately $6.2kcal/mol$ at $310K$ for our $G3$ dendrimers. This value is lower than that previously observed by Kelly *et al.* [57]. However, such differences are expected since we did not account for hydrophobic interactions between the dendrimers and lipid interiors.

The broad and deep potential wells seen in the results of Fig. 6.7 indicate that the dendrimers will experience a strong driving force for binding to the bilayer membrane. However, such an attraction will also serve as a significant barrier for the escape of the dendrimer upon adsorption to the membrane. Thus, passive transport of the dendrimer through a tensionless bilayer into the cellular environment would require very long time scales. Hence, it is not surprising that even for small dendrimers, active transport (endocytosis) has been suggested as the main mechanism for internalization of dendrimers into the cell [53].

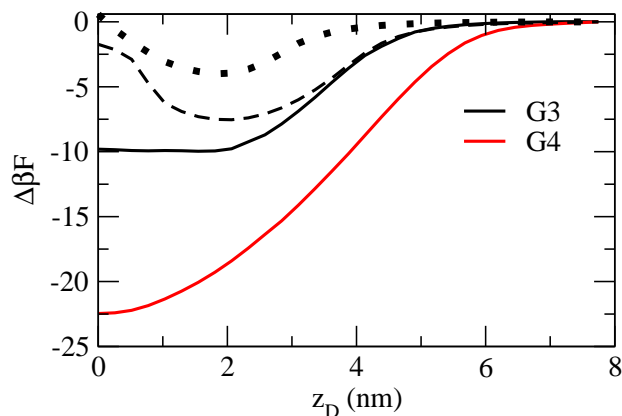


Figure 6.7: The dendrimer-membrane potential of mean force, $\Delta\beta F$, for a $G3$ dendrimer (solid black line), $NDG3$ dendrimer (dashed black line), HS representing a $G3$ dendrimer (dotted black line), and $G4$ dendrimer (solid red line) as a function of distance between the dendrimer core monomer and the bilayer midplane.

6.3.2 Influence of Dendrimer Flexibility and Porosity

A number of works have considered the model of nanoparticles interacting with membranes, and have observed results qualitatively similar to those discussed in the preceding section [160]. Based on such comparisons, one may query what, if any, are the differences in the characteristics of interactions between nanoparticles and dendrimers with membranes. In this regard, we note that our dendrimer model differs from those commonly used for nanoparticles in at least two respects: (i) Our model allows for conformational modulations of the dendrimer molecule (*i.e.*, the dendrimer density profile is not fixed and changes as a function of distance from the membrane); (ii) Our model allows for penetration of the dendrimer by lipid and solvent components (*i.e.* the dendrimer is porous). Hence, the outstanding questions are, “What are the

specific roles played by the flexibility of the dendrimer conformations and the porosity of the dendrimer in influencing its interactions with the membrane?” Below we examine two variants of our model to address the specific roles of such features.

(i) In order to clarify the role of conformational flexibility, we considered a dendrimer of fixed conformation by constraining the density profile of the dendrimer to remain fixed to its conformation far from the membrane. Henceforth, we refer to the $G3$ dendrimers of fixed conformation as $NDG3$ dendrimers. The corresponding PMF profile for the $NDG3$ dendrimer is displayed by the dashed line in Fig. 6.7. As expected, we see that at far distances, the PMFs of the deformable $G3$ (solid black line) and $NDG3$ (dashed black line) dendrimers match. However, at approximately $z_D = 4nm$ (the location at which distortions in the deformable dendrimers manifest, *c.f.* Fig. 6.4a) the PMF profiles begin to differ. Explicitly, we see that the deformable dendrimers exhibit more attractive interactions as compared to the $NDG3$ dendrimers. Interestingly, we observe that the minimum in the dendrimer-membrane PMF profiles for the $NDG3$ dendrimer is offset from $z_D = 0$, indicating that if the dendrimer conformations are rigidly fixed, there is a barrier to permeation of the dendrimer through our model membrane.

We can better understand the differing trends in the $G3$ and $NDG3$ dendrimer-membrane PMF profiles by comparing the plots in Figs. 6.3d-f with those of Figs. 6.8a-c, which display the color density plots of the $NDG3$ dendrimer at $z_D = 2.1nm$, $1.0nm$, and $0nm$ respectively. For the deformable

dendrimer, the membrane is observed to be almost unperturbed during the approach of the dendrimer, while the dendrimer itself undergoes significant conformational changes. In contrast, for the case of the *NDG3* dendrimer, as the dendrimer approaches the membrane, the bilayer is seen to bend substantially in order to initiate dendrimer-membrane electrostatic contacts. Moreover, in the previous section, we saw that the dendrimer deformations allows them to position their charged monomers near the lipid head groups to take advantage of favorable electrostatic interactions. We observe that while the *NDG3* dendrimer is also able to insert itself into the membrane to make contact with the leaflets of the bilayer (Fig. 6.8c), the *NDG3* dendrimer causes more thinning of the membrane as compared to the deformable dendrimer (*c.f.* Fig. 6.3f). The latter can be understood to be a result of the *NDG3* dendrimer rigidity, which leads to a larger number of dendrimer monomers residing in the hydrophobic region of the bilayer where the lipid density is highest (*c.f.* Fig. 6.2a), resulting in higher steric interactions and membrane thinning. Such effects also incur energetic costs that serve to both reduce the attractive wells of the *NDG3* dendrimer-membrane PMF profile and create the energetic barrier seen in the insertion of the *NDG3* dendrimers into the membrane.

Although our *NDG3* conformations were obtained initially from a highly flexible *G3* dendrimer, we believe that the above results may also be used to infer the influence of semiflexibility of the dendrimer bonds on dendrimer-membrane interactions. Indeed, as a crude approximation, the dendrimer with

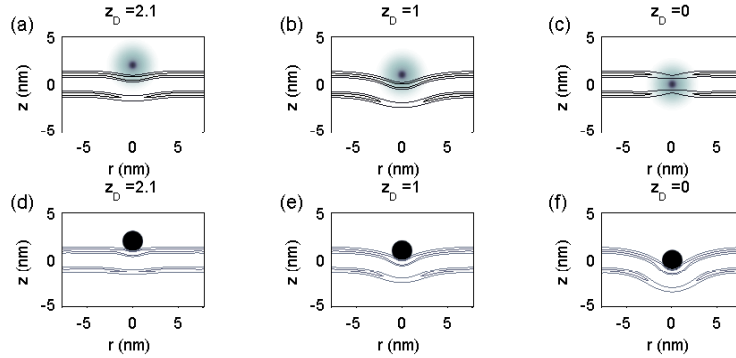


Figure 6.8: Color plots displaying the volume fraction values of fixed conformation *NDG3* dendrimers (a-c) and *HS* representing *G3* dendrimers (d-f) in a $pH = 7$ solution at varying distances from the center of the lipid bilayer, z_D . The lipid bilayer head group volume fraction values are shown through the contour lines, which correspond to values of $\varphi_H = 0.07$ and $\varphi_H = 0.14$.

fixed conformations can be considered to be a model for rigid dendrimers. For the highly flexible dendrimers, the conformational rearrangements undergone by the dendrimer are seen to reduce energy barriers for crossing the membrane. In contrast, based on the behavior of the *NDG3* dendrimer one may expect that for a rigid dendrimer, the membrane would distort significantly during the insertion of the dendrimer. Moreover, the PMFs in such cases can also be expected to involve an energy barrier during the permeation of the dendrimer.

(ii) In order to examine the effect of the dendrimer porosity, we considered a model of a hard sphere (HS) whose volume ($V = M(g)/\rho_0$) equalled that of our single *G3* dendrimers. For our *G3* dendrimers, this corresponded to a hard sphere of radius $R = 1.1nm$. We assume that the HS contains a

uniform distribution of the NH and NH_2 groups and fix the total number of dissociable charge groups to match with our $G3$ dendrimer.

The results for the HS-membrane PMF are represented in Fig. 6.7 by the black dotted line. Here we notice that, similar to the $NDG3$ dendrimer, the location of the PMF minimum ($z_D \approx 2nm$) is offset from the bilayer midplane. More interestingly, the attraction between the HS and membrane is seen to be weaker than that of the $NDG3$ dendrimer. These trends can be rationalized by comparing the morphologies resulting in the $NDG3$ (Figs. 6.8a-c) and HS models (Figs. 6.8d-f). In both cases, we observe that the bilayer begins to deform to initiate contact as the charged dendrimers approach the membrane, which occurs at the cost of an energetic penalty arising from the membrane rigidity. However, we notice an overlap between the dendrimer monomers and the charged lipid head groups in the case of the $NDG3$ dendrimer, whereas in the case of the HS, there is no possibility for such overlap. Moreover, while the $NDG3$ dendrimer still maintains its ability to insert itself within the membrane, in the case of the HS dendrimer, even for $z_D = 0$, we observe that the membrane has to deform to wrap the HS. Hence, the electrostatic interactions are expected to be less significant for the HS dendrimer, which is consistent with the observed weaker attractions.

The results presented in this section serve to clarify the influences of dendrimer porosity and flexibility on its interactions with membranes. Overall, both the lipid molecule penetration within dendrimer voids and conformational changes of the dendrimer were seen to play important roles in modulating

the energetic interactions between dendrimer and membranes. By choosing a model wherein the volume and charges of the idealized model were chosen to match that of the corresponding flexible dendrimer model, we were able to achieve a more direct and quantitative comparison with the flexible dendrimer model.

6.3.3 Effect of Neutral Grafts

As discussed in the introduction, the addition of neutral PEG grafts to dendrimers has been shown to reduce the cytotoxicities of the latter [30, 54, 169]. It has been speculated that the presence of grafts reduce the exposed charges of the dendrimer and thereby modulate its interaction with membranes. In this section, we present results quantifying the interactions between grafted dendrimers and membranes to clarify the mechanisms by which grafts influence the permeation processes.

We begin by discussing the influence of grafts on the conformational changes undergone by the dendrimer during its approach and permeation into the dendrimer. We recall our results from Sec. 6.3.1, wherein we observed that the conformational changes of the dendrimer (*c.f.* Fig. 6.3) played a significant role in their interactions with the membrane. In order to quantify the effect of N_G on the dendrimer shapes during permeation, in Fig. 6.9, we present results that quantify the relative shape anisotropies (a and c), sizes (a and c insets), and aspect ratios (b and d) of the $G3$ and $G4$ dendrimers as a function of z_D for varying N_G values. The solid lines represent the values when

only the dendrimer monomer density profiles are considered, while the dashed lines correspond to the conformations of the dendrimer and graft monomers considered together. In Figs. 6.9a and c, we observe that adding grafts to the dendrimer results in a qualitative change in the asphericity profiles for the $G3$ and $G4$ dendrimers. Explicitly, we notice that the two maxima present in the *non-grafted* $G3$ and $G4$ dendrimers (denoted in the figure as 1 and 2 respectively) are shifted to farther z_D values. Moreover, the magnitude of the maxima for the grafted dendrimers (1 and 2) decreases as N_G is increased. The *shift* to larger z_D for the first two maxima can be attributed to the fact that the presence of the corona from the grafted polymers increases the distance at which the dendrimer “feels” the membrane. The *decrease in the magnitude* of the peaks can be attributed to the fact that the addition of grafts creates results in more steric interactions between the dendrimer and membrane and also shields the electrostatic interactions between the charged dendrimer and lipid monomers. Hence the dendrimers exhibit less propensity to deform and contact the membrane. Thus, the grafted dendrimers maintain more spherically symmetric conformations.

For smaller values of z_D (when the dendrimer is inside the membrane), we notice in Figs. 6.9a and c that $G3$ and $G4$ dendrimers exhibit different trends when N_G is increased. For the $G3$ dendrimers, the asphericity at small z_D increases with increasing N_G , whereas, for $G4$ dendrimers, we observe that the A_S values decrease with N_G . To understand these behaviors, in Fig. 6.10, we present color plots for the density values of the (interior) dendrimer (a-

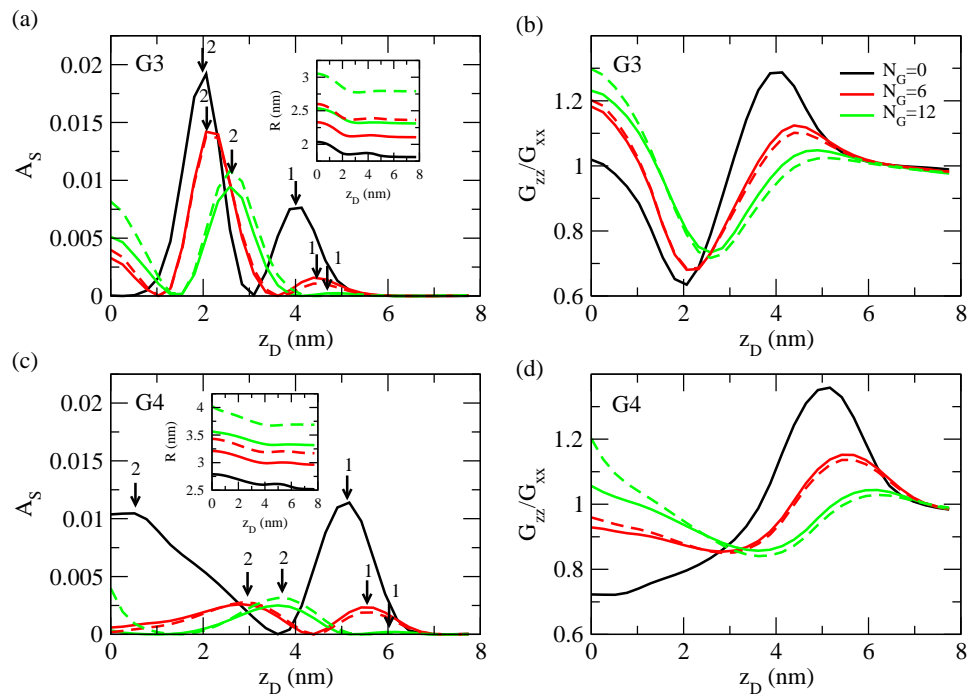


Figure 6.9: The dendrimer asphericity (a and b) and G_{zz}/G_{xx} ratios (b and d) as a function of z_D for G3 (a and b) and G4 (c and d) dendrimers. The insets quantify the dendrimer radius of gyration values for the G3 and G4 dendrimers as a function of z_D .

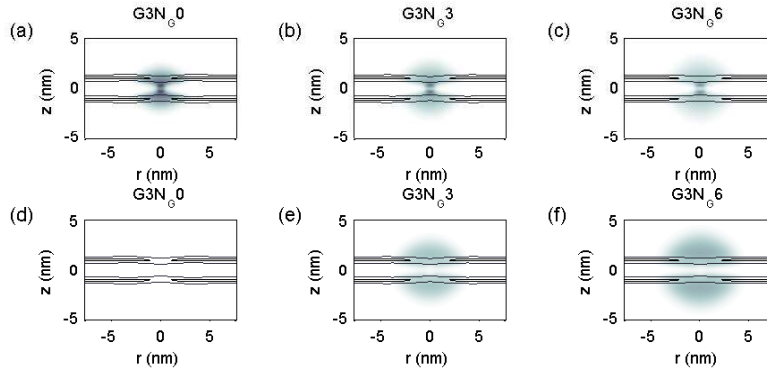


Figure 6.10: Color plots displaying the volume fraction values of $G3$ dendrimer interior (a)-(c) and graft (d)-(f) monomers in a $pH = 7$ solution at varying values of N_G and separation distance $z_D = 0$. The lipid bilayer head group volume fraction values are shown through the contour lines, which correspond to values of $\varphi_H = 0.07$ and $\varphi_H = 0.14$.

c) and (exterior) graft (d-f) monomers for $G3$ dendrimers of grafting lengths $N_G = 0$ (non-grafted dendrimer, a and d), $N_G = 6$ (b and e), and $N_G = 12$ (c and f) when the dendrimers are located at $z_D = 0$, which corresponds to the center of the lipid membrane. We observe that adding grafts to the dendrimers causes the latter to stretch in the z direction, which reduces the density of dendrimer monomers that are near the charged lipid monomers. Correspondingly, the corona evident in the density profiles of the grafted material (displayed in Figs. 6.10d-f) is seen to increase in both magnitude and extent.

Based on the density profiles displayed in Fig. 6.10, the asphericity trends of $G3$ dendrimers can be attributed to the increased stretching of the dendrimer along the z -axis (*c.f.* Figs. 6.10a-c and 6.9b), which results from the steric repulsions between the graft and membrane monomers. By stretch-

ing along the z -axis, the dendrimer assumes a conformation which reduces the entropic costs associated with crowding of the grafted chains. To rationalize the behavior of $G4$ dendrimers, we recall that in Fig. 6.4a, we demonstrated that the increased asphericity of non-grafted $G4$ dendrimers relative to non-grafted $G3$ dendrimers arose from the fact that the charged monomer groups spread out more in the r -direction relative to the z -direction. However, when grafts are attached to the dendrimer, the grafts cause stretching of the dendrimer along the z -axis for the reasons discussed above within the context of $G3$ dendrimers. The latter is reflected in the decreased A_S values as seen in Fig. 6.9c, which results in more spherical shapes.

While the above results indicate that the addition of grafts leads to increased steric repulsions, we note that grafts also have an influence upon the electrostatic interactions between the dendrimer monomers and the lipid head groups. To quantify such effects, we use the following measure,

$$Q_{Contact} = \int d\mathbf{r} \left(\sum_{j=NH, NH_2} \alpha_{P_j} f_j(\mathbf{r}) \varphi_{P_j}(\mathbf{r}) \right) \alpha_H \varphi_H(\mathbf{r}), \quad (6.43)$$

which is proportional to the overlap of the charge densities of the lipid and dendrimer monomers. A small value of $Q_{Contact}$ indicates little overlap, whereas a large value corresponds a high amount of contact between the charged lipid and dendrimer monomers. In Fig. 6.11, we display the $Q_{Contact}$ values as a function of z_D for the dendrimers. Not surprisingly, we observe higher $Q_{Contact}$ values in general for $G4$ dendrimers which arise as a consequence of the larger number of charged monomers. More interestingly, we observe that increasing the

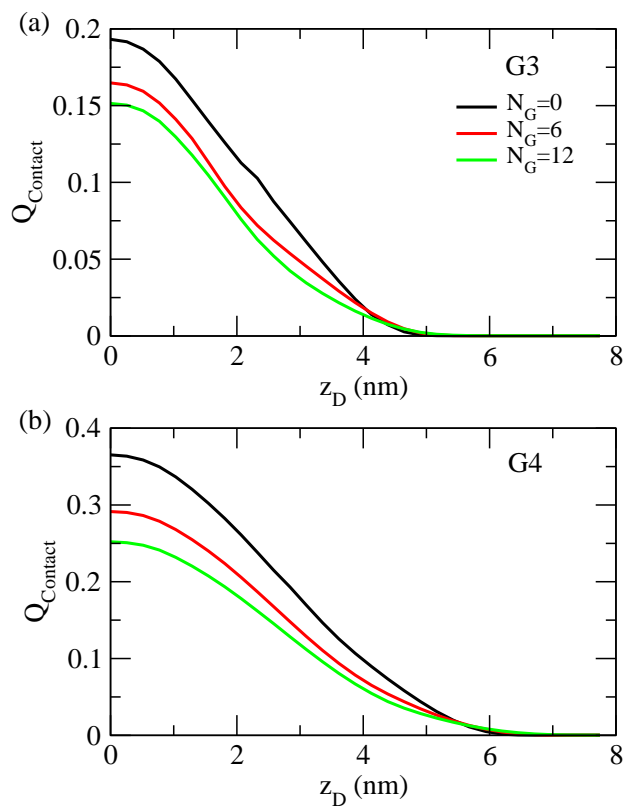


Figure 6.11: The Q_{Contact} values (eq 6.43) between charged $G3$ (a) and $G4$ (b) dendrimer monomers and charged lipid head groups.

grafting length of the dendrimers reduces the contact between the dendrimer and lipids for all z_D . The latter result validates the hypothesis that the addition of grafted chains to the dendrimer periphery reduces electrostatic contact between the charged dendrimer and lipid head group monomers.

The results presented in Figs. 6.9 - 6.11 indicate that neutral grafts influence both the steric and electrostatic components of the dendrimer-membrane interactions. As a direct measure of the influence of grafts on the dendrimer-

membrane interactions, we present the PMF profiles of $G3$ and $G4$ dendrimers as a function of N_G in Fig. 6.12. For both $G3$ and $G4$ dendrimers, we observe that the addition of grafts to the dendrimer has a significant effect on the PMFs between the dendrimers and charged bilayers. Explicitly, the interactions change from being attractive to becoming repulsive as the dendrimer graft length is increased from $N_G = 0$ to $N_G = 12$. For the intermediate grafting length $N_G = 6$, we observe small regions of attractive interaction when the dendrimer and membrane centers are separated by $3 - 4nm$. However, this attraction is significantly smaller than the energy barrier required for the dendrimer to penetrate inside of the membrane. Comparing the results of $G3$ and $G4$ dendrimers, we observe that they exhibit qualitatively similar trends, with however the range and magnitude of the repulsive barrier being larger for the $G4$ dendrimers. Such trends can be rationalized by noting that $G4$ dendrimers are of larger size and also contain larger number of grafts.

In sum, the results presented in this section clarify the effect of neutral grafts on dendrimer-membrane interactions. Explicitly, the presence of grafts was seen to contribute to the steric interactions between the grafts and membrane contribute to repulsive interactions between the dendrimer and membrane. Moreover, the electrostatic contact between the charged dendrimer and lipid head monomers was also seen to be reduced. The combination of the preceding effects results in a decrease in the magnitude of attraction and introduces a repulsive barrier in the interactions between between the dendrimer and the membrane. As a consequence, grafted dendrimers can be expected to

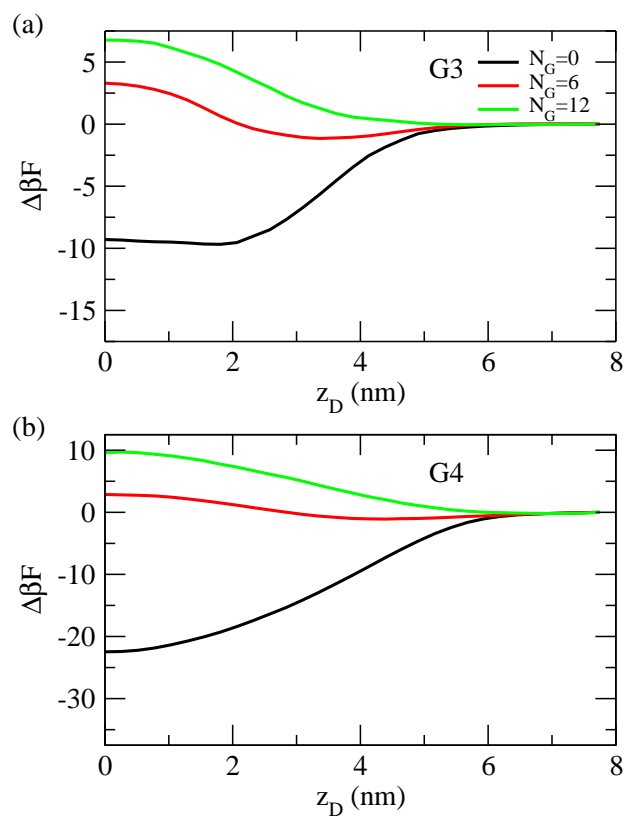


Figure 6.12: The effect of N_G on the dendrimer-membrane potential of mean force, $\Delta\beta F$, as a function of distance between the dendrimer core monomer and the bilayer midplane for $G3$ (a) and $G4$ (b) dendrimers.

exhibit significantly lower propensity for insertion into the membranes, which rationalizes the experimentally reported lower cytotoxicities in such systems.

6.3.4 Effect of pH and Membrane Tension

In this final section of our results, we discuss the effects of pH and the membrane tension upon the interaction between dendrimers and anionic membranes. The motivation for such studies comes from the fact that endocytosis of gene delivery vehicles results in their internalization within a lipid endosomal vesicle [6, 143]. The pH inside such vesicles are modulated through the addition of H^+ ions by endosomal ATPase. As a consequence of such pH changes, the vesicle osmotic pressure and surface tension of the endosomal membrane increases [6, 143, 185]. Hence, it is of interest to understand the influence of pH and membrane tensions on the characteristics of dendrimer-membrane interactions.

Since our model directly incorporates the weakly basic nature of the dendrimer molecules, the modulation of the dendrimer charge arising from the variation of solution pH is rigorously accounted. To quantify the effect of solution pH on dendrimer membrane interactions, in Fig. 6.13, we display PMF profiles for the grafted and non-grafted $G3$ and $G4$ dendrimers as a function of pH . Overall, we observe that decreasing the solution pH results in a stronger attractive interaction between the dendrimers and the membrane. The latter can be understood to be a result of the enhancement in the total dendrimer charge, Q_P , with decreasing pH (see the insets of Fig. 6.13). Interestingly,

our results suggest that the interactions between the N_G6 dendrimers and the membrane can actually switch from being repulsive to becoming attractive as pH is decreased. These results demonstrate that despite the additional steric interactions brought about by the addition of neutral grafts, the electrostatic interactions between the dendrimer and the lipids may be tuned so as to become dominant at lower pHs to facilitate the insertion of dendrimers into membranes.

To examine the impact of the membrane tension, in Fig. 6.14, we compare the PMF profiles between dendrimers and membranes when $\gamma = 0.0k_B T/nm^2$ and $\gamma = 0.74k_B T/nm^2$. Interestingly, we witness only minor changes in the dendrimer-membrane PMFs upon variation of membrane tensions. Such a behavior contrasts significantly with the results of Ting and Wang in which they observed that the attraction between impenetrable nanoparticles and membranes decreased significantly (potential well depth shifted from $\approx -31k_B T$ to $\approx -21k_B T$ for a $G5$ dendrimer) when the membrane surface tension increased from $\gamma = 0.0k_B T/nm^2$ and $\gamma = 0.74k_B T/nm^2$ [160]. Since the energetics of nanoparticle interaction with the membrane are influenced by the membrane deformations (see discussion in the context of Fig. 6.8), their results can be straightforwardly understood to be a consequence of the increased energy required to deform the membrane to wrap around the nanoparticle. In contrast, the porosity and flexibility of our dendrimer model significantly reduces the extent to which the membranes deform during dendrimer-membrane insertion (*c.f.* Fig. 6.3). Hence, it is not surprising that the dendrimer-

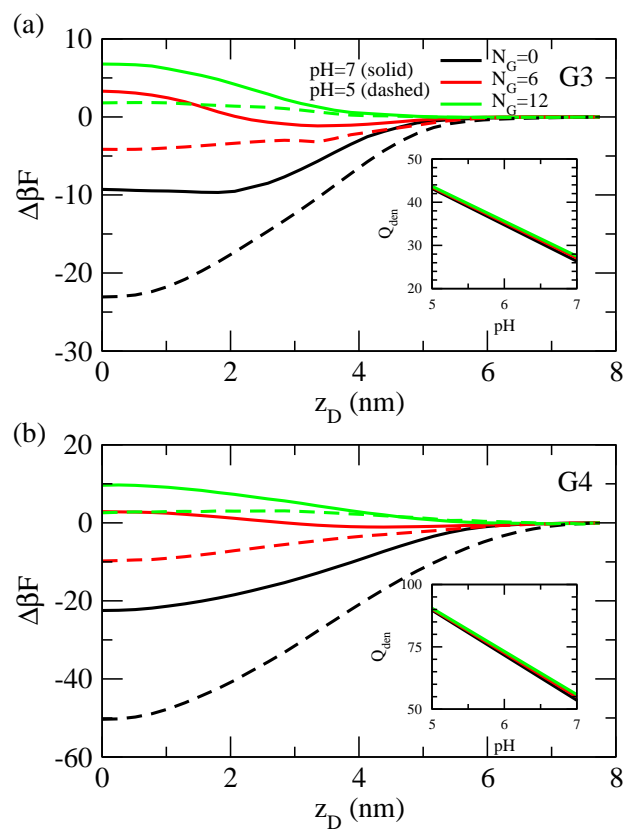


Figure 6.13: The effect of solution pH on the dendrimer-membrane potential of mean force, $\Delta\beta F$, as a function of distance between the dendrimer core monomer and the bilayer midplane for G3 (a) and G4 (b) dendrimers. The insets quantify the dendrimer charge, Q_{den} for an individual dendrimer in the absence of a membrane.

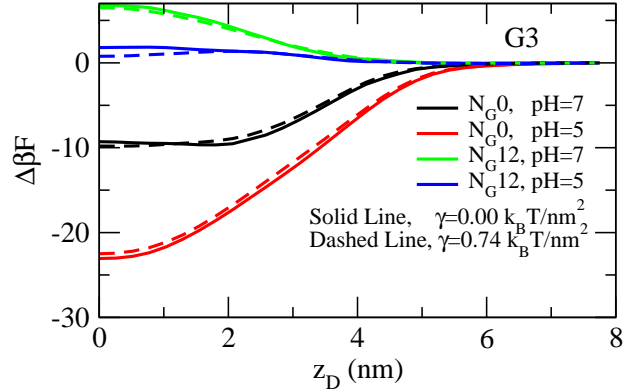


Figure 6.14: The effect of membrane tension, grafting length, and pH on the potential of mean, $\Delta\beta F$, between $G3$ dendrimers and an anionic lipid bilayer. Solid lines represent $\gamma = 0.0 \text{ k}_B T/nm^2$ while dashed lines represent $\gamma = 0.74 \text{ k}_B T/nm^2$.

membrane PMF exhibits only a weak dependence on membrane tension.

Previous works have shown that the rupture tension of membranes, γ_r , can be reduced in the presence of dendrimers, and so it is of interest to understand how the addition of grafts to dendrimer molecules affects their ability to modulate the rupture tension. To determine the effect of dendrimer insertion on the membrane rupture tension, we simulate a dendrimer-membrane system with the dendrimer center of mass situated at $z_D = 0$ for increasing values of membrane surface tension. As we increase γ , we eventually see the formation of a pore which expands indefinitely, and the membrane components in our simulation vanish, which corresponds to the rupture tension of the dendrimer-membrane system.

In Fig. 6.15, we display the rupture tension, γ_r , observed for bilayer membranes in the presence of $G3N_G0$ and $G3N_G12$ dendrimers as a function

of pH . Here we observe that the membrane rupture tensions are uniformly lower in the presence of the dendrimer as compared to the bare membrane ($\gamma = 3.03k_B T/nm^2$, indicated by dotted line in Fig. 6.15). The reduction in rupture tension by dendrimers can be understood to be a consequence of dendrimer-induced disruption of lipid arrangement, which is expected to lower the energy barrier for pore formation [181,182]. As the charge on the dendrimer is increased (by decreasing the solution pH), the rupture tension of the membrane is seen to increase. Such an effect has also been previously witnessed in the context of nanoparticles and results from the enhanced adhesion between the charged dendrimer and lipid head monomers resulting from the increased dendrimer charge [160]. However, when grafts are added to the dendrimers, we observe a reduction in the rupture tension. This reduction in rupture tension can be attributed to the decreased dendrimer-membrane adhesion strength which results from the steric repulsions between the grafts and the membrane. Since rupture tension provides a measure for the ease of releasing the gene delivery vehicles, the above results indicate that the addition of grafts may promote the ease with which dendrimers are released from the endosome.

6.4 Summary

In this article, we reported results of polymer SCFT calculations which examined the interactions between charged dendrimers (with and without neutral grafts) and anionic lipid bilayer membranes. Our results were in qualita-

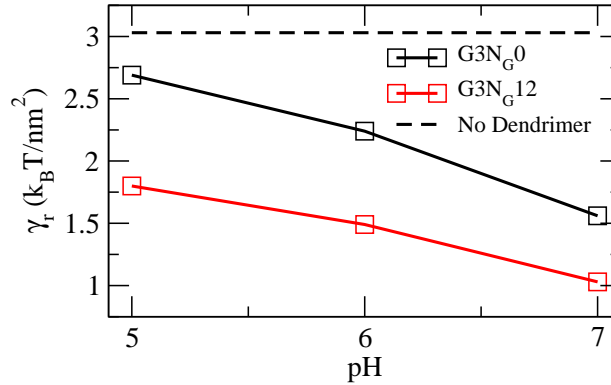


Figure 6.15: The effect of pH and neutral grafts on the rupture tension, γ_r , of anionic bilayer membranes.

tive agreement with observations from previous molecular dynamics simulation studies [57, 58, 73]. We observed that dendrimers undergo significant conformational changes to maximize contact between their monomers and the negatively charged lipid head groups. By performing corresponding calculations for interactions between membranes and (i) non-deformable, porous dendrimers and (ii) charged hard spheres, we were able to delineate the influences of the penetrability and deformability of the dendrimer on the PMFs for dendrimer-membrane interactions. For flexible dendrimers, there was a strong attraction seen between the dendrimer and membrane, with no energy barriers in the insertion of the dendrimer into the membrane. In contrast, the non-deformable dendrimers and charged hard spheres exhibit an energy barrier with an effective well at a finite distance from the membrane. The dendrimer-membrane attraction was seen to be strongest for the deformable dendrimers and weakest for the charged hard spheres.

The addition of neutral grafts to the dendrimer exterior was shown to affect the attraction between the dendrimer and the membrane. In general, we observed that at neutral pH , the grafted dendrimers experienced a repulsive dendrimer-membrane potential, which arose from the increase in steric repulsions between the grafts and the membrane. However, when the pH was lowered to 5 (representative of the environment in the endosome), both the $G3N_G6$ and $G4N_G6$ dendrimers developed an attractive well in their PMF profiles. Furthermore, the addition of grafts to the dendrimer were seen to reduce the required tension for membrane rupture and release the genetic material.

The results in this work provide perspective on both the general manner through which dendrimers permeate cellular membranes and how neutral grafts affect dendrimer-membrane interactions. When the optimally designed grafted dendrimers are near the cell membrane at physiological pH , they will not insert themselves into the membrane; however, upon internalization, the drop in pH and corresponding protonation of the tertiary amine groups results in favorable dendrimer-membrane interaction. The insertion of the dendrimer into the bilayer in turn reduces the tension required for the endosomal membrane to rupture which helps to release the internalized material.

Chapter 7

Summary and Future Work

In this chapter, we summarize the work presented in this dissertation and provide future directions for research on modeling dendrimers, including incorporation of dendrimer semi-flexibility, inclusion of explicit hydrogen bonding sites on the dendrimer, examination of multibody dendrimer-linear polyelectrolyte interactions, and examination of dendrimer-linear polyelectrolyte interactions with anionic membranes.

7.1 Summary of Research

In this body of work, we have developed self-consistent field theory models which examine the conformations and interactions of dendrimers in the presence of model drugs, linear polyelectrolytes, and bilayer membranes. These studies were motivated by the application of dendrimers as drug and gene delivery vectors. An important contribution of this work was the insight on how the connectivity of the dendrimer monomers affects the resulting localization of counterions and charge dissociation of the weakly basic monomers. Because of such effects, we demonstrated that the resulting charge carried by dendrimers could not be known *a priori*. Furthermore, modifications to

the dendrimer architecture and the presence of charged drug, linear polyelectrolyte, and lipid molecules was seen to further influence the total charge carried by dendrimers, effects which can not be accounted for if the acid-base equilibrium reaction is not explicitly accounted for by the model.

By incorporating grafted chains within our dendrimer model, we provided insights into how the presence and length of neutral grafts influence the conformations, drug and linear-polyelectrolyte binding efficacies, and membrane interactions of the dendrimers. We observed that adding grafts created a relatively hydrophobic corona around the dendrimer, which enhanced the binding between hydrophobic drugs and dendrimer molecules. Furthermore, the corona of grafted monomers increased the dendrimer's ability to shield linear polyelectrolyte material and affect the conformations and charge distributions of the dendrimer-linear polyelectrolyte complexes. Lastly, we obtained results which suggested that the addition of grafts to dendrimers can provide experimentalists with the ability to tune the membrane permeability of the dendrimers at different pH values, which would be beneficial for the development of effective, non-cytotoxic delivery vectors.

7.2 Recommendations for Future Work

The models used in this dissertation may be extended to examine other issues relevant to dendrimer applications in drug and gene delivery systems. Below we discuss modifications and additions to our models which would be beneficial in such endeavors.

7.2.1 Dendrimer Flexibility

In our work, we modeled the dendrimer chains by employing a continuous Gaussian chain model, which assumes that the dendrimer backbone is a linearly elastic filament and capable of stretching [35]. However, physically realizable dendrimers are connected by relatively short spacer molecules such that the bond vectors are not necessarily uncorrelated on the length scales assumed in our calculations (*c.f.* Fig. 1.1). Therefore, the dendrimer segments might be more accurately represented through a semiflexible, wormlike chain model such that the length of the dendrimer backbone is fixed and the bending of the dendrimer chain occurs at the cost of a harmonic energy penalty [35].

Incorporation of chain bending rigidity requires not only accounting for the location of the individual monomers, but also the local orientation of the polymer bonds [35]. Determination of such information does occur at a computational expense. However, by using the spherically symmetric wormlike chain framework developed in our group [36], calculations which examine the effect of dendrimer rigidity on the conformations of dendrimers may prove to be computationally tractable. This framework could then be extended to examine how dendrimer flexibility affects their interactions with drug molecules, linear polyelectrolytes, and lipid bilayers.

7.2.2 Incorporating Explicit Hydrogen Bonding

Perhaps one of the most widely used type of dendrimers is the polyamidoamine (PAMAM) dendrimer. PAMAM dendrimers have a number of chemical groups capable of participating in hydrogen (H) bonding interactions. In fact, atomistic simulations have demonstrated that intramolecular H-bonds between the PAMAM primary amine hydrogens and carbonyl oxygens contribute to the backfolding of dendrimer chains [14, 149]. Furthermore, it has been shown that the ether oxygen groups of polyethylene glycol (PEG, a common neutral polymer used to graft dendrimers) are capable of forming H-bonds with the PAMAM amine hydrogens, and such bonding has been observed to compete with PAMAM-water H-bonding [149].

Many weakly soluble drugs carry carbonyl and hydroxyl groups which have been shown to contribute to the binding efficacy between dendrimers and drugs through H-bonding [22, 130, 148]. Thus, it is relevant to query whether H-bonds between the PAMAM amine hydrogen and PEG ether oxygen groups could compete with H-bonding interactions between the dendrimers and drug molecules. Previous SCFT studies have incorporated the effects of reversible hydrogen bonding interactions in a manner similar to way that the acid-base equilibrium reactions of the dendrimer monomers were accounted in this dissertation [32, 80]. Thus, by incorporating such reversible hydrogen bonding interactions to our model, we could explicitly examine the role of grafted chains on the H-bond interactions on the binding efficacies between dendrimers and drug molecules.

7.2.3 Multibody Dendrimer-Linear Polyelectrolyte Interactions

Our work on dendrimer-linear polyelectrolyte complex (dendriplex) formation has provided valuable insights into the physical mechanisms governing their formation. However, the length scales of experimentally relevant dendriplexes ($50 - 250nm$) have indicated that they are composed of multiple dendrimers and nucleic acid (NA) chains [18, 147, 150]. Furthermore, the resulting dendriplex morphologies have been shown to depend on a multitude of parameters including the dendrimer architecture, the dendrimer/NA chain charge ratio, and the size and type of genetic material used. For instance, by using cryo-TEM, Ainalam *et al.* were able to observe that $G1$ and $G2$ PAMAM dendrimers complexed with Luciferase T7 Control DNA (4331 base pair) were able to form well structured rods toroids whereas $G4$, $G6$, and $G8$ PAMAM dendrimers formed globular and less defined aggregates upon complexation [2].

Motivated by the multibody nature of dendriplexes, there have been some simulation studies which examined the binding between two cationic dendrimers and a single anionic linear polyelectrolyte (LPE) [71, 166]. However, these studies did not probe how such parameters affect the potentials of mean force between dendrimers in the presence of LPE molecules. Furthermore, they have not examined how adding neutral grafts would affect such interactions. By utilizing our SCFT dendrimer model in cylindrical coordinates, the effect of dendrimer architecture, LPE concentration, and LPE chain length on the resulting dendrimer-dendrimer PMF profiles could be computed. Such

results would compliment our dendrimer-LPE PMF calculations and could be used to obtain further insights into the role of multibody effects on dendriplex morphology which would be relevant to the experimental systems.

7.2.4 Dendriplex Interactions with a Membrane

The interactions between dendrimers and bilayer membranes are relevant for both drug and gene delivery applications. However, within the context of gene delivery, the dendrimer molecules are complexed with NA materials. Because the NA chains carry negative charges, it is reasonable to expect a dendrimer-LPE complex to interact differently with a membrane than an individual, non-complexed dendrimer. In fact, Monte Carlo simulations have shown that, under certain conditions, anionic LPEs are capable of dissociating from cationic dendrimers when in the presence of a negatively charged, rigid wall [167].

In order to better understand the physics involved in cellular internalization and subsequent endosomal escape of dendriplexes, we propose extend our dendrimer-membrane SCFT model to include the presence of LPEs. By doing so, we could examine the effect of dendrimer architecture and LPE stiffness and size on the stability of the dendrimer-LPE complex and the resulting dendriplex-membrane PMFs. Furthermore, by incorporating the self-consistently determined LPE potential fields into Monte Carlo simulations, we could determine the dendrimer-LPE PMF profiles when in the presence of a membrane.

Bibliography

- [1] M. L. Ainalem, R. A. Campbell, S. Khalid, R. J. Gillams, A. R. Rennie, and T. Nylander. On the ability of pamam dendrimers and dendrimer/dna aggregates to penetrate popc model biomembranes. *Journal of Physical Chemistry B*, 114(21):7229–7244, June 2010.
- [2] M. L. Ainalem, A. M. Carnerup, J. Janiak, V. Alfredsson, T. Nylander, and K. Schillen. Condensing dna with poly(amido amine) dendrimers of different generations: means of controlling aggregate morphology. *Soft Matter*, 5(11):2310–2320, 2009.
- [3] D. Astruc, E. Boisselier, and C. Ornelas. Dendrimers designed for functions: From physical, photophysical, and supramolecular properties to applications in sensing, catalysis, molecular electronics, photonics, and nanomedicine. *Chemical Reviews*, 110(4):1857–1959, April 2010.
- [4] R. C. Ball, J. F. Marko, S. T. Milner, and T. A. Witten. Polymers grafted to a convex surface. *Macromolecules*, 24(3):693–703, February 1991.
- [5] A. E. Beezer, A. S. H. King, I. K. Martin, J. C. Mitchell, L. J. Twyman, and C. F. Wain. Dendrimers as potential drug carriers; encapsulation

- of acidic hydrophobes within water soluble pamam derivatives. *Tetrahedron*, 59(22):3873–3880, May 2003.
- [6] J. P. Behr. The proton sponge: A trick to enter cells the viruses did not exploit. *Chimia*, 51(1-2):34–36, January 1997.
- [7] D. Bhadra, S. Bhadra, S. Jain, and N. K. Jain. A pegylated dendritic nanoparticulate carrier of fluorouracil. *International Journal of Pharmaceutics*, 257(1-2):111–124, May 2003.
- [8] R. Blaak, S. Lehmann, and C. N. Likos. Charge-induced conformational changes of dendrimers. *Macromolecules*, 41(12):4452–4458, June 2008.
- [9] U. Boas and P. M. H. Heegaard. Dendrimers in drug research. *Chemical Society Reviews*, 33(1):43–63, January 2004.
- [10] D. Boris and M. Rubinstein. A self-consistent mean field model of a starburst dendrimer: Dense core vs dense shell. *Macromolecules*, 29(22):7251–7260, October 1996.
- [11] O. V. Borisov and E. B. Zhulina. Effects of ionic strength and charge annealing in star-branched polyelectrolytes. *European Physical Journal B*, 4(2):205–217, July 1998.
- [12] I. Borukhov, D. Andelman, and H. Orland. Random polyelectrolytes and polyampholytes in solution. *European Physical Journal B*, 5(4):869–880, October 1998.

- [13] I. Borukhov and L. Leibler. Enthalpic stabilization of brush-coated particles in a polymer melt. *Macromolecules*, 35(13):5171–5182, June 2002.
- [14] P. Carbone and F. Muller-Plathe. Molecular dynamics simulations of polyaminoamide (pamam) dendrimer aggregates: molecular shape, hydrogen bonds and local dynamics. *Soft Matter*, 5(13):2638–2647, 2009.
- [15] P. Carbone, F. Negri, and F. Muller-Plathe. A coarse-grained model for polyphenylene dendrimers: Switching and backfolding of planar three-fold core dendrimers. *Macromolecules*, 40(19):7044–7055, September 2007.
- [16] W. Carl. A monte carlo study of model dendrimers. *Journal of the Chemical Society-faraday Transactions*, 92(21):4151–4154, November 1996.
- [17] T. L. Chasse, R. Sachdeva, C. Li, Z. M. Li, R. J. Petrie, and C. B. Gorman. Structural effects on encapsulation as probed in redox-active core dendrimer isomers. *Journal of the American Chemical Society*, 125(27):8250–8254, July 2003.
- [18] A. M. Chen, L. M. Santhakumaran, S. K. Nair, P. S. Amenta, T. Thomas, H. X. He, and T. J. Thomas. Oligodeoxynucleotide nanostructure formation in the presence of polypropyleneimine dendrimers and their uptake in breast cancer cells. *Nanotechnology*, 17(21):5449–5460, November 2006.

- [19] W. R. Chen, L. Porcar, Y. Liu, P. D. Butler, and L. J. Magid. Small angle neutron scattering studies of the counterion effects on the molecular conformation and structure of charged g4 pamam dendrimers in aqueous solutions. *Macromolecules*, 40(16):5887–5898, August 2007.
- [20] Y. Y. Cheng, Y. W. Li, Q. L. Wu, H. H. Zhang, and T. W. Xu. Generation-dependent encapsulation/electrostatic attachment of phenobarbital molecules by poly(amidoamine) dendrimers: Evidence from 2d-noesy investigations. *European Journal of Medicinal Chemistry*, 44(5):2219–2223, May 2009.
- [21] Y. Y. Cheng, Q. L. Wu, Y. W. Li, and T. W. Xu. External electrostatic interaction versus internal encapsulation between cationic dendrimers and negatively charged drugs: Which contributes more to solubility enhancement of the drugs? *Journal of Physical Chemistry B*, 112(30):8884–8890, July 2008.
- [22] Y. Y. Cheng and T. W. Xu. Dendrimers as potential drug carriers. part i. solubilization of non-steroidal anti-inflammatory drugs in the presence of polyamidoamine dendrimers. *European Journal of Medicinal Chemistry*, 40(11):1188–1192, November 2005.
- [23] Y. Y. Cheng, Z. H. Xu, M. L. Ma, and T. W. Xu. Dendrimers as drug carriers: Applications in different routes of drug administration. *Journal of Pharmaceutical Sciences*, 97(1):123–143, January 2008.

- [24] J. S. Choi, K. Nam, J. Park, J. B. Kim, J. K. Lee, and J. Park. Enhanced transfection efficiency of pamam dendrimer by surface modification with l-arginine. *Journal of Controlled Release*, 99(3):445–456, October 2004.
- [25] M. Daoud and J. P. Cotton. Star shaped polymers - a model for the conformation and its concentration-dependence. *Journal De Physique*, 43(3):531–538, 1982.
- [26] Kurt Binder David P. Landau. *A guide to Monte Carlo simulations in statistical physics*. Cambridge University Press, 2009.
- [27] P. G. Degennes and H. Hervet. Statistics of starburst polymers. *Journal De Physique Lettres*, 44(9):L351–L360, 1983.
- [28] H. M. Ding, W. D. Tian, and Y. Q. Ma. Designing nanoparticle translocation through membranes by computer simulations. *Acs Nano*, 6(2):1230–1238, February 2012.
- [29] A. Evangelista-Lara and P. Guadarrama. Theoretical evaluation of the nanocarrier properties of two families of functionalized dendrimers. *International Journal of Quantum Chemistry*, 103(4):460–470, June 2005.
- [30] K. Fant, E. K. Eshjorner, A. Jenkins, M. C. Grossel, P. Lincoln, and B. Norden. Effects of pegylation and acetylation of pamam dendrimers on dna binding, cytotoxicity and in vitro transfection efficiency. *Molecular Pharmaceutics*, 7(5):1734–1746, September 2010.

- [31] K. Fant, B. Norden, and P. Lincoln. Using ethidium to probe nonequilibrium states of dna condensed for gene delivery. *Biochemistry*, 50(7):1125–1127, February 2011.
- [32] E. H. Feng, W. B. Lee, and G. H. Fredrickson. Supramolecular diblock copolymers: A field-theoretic model and mean-field solution. *Macromolecules*, 40(3):693–702, February 2007.
- [33] P. J. Flory. Statistical thermodynamics of liquid mixtures. *Journal of the American Chemical Society*, 87(9):1833–&, 1965.
- [34] G. H. Fredrickson, V. Ganesan, and F. Drolet. Field-theoretic computer simulation methods for polymers and complex fluids. *Macromolecules*, 35(1):16–39, January 2002.
- [35] Glenn Fredrickson. *The Equilibrium Theory of Inhomogeneous Polymers*. Oxford University Press, 2005.
- [36] V. Ganesan, L. Khounlavong, and V. Pryamitsyn. Equilibrium characteristics of semiflexible polymer solutions near probe particles. *Physical Review E*, 78(5):051804, November 2008.
- [37] V. V. Ginzburg and S. Balijepailli. Modeling the thermodynamics of the interaction of nanoparticles with cell membranes. *Nano Letters*, 7(12):3716–3722, December 2007.

- [38] G. Giupponi, D. M. A. Buzza, and D. B. Adolf. Are polyelectrolyte dendrimers stimuli responsive? *Macromolecules*, 40(16):5959–5965, August 2007.
- [39] P. Gong, J. Genzer, and I. Szleifer. Phase behavior and charge regulation of weak polyelectrolyte grafted layers. *Physical Review Letters*, 98(1):018302, January 2007.
- [40] E. N. Govorun, K. B. Zeldovich, and A. R. Khokhlov. Structure of charged poly(propylene imine) dendrimers: Theoretical investigation. *Macromolecular Theory and Simulations*, 12(9):705–713, December 2003.
- [41] G. M. Grason and R. D. Kamien. Self-consistent field theory of multiply branched block copolymer melts. *Physical Review E*, 71(5):051801, May 2005.
- [42] G. S. Grest. Structure of many-arm star polymers in solvents of varying quality - a molecular-dynamics study. *Macromolecules*, 27(13):3493–3500, June 1994.
- [43] A. A. Gurtovenko, S. V. Lyulin, M. Karttunen, and I. Vattulainen. Molecular dynamics study of charged dendrimers in salt-free solution: Effect of counterions. *Journal of Chemical Physics*, 124(9):094904, March 2006.
- [44] Y. Haba, C. Kojima, A. Harada, T. Ura, H. Horinaka, and K. Kono. Preparation of poly(ethylene glycol)-modified poly(amido amine) den-

- drimers encapsulating gold nanoparticles and their heat-generating ability. *Langmuir*, 23(10):5243–5246, May 2007.
- [45] R. C. Hedden and B. J. Bauer. Structure and dimensions of pamam/peg dendrimer-star polymers. *Macromolecules*, 36(6):1829–1835, March 2003.
- [46] R. C. Hedden, B. J. Bauer, A. P. Smith, F. Grohn, and E. Amis. Templating of inorganic nanoparticles by pamam/peg dendrimer-star polymers. *Polymer*, 43(20):5473–5481, September 2002.
- [47] S. P. Hong, A. U. Bielinska, A. Mecke, B. Keszler, J. L. Beals, X. Y. Shi, L. Balogh, B. G. Orr, J. R. Baker, and M. M. B. Holl. Interaction of poly(amidoamine) dendrimers with supported lipid bilayers and cells: Hole formation and the relation to transport. *Bioconjugate Chemistry*, 15(4):774–782, July 2004.
- [48] S. Huissmann, A. Wynveen, C. N. Likos, and R. Blaak. The effects of ph, salt and bond stiffness on charged dendrimers. *Journal of Physics-condensed Matter*, 22(23):232101, June 2010.
- [49] J. Hur, K. N. Witte, W. Sun, and Y. Y. Won. On the origins of the salt-concentration-dependent instability and lateral nanoscale heterogeneities of weak polyelectrolyte brushes: Gradient brush experiment and flory-type theoretical analysis. *Langmuir*, 26(3):2021–2034, February 2010.

- [50] A. A. Ivanov and K. A. Jacobson. Molecular modeling of a pamam-cgs21680 dendrimer bound to an a(2a) adenosine receptor homodimer. *Bioorganic & Medicinal Chemistry Letters*, 18(15):4312–4315, August 2008.
- [51] K. Jain, P. Kesharwani, U. Gupta, and N. K. Jain. Dendrimer toxicity: Let’s meet the challenge. *International Journal of Pharmaceutics*, 394(1-2):122–142, July 2010.
- [52] L. B. Jensen, G. M. Pavan, M. R. Kasimova, S. Rutherford, A. Danani, H. M. Nielsen, and C. Foged. Elucidating the molecular mechanism of pamam-sirna dendriplex self-assembly: Effect of dendrimer charge density. *International Journal of Pharmaceutics*, 416(2):410–418, September 2011.
- [53] R. Jevprasesphant, J. Penny, D. Attwood, and A. D’Emanuele. Transport of dendrimer nanocarriers through epithelial cells via the transcellular route. *Journal of Controlled Release*, 97(2):259–267, June 2004.
- [54] R. Jevprasesphant, J. Penny, R. Jalal, D. Attwood, N. B. McKeown, and A. D’Emanuele. The influence of surface modification on the cytotoxicity of pamam dendrimers. *International Journal of Pharmaceutics*, 252(1-2):263–266, February 2003.
- [55] D. Kannaiyan and T. Imae. pH-dependent encapsulation of pyrene in ppi-core:pamam-shell dendrimers. *Langmuir*, 25(9):5282–5285, May 2009.

- [56] K. Karatasos, P. Posocco, E. Laurini, and S. Pricl. Poly(amidoamine)-based dendrimer/sirna complexation studied by computer simulations: Effects of ph and generation on dendrimer structure and sirna binding. *Macromolecular Bioscience*, 12(2):225–240, February 2012.
- [57] C. V. Kelly, P. R. Leroueil, E. K. Nett, J. M. Wereszczynski, J. R. Baker, B. G. Orr, M. M. B. Holl, and I. Andricioaei. Poly(amidoamine) dendrimers on lipid bilayers i: Free energy and conformation of binding. *Journal of Physical Chemistry B*, 112(31):9337–9345, August 2008.
- [58] C. V. Kelly, P. R. Leroueil, B. G. Orr, M. M. B. Holl, and I. Andricioaei. Poly(amidoamine) dendrimers on lipid bilayers ii: Effects of bilayer phase and dendrimer termination. *Journal of Physical Chemistry B*, 112(31):9346–9353, August 2008.
- [59] C. V. Kelly, M. G. Liroff, L. D. Triplett, P. R. Leroueil, D. G. Mullen, J. M. Wallace, S. Meshinchi, J. R. Baker, B. G. Orr, and M. M. B. Holl. Stoichiometry and structure of poly(amidoamine) dendrimer-lipid complexes. *Acs Nano*, 3(7):1886–1896, July 2009.
- [60] Y. Kim, A. M. Klutz, and K. A. Jacobson. Systematic investigation of polyamidoamine dendrimers surface-modified with poly(ethylene glycol) for drug delivery applications: Synthesis, characterization, and evaluation of cytotoxicity. *Bioconjugate Chemistry*, 19(8):1660–1672, August 2008.

- [61] J. S. Klos and J. U. Sommer. Properties of dendrimers with flexible spacer-chains: A monte carlo study. *Macromolecules*, 42(13):4878–4886, July 2009.
- [62] J. S. Klos and J. U. Sommer. Simulations of dendrimers with flexible spacer chains and explicit counterions under low and neutral ph conditions. *Macromolecules*, 43(24):10659–10667, December 2010.
- [63] J. S. Klos and J. U. Sommer. Monte carlo simulations of charged dendrimer-linear polyelectrolyte complexes and explicit counterions. *Journal of Chemical Physics*, 134(20):204902, May 2011.
- [64] J. S. Klos and J. U. Sommer. Simulation of complexes between a charged dendrimer and a linear polyelectrolyte with finite rigidity. *Macromolecular Theory and Simulations*, 21(7):448–460, August 2012.
- [65] C. Kojima, K. Kono, K. Maruyama, and T. Takagishi. Synthesis of polyamidoamine dendrimers having poly(ethylene glycol) grafts and their ability to encapsulate anticancer drugs. *Bioconjugate Chemistry*, 11(6):910–917, November 2000.
- [66] C. Kojima, B. Turkbey, M. Ogawa, M. Bernardo, C. A. S. Regino, L. H. Bryant, P. L. Choyke, K. Kono, and H. Kobayashi. Dendrimer-based mri contrast agents: the effects of pegylation on relaxivity and pharmacokinetics. *Nanomedicine-nanotechnology Biology and Medicine*, 7(6):1001–1008, December 2011.

- [67] P. Kolhe, J. Khandare, O. Pillai, S. Kannan, M. Lieh-Lai, and R. M. Kannan. Preparation, cellular transport, and activity of polyamidoamine-based dendritic nanodevices with a high drug payload. *Biomaterials*, 27(4):660–669, February 2006.
- [68] P. Kolhe, E. Misra, R. M. Kannan, S. Kannan, and M. Lieh-Lai. Drug complexation, in vitro release and cellular entry of dendrimers and hyperbranched polymers. *International Journal of Pharmaceutics*, 259(1-2):143–160, June 2003.
- [69] J. F. KukowskaLatallo, A. U. Bielinska, J. Johnson, R. Spindler, D. A. Tomalia, and J. R. Baker. Efficient transfer of genetic material into mammalian cells using starburst polyamidoamine dendrimers. *Proceedings of the National Academy of Sciences of the United States of America*, 93(10):4897–4902, May 1996.
- [70] M. Lard, S. H. Kim, S. Lin, P. Bhattacharya, P. C. Ke, and M. H. Lamm. Fluorescence resonance energy transfer between phenanthrene and pamam dendrimers. *Physical Chemistry Chemical Physics*, 12(32):9285–9291, 2010.
- [71] S. V. Larin, A. A. Darinskii, A. V. Lyulin, and S. V. Lyulin. Linker formation in an overcharged complex of two dendrimers and linear polyelectrolyte. *Journal of Physical Chemistry B*, 114(8):2910–2919, March 2010.

- [72] S. V. Larin, S. V. Lyulin, A. V. Lyulin, and A. A. Darinskii. Charge inversion of dendrimers in complexes with linear polyelectrolytes in the solutions with low ph. *Polymer Science Series A*, 51(4):459–468, April 2009.
- [73] H. Lee and R. Larson. Molecular dynamics simulations of pamam dendrimer-induced pore formation in dppc bilayers using a coarse grained model. *Abstracts of Papers of the American Chemical Society*, 232:342–342, September 2006.
- [74] H. Lee and R. G. Larson. Coarse-grained molecular dynamics studies of the concentration and size dependence of fifth- and seventh-generation pamam dendrimers on pore formation in dmpe bilayer. *Journal of Physical Chemistry B*, 112(26):7778–7784, July 2008.
- [75] H. Lee and R. G. Larson. Lipid bilayer curvature and pore formation induced by charged linear polymers and dendrimers: The effect of molecular shape. *Journal of Physical Chemistry B*, 112(39):12279–12285, October 2008.
- [76] H. Lee and R. G. Larson. Molecular dynamics study of the structure and interparticle interactions of polyethylene glycol-conjugated pamam dendrimers. *Journal of Physical Chemistry B*, 113(40):13202–13207, October 2009.
- [77] H. Lee and R. G. Larson. Effects of pegylation on the size and internal

- structure of dendrimers: Self-penetration of long peg chains into the dendrimer core. *Macromolecules*, 44(7):2291–2298, April 2011.
- [78] H. Lee and R. G. Larson. Membrane pore formation induced by acetylated and polyethylene glycol-conjugated polyamidoamine dendrimers. *Journal of Physical Chemistry C*, 115(13):5316–5322, April 2011.
- [79] I. Lee, B. D. Athey, A. W. Wetzel, W. Meixner, and J. R. Baker. Structural molecular dynamics studies on polyamidoamine dendrimers for a therapeutic application: Effects of ph and generation. *Macromolecules*, 35(11):4510–4520, May 2002.
- [80] W. B. Lee, R. Mezzenga, and G. H. Fredrickson. Self-consistent field theory for lipid-based liquid crystals: Hydrogen bonding effect. *Journal of Chemical Physics*, 128(7):074504, February 2008.
- [81] P. R. Leroueil, S. A. Berry, K. Duthie, G. Han, V. M. Rotello, D. Q. McNerny, J. R. Baker, B. G. Orr, and M. M. B. Holl. Wide varieties of cationic nanoparticles induce defects in supported lipid bilayers. *Nano Letters*, 8(2):420–424, February 2008.
- [82] R. L. Lescanec and M. Muthukumar. Configurational characteristics and scaling behavior of starburst molecules - a computational study. *Macromolecules*, 23(8):2280–2288, April 1990.
- [83] Thomas Lewis and Venkat Ganesan. Conjugation of polybasic dendrimers with neutral grafts: effect on conformation and encapsulation of

- acidic drugs. *Soft Matter*, 8:11817–11830, September 2012.
- [84] Thomas Lewis and Venkat Ganesan. Mean-field modeling of the encapsulation of weakly acidic molecules in polyelectrolyte dendrimers. *The Journal of Physical Chemistry B*, 116(28):8269–8281, 2012.
- [85] Thomas Lewis, Gunja Pandav, Ahmad Omar, and Venkat Ganesan. Complexation between weakly basic dendrimers and linear polyelectrolytes: effects of grafts, chain stiffness, and poh. *Soft Matter*, pages –, 2013.
- [86] Thomas Lewis, Victor Pryamitsyn, and Venkat Ganesan. Mean field theory of charged dendrimer molecules. *The Journal of Chemical Physics*, 135(20):204902, 2011.
- [87] Y. Li and N. Gu. Thermodynamics of charged nanoparticle adsorption on charge-neutral membranes: A simulation study. *Journal of Physical Chemistry B*, 114(8):2749–2754, March 2010.
- [88] W. B. Liechty, D. R. Kryscio, B. V. Slaughter, and N. A. Peppas. Polymers for drug delivery systems. *Annual Review of Chemical and Biomolecular Engineering, Vol 1*, 1:149–173, 2010.
- [89] X. B. Lin, Y. Li, and N. Gu. Molecular dynamics simulations of the interactions of charge-neutral pamam dendrimers with pulmonary surfactant. *Soft Matter*, 7(8):3882–3888, 2011.

- [90] Y. Lin, Q. Liao, and X. G. Jin. Molecular dynamics simulations of dendritic polyelectrolytes with flexible spacers in salt free solution. *Journal of Physical Chemistry B*, 111(21):5819–5828, May 2007.
- [91] C. A. Lipinski. Drug-like properties and the causes of poor solubility and poor permeability. *Journal of Pharmacological and Toxicological Methods*, 44(1):235–249, July 2000.
- [92] Y. Liu, V. S. Bryantsev, M. S. Diallo, and W. A. Goddard. Pamam dendrimers undergo ph responsive conformational changes without swelling. *Journal of the American Chemical Society*, 131(8):2798–+, March 2009.
- [93] Y. Liu, L. Porcar, K. L. Hong, C. Y. Shew, X. Li, E. Liu, P. D. Butler, K. W. Herwig, G. S. Smith, and W. R. Chen. Effect of counterion valence on the ph responsiveness of polyamidoamine dendrimer structure. *Journal of Chemical Physics*, 132(12):124901, March 2010.
- [94] D. Luo, K. Haverstick, N. Belcheva, E. Han, and W. M. Saltzman. Poly(ethylene glycol)-conjugated pamam dendrimer for biocompatible, high-efficiency dna delivery. *Macromolecules*, 35(9):3456–3462, April 2002.
- [95] Y. V. Lyatskaya, F. A. M. Leermakers, G. J. Fleer, E. B. Zhulina, and T. M. Birshstein. Analytical self-consistent-field model of weak polyacid brushes. *Macromolecules*, 28(10):3562–3569, May 1995.

- [96] S. V. Lyulin, A. A. Darinskii, and A. V. Lyulin. Computer simulation of complexes of dendrimers with linear polyelectrolytes. *Macromolecules*, 38(9):3990–3998, May 2005.
- [97] S. V. Lyulin, A. A. Darinskii, and A. V. Lyulin. Energetic and conformational aspects of dendrimer overcharging by linear polyelectrolytes. *Physical Review E*, 78(4):041801, October 2008.
- [98] S. V. Lyulin, L. J. Evers, P. van der Schoot, A. A. Darinskii, A. V. Lyulin, and M. A. J. Michels. Effect of solvent quality and electrostatic interactions on size and structure of dendrimers. brownian dynamics simulation and mean-field theory. *Macromolecules*, 37(8):3049–3063, April 2004.
- [99] S. V. Lyulin, I. Vattulainen, and A. A. Gurtovenko. Complexes comprised of charged dendrimers, linear polyelectrolytes, and counterions: Insight through coarse-grained molecular dynamics simulations. *Macromolecules*, 41(13):4961–4968, July 2008.
- [100] V. Maingi, M. V. S. Kumar, and P. K. Maiti. Pamam dendrimer-drug interactions: Effect of ph on the binding and release pattern. *Journal of Physical Chemistry B*, 116(14):4370–4376, April 2012.
- [101] P. K. Maiti and B. Bagchi. Structure and dynamics of dna-dendrimer complexation: Role of counterions, water, and base pair sequence. *Nano Letters*, 6(11):2478–2485, November 2006.

- [102] P. K. Maiti and B. Bagchi. Diffusion of flexible, charged, nanoscopic molecules in solution: Size and ph dependence for pamam dendrimer. *Journal of Chemical Physics*, 131(21):214901, December 2009.
- [103] P. K. Maiti, T. Cagin, S. T. Lin, and W. A. Goddard. Effect of solvent and ph on the structure of pamam dendrimers. *Macromolecules*, 38(3):979–991, February 2005.
- [104] P. K. Maiti, T. Cagin, G. F. Wang, and W. A. Goddard. Structure of pamam dendrimers: Generations 1 through 11. *Macromolecules*, 37(16):6236–6254, August 2004.
- [105] P. K. Maiti, Y. Y. Li, T. Cagin, and W. A. Goddard. Structure of polyamidoamide dendrimers up to limiting generations: A mesoscale description. *Journal of Chemical Physics*, 130(14):144902, April 2009.
- [106] P. K. Maiti and R. Messina. Counterion distribution and zeta-potential in pamam dendrimer. *Macromolecules*, 41(13):5002–5006, July 2008.
- [107] M. Majtyka and J. Klos. Computer simulations of dendrimers with charged terminal groups. *Journal of Physics-condensed Matter*, 18(15):3581–3589, April 2006.
- [108] M. Majtyka and J. Klos. Monte carlo simulations of a charged dendrimer with explicit counterions and salt ions. *Physical Chemistry Chemical Physics*, 9(18):2284–2292, 2007.

- [109] M. L. Mansfield and L. I. Klushin. Monte-carlo studies of dendrimer macromolecules. *Macromolecules*, 26(16):4262–4268, August 1993.
- [110] A. Mecke, I. J. Majoros, A. K. Patri, J. R. Baker, M. M. B. Holl, and B. G. Orr. Lipid bilayer disruption by polycationic polymers: The roles of size and chemical functional group. *Langmuir*, 21(23):10348–10354, November 2005.
- [111] N. Metropolis, A. W. Rosenbluth, M. N. Rosenbluth, A. H. Teller, and E. Teller. Equation of state calculations by fast computing machines. *Journal of Chemical Physics*, 21(6):1087–1092, 1953.
- [112] P. Miklis, T. Cagin, and W. A. Goddard. Dynamics of bengal rose encapsulated in the meijer dendrimer box. *Journal of the American Chemical Society*, 119(32):7458–7462, August 1997.
- [113] S. T. Milner, T. A. Witten, and M. E. Cates. Theory of the grafted polymer brush. *Macromolecules*, 21(8):2610–2619, August 1988.
- [114] M. A. Mintzer and M. W. Grinstaff. Biomedical applications of dendrimers: a tutorial. *Chemical Society Reviews*, 40(1):173–190, 2011.
- [115] M. T. Morgan, M. A. Carnahan, C. E. Immoos, A. A. Ribeiro, S. Finkelstein, S. J. Lee, and M. W. Grinstaff. Dendritic molecular capsules for hydrophobic compounds. *Journal of the American Chemical Society*, 125(50):15485–15489, December 2003.

- [116] M. Murat and G. S. Grest. Molecular dynamics study of dendrimer molecules in solvents of varying quality. *Macromolecules*, 29(4):1278–1285, February 1996.
- [117] V. S. Myers, M. G. Weir, E. V. Carino, D. F. Yancey, S. Pande, and R. M. Crooks. Dendrimer-encapsulated nanoparticles: New synthetic and characterization methods and catalytic applications. *Chemical Science*, 2(9):1632–1646, 2011.
- [118] J. F. Nagle and S. Tristram-Nagle. Structure of lipid bilayers. *Biochimica Et Biophysica Acta-reviews On Biomembranes*, 1469(3):159–195, November 2000.
- [119] U. Nagpal, F. A. Detcheverry, P. F. Nealey, and J. J. de Pablo. Morphologies of linear triblock copolymers from monte carlo simulations. *Macromolecules*, 44(13):5490–5497, July 2011.
- [120] B. Nandy and P. K. Maiti. Dna compaction by a dendrimer. *Journal of Physical Chemistry B*, 115(2):217–230, January 2011.
- [121] R. Nap, P. Gong, and I. Szleifer. Weak polyelectrolytes tethered to surfaces: Effect of geometry, acid-base equilibrium and electrical permittivity. *Journal of Polymer Science Part B-polymer Physics*, 44(18):2638–2662, September 2006.
- [122] B. Natarajan, S. Gupta, V. Ramamurthy, and N. Jayaraman. Interfacial regions governing internal cavities of dendrimers. studies of poly(alkyl

- aryl ether) dendrimers constituted with linkers of varying alkyl chain length. *Journal of Organic Chemistry*, 76(10):4018–4026, May 2011.
- [123] M. F. Neerman. The efficiency of a pamam dendrimer toward the encapsulation of the antileukemic drug 6-mercaptopurine. *Anti-cancer Drugs*, 18(7):839–842, August 2007.
- [124] R. R. Netz and H. Orland. Variational theory for a single polyelectrolyte chain. *European Physical Journal B*, 8(1):81–98, March 1999.
- [125] G. Nisato, R. Ivkov, and E. J. Amis. Size invariance of polyelectrolyte dendrimers. *Macromolecules*, 33(11):4172–4176, May 2000.
- [126] Y. H. Niu, L. Sun, and R. A. Crooks. Determination of the intrinsic proton binding constants for poly(amidoamine) dendrimers via potentiometric pH titration. *Macromolecules*, 36(15):5725–5731, July 2003.
- [127] K. Olbrich, W. Rawicz, D. Needham, and E. Evans. Water permeability and mechanical strength of polyunsaturated lipid bilayers. *Biophysical Journal*, 79(1):321–327, July 2000.
- [128] P. D. Olmsted and S. T. Milner. Strong segregation theory of bicontinuous phases in block copolymers. *Macromolecules*, 31(12):4011–4022, June 1998.
- [129] D. Ouyang, H. Zhang, H. S. Parekh, and S. C. Smith. The effect of pH on pamam dendrimer-sirna complexation - endosomal considerations as

- determined by molecular dynamics simulation. *Biophysical Chemistry*, 158(2-3):126–133, October 2011.
- [130] L. Ouyang, L. F. Ma, B. Jiang, Y. H. Li, D. S. He, and L. Guo. Synthesis of novel dendrimers having aspartate grafts and their ability to enhance the aqueous solubility of model drugs. *European Journal of Medicinal Chemistry*, 45(6):2705–2711, June 2010.
- [131] M. L. Patil, M. Zhang, S. Betigeri, O. Taratula, H. He, and T. Minko. Surface-modified and internally cationic polyamidoamine dendrimers for efficient sirna delivery. *Bioconjugate Chemistry*, 19(7):1396–1403, July 2008.
- [132] G. M. Pavan, M. A. Mintzer, E. E. Simanek, O. M. Merkel, T. Kissel, and A. Danani. Computational insights into the interactions between dna and sirna with "rigid" and "flexible" triazine dendrimers. *Biomacromolecules*, 11(3):721–730, March 2010.
- [133] S. Phan and G. H. Fredrickson. Morphology of symmetric abc triblock copolymers in the strong segregation limit. *Macromolecules*, 31(1):59–63, January 1998.
- [134] G. T. Pickett. Classical path analysis of end-grafted dendrimers: Dendrimer forest. *Macromolecules*, 34(25):8784–8791, December 2001.
- [135] A. A. Polotsky, E. B. Zhulina, T. M. Birshtein, and O. V. Borisov. Effect of the ionic strength on collapse transition in star-like polyelectrolytes.

Macromolecular Symposia, 278:24–31, 2009.

- [136] L. Porcar, K. L. Hong, P. D. Butler, K. W. Herwig, G. S. Smith, Y. Liu, and W. R. Chen. Intramolecular structural change of pamam dendrimers in aqueous solutions revealed by small-angle neutron scattering. *Journal of Physical Chemistry B*, 114(5):1751–1756, February 2010.
- [137] W. H. Press, S. A. Teukolsky, W. T. Vetterling, and B. P. Flannery. *Numerical Recipes: The Art of Scientific Computing*. Cambridge University Press, 2007.
- [138] V. Pryamitsyn and V. Ganesan. Strong segregation theory of block copolymer-nanoparticle composites. *Macromolecules*, 39(24):8499–8510, November 2006.
- [139] V. A. Pryamitsyn, F. A. M. Leermakers, G. J. Fleer, and E. B. Zhulina. Theory of the collapse of the polyelectrolyte brush. *Macromolecules*, 29(25):8260–8270, December 1996.
- [140] A. N. Semenov. Contribution to the theory of microphase layering in block-copolymer melts. *Zhurnal Eksperimentalnoi I Teoreticheskoi Fiziki*, 88(4):1242–1256, 1985.
- [141] D. G. Shcharbin, B. Klajnert, and M. Bryszewska. Dendrimers in gene transfection. *Biochemistry-moscow*, 74(10):1070–1079, October 2009.
- [142] P. E. S. Smith, J. R. Brender, U. H. N. Durr, J. D. Xu, D. G. Mullen, M. M. B. Holl, and A. Ramamoorthy. Solid-state nmr reveals the

- hydrophobic-core location of poly(amidoamine) dendrimers in biomembranes. *Journal of the American Chemical Society*, 132(23):8087–8097, June 2010.
- [143] N. D. Sonawane, F. C. Szoka, and A. S. Verkman. Chloride accumulation and swelling in endosomes enhances dna transfer by polyamine-dna polyplexes. *Journal of Biological Chemistry*, 278(45):44826–44831, November 2003.
- [144] L. Sun and R. M. Crooks. Interactions between dendrimers and charged probe molecules. 1. theoretical methods for simulating proton and metal ion binding to symmetric polydentate ligands. *Journal of Physical Chemistry B*, 106(23):5864–5872, June 2002.
- [145] S. Svenson. Dendrimers as versatile platform in drug delivery applications. *European Journal of Pharmaceutics and Biopharmaceutics*, 71(3):445–462, March 2009.
- [146] F. Tack, A. Bakker, S. Maes, N. Dekeyser, M. Bruining, C. Elissen-Roman, M. Janicot, M. Brewster, H. M. Janssen, B. F. M. De Waal, P. M. Fransen, X. Lou, and E. W. Meijer. Modified poly(propylene imine) dendrimers as effective transfection agents for catalytic dna enzymes (dnazymes). *Journal of Drug Targeting*, 14(2):69–86, February 2006.
- [147] Yin Tang, Yang-Bing Li, Bo Wang, Ri-Yuan Lin, Mallory van Dongen, Danielle M. Zurcher, Xiao-Yan Gu, Mark M. Banaszak Holl, George Liu,

- and Rong Qi. Efficient in vitro sirna delivery and intramuscular gene silencing using peg-modified pamam dendrimers. *Molecular Pharmaceutics*, 9(6):1812–1821, 2012.
- [148] I. Tanis and K. Karatasos. Association of a weakly acidic anti-inflammatory drug (ibuprofen) with a poly(amidoamine) dendrimer as studied by molecular dynamics simulations. *Journal of Physical Chemistry B*, 113(31):10984–10993, August 2009.
- [149] I. Tanis and K. Karatasos. Molecular dynamics simulations of polyamidoamine dendrimers and their complexes with linear poly(ethylene oxide) at different ph conditions: static properties and hydrogen bonding. *Physical Chemistry Chemical Physics*, 11(43):10017–10028, 2009.
- [150] O. Taratula, O. B. Garbuzenko, P. Kirkpatrick, I. Pandya, R. Savla, V. P. Pozharov, H. X. He, and T. Minko. Surface-engineered targeted ppi dendrimer for efficient intracellular and intratumoral sirna delivery. *Journal of Controlled Release*, 140(3):284–293, December 2009.
- [151] P. Tarazona. A density functional theory of melting. *Molecular Physics*, 52(1):81–96, 1984.
- [152] R. K. Tekade, T. Dutta, V. Gajbhiye, and N. K. Jain. Exploring dendrimer towards dual drug delivery: ph responsive simultaneous drug-release kinetics. *Journal of Microencapsulation*, 26(4):287–296, 2009.

- [153] G. Teobaldi and F. Zerbetto. Molecular dynamics of a dendrimer-dye guest-host system. *Journal of the American Chemical Society*, 125(24):7388–7393, June 2003.
- [154] G. Teobaldi and F. Zerbetto. Simulation of some dynamical aspects of the photophysics of dye molecules encapsulated in a dendrimer. *Journal of Luminescence*, 111(4):335–342, March 2005.
- [155] R. B. Thompson, V. V. Ginzburg, M. W. Matsen, and A. C. Balazs. Block copolymer-directed assembly of nanoparticles: Forming mesoscopically ordered hybrid materials. *Macromolecules*, 35(3):1060–1071, January 2002.
- [156] W. D. Tian and Y. Q. Ma. Complexation of a linear polyelectrolyte with a charged dendrimer: Polyelectrolyte stiffness effects. *Macromolecules*, 43(3):1575–1582, February 2010.
- [157] W. D. Tian and Y. Q. Ma. Effects of valences of salt ions at various concentrations on charged dendrimers. *Soft Matter*, 6(6):1308–1316, 2010.
- [158] W. D. Tian and Y. Q. Ma. Insights into the endosomal escape mechanism via investigation of dendrimer-membrane interactions. *Soft Matter*, 8(23):6378–6384, 2012.
- [159] Wen-de Tian and Yu-qiang Ma. Theoretical and computational studies of dendrimers as delivery vectors. *Chem. Soc. Rev.*, 42:705–727, 2013.

- [160] C. L. Ting and Z. G. Wang. Interactions of a charged nanoparticle with a lipid membrane: Implications for gene delivery. *Biophysical Journal*, 100(5):1288–1297, March 2011.
- [161] C. L. Ting and Z. G. Wang. Minimum free energy paths for a nanoparticle crossing the lipid membrane. *Soft Matter*, 8(48):12066–12071, 2012.
- [162] D. A. Tomalia, A. M. Naylor, and W. A. Goddard. Starburst dendrimers - molecular-level control of size, shape, surface-chemistry, topology, and flexibility from atoms to macroscopic matter. *Angewandte Chemie-international Edition In English*, 29(2):138–175, February 1990.
- [163] D. Trombly and V. Ganesan. Interactions between polymer-grafted particles and bare particles for biocompatibility applications. *Journal of Polymer Science Part B-polymer Physics*, 47(24):2566–2577, December 2009.
- [164] Y. J. Tsai, C. C. Hu, C. C. Chu, and I. Toyoko. Intrinsically fluorescent pamam dendrimer as gene carrier and nanoprobe for nucleic acids delivery: Bioimaging and transfection study. *Biomacromolecules*, 12(12):4283–4290, December 2011.
- [165] M. J. Uline, Y. Rabin, and I. Szleifer. Effects of the salt concentration on charge regulation in tethered polyacid monolayers. *Langmuir*, 27(8):4679–4689, April 2011.

- [166] V. Vasumathi and P. K. Maiti. Complexation of sirna with dendrimer: A molecular modeling approach. *Macromolecules*, 43(19):8264–8274, October 2010.
- [167] N. K. Voulgarakis, K. O. Rasmussen, and P. M. Welch. Dendrimers as synthetic gene vectors: Cell membrane attachment. *Journal of Chemical Physics*, 130(15):155101, April 2009.
- [168] Q. Wang, T. Taniguchi, and G. H. Fredrickson. Self-consistent field theory of polyelectrolyte systems. *Journal of Physical Chemistry B*, 108(21):6733–6744, May 2004.
- [169] W. Wang, W. Xiong, J. L. Wan, X. H. Sun, H. B. Xu, and X. L. Yang. The decrease of pamam dendrimer-induced cytotoxicity by pegylation via attenuation of oxidative stress. *Nanotechnology*, 20(10):105103, March 2009.
- [170] Y. L. Wang, Z. Y. Lu, and A. Laaksonen. Specific binding structures of dendrimers on lipid bilayer membranes. *Physical Chemistry Chemical Physics*, 14(23):8348–8359, 2012.
- [171] P. Welch and M. Muthukumar. Tuning the density profile of dendritic polyelectrolytes. *Macromolecules*, 31(17):5892–5897, August 1998.
- [172] P. Welch and M. Muthukumar. Dendrimer-polyelectrolyte complexation: A model guest-host system. *Macromolecules*, 33(16):6159–6167, August 2000.

- [173] C. M. Wijmans and E. B. Zhulina. Polymer brushes at curved surfaces. *Macromolecules*, 26(26):7214–7224, December 1993.
- [174] K. N. Witte, S. Kim, and Y. Y. Won. Self-consistent field theory study of the effect of grafting density on the height of a weak polyelectrolyte brush. *Journal of Physical Chemistry B*, 113(32):11076–11084, August 2009.
- [175] K. N. Witte and Y. Y. Won. Self-consistent-field analysis of mixed polyelectrolyte and neutral polymer brushes. *Macromolecules*, 39(22):7757–7768, October 2006.
- [176] J. K. Wolterink, F. A. M. Leermakers, G. J. Fleer, L. K. Koopal, E. B. Zhulina, and O. V. Borisov. Screening in solutions of star-branched polyelectrolytes. *Macromolecules*, 32(7):2365–2377, April 1999.
- [177] J. K. Wolterink, J. van Male, M. Daoud, and O. V. Borisov. Starburst polyelectrolytes: Scaling and self-consistent-field theory. *Macromolecules*, 36(17):6624–6631, August 2003.
- [178] J. K. Wolterink, J. van Male, M. A. C. Stuart, L. K. Koopal, E. B. Zhulina, and O. V. Borisov. Annealed star-branched polyelectrolytes in solution. *Macromolecules*, 35(24):9176–9190, November 2002.
- [179] B. Wu, W. R. Chen, T. Egami, X. Li, Y. Liu, Y. M. Wang, C. Do, L. Porcar, K. L. Hong, L. Liu, G. S. Smith, and S. C. Smith. Molecular

- dynamics and neutron scattering study of the dependence of polyelectrolyte dendrimer conformation on counterion behavior. *Journal of Chemical Physics*, 137(6):064902, August 2012.
- [180] D. T. Wu, G. H. Fredrickson, J. P. Carton, A. Ajdari, and L. Leibler. Distribution of chain-ends at the surface of a polymer melt - compensation effects and surface-tension. *Journal of Polymer Science Part B-polymer Physics*, 33(17):2373–2389, December 1995.
- [181] L. T. Yan and X. B. Yu. Charged dendrimers on lipid bilayer membranes: Insight through dissipative particle dynamics simulations. *Macromolecules*, 42(16):6277–6283, August 2009.
- [182] L. T. Yan and X. B. Yu. Enhanced permeability of charged dendrimers across tense lipid bilayer membranes. *Acs Nano*, 3(8):2171–2176, August 2009.
- [183] H. Yang, J. J. Morris, and S. T. Lopina. Polyethylene glycol-polyamidoamine dendritic micelle as solubility enhancer and the effect of the length of polyethylene glycol arms on the solubility of pyrene in water. *Journal of Colloid and Interface Science*, 273(1):148–154, May 2004.
- [184] K. Yang, L. A. Weng, Y. Y. Cheng, H. F. Zhang, J. H. Zhang, Q. L. Wu, and T. W. Xu. Host-guest chemistry of dendrimer-drug complexes. 6. fully acetylated dendrimers as biocompatible drug vehicles using dexamethasone 21-phosphate as a model drug. *Journal of Physical Chemistry B*, 115(10):2185–2195, March 2011.

- [185] S. Yang and S. May. Release of cationic polymer-dna complexes from the endosome: A theoretical investigation of the proton sponge hypothesis. *Journal of Chemical Physics*, 129(18):185105, November 2008.
- [186] Cheng Yiyun, Xu Tongwen, and Fu Rongqiang. Polyamidoamine dendrimers used as solubility enhancers of ketoprofen. *European Journal of Medicinal Chemistry*, 40(12):1390 – 1393, 2005.
- [187] H. Yoo, P. Sazani, and R. L. Juliano. Pamam dendrimers as delivery agents for antisense oligonucleotides. *Pharmaceutical Research*, 16(12):1799–1804, December 1999.
- [188] G. S. Yu, Y. M. Bae, H. Choi, B. Kong, I. S. Choi, and J. S. Choi. Synthesis of pamam dendrimer derivatives with enhanced buffering capacity and remarkable gene transfection efficiency. *Bioconjugate Chemistry*, 22(6):1046–1055, June 2011.
- [189] Libo Zhao, Qinglin Wu, Yiyun Cheng, Jiahai Zhang, Jihui Wu, and Tongwen Xu. High-throughput screening of dendrimer-binding drugs. *Journal of the American Chemical Society*, 132(38):13182–13184, 2010.
- [190] T. Zhou and S. B. Chen. Monte carlo simulations of dendrimer-polymer conjugates. *Macromolecules*, 38(20):8554–8561, October 2005.
- [191] T. Zhou and S. B. Chen. A simulation study on dynamics of dendrimer-polymer conjugates. *Macromolecules*, 39(19):6686–6692, September 2006.

- [192] E. B. Zhulina and O. V. Borisov. Polyelectrolytes grafted to curved surfaces. *Macromolecules*, 29(7):2618–2626, March 1996.
- [193] Y. B. Zhulina, V. A. Pryamitsyn, and O. V. Borisov. Structure and conformational transitions in grafted polymer-chains layers - new theory. *Vysokomolekulyarnye Soedineniya Seriya A*, 31(1):185–194, January 1989.
- [194] T. C. Zook and G. T. Pickett. Hollow-core dendrimers revisited. *Physical Review Letters*, 90(1):015502, January 2003.